The role of USP22 in nucleic acid sensing pathways and interferon-induced necroptotic cell death

Dissertation

zur Erlangung des Doktorgrades der Naturwissenschaften

vorgelegt beim Fachbereich 14 Biochemie, Chemie und Pharmazie

der Johann Wolfgang Goethe-Universität

in Frankfurt am Main

von

Rebekka Karlowitz

aus Heilbronn

Frankfurt am Main, 2023

(D 30)

Vom Fachbereich 14 der Johann Wolfgang Goethe-Universität als Dissertation angenommen.

Dekan: Prof. Dr. Clemens Glaubitz, FB14

1. Gutachter: Prof. Dr. Volker Dötsch, FB14

2. Gutachter: Dr. rer. nat. habil. Sjoerd J.L. van Wijk, FB16

Datum der Disputation: 29.01.2024

Table of Contents

List of abbreviations

2’3’-cGAMP, cGAMP	Cyclic guanosine monophosphate (GMP) adenosine monophosphate (AMP)
3CLpro	3C-like protease
ABCG2	Adenosine triphosphate (ATP)-binding cassette subfamily G member 2
ACE2	Angiotensin-converting enzyme 2
AIM2	Absent in melanoma-2
AK4	Adenylate kinase 4
ALKB	Alkylation B
ALKBH	ALKB homolog
ALR	AIM2-like receptor
AMFR	Autocrine motility factor receptor
AML	Acute myeloid leukemia
AMP	Adenosine monophosphate
APS	Ammonium persulfate
ATG	Autophagy-related protein
ATP	Adenosine triphosphate
ATXN7	Ataxin 7
ATXN7L3	ATXN7 like 3
BSA	Albumin fraction V
BST2	Bone marrow stromal cell antigen 2
BV6, B	Smac mimetic
CARD	Caspase activation and recruitment domain
CD4	Cluster of differentiation 4
CDK	Cyclin dependent kinase
CDN	Cyclic dinucleotides
cDNA	Cyclic deoxyribonucleic acid (DNA)
cGAS	Cyclic guanosine monophosphate (GMP)-AMP synthase
CHX	Cycloheximide
cIAP	Cellular inhibitor of apoptosis protein
CLR	C-type lectin receptor
CO_2	Carbon dioxide
COP-II	Coatomer protein complex II
COVID-19	Coronavirus disease 2019
CRISPR	Clustered regularly interspaced short palindromic repeats
CXCL-10	C-X-C motif chemokine ligand 10

CXCR	C-X-C motif chemokine receptor
CYLD	Cylindromatosis
DAI	Deoxyribonucleic acid (DNA)-dependent activator of interferon (IFN)-regulatory factors
DAMP	Damage-associated molecular pattern
DDX	DEAD-box helicase
diABZI	Di-amidobenzimidazoles
dKO	Double KO
DMEM	Dulbecco's Modified Eagle Medium
DMSO	Dimethyl sulfoxide
DNA	Deoxyribonucleic acid
DNA-PK	DNA-dependent protein kinase
DPB	Digitonin permeabilization buffer
DPBS	Dulbecco's phosphate buffered saline
DSMZ	*Deutsche Sammlung von Mikroorganismen und Zellkulturen*
DTT	Dithiothreitol
DUB	Deubiquitylating enzyme, deubiquitylase
E protein	Envelope protein (coronavirus protein)
EDTA	Ethylenediaminetetraacetic acid
EEF1A2	Eukaryotic translation elongation factor 1 alpha 2
EIF3S5	Eukaryotic translation initiation factor 3 subunit 5
ENY2	ENY2 transcription and export complex 2 subunit
EpiCM	Epithelial Cell Medium
ER	Endoplasmic reticulum
ERGIC	ER-Golgi intermediate compartment
FACS	Fluorescence-activated cell sorting
FACT	Facilitates chromatin transcription
FADD	Fas-associated death domain protein
FASL	Fas ligand
FBP1	Far upstream element (FUSE) binding protein 1
FCCP	Carbonyl cyanide-4-(trifluoromethoxy)phenylhydrazone
FCS	Fetal calf serum
FDA	Food and Drug Administration
FoxM1	Forkhead box M1
FUSE	Far upstream element
GAS	Interferon (IFN)γ-activated site
GFP	Green fluorescent protein

GM-CSF	Granulocyte-macrophage colony-stimulating factor
GMP	Guanosine monophosphate
GO	Gene ontology
gRNA	Genomic ribonucleic acid (RNA)
GTP	Guanosine triphosphate
H	Histone
HAT	Histone acetyltransferase
HCl	Hydrochloric acid
HCoV	Human coronavirus
HECT	Homologous to the E6-AP carboxyl terminus
HER2	Human epidermal growth factor receptor 2
hIEC	Human intestinal epithelial cell
HIV-1	Human immunodeficiency virus type 1
HMGB1	High mobility group-box protein 1
HOIL-1	Heme-oxidized iron regulatory protein (IRP) 2 ubiquitin ligase 1
HOIP	HOIL-1 interacting protein
HRP	Horseradish peroxidase
HSPA5	Heat shock protein family A (Hsp70) member 5
HSV-1	Herpes simplex virus 1
IFI	Interferon (IFN) gamma inducible protein
IFIT	Interferon (IFN)-induced protein with tetratricopeptide repeats
IFITM	Interferon (IFN)-induced transmembrane protein
IFN, I	Interferon
IFNAR	IFN alpha receptor
IFNGR	IFN gamma receptor
IFNLR	IFN lambda receptor
IKK	IκB kinase
IL	Interleukin
IL-10R	IL-10 receptor
IP-10	IFN-gamma induced protein 10 kilodalton (kDa)
IRF	IFN regulatory factor
iRHOM2	Inactive rhomboid protein 2
IRP	Iron regulatory protein
ISD	IFN-stimulatory DNA
ISG	IFN-stimulated gene
ISGF3	ISG factor 3
ISRE	IFN-stimulated response elements

JAK	Janus kinase
JAMM	Zinc metalloproteases JAB1/MPN/MOV34
K	Lysine
KCl	Potassium chloride
kDa	Kilodalton, unified atomic mass unit
KO	Knockout
KPNA2	Importin subunit alpha-1, karyopherin subunit alpha-2
LC3	Light chain 3
LPG2	Laboratory of genetics and physiology 2
LPS	Lipopolysaccharide
LRR	Leucine-rich repeat
M	Methionine
M protein	Membrane protein (coronavirus protein)
MAPK	Mitogen-activated protein kinase
MAVS	Mitochondrial antiviral-signaling protein
MBOAT2	Membrane bound O-acyltransferase domain containing 2
MCMV	Murine cytomegalovirus
MDA5	Melanoma differentiation-associated gene 5
MEM	Minimum Essential Medium Eagle
MERS	Middle east respiratory syndrome
MERTK	Tyrosine-protein kinase Mer
$MgCl_2$	Magnesium chloride
MINDY	Motif interacting with ubiquitin-containing novel DUB family
MJD	Machado-Joseph domain-containing proteases
MLKL	Mixed-lineage kinase-like
mRNA	Messenger ribonucleic acid (RNA)
mtDNA	Mitochondrial DNA
mTORC1	Rapamycin complex 1
MUL1	Mitochondrial E3 ubiquitin protein ligase 1
MX1	MX dynamin like GTPase 1
MyD88	Myeloid differentiation primary response 88
MYSM1	Myb like, SWIRM and MPN domains 1
N/A	Not applicable
Na_2HPO_4	Disodium hydrogen phosphate
NaCl	Sodium chloride
ncRNA	Non-coding ribonucleic acid (RNA)
NECTIN3	Nectin cell adhesion molecule 3

NEDD8	Neural precursor cell expressed, developmentally down-regulated 8
NEMO	Nuclear factor kappa-light-chain-enhancer of activated B cells (NF-κB) essential modulator
NF-κB	Nuclear factor kappa-light-chain-enhancer of activated B cells
NHT	Non-human target
NIK	NF-κB-inducing kinase
NK	Natural killer
NLR	Nucleotide-binding oligomerization domain (NOD)-like receptor
NOD	Nucleotide-binding oligomerization domain
NP	Nucleoprotein
NP-40	Nonident-40
Nsp	Non-structural protein
OAS	2'-5'-oligoadenylate synthetase
ORF	Open reading frame
OTU	Ovarian tumor
OTUB1	Otubain
OTUD	OTU deubiquitylase
OUT	Ovarian tumor
P/S	Penicillin/streptomycin
P3H2	Prolyl 3-hydroxylase 2
PAGE	Polyacrylamide gel electrophoresis
PAMP	Pathogen-associated molecular pattern
PARP9	Poly(ADP-Ribose) polymerase family member 9
PBS	Phosphate buffered saline
PBS-T	PBS-Tween-20
PC	Pancreatic cancer
PCR	Polymerase chain reaction
PD-L1	Programmed death-ligand 1
PI	Propidium iodide
PIC	Protease Inhibitor Cocktail
PKR	Protein kinase R
PLpro	Papain-like protease
poly(I:C)	Polyinosinic:polycytidylic acid
PRR	Pattern recognition receptor
qRT-PCR	Quantitative real-time PCR
RBR	Really interesting new gene (RING)-between-RING
RCAN1	Regulator of calcineurin

REG4	Regenerating family member 4
RHIM	Receptor-interacting protein (RIP) homotypic interaction motif
RIG-I	Retinoic acid-inducible gene I
RING	Really interesting new gene
RIP	Receptor-interacting protein
RIPK	RIP kinase
RLR	RIG-I-like receptors
RNA	Ribonucleic acid
RNF	Ring finger protein
rRNA	Ribosomal RNA
RT	Room temperature
S protein	Spike protein (coronavirus protein)
SAGA	Spt-Ada-Gcn5-acetyltransferase
SAMD5	Sterile alpha motif domain containing 5
SARS-CoV	Severe Acute Respiratory Syndrome Coronavirus
SARS-CoV-2	Severe Acute Respiratory Syndrome Coronavirus 2
SAVI	STING-associated vasculopathy with onset in infancy
SD	Standard deviation
SDS	Sodium dodecyl sulfate
SEAP	Secreted embryonic alkaline phosphatase
SeV	Sendai virus
sgRNA	Small guide RNA
SHARPIN	Shank-associated RH domain-interacting protein
siCtrl	Non-silencing control (siRNA)
siRNA	Silencing RNA
SIRT1	Sirtuin 1
SLFN4	Schlafen 5
SQSTM1	Sequestosome 1
STAT	Signal transducer and activator of transcription
STIM1	Stromal interaction molecule 1
STING	Stimulator of IFN genes
STR	Short tandem repeat
SUMO	Small ubiquitin-related modifier
TAB	TGF-β activated kinase 1 (TAK1) binding protein 1
TACSTD2	Tumor-associated calcium signal transducer 2
TAK1	Transforming growth factor-β (TGF-β)-activated kinase 1
TBK1	Tank-binding kinase 1

TEMED	Tetramethyletylenediamine
TFAM	Mitochondrial transcription factor A
TGF-β	Transforming growth factor-β
TGM2	Transglutaminase 2
TIR	Toll/IL-1 receptor
TIRAP	TIR domain containing adaptor protein
TLR	Toll-like receptor
TMB	3,3',5,5'-Tetramethylbenzidine
TMRM	Tetramethylrhodamine methylester
TNFR	Tumor necrosis factor (TNF) receptor
TNFα	Tumor necrosis factor α
TRADD	TNFR type 1-associated death domain protein
TRAF	TNFR-associated factor 2
TRAIL	TNF-related apoptosis-inducing ligand
TRAM	Translocating chain-associating membrane protein
TRF1	Telomeric repeat factor 1
TRIF	TIR domain-containing adaptor protein inducing IFN beta
TRIM	Tripartite motif containing
tRNA	Transfer RNA
TRRAP	Transformation/transcription domain associated protein
TUBE	Tandem ubiquitin binding entities
TYK2	Tyrosine kinase 2
UBD	Ubiquitin-binding domain
Ubp8p	Ubiquitin-specific-processing protease 8
UCH	Ubiquitin C-terminal hydrolase
UPR	Unfolded protein response
USP	Ubiquitin-specific protease
USP22	Ubiquitin-specific peptidase 22
vIRD	Viral inducer of RIPK3 degradation
Vpu	Viral protein U
WIPI2	WD repeat domain phosphoinositide-interacting protein 2
ZBP1	Z-DNA binding protein 1
ZnF	Zinc finger
ZUFSP/ZUP1	Zinc finger with UFM1-specific peptidase domain protein
zVAD.fmk, Z	N-benzyloxycarbonyl-Val-Ala-Asp(O-Me)fluoromethylketone

List of tables

List of figures

1 Abstract

Every day, living organisms are challenged by internal and external factors that threaten to bring imbalance to their tightly regulated systems and disrupt homeostasis, leading to degeneration, and ultimately death. More than ever, we face the challenge of combating diseases such as COVID-19 caused by infection with the SARS-CoV-2 coronavirus. It is therefore crucial to identify host factors that control antiviral defense mechanisms. In addition, in the fight against cancer, it is becoming increasingly important to identify markers that could be used for targeted therapy to influence cellular processes and determine cell fate.

As a deubiquitylating enzyme, ubiquitin specific peptidase 22 (USP22) mediates the removal of the small molecule ubiquitin, which is post-translationally added to target proteins, thereby regulating several important processes such as protein degradation, activation or localization. Through its deubiquitylating function, USP22 controls several biological processes such as cell cycle regulation, proliferation and cancer immunoresistance by modulating key proteins involved in these pathways. Lately, USP22 was reported to positively regulate TNFα-mediated necroptosis, an inflammatory type of programmed cell death, in various human tumor cell lines by affecting RIPK3 phosphorylation. In addition, USP22 as a part of the Spt-Ada-Gcn5 acetyltransferase (SAGA) transcription complex is known to regulate gene expression by removing ubiquitin from histones H2A and H2B. However, little is known about the role of USP22 in global gene expression.

In this study, we performed a genome-wide screen in the human colon carcinoma cell line HT-29 and identified USP22 as a key negative regulator of basal interferon (IFN) expression. We further demonstrated that the absence of USP22 results in increased STING activity and ubiquitylation, both basally and in response to stimulation with the STING agonist 2'3'-cGAMP, thereby affecting IFNλ1 expression and basal expression of antiviral ISGs. In addition, we were able to establish USP22 as a critical host factor in controlling SARS-CoV-2 infection by regulating infection, replication, and the generation of infectious virus particles, which we attribute in part to its role in regulating STING signaling.

In the second part of the study, we connected the findings of USP22-dependent regulation of IFN signaling and TNFα-induced necroptosis and investigated the role of USP22 during necroptosis induced by the synergistic action of IFN and the Smac mimetic BV6 in caspase-deficient settings. We identified USP22 as a negative regulator of IFN-induced necroptosis, which does not depend on STING expression, but relies on a yet unknown mechanism.

In summary, we identify USP22 as an important regulator of IFN signaling with important implications for the defense against viral infections and regulation of the necroptotic pathway

that could be exploited for devising targeted therapeutic strategies against viral infections and related diseases like COVID-19, and advancing precision medicine in cancer treatment.

2 Introduction

2.1 The ubiquitin system

2.1.1 Ubiquitylation

Ubiquitylation, the covalent attachment of the 8.6 kDa protein ubiquitin to substrate proteins, is an integral part of the fine-tuning and regulation of many cellular processes [1, 2]. Ubiquitylation is one of several forms of post-translational modifications, like modification with ubiquitin-like proteins such as small ubiquitin-related modifier (SUMO), interferon stimulated gene (ISG) 15, neural precursor cell expressed, developmentally down-regulated 8 (NEDD8), and autophagy-related protein 8 (ATG8) [3], and is mediated by a series of ubiquitin-activating (E1), -conjugating (E2), and -ligating (E3) enzymes in an adenosine triphosphate (ATP)-dependent manner [4].

The first step in linking ubiquitin to target proteins is mediated by E1 enzymes, which activate ubiquitin by adenylation, allowing the formation of a thioester bond between ubiquitin and the active site of E1. In a next step, the activated ubiquitin is transferred to E2 enzymes, which act as donors for E3 ligases to transfer ubiquitin to their intended protein substrates [5-7]. Three types of E3 ligases mediate the final step of coupling ubiquitin to its target substrate [8]. In the case of really interesting new gene (RING) ligases, ubiquitin is transferred directly from the donor E2 enzyme to the substrate, during which the E3 ligase binds to both the E2 and the target protein to facilitate the transfer [9]. Homologous to the E6-AP carboxyl terminus (HECT) ligases form a transient thioester bond with ubiquitin before isopeptide bond-mediated substrate modification [10, 11]. Finally, RING-between-RING (RBR) ligases use both mechanisms by directly binding E2s and the formation of transient bonds with ubiquitin before target transfer [12, 13].

The versatile signaling outcomes of ubiquitylation proteins can be attributed to the variability in ubiquitin modification, e.g. monoubiquitin or ubiquitin chains, chain length, and type of inter-ubiquitin linkages, as shown in Figure 1. Target proteins can be covalently linked to either mono- or polyubiquitin, i.e. ubiquitin chains that are generated through the lysine (K) residues K6, K11, K27, K29, K33, K48, or K63, or via the N-terminal methionine (M) at position 1 (M1), or heterotypic combinations thereof, creating distinct three-dimensional topologies that allow precise recognition by ubiquitin-binding domain (UBD) proteins [8, 14]. Depending on the linkage type, target proteins are degraded by the proteasome (for K48- and K63-linked chains) while other linkages lead to stabilization or activation of the ubiquitylated protein or act as scaffolds for the recruitment of additional signaling components [2, 15]. Adding additional complexity, ubiquitin itself can be modified with phosphorylation or acetylation, although the implications of these modifications remain unclear in some cases (Figure 1) [16, 17].

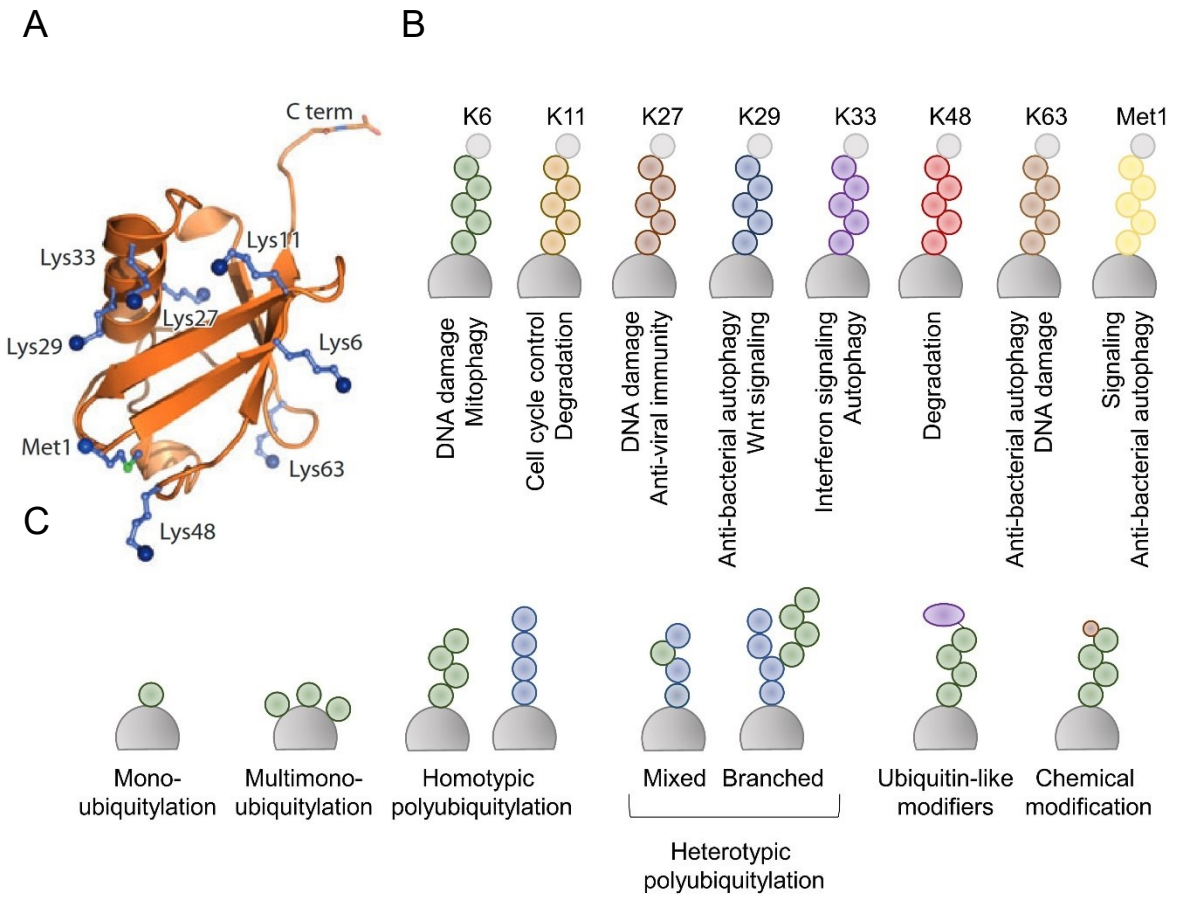

Figure 1: The multiple forms of ubiquitylation. A. The structure of ubiquitin, including the lysine (Lys) and methionine (Met1) residues that are used for differentially-linked ubiquitin chains. B. Ubiquitin chain types and their predominant cellular functions. C. Forms of ubiquitylation, including heterotypic polyubiquitylation with mixed ubiquitin linkage types, the addition of ubiquitin-like modifiers (such as SUMO, NEDD8) to existing ubiquitin-chains, and the chemical modification (phosphorylation, acetylation, deamidation) of existing ubiquitin chains. Adapted from [2, 18-20].

2.1.2 Deubiquitylating enzymes

Ubiquitylation is counteracted by the superfamily of deubiquitylating enzymes (or deubiquitylases, DUBs). To date, about 100 DUBs have been identified, which can be classified according to their domain structure into the cysteine proteases ubiquitin-specific proteases (USP), ubiquitin C-terminal hydrolases (UCH), ovarian tumor (OTU) DUBs, Machado-Joseph domain-containing proteases (MJDs), the zinc metalloproteases JAB1/MPN/MOV34 (JAMM) family DUBs, the zinc finger (ZnF) with UFM1-specific peptidase domain protein (ZUFSP/ZUP1) DUBs, and motif interacting with ubiquitin-containing novel DUB family (MINDY) [4, 21-24].

The most common group of cysteine proteases, comprising the USPs, OTUs, UCHs, MJDs and MINDY family [25], cleave ubiquitin through action of the catalytic triad containing a cysteine, histidine, and acidic residue. Upon binding of ubiquitin to the DUB catalytic site, the isopeptide linkage is attacked by the catalytic cysteine residue. During the deubiquitylation

process, the proximal ubiquitin is released and the newly formed acyl intermediate deacetylated by a water molecule, leading to release of the distal ubiquitin [25].

In addition to the removal of ubiquitin, some DUBs are able to remove ubiquitin-like modifiers, e.g. NEDD8, ISG15, and SUMO, such as USP21, which cleaves both neddylated and ubiquitylated proteins, or USP18, which specifically cleaves ISG15 [26-28].

The exact mechanisms how DUBs discriminate between ubiquitylated proteins, ubiquitin chain linkages and ubiquitin-like molecules are still unclear. Primarily, ubiquitin is directed to the DUB catalytic center by interaction of its Ile44 or Ile36 patch with the ubiquitin-binding site (S1) at the DUB surface [29-31]. Further specificity of DUBs can be mediated by the presence of additional binding sites at the DUB surface that offer substrate-, sequence- or ubiquitin-linkage specificity, or discrimination between ubiquitin and ubiquitin-like modifiers, as nicely reviewed by Mevissen and Komander [25]. For instance, during ubiquitin-DUB interactions, the C-terminal amino acids of ubiquitin stretch towards the DUB catalytic center, which allows discrimination between ubiquitin and the ubiquitin-like modifiers NEDD8 and SUMO that have different C-terminal sequences [24]. A similar mechanism of predetermined orientation of the ubiquitin moieties in respect to each other and in respect to the ubiquitin binding sites is proposed for distinguishing between ubiquitin linkage types [30], e.g. between the extended K63- or M1-linked and the more densely packed K48-linked ubiquitin chains [24, 30], as well as the decision between cleavage of a distal ubiquitin (endo) or between ubiquitin molecules (exo) [24].

Interestingly, many diseases, including cancer, can be traced to the dysfunction of the ubiquitin system [5]. The DUB Otubain 1 (OTUB1) is involved in the regulation of cancer-associated signaling pathways, such as mitogen-activated protein kinase (MAPK), rapamycin complex 1 (mTORC1) and p53 signaling, and is overexpressed in several tumor entities, including colon cancer [32, 33]. Additionally, mutations in the ubiquitin carboxyl-terminal hydrolase cylindromatosis (CYLD) are responsible for the phenotype of skin tumor cylindromatosis [34, 35], and mutations in A20 can lead to a form of autoinflammatory disorder [36].

In addition to mammalian organisms, many viruses contain the genetic information for viral DUBs that counteract the advanced ubiquitin system of the innate immune response or otherwise alter ubiquitin signaling to avoid neutralization by the host immune response [37, 38]. Examples include the DUB domain papain-like protease (PLpro) of the coronaviruses Severe Acute Respiratory Syndrome Coronavirus (SARS-CoV) and SARS-CoV-2 that interfere with nucleic acid sensing pathways and the interferon (IFN) response [39, 40], and the human immunodeficiency virus type 1 (HIV-1) protein viral protein U (Vpu), which recruits an E3 ubiquitin ligase complex for cluster of differentiation 4 (CD4) degradation [41].

2.1.3 Ubiquitin-specific peptidase 22

Ubiquitin-specific peptidase 22 (USP22) belongs to the superfamily of USPs and was first described as part of an 11-gene signature that predicts poor patient outcome, such as a short interval to disease recurrence, metastasis and death [42, 43]. Subsequent studies performed in yeast and humans have identified USP22 as part of the Spt-Ada-Gcn5-acetyltransferase (SAGA) transcription complex [44, 45]. Extensive studies on USP22 yeast homolog ubiquitin-specific-processing protease 8 (Ubp8p) have revealed the structure of USP22 and its integration into the SAGA module. Both USP22 and Ubp8p contain an N-terminal ZnF and a C-terminal catalytic domain. In contrast to the majority of DUBs in the USP family, the ZnF domain of USP22 does not contain the Arg221 residue that is crucial for binding to free ubiquitin [46], but mediates binding to ataxin 7 like 3 (ATXN7L3) and ataxin 7 (ATXN7) (or yeast homologs Sgf11 and Sgf73), which are required for incorporation into the SAGA complex. Within the human SAGA complex, the N-terminal ZnF motif of USP22 forms the assembly lobe together with ENY2 transcription and export complex 2 (ENY2) and the N-terminal helix of ATXN7L3, while the C-terminal ubiquitin hydrolase domain of USP22 forms the catalytic lobe together with the N-terminal ZnF domain of ATXN7L3 [47].

The human SAGA complex consists of 20 known subunits and is divided into five separate modules with functionally distinct roles, including a scaffolding core, a module for histone acetylation (histone acetyltransferases, HAT), a deubiquitylation module, a metazoan-specific splicing module, and the multidomain protein kinase transformation/transcription domain associated protein (TRRAP) [48-50]. While the HAT module catalyzes the acetylation of histone (H) 3 to allow chromatin opening, binding of transcription factors and the pre-initiation complex, USP22 embedded in the DUB module contributes to the deubiquitylation of histone H2B at K120 and histone H2A at K119 [51-53].

Histone (de)ubiquitylation is a powerful tool to regulate gene expression. As a regulator of H2A monoubiquitylation, USP22 is suggested to repress Polycomb gene transcription [53-55]. In addition, increased monoubiquitylation of H2B increases transcription of genes by inhibiting the tight packing of histones to allow the recruitment of histone modifying and remodeling proteins [56, 57] and H2Bub1 facilitates the function of the chaperone facilitates chromatin transcription (FACT) and transcriptional elongation [58]. Interestingly, several studies highlight the necessity of both H2B ubiquitylation and subsequent deubiquitylation by Ubp8p for the recruitment of the ribonucleic acid (RNA) polymerase II kinase Ctk1 and messenger RNA (mRNA) elongation [59, 60].

Besides regulating gene transcription through its deubiquitinating role in the SAGA complex, USP22 plays a significant role in promoting cell cycle progression by affecting the stability of cell cycle regulators. Through K63-linked deubiquitylation of far upstream element (FUSE)

binding protein 1 (FBP1), USP22 negatively regulates the expression of the cyclin-dependent kinase inhibitor p21. Knockdown of USP22 resulted in increased FBP1 ubiquitylation, decreased FBP1 occupancy at the p21 gene, and increased p21 expression, leading to the inhibition of cyclin dependent kinase (CDK) complexes and increased accumulation in G1 [61, 62]. A similar mechanism was observed in pancreatic cancer (PC), where USP22 downregulated p21 and p27 through regulating their inhibitor forkhead Box M1 (FoxM1), strengthening reports of USP22 in promoting G1 progression [63]. In addition, some studies have also suggested a role for USP22 in G2/M progression [64, 65].

Several studies have reported USP22 to mediate resistance to cell death, an additional important hallmark of cancer besides the regulation of cell cycle progression [66]. Two mechanisms mainly account for the protective role of USP22 during cell death. Through its role in SAGA, USP22 regulates transcription of c-Myc, the androgen receptor and p53, which are important transcription factors for cancer progression [51, 67]. Additionally, USP22 contributes to the regulation of cancer-related genes by stabilizing the deacetylase Sirtuin 1 (SIRT1). SIRT1 in turn decreases p53 acetylation and downstream transcription, leading to impaired apoptosis [68]. In addition, c-Myc is stabilized through SIRT1-mediated deacetylation [69], which adds to the USP22-dependent SAGA-mediated regulation and detrimental role of USP22 in apoptosis outcome. Several additional reports of USP22-regulated proteins and pathways underline the role of USP22 in regulation of cancer-related pathways, including the ER chaperone heat shock protein family A (HSP70) member 5 (HSPA5), whose stabilization leads to suppression of the unfolded protein response (UPR) in human epidermal growth factor receptor 2 (HER2)-driven breast cancer and decreased sensitization to UPR-targeting apoptosis [70], regulation of the Wnt/β-catenin pathway, which adds to USP22-mediated chemoresistance [71], and USP22-dependent deubiquitylation of receptor-interacting protein kinase (RIPK) 3 which affects tumor necrosis factor α (TNFα)-induced RIPK3 phosphorylation and necroptotic cell death [72]. In addition, USP22 regulates ATG7- and ATG5-mediated autophagy, a lysosomal degradation pathway indispensable for cell recycling and cellular metabolism that has been implicated in tumor survival and treatment resistance, through regulation of SIRT1 [47, 73].

2.2 Interferon signaling

IFNs were first discovered in 1957 as factors capable of interfering with the replication of influenza virus [74]. Now, they are well known as cytokines with a wide-ranging role in antiviral and antiproliferative signaling and immunomodulation in response to the detection of pathogens or damaged cells [75].

There are three classes of IFNs in humans. The first class of type I IFNs includes IFNα, IFNβ, IFNε, IFNκ and IFNω, with IFNα being divided into 13 different subtypes, namely IFNα1, IFNα2,

IFNα4, IFNα5, IFNα6, IFNα7, IFNα8, IFNα10, IFNα13, IFNα14, IFNα16, IFNα17, and IFNα21, with all type I IFNs engaging the same receptor, the IFN alpha receptor (IFNAR). IFNγ is the only member of the type II IFNs and binds to the heterodimeric IFN gamma receptor (IFNGR), which consists of the ligand-binding IFNGR1 chain and the IFNGR2 chain that is required for signal transduction [76]. Lambda IFNs are the third class of IFNs identified in 2003 along with their receptor subunits IFN lambda receptor (IFNLR) 1 and interleukin (IL)-10 receptor (IL-10R) 2. Type III IFNs comprise IFNλ1 (also known as IL-29), IFNλ2 (also known as IL-28A), and IFNλ3 (also known as IL-28B), as well as a later discovered fourth IFNλ (IFNλ4) [77, 78].

Type I and III IFN signaling is typically induced by activation of IFN regulatory factors (IRFs) downstream of nucleic acid sensing signaling [79]. The type of IFN expressed depends on the nucleic acid sensing stimulus and sometimes the location of the sensing receptors, as demonstrated for the toll-like receptor (TLR) 4, whose endosomal engagement results in type I IFN induction, whereas TLR4 in the plasma membrane has been shown to transmit type III IFN signaling [80, 81]. IFNα subtypes or IFNβ are expressed downstream of IRF3, IRF7 or IRF5, sometimes in a time-dependent manner [82-84]. While translocation of IRF3 and IRF7 to the nucleus has been shown to lead to the expression of both type I and type III IFNs, IFNλ1 can also be induced by IRF1 [85, 86]. IFNγ is a major driver of adaptive immune signaling and is primarily produced by cells of the adaptive immune system, such as $CD4^+$ T helper 1 cells, $CD8^+$ cytotoxic T cells, and natural killer (NK) cells [87-89], contributing to immune cell homeostasis [90].

Naturally, the transmission of IFN signaling depends on the expression of the respective receptors. With few exceptions, type I and II IFN receptors, as well as IFNLR2, are widely distributed and ubiquitously expressed, whereas IFNλ signaling is restricted by the limited expression of IFNLR1 to lung, intestine, liver tissue, and some immune cells [79, 91-93]. Type I, II, and III IFNs share similar, yet distinct mechanisms of IFNR engagement and downstream signaling. Both IFNα and IFNλ receptor complexes associate with Janus kinase (JAK) family members JAK1 and tyrosine kinase 2 (TYK2), whereas IFNGR1 and IFNGR2 associate with JAK1 and JAK2, respectively [76, 94, 95]. In response to ligand binding, receptor subunits dimerize, inducing autophosphorylation and phosphorylation of the associated JAK adaptor proteins. Several post-translational modifications, including ubiquitylation, ensure internalization of the IFNAR complex, a feature required for downstream signaling, whereas IFNGR signaling is not dependent on endocytosis, but on association with cholesterol/sphingolipid-enriched post-translational nanodomains [96-100]. Activation of the JAK adaptor proteins results in recruitment and phosphorylation of signal transducer and activator of transcription (STAT) proteins and formation of STAT homo- or heterodimers that translocate to the nucleus and function as a transcription factor to ensure expression of a

specific subset of target genes called IFN-stimulated genes (ISGs) [101], as depicted in Figure 2. Type I and III IFNs commonly induce the formation of phosphorylated STAT1-homodimers as well as phosphorylated STAT1-STAT2 heterodimers that bind to specific ISG promoter sequences known as IFN-stimulated response elements (ISREs) in a complex with IRF9 called ISG factor 3 (ISGF3). Other complexes formed include STAT3, STAT4, STAT5, and STAT6 homodimers and heterodimeric combinations thereof [75]. STAT1-homodimers are the main transcription factor for induction of IFNγ-dependent genes and bind to IFNγ-activated site (GAS) promoter elements [102]. Together, the heterogeneity of activated complexes, the restricted expression of components of the IFN signaling cascade, the differential receptor affinities of IFN classes and subtypes, and the kinetics of subsequent STAT phosphorylation allow for distinct transcription of a diverse array of ISGs and fine-tuning of the IFN signaling response [103-108].

Although best described for their response to cytosolic abnormal DNA, sensing of bacterial components, or viral infection, IFNs are also constitutively expressed at low levels in many cell types, including epithelial cells, and play a critical role in mediating antiviral responses after infection by ensuring basal expression of key signaling components such as IRFs and STATs [109-113].

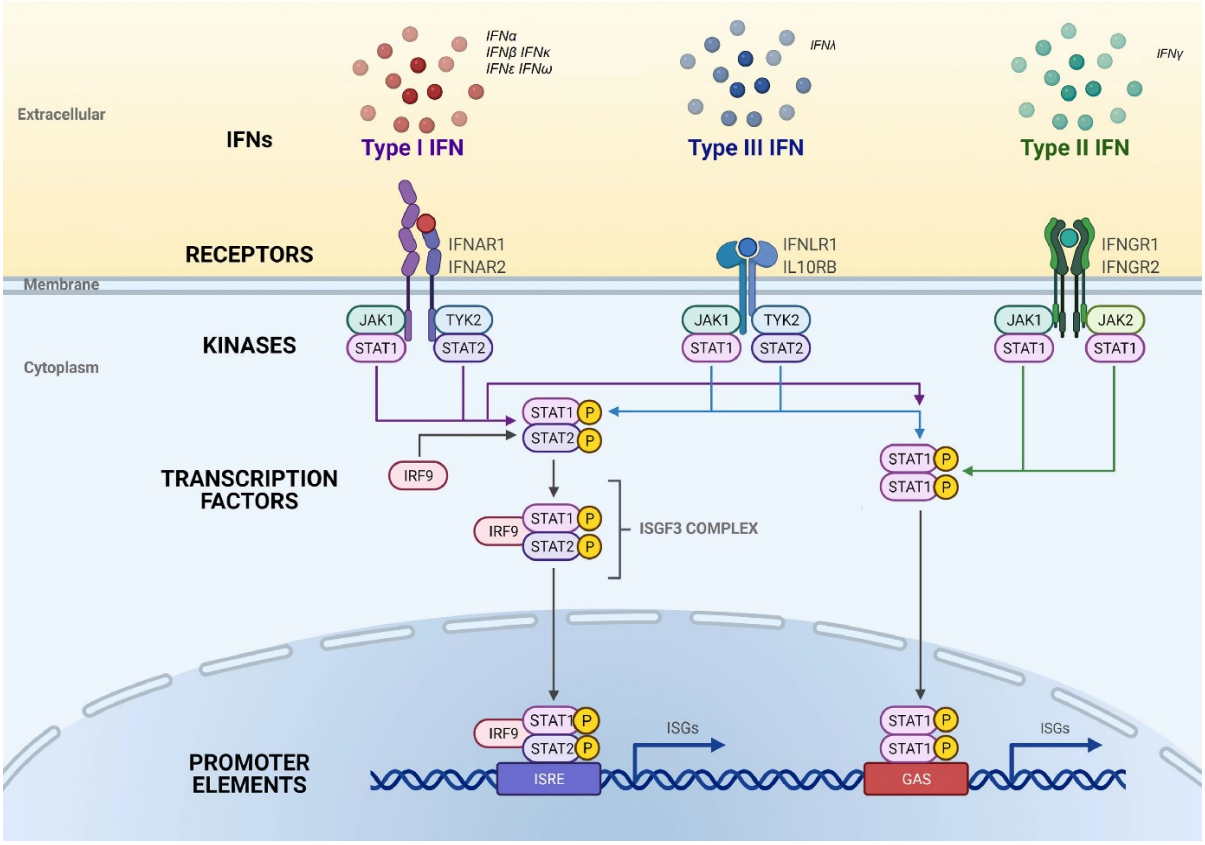

Figure 2: Classical type I, II and III IFN signaling. Upon binding of IFNs to the respective receptors, the receptor associated JAKs are activated and phosphorylate the transcription factor STAT1, leading to STAT dimerization and translocation to GAS promoter elements in the nucleus. In addition to STAT1, STAT2 can be phosphorylated, leading to the formation of STAT1-STAT2 heterodimers and formation

of the ISGF3 complex together with IRF9, which binds to ISRE promoter elements. Binding of ISGF3 or STAT1-homodimersto promoter elements then leads to the expression of IFN-specific ISGs. Adapted from [114].

2.3 Nucleic acid sensing

The human innate immune system provides rapid protection against a broad range of threats, whereas the pathogen-specific responses of the adaptive immune system are delayed due to the need for time-consuming clonal expansion of effector T and B cells [115, 116]. Several mechanisms impede pathogen invasion from the very beginning, such as the mechanical barrier of the skin or tight junctions, unfavorable conditions such as pH, or colonization with commensal bacteria [116]. Other more specific mechanisms activate a first line of defense once the pathogen has been internalized.

2.3.1 Pattern recognition receptors

A vital component of the mammalian innate immune system is the expression of pattern recognition receptors (PRRs) on a variety of cell types, including epithelial cells and cells of the immune system, such as macrophages, dendritic cells, and monocytes. PRRs are capable of recognizing specific sequences of bacterial or viral components, so called pathogen-associated molecular patterns (PAMPs) or damage-associated molecular patterns (DAMPs), e.g. abnormal self-deoxyribonucleic acid (DNA) and (mitochondrial) RNA, lipopolysaccharides (LPS) or high mobility group-box protein (HMGB)-1 which is released during cell death [117, 118]. Ultimately, recognition of PAMPs leads to the expression of IFNs and induction of inflammatory processes to fight off infection [119].

Based on their protein domain homology, PRRs can be classified into one of five classes: Toll-like receptors (TLRs), nucleotide-binding oligomerization domain (NOD)-like receptors (NLRs), C-type lectin receptors (CLRs), retinoic acid-inducible gene (RIG)-I-like receptors (RLRs) and absent in melanoma-2 (AIM2)-like receptors (ALRs). The most relevant for recognition of viral DNA are TLRs, RLRs, and the cGAS-STING signaling pathway, which are presented below.

TLRs recognize pathogens and pathogen-derived ligands through N-terminal conserved short tandem leucine-rich repeat (LRR) motifs or glycan moieties, often before the cell is infected, while their cytosolic C-terminal Toll/IL-1 receptor (TIR) domain is responsible for downstream signaling through interaction with transduction adaptors [120]. To date, ten TLRs have been identified in humans of which the homodimerizing TLR3, -7, -8 and -9 sense nucleic acids and are located in intracellular vesicles such as the endoplasmic reticulum (ER), lysosomal membranes and endosomes [121-123]. The fine-tuning and outcome of TLR downstream signaling is tightly regulated by the nature of the recruited TIR-containing adaptor molecules myeloid differentiation primary response 88 (MyD88), TIR domain containing adaptor protein (TIRAP), translocating chain-associating membrane protein (TRAM) or TIR domain-containing

adaptor protein inducing IFN beta (TRIF) [124]. TLR3 was the first TLR identified to recognize viral double-stranded (ds) RNA, and its activation leads to the recruitment of TRIF and downstream expression of IFNα/β and additional antiviral proteins in a nuclear factor kappa-light-chain-enhancer of activated B cells (NF-κB)- and IRF3- and -7-dependent manner [125, 126].

The family of RLRs consists of the three currently known members, RIG-I and melanoma differentiation-associated gene 5 (MDA5), which both detect short or longer viral dsRNA, respectively [127], and laboratory of genetics and physiology 2 (LPG2). RLRs all contain a central helicase DExD/H box-motif domain and a carboxy-terminal domain through which RNAs are detected, and all but LGP2 contain two N-terminal caspase activation and recruitment domains (CARDs) to mediate downstream signaling [128]. Association of the RLR N-terminal CARD domains with the CARD domain of the mitochondria-localized adapter protein mitochondrial antiviral-signaling protein (MAVS) leads to the aggregation of MAVS CARDs.

In addition to the PRRs described above, many cytosolic sensors have emerged that add to the complexity of nucleic acid sensing, including IFN gamma inducible protein 16 (IFI16) [129], DNA-dependent activator of IFN-regulatory factors (DAI)/Z-DNA binding protein 1 (ZBP1) [130], AIM2 [131] and RNA polymerase III [132].

2.3.2 The cGAS-STING pathway

A key factor in intrinsic innate immune signaling is stimulator of IFN genes (STING; encoded by TMEM173), a dimeric protein of 378 amino acids located in the endoplasmic ER membrane. Canonical activation of STING occurs when the cyclic guanosine monophosphate (GMP)-adenosine monophosphate (AMP) synthase cGAS recognizes and binds dsDNA in the cytosol [133]. Here, the negatively charged backbone of cytosol-localized dsDNA molecules binds to positively charged DNA-binding sites on the C-terminal tail of cGAS, inducing conformational changes and enabling the catalysis of ATP and guanosine triphosphate (GTP) to form the second messenger cyclic GMP-AMP (2’3’-cGAMP) [134-137], which in turn activates STING [138]. In its basal state, the four transmembrane helices of each STING subunit package with the transmembrane helices of the other subunit to form an integrated structure that is linked by a connector loop to the two C-terminal ligand-binding domains of the STING dimer that form the ligand binding pocket [138] (Figure 3). Binding of 2’3’-cGAMP or other dinucleotides confers a 180° rotation of the STING ligand binding pockets in relation to its transmembrane region, allowing the formation of higher-order oligomers and activation of the serine/threonine protein kinase tank-binding kinase 1 (TBK1), which mediates the trans-phosphorylation of neighboring TBK1 dimers and STING itself at Ser366 [139], as shown in Figure 3. Phosphorylation of Ser366 in the pLxIS (p = hydrophilic amino acid, x = any amino acid) motif

of the C-terminal STING tail leads to the recruitment of IRF3, which is subsequently activated by phosphorylation via neighboring TBK1 molecules and translocates to the nucleus, initiating the transcription of downstream genes, such as type I, II, or III IFNs [140].

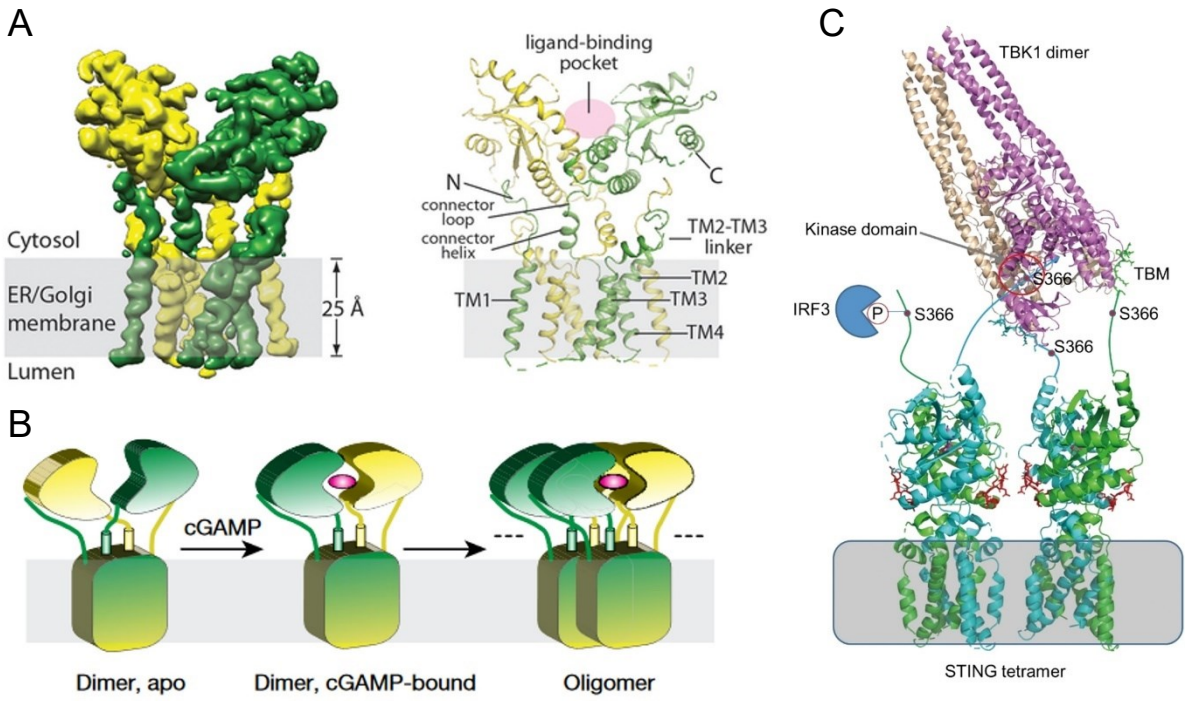

Figure 3: STING structure and activation. A. Two STING subunits (green and yellow) form the STING-dimer in its ligand-free state, anchored to the ER or Golgi membrane via transmembrane (TM) regions. B. Binding of cGAMP to the ligand-binding pocket induces lid-closure and 180° rotation of the ligand binding domains of the STING dimer, followed by oligomerization. C. Model of TBK1 and IRF3 recruitment. TBK1 binds as a dimer to a STING dimer through the TBK1-binding motif (TBM). IRF3 is recruited to phosphorylated S366 at the STING C-terminal tail, where it is phosphorylated by TBK1, dissociates and translocates to the nucleus. Adapted from [141] and [138].

An indispensable part of STING activation is its trafficking from the ER to the ER-Golgi intermediate compartment (ERGIC) and Golgi [142-144], as shown in Figure 4**.** In a process resembling autophagy, STING is translocated via coatomer protein complex II (COP-II) component SEC24C after the interaction of STING with ER-protein stromal interaction molecule 1 (STIM1) is disrupted upon binding of cGAMP [145, 146]. Other factors contributing to STING trafficking are currently investigated and will be required to fully understand its implications [147]. It is not yet clear at which step during trafficking TBK1 and IRF3 are recruited and activated. While some studies place TBK1 interaction with STING already at the ER, even in the absence of cGAMP, others describe both TBK1 and IRF3 recruitment at later stages at the ERGIC and Golgi compartments [140, 148-150]. Indisputable remains that trafficking is an indispensable mechanism for activation of downstream signaling. Following activation and trafficking, STING is targeted for degradation by TBK1-mediated phosphorylation of p62/sequestosome 1 (SQSTM1), which directs STING to autophagosomes and disrupts the STING signaling cascade [151]. Interestingly, a model of steady-state basal

STING signaling has been proposed, in which STING is continuously trafficked between the ER and ERGIC, and inhibition of retrograde transport leads to activation of the STING pathway independent from cGAS [152]. In addition, disruption of post-Golgi trafficking and degradation resulted in tonic IFN signaling [150], the implications of which were described in more detail in Chapter 2.2. Interestingly, the two autoinflammatory, STING-associated diseases STING-associated vasculopathy with onset in infancy (SAVI) and COPA syndrome are based on mutations in STING and COPI, respectively, that cause constant trafficking of STING and activation of downstream IFN signaling [140].

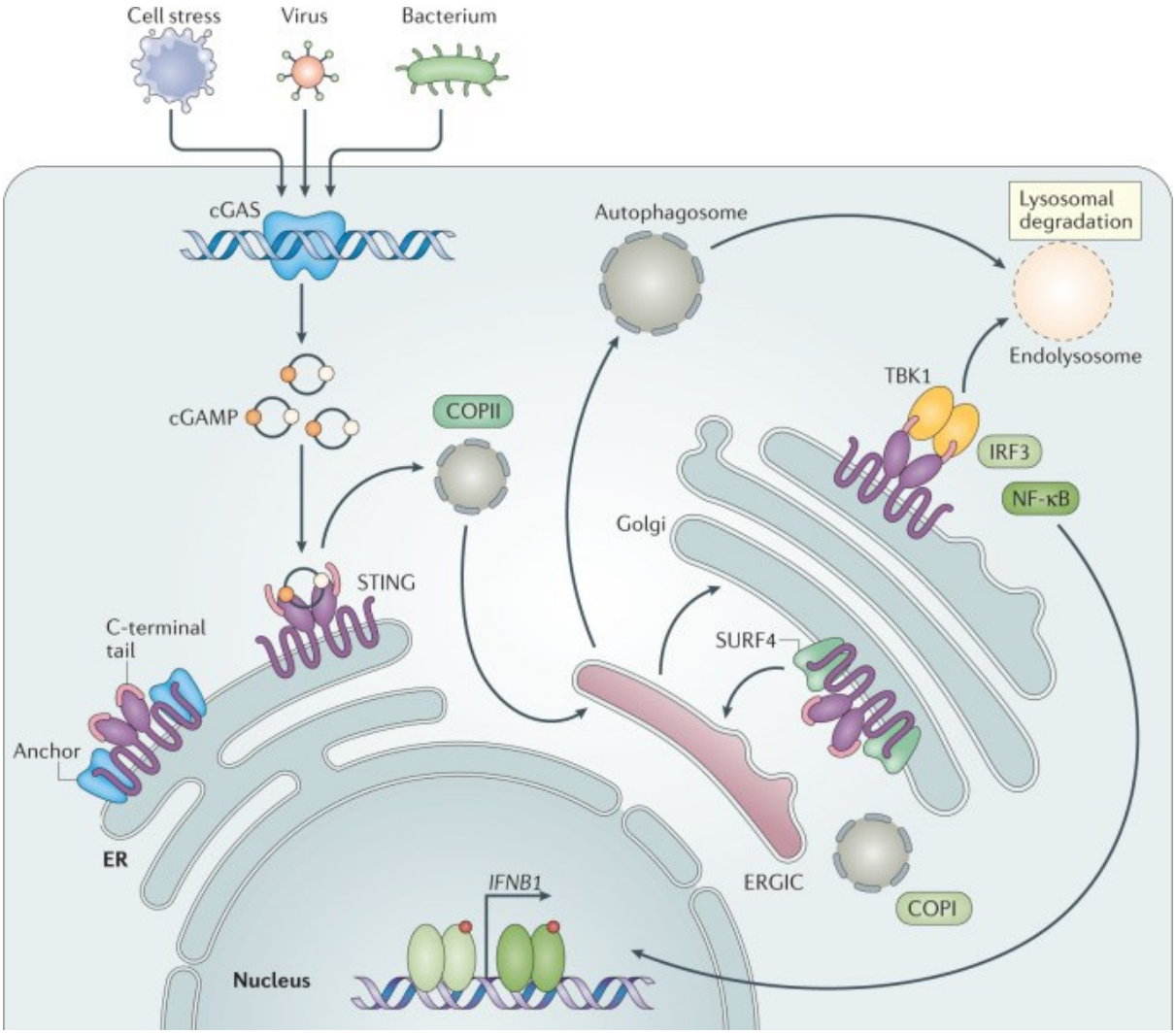

Figure 4: Mechanism of STING signaling and trafficking. Upon binding of nucleic acids to cGAS due to cellular stress, viral or bacterial invasion, cGAMP is generated. cGAMP is an activator of ER-localized STING and induces conformational changes and subsequent activation of STING. STING is transported to the ERGIC and Golgi in a COPII-dependent manner. At the Golgi, TBK1 is recruited to STING, leading to TBK1 phosphorylation, recruitment and subsequent phosphorylation of IRF3. In addition, NF-κB can be activated. Both IRF3 and NF-κB act as transcription factors to induce the transcription of target genes, including IFNs. Activated STING is degraded in the endolysosome. In addition, there is constant trafficking between the Golgi and ERGIC via COPI-dependent transport. Adapted from [140].

In addition to its function in IRF3 activation, STING is also known to induce autophagy through lipidation of microtubule-associated protein 1 A/1B-light chain 3 (LC3), a function that is

independent of TBK1 and IRF3 [153]. Upon activation and transport of STING to the ERGIC, LC3 is lipidated in a WD repeat domain phosphoinositide-interacting protein 2 (WIPI2)- and ATG5-dependent manner, leading to autophagosome formation [146]. Another study reports the presence of LC3-interacting regions through which STING directly recruits LC3 and activates autophagy [153]. Recently, evidence emerged that the evolutionarily older sea anemone homolog of STING, which lacks the C-terminal TBK1-recruiting domain, still induces autophagy upon activation, suggesting that autophagy is the original function of the cGAS-STING pathway [146].

Lastly, STING also promotes NF-κB signaling [142, 154]. The family of NF-κB transcription factors includes the five proteins p50, p52, p65 (or RelA), RelB and c-Rel, which upon activation bind to κB-elements on DNA and allow transcription of downstream genes [155, 156]. In the resting state, NF-κB transcription factors are bound by IκB family members, preventing their nuclear translocation and binding to κB elements. Various triggers can initiate the degradation of IκB proteins by phosphorylating the components of the IκB kinase (IKK) complex, IKKα, IKKβ and NF-κB essential modulator (NEMO, also known as IKKγ). In canonical signaling, IκBα is phosphorylated by IKK, leading to its ubiquitin-mediated degradation and the release of p50/p65 or p50/c-Rel dimers and their translocation to the nucleus [157, 158]. Non-canonical NF-κB signaling is dependent on the precursor protein p100, which is phosphorylated by NF-κB-inducing kinase (NIK) and IKKα, leading to subsequent ubiquitylation and processing of p100 to mature p52, which then complexes with RelB to translocate to the nucleus [159]. Although NF-κB signaling is well understood, the exact mechanisms how STING mediates NF-κB signaling remain unclear. The serine/threonine kinases TBK1 and IKKε have both been implicated in separate models of STING-mediated canonical NF-κB signaling [160, 161], and TBK1 seems to be necessary to induce the nuclear translocation of p52-RelB [162].

The diverse outcome and activation of signaling pathways downstream of STING may be owed to its not less versatile modes of activation and the associated recruitment of different adaptor proteins, recruitment kinetics or conformational states [140, 163, 164]. Besides canonical activation of STING through binding of cyclic dinucleotides (CDNs) like 2'3'-cGAMP, several signals from additional upstream cytosolic sensors converge on the level of STING, as is described for IFI16, DEAD-box helicase (DDX) 41 and DNA-dependent protein kinase (DNA-PK) [129, 165-167]. Furthermore, several PRRs including STING and RIG-I are described to cross-activate downstream signaling pathways, as nicely reviewed by Zevini et al. [168].

2.4 Immune responses to SARS-CoV-2 infection

The novel severe acute respiratory syndrome coronavirus (SARS-CoV)-2 and the associated coronavirus disease 2019 (COVID-19) have been an emerging threat for the past two years,

and although most cases of COVID-19 present with mild symptoms, severe cases are often associated with induction of inflammatory cytokines and low antiviral response [169]. Consequently, elucidating the role of ubiquitylation in immune signaling became paramount in light of the recent SARS-CoV-2 pandemic, as has the identification of critical factors regulating the coordinated response of the infected host.

Like the human coronaviruses SARS-CoV and middle east respiratory syndrome (MERS)-CoV, SARS-CoV-2 consists of an approximately 30 kb positive-sense single-stranded RNA genome, which is enclosed by the nucleocapsid proteins, lipids and the three proteins spike (S), envelope (E), and membrane (M) [170, 171]. SARS-CoV-2 entry is mediated by binding of the receptor binding domain at the C-terminus of spike protein subunit S1 to angiotensin-converting enzyme 2 (ACE2) on the cell surface [172-174], as depicted in Figure 5**.** In addition, several cellular proteases are involved in the cleavage of the S protein, which allows endocytic entry of the virus [172]. Once inside the cell, viral RNA is released and translated into the polyprotein open reading frame (ORF) 1a and ORF1b by components of the host cell replication machinery. These polyproteins are then further processed into non-structural proteins (Nsp1-16) for RNA synthesis, proofreading and capping. In addition, SARS-CoV-2 RNA serves as a template for the generation of genomic and subgenomic RNA through negative-strand transcription, which is enabled by proteins cleaved from the ORF polyproteins inside double-membrane vesicles. S, M, E and N proteins are translated from plus-stranded subgenomic DNA, and are used to encapsulate a newly synthesized genomic (g) RNA, which is then released as a new virion through exocytosis [175-177].

Although SARS-CoV-2 is recognized by several components of the innate immune system, including CLR family members DC-SIGN, L-SIGN, LSECtin, ASGR1, CLEC10A and TTYH2 [178-180], several TLR family members [181-185], and RLR members RIG-I and MDA5 [186, 187], viral clearance is often evaded by interference of SARS-CoV-2-encoded proteins with the type I IFN host response. Mechanisms such as inhibition of RIG-I-MAVS interaction by viral protein 9b, destabilization of TBK1 by viral protein 7a, or modulation of K63-linked ubiquitylation of NEMO that is required for NF-κB activation often render cells unable to defend themselves against the viral threat [186, 188].

Administration of type I and type III IFNs prior to SARS-CoV-2 infection has been proposed as an effective means of boosting the innate immune system and overcoming SARS-CoV-2-mediated inhibition of the IFN signaling pathway [189, 190]. Indeed, pre-treatment of human airway epithelial cells with type I or type III IFNs or their administration even during infection significantly induced transcription of antiviral genes and protected against viral replication, as did administration of IFNβ or IFNλ1 in primary human bronchial epithelial cells [191, 192]. Interestingly, activation of STING by pharmacological agonists could also protect epithelial

cells from SARS-CoV-2 infection [193, 194]. On the other hand, activation of STING has also been implicated in the induction of pro-inflammatory cytokines and could be a driver for severe disease outcome and overproduction of cytokines, e.g. ILs, IFNs and TNFα, with devastating consequences for affected cells and the host organism [195], as seen in severe cases of COVID-19, where respiratory failure and destruction of lung tissue are often accompanied by high levels of IL-6 and TNFα [196, 197]. It is critical to investigate how SARS-CoV-2 is detected inside the cell and how treatment can be offered to limit viral replication without inducing an undesirable immune overreaction.

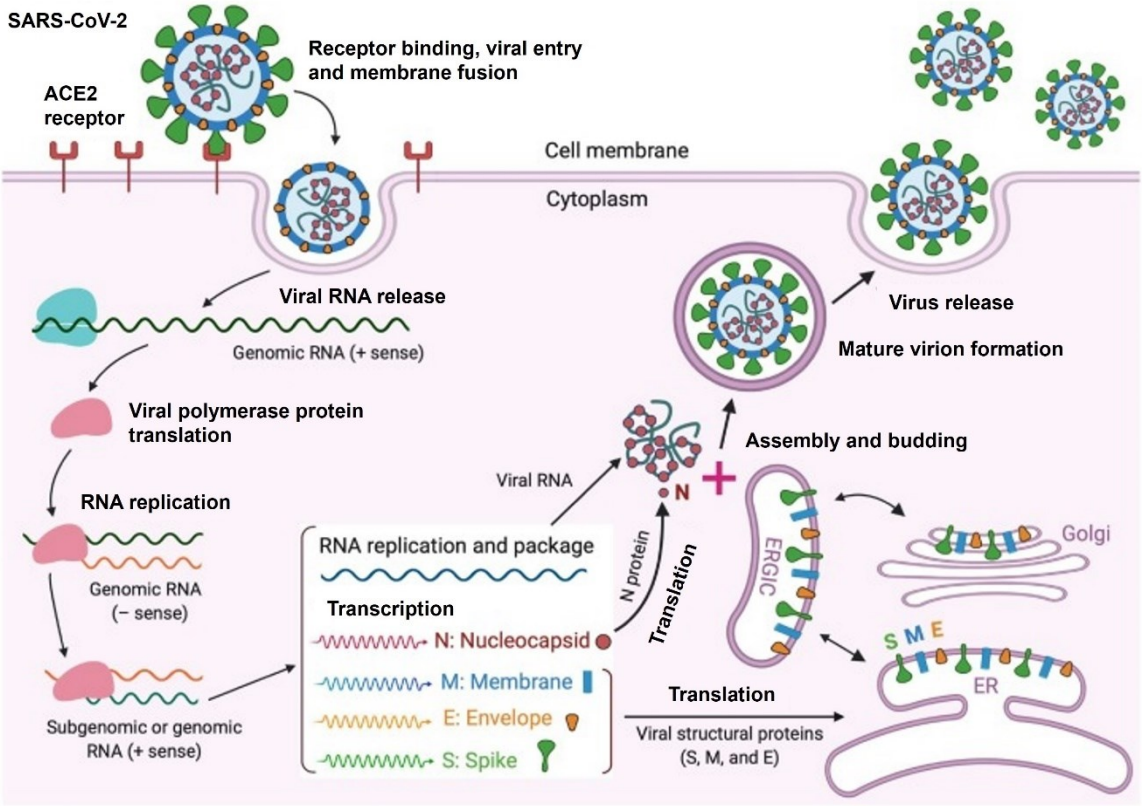

Figure 5: Life cycle of SARS-CoV-2. SARS-CoV-2 enters the cell by binding to the cellular receptor ACE2 via the spike (S) protein, inducing endocytic uptake of the virus. Upon release of viral RNA into the cell, translation of viral proteins from the + sense genomic RNA enables replication and transcription of - sense genomic RNA and + sense subgenomic or genomic RNA. Viral RNA assembles with nucleocapsid protein (N) and is assembled into new virions with viral structural proteins S, membrane (M) and envelope (E). Adapted from [198].

2.5 The role of USP22 in the regulation of STING and response to virus infection

Given the growing knowledge of the significance of ubiquitylation in the context of viral infections and the intricate strategies employed by viruses like SARS-CoV-2 to manipulate or exploit ubiquitylation processes, it is intriguing that STING activity and stability are heavily regulated by post-translational modifications. On the other hand, several studies have linked the deubiquitylase USP22 to the regulation of IFN signaling and viral defense, making it an interesting research target in the context of viral defense.

Several E3 ligases and deubiquitylating proteins have been described to alter STING ubiquitylation. The E3 ligases tripartite motif containing (TRIM) 56 [199], TRIM32 [200], mitochondrial E3 ubiquitin protein ligase 1 (MUL1) [201] and ring finger protein 115 (RNF115) [202] mediate K63-linked polyubiquitylation of STING, whereas K27-linked ubiquitin is added to STING by autocrine motility factor receptor (AMFR) [203], both of which promote its interaction with TBK1. In contrast, K48-linked chains that target STING for proteasomal degradation are conjugated after DNA recognition by RNF5 [204], TRIM30α [205] and TRIM29 [206]. Proteasomal degradation was also mediated by TRIM13-induced K6-linked ubiquitylation [207]. In addition, several E3 ligases are involved in the regulation of STING by competing for lysine sites at their target protein, such as RNF26, which conjugates K11 to STING K150, the target lysine for RNF5 [208, 209]. Several deubiquitylases, in turn, remove ubiquitin from STING, while other proteins act as scaffolds to recruit deubiquitylases. The pseudoprotease inactive rhomboid protein 2 (iRhom2) recruits eukaryotic translation initiation factor 3 subunit 5 (EIF3S5) to STING to remove K48-linked ubiquitin and prevent proteasomal degradation [210]. USP13 removes K27- and K33-linked ubiquitin from STING, thereby reducing TBK1 recruitment [211]. USP35 also deubiquitylates STING, thereby limiting STING activation [212]. CYLD removes K48 from STING in response to viral infection, prolonging its signaling [213]. In a competitive event leading to increased type I IFN production, the E3 ligase RNF26 adds K11-linked polyubiquitin to STING K150, protecting STING from K48-linked ubiquitylation and subsequent degradation mediated by RNF5 [204]. Interestingly, RNF26 also mediates autophagic degradation of IRF3, thereby limiting excessive IFN production [209]. Phosphorylated USP21 removes K27/63-linked polyubiquitin chains on STING after herpes simplex virus 1 (HSV-1) infection [214], Myb like, SWIRM and MPN domains 1 (MYSM1) inhibits STING signaling by removing K63-linked ubiquitin [215], and OTU deubiquitylase 5 (OTUD5) and USP20 remove K48-linked chains from STING to inhibit proteasomal degradation of STING [216-218].

Intriguingly, also USP22 is described as a regulator of STING ubiquitylation. In an extended screen for DUB-mediated regulation upon virus infection, Liu et al. reports the cooperation of USP22 and USP13 to mediate the deubiquitylation of K27-linked STING, presenting USP22 as a negative regulator of IFNβ, NF-κB and ISRE activation upon Sendai virus (SeV) infection [219]. An additional study links USP22 with the regulation of the IFN signaling mediator STAT3 through modulating SIRT1 ubiquitylation [220, 221], and Dietlein et al. reinforce the role of USP22 as a negative regulator of viral and IFN signaling by proposing that increased H2B ubiquitylation after USP22 loss leads to increased innate and adaptive immunity and inflammation [222].

However, USP22 has also been proposed as a positive regulator of IFN signaling. Cai et al. reported increased IRF3 nuclear translocation and antiviral response dependent on USP22-mediated deubiquitylation and subsequent stabilization of importin subunit alpha-1 (karyopherin subunit alpha-2, KPNA2) after infection with SeV or HSV-1 [223]. In another study, USP22 deubiquitylated STAT1, resulting in protection from proteasomal degradation and stabilization of the protein. In accordance, USP22 levels were positively correlated with IFNGR1, IFNGR2, JAK1, JAK2 and STAT1 expression, and USP22 deficiency in mouse and human melanoma cells impaired sensitivity to IFN and induced resistance to T-cell-mediated killing [224].

The discrepancy in reports of USP22-mediated regulation of IFN and antiviral signaling may be explained by the use of different cancer models and the presence or absence of viral stimuli, as USP22 interaction can also be affected by IFN stimulation, as shown by the study by Hong et al. where treatment with IFNα caused dissociation of regulator of calcineurin (RCAN1) from USP22 [59]. Further studies are needed to elucidate the multiple roles of USP22 in viral defense signaling and how it can be exploited against pathogen threats.

2.6 Programmed cell death

The elimination of dysregulated, infected, or otherwise dispensable cells is critical to the survival and development of an organism. To ensure controlled elimination, human cells have implemented a rich selection of pathways that respond flexibly to cell intrinsic or extrinsic stimuli to eliminate the threat of an infected or otherwise dangerous cell, killing some cells to ensure the survival of the whole organism. Programmed cell death was first discovered in silkworms, where specific cells died during metamorphosis, indicating that some form of regulation is already implemented in the organism [225, 226]. To date, about 15 different modes of cell death have been discovered, classified according to their respective indispensable molecular aspects, although emerging evidence suggests some interconnectivity between the pathways [227, 228].

Necroptosis is a highly inflammatory form of programmed cell death mediated by the key proteins receptor interacting protein kinase (RIPK) 1, RIPK3 and mixed-lineage kinase-like (MLKL) that can be induced primarily when key players of the apoptotic signaling pathway are compromised. Morphologically, necroptosis is characterized by cell swelling, cytoplasmic granulation, and disruption of the plasma membrane, combining features of both apoptotic cell death and the uncontrolled form of cell death, necrosis [229-231]. Several necroptotic stimuli can induce the activation of RIPK1, RIPK3 and MLKL for necroptosis execution. Among them is the engagement of cell surface receptors using members of the TNF superfamily, such as TNFα, TNF-related apoptosis-inducing ligand (TRAIL) or Fas ligand (FASL), IFNs, or the engagement of nucleic acid sensors such as ZBP1, cGAS and TLRs [232-237]. While the

mechanisms of necroptosis induction via IFNs or nucleic acid sensors are less clear, induction of cell death pathways using TNFα is well studied.

TNFα is expressed downstream of several signaling cascades that sense DAMPs and PAMPs in response to tissue injury or infection and is a major contributor to maintaining or restoring tissue homeostasis [238]. Although commonly employed as an inducer of regulated cell death, it is also a major mediator of inflammatory responses or pro-survival signaling by inducing NF-κB- and MAPK-dependent gene transcription through the assembly of the TNF receptor (TNFR) complex [239]. Upon binding of TNFα, a pro-survival signaling complex comprising TNFR1, TNF receptor type 1-associated death domain protein (TRADD), RIPK1, TNFR-associated factor 2 (TRAF2), and cellular inhibitor of apoptosis protein (cIAP) 1/2 (complex I) forms, enabling the ubiquitylation of RIPK1 through the E3 ubiquitin ligases cIAP1 and cIAP2. This in turn facilitates the recruitment of heme-oxidized iron regulatory protein (IRP) 2 ubiquitin ligase 1 (HOIL-1), HOIL-1 interacting protein (HOIP) and shank-associated RH domain-interacting protein (SHARPIN), also called the LUBAC complex, and the subsequent addition of M1-linked polyubiquitin chains to TRADD, TNFR1 and RIPK1 [240, 241]. In turn, the transforming growth factor-β (TGF-β)-activated kinase 1 (TAK1)/TAK1 binding protein (TAB) 1/TAB2/3 kinase complex and IKKα/IKKβ/IKKγ (IKK complex) are recruited. TAK1 phosphorylates IKKβ, leading to phosphorylation, ubiquitylation, and subsequent degradation of IκB, which enables the release of NF-κB subunits, translocation to the nucleus, and transcription of target genes [242].

Inhibition of complex I, for example by deubiquitylation of RIPK1 by the deubiquitylating proteins CYLD and A20, leads to the formation of the cell death-inducing complex II and, in most cases, to the abrogation of pro-survival signaling [243, 244]. In the case of necroptosis, TNFα stimulation induces the formation of a signaling complex containing RIPK1 and RIPK3. The additional depletion of caspases, e.g. by N-benzyloxycarbonyl-Val-Ala-Asp(O-Me)fluoromethylketone (zVAD.fmk), prevents the caspase-mediated degradation of RIPK1 and RIPK3, followed by RIPK1 and RIPK3 auto- and transphosphorylation and oligomerization with MLKL in the necrosome [245-248]. Subsequent translocation of MLKL into the cell membrane leads to pore formation and leakage of inflammatory signals into the outer membrane space, ultimately resulting in necroptotic cell death [249].

In addition to stimulating necroptosis using the well-studied approach with members of the TNF superfamily, alternative necroptosis-inducing pathways are possible. In contrast to the high doses of type I and II IFNs needed for the induction of the apoptotic cell death [250, 251], Thapa et al. demonstrated in murine embryonic fibroblasts that administration of low doses of type I and type II IFNs could induce necroptosis under Fas-associated death domain protein (FADD)- or caspase deficiency in a transcription- and protein kinase R (PKR)-dependent

mechanism [234]. Necroptosis was also induced using IFNγ in lung epithelial cells [252] and in RIPK1-, FADD-, or caspase-8 deficient cells, and was dependent on IFN-induced ZBP1 interaction with RIPK3 [253]. Recent evidence shows that the combination of IFNs with cell cycle inhibitors induces necroptosis via ZBP1 expression [254]. Notably, IFNs are also able to increase MLKL expression in cancer cells [255]. Interestingly, IFNγ also activates IKKβ-dependent NF-κB signaling, which can counteract the pro-necroptotic effects of IFN [256].

Similar to the induction of necroptosis by direct administration of IFNs, activation of STING can be used to achieve a necroptotic outcome through transcription of IFN genes via the STING-TBK1-IRF3 axis. Two independent studies have shown that engagement of STING can robustly induce necroptosis through both the activation of JAK/STAT signaling and the upregulation of TNFα [257, 258]. Further studies support an additional function of STING as an amplifier of inflammatory signaling during ZBP1-MLKL-mediated necroptosis after tumor cell irradiation by creating a positive feedback loop between both pathways [259].

3 Aim of the study

The deubiquitylation of specific substrates is a critical factor in maintaining ubiquitin homeostasis, governing receptor activation, internalization, proteasomal degradation, and transcriptional processes.

As part of the SAGA complex, the ubiquitin-specific protease USP22 regulates gene transcription through deubiquitylation of H2A and H2B, but several other non-histone targets have been described. Previous studies in our group have shown that USP22 affects necroptosis outcome by affecting RIPK3 ubiquitylation, but without altering gene expression of the key necroptosis players RIPK1, RIPK3 or MLKL, suggesting a selectivity of USP22-dependent gene regulation. Therefore, we started this study with a genome-wide screen of a USP22 KO model of human intestinal epithelial cells (hIECs) in order to identify pathways specifically regulated by USP22. Based on our findings, we focused our studies on the regulation of USP22 in IFN signalling and nucleic acid sensing pathways. Translating our findings to the current pandemic, we further aimed to investigate how USP22 affects infection of hIECs with the novel coronavirus SARS-CoV-2.

The second part of this study builds on the findings of the first part of this study that USP22 is an important regulator of IFN and STING signalling. In the ongoing race between tumor immune evasion and resistance to chemotherapeutic elimination of cancer, administration of IFNs to induce apoptotic cell death is a promising therapeutic approach [260-262]. However, the mechanisms by which IFNs induce necroptotic cell death remain to be elucidated. Based on the results of previous research in our group that USP22 regulates necroptotic signaling by affecting RIPK3 ubiquitylation, we aimed to understand the signaling pathway of IFN- and STING-induced necroptosis in HT-29 cells and the role of USP22 in its regulation.

4 Materials and Methods

4.1 Materials

4.1.1 Human cell lines

All cell lines were authenticated by short tandem repeat (STR) profiling/DNA fingerprinting at Leibniz Institute, German Collection of Microorganisms and Cell Cultures (DSMZ, *Deutsche Sammlung von Mikroorganismen und Zellkulturen*) and regularly tested for mycoplasma contamination by PCR.

Table 1: Human cell lines

Cell line	Origin	Source
HT-29	Human colon carcinoma	DSMZ
HT-29 non-human target (NHT)	Human colon carcinoma	Roedig et al. [72]
HT-29 USP22 KO clones #8, #16, #62	Human colon carcinoma	Roedig et al. [72]
HT-29 NHT-STING KO	Human colon carcinoma	This study
HT-29 USP22 KO #62-STING KO	Human colon carcinoma	This study
HeLa	Human cervix carcinoma	DSMZ
HeLa NHT	Human cervix carcinoma	Roedig et al. [72]
HeLa USP22 KO	Human cervix carcinoma	Roedig et al. [72]
Caco-2	Human colorectal adenocarcinoma	Jindrich Cinatl Jr.
Caco-2 NHT	Human colorectal adenocarcinoma	This study
Caco-2 USP22 KO #1, #6	Human colorectal adenocarcinoma	This study
Caco-2 NHT-STING KO	Human colorectal adenocarcinoma	This study
Caco-2 USP22 KO #1, #6 – STING KO	Human colorectal adenocarcinoma	This study
HEK293T	Human embryonic kidney	ATCC
HEK-Blue IFNα/β reporter cells	Human embryonic kidney	Invivogen
HEK-Blue IFNλ reporter cells	Human embryonic kidney	Invivogen
HCoEpiC	Human colonic epithelial cells	Jindrich Cinatl Jr.

4.1.2 Materials used in cell culture

4.1.2.1 Cell culture media

Table 2: Cell culture media

Medium	Company
Dulbecco's Modified Eagle Medium (DMEM) GlutaMAX™	Thermo Fisher Scientific
Epithelial Cell Medium (EpiCM)	ScienCell Research Laboratories
McCoy's 5A (Modified) Medium GlutaMAX™-I	Thermo Fisher Scientific
Minimum Essential Medium Eagle (MEM)	Merck Sigma

4.1.2.2 Medium supplements and additional cell culture reagents

Table 3: Medium supplements and cell culture reagents

Reagent	Company
Blasticidin	Invivogen
Dimethyl sulfoxide (DMSO)	Sigma
Dulbecco's phosphate buffered saline (DPBS)	Thermo Fisher Scientific
Epithelial Cell Growth Supplement	ScienCell Research Laboratories
Fetal calf serum (FCS)	Thermo Fisher Scientific
L-glutamine	Thermo Fisher Scientific
Normocin	Invivogen
Penicillin/streptomycin (10000 U/ml)	Thermo Fisher Scientific
Puromycin	Clontech Laboratories
Trypsin/Ethylenediaminetetraacetic acid (EDTA) solution (0.05%), phenol red	Thermo Fisher Scientific
Zeocin	Invivogen

4.1.2.3 Chemicals, compounds and inhibitors used as treatment in cell culture

Table 4: Chemicals, compounds and inhibitors for treatment

Reagent	Function	Company
2'3'-cGAMP	STING agonist	Invivogen
BV6	Smac mimetic	Genentech
Carbonyl cyanide-4-(trifluoromethoxy)phenylhydrazone (FCCP)	Uncoupler of mitochondrial oxidative phosphorylation	Merck Sigma
Cycloheximide (CHX)	Protein synthesis inhibitor	Sigma
Di-amidobenzimidazoles (diABZI)	STING agonist	Invivogen
Enbrel	TNF inhibitor	Pfizer
Etoposide	Inducer of DNA double-strand breaks	TEVA
GSK'872	RIPK3 inhibitor	Merck
Interferon-stimulating DNA (ISD)	PRR agonist	Invivogen
Interferon α (IFNα)	Cytokine	Merck Sigma
Interferon β (IFNβ)	Cytokine	Merck Sigma
Interferon γ (IFNγ)	Cytokine	Merck
Interferon λ1 (IFNλ1)	Cytokine	Peprotech
Interferon λ2 (IFNλ2)	Cytokine	Peprotech
Interferon λ3 (IFNλ3)	Cytokine	Biomol
N-benzyloxycarbonyl-Val-Ala-Asp(O-Me)fluoromethylketone (zVAD.fmk)	Caspase inhibitor	Bachem
Nec-1s	RIPK1 inhibitor	Merck
Poly(I:C)	PRR agonist	Invivogen
Ruxolitinib	JAK/STAT inhibitor	Selleckchem
Tumor necrosis factor α (TNFα)	Cytokine	Biochrom
α-IFNAR2 clone MMHAR-2	IFNAR2 blocking antibody	PBL Assay Science

4.1.2.4 Fluorescent dyes used in cell culture

Table 5: Fluorescent dyes used in cell culture

Reagent	Company
Hoechst 33342	Thermo Fisher Scientific
Propidium iodide (PI)	Thermo Fisher Scientific
Tetramethylrhodamine methylester (TMRM)	Thermo Fisher Scientific

4.1.2.5 Reagents and buffers used for drug delivery, transduction and transfection

Table 6: Reagents and buffers used for drug delivery, transduction and transfection

Reagent	Company
Digitonin Permeabilization Buffer (DPB)	50 mM HEPES, 100 mM potassium chloride (KCl), 3 mM magnesium chloride ($MgCl_2$), 85 mM sucrose, 0.2% bovine serum albumin (BSA), 1 mM ATP, 5 µg/ml digitonin, 0.1 mM Dithiothreitol (DTT); pH 7
FuGENE HD Transfection Reagent	Promega
Lipofectamine 2000	Thermo Fisher Scientific
Lipofectamine RNAiMAX	Thermo Fisher Scientific
LyoVec Transfection Reagent	Invivogen
OptiMEM	Thermo Fisher Scientific
Polybrene	Merck Sigma
Resuspension buffer R	Thermo Fisher Scientific

4.1.2.6 Small-interfering RNA (siRNA) constructs used for gene knockdown

Table 7: siRNA constructs for gene knockdown

Target gene/construct number	Identifier
IRF1 #1	s7501
IRF1 #2	s7502
IRF1 #3	s7503
Non-silencing control (siCtrl)	4390843
TFAM #1	279141
TFAM #2	279142

Target gene/construct number	Identifier
TFAM #3	279143
TRIM29 #1	133796
TRIM29 #2	133797
TRIM29 #3	133798
USP22 #1	s23566
USP22 #2	s23568

All siRNA constructs were ordered from Thermo Fisher Scientific.

4.1.2.7 Plasmids and guide RNA sequences used for CRISPR/Cas9-mediated gene knockout

Table 8: Plasmids and guide RNA sequences used for CRISPR/Cas9-mediated gene knockout

Target gene/Plasmid	Guide RNA sequence (5' → 3')	Source
Plasmid plentiCRISPR v2	N/A	Sanjana et al.; [263] Addgene plasmid #52961
Plasmid pMD2.G	N/A	Gift from Didier Trono; Addgene plasmid #12259
Plasmid psPAX2	N/A	Gift from Didier Trono; Addgene plasmid #12260
USP22	#1: GCCATTGATCTGATGTACGG	
	#2: CCTCGAACTGCACCATAGGT	
	#3: ACCTGGTGTGGACCCACGCG	
TMEM173	#1: CATTACAACAACCTGCTACG	
	#2: GCTGGGACTGCTGTTAAACG	
	#3: GCAGGCACTCAGCAGAACCA	
DDX58	#1: CATCTTAAAAAATTCCCACA	
	#2: GGAACAAGTTCAGTGAACTG	
	#3: TGCATGCTCACTGATAATGA	
IFIH1	#1: CTTGGACATAACAGCAACAT	
	#2: TGAGTTCCAAAATCTGACAT	

Target gene/Plasmid	Guide RNA sequence (5' → 3')	Source	
TLR3	#1: ACGACTGATGCTCCGAAGGG		
	#2: ACTTACCTTCTGCTTGACAA		
	#3: GGAAATAAATGGGACCACCA		
Control NHT	#1: N/A	Addgene #51763	plasmid
	#2: N/A	Addgene #51762	plasmid
	#3: N/A	Addgene #51760	plasmid

Oligonucleotides were designed individually, if not stated otherwise, and purchased from Eurofins.

4.1.3 Materials used in the assessment of gene expression

4.1.3.1 Reagents and commercial kits used for RNA isolation, cDNA synthesis and qRT-PCR

Table 9: Reagents and commercial kits used for RNA isolation, cDNA synthesis and qRT-PCR

Reagent	Company
peqGold DNase I Digest Kit	VWR Life Science
peqGOLD total RNA isolation kit	VWR Life Science
RevertAid H Minus First Strand Kit	Thermo Fisher Scientific
SYBR-Green PCR Master Mix	Thermo Fisher Scientific

4.1.3.2 Oligonucleotides used in qRT-PCR

Table 10: List of oligonucleotides used in qRT-PCR

Target gene	Forward primer	Reverse primer
AK4	CACTGGTGAACCGTTAGTCCA	AGCACTCCTCGGCTCTTGT
BST2	CCACCTGCAACCACACTG	CCTGAAGCTTATGGTTTAATGTAGTG
COV1	GCCTCTTCTGTTCCTCATCAC	AGACAGCATCACCGCCATTG
CXCR4	GGCCCTCAAGACCACAGTCA	TTAGCTGGAGTGAAAACTTGAAG
DDX58	TGTGGGCAATGTCATCAAAA	GAAGCACTTGCTACCTCTTGC
DDX60	AATCCCACAGGACTGCACA	TCGACCAAATACCTTCTGCAA

Target gene	Forward primer	Reverse primer
IFI27	GTGGCCAAAGTGGTCAGG	CCAATCACAACTGTAGCAATCC
IFI6	AACCGTTTACTCGCTGCTGT	GGGCTCCGTCACTAGACCT
IFIH1	TTTTGCAGATTCTTCTGTAGTTTCA	TGCTGTTATGTCCAAGACTTTCA
IFIT1	CTTGTGGGTAATACAGTGGAGATG	GCTCCAGACTATCCTTGACCTG
IFNA5	CAAGGTTCAGGGTCACTCAAT	CACCAGGGCCATCAGTAAAAC
IFNA6	ATCTGTTGCTTGGGATGAGAGG	AGGCACAAGGGCTGTACTTTT
IFNA7	CCCACCTCAGGTAGCCTAGTGAT	TCACAGCCCAGAGAGCAGAT
IFNA8	CTGTTCAGCTGTATGGGCAC	GCACAATCAGGGTTGGAGTTC
IFNB1	ATGACCAACAAGTGTCTCCTCC	GGAATCCAAGCAAGTTGTAGCTC
IFNL1	GGACGCCTTGGAAGAGTCAC	AGCTGGGAGAGGATGTGGT
IFNλ1	TCAAAGACTCTCACCCCTGC	CAGTGTAAAGGTGCACATGACG
IFNλ10	CACGACGCGTTGAATCAAAAT	ACATTAACCACAATGTAAAGCGAC
IFNλ14	CATCTTCGGGATTCCCAATGGC	TTACAGCCCAGAGAGCAGCTT
IFNλ16	GGATTCATCTGCTGCTTGGGATG	GAGTCCTCATTCATCAGGGCAA
IFNλ17	TGCTGGTGCTCAGCTACAAA	TCCTCCTGGGGAAGTCCAAA
IFNλ2	TTTCAACCAGTCTAGCAGCATCT	TCAAGGTCCTCCTGCTACCC
IFNλ21	TCCACACTTCTATGACTTCTGCC	TGCCTGCACAGGTAAACATGA
IFNλ4	AGAGGCCGAAGTTCAAGGTTA	ACTGGTGGCCATCAAACTCC
IRF9	AGCCTGGACAGCAACTCAG	GAAACTGCCCACTCTCCACT
ISG15	GAGGCAGCGAACTCATCTTT	AGCATCTTCACCGTCAGGTC
OAS2	TGCAGGGAGTGGCCATAG	TCTGATCCTGGAATTGTTTTAAGTC
OAS3	TCCCATCAAAGTGATCAAGGT	ACGAGGTCGGCATCTGAG
panIFNA	TCCATGAGVTGATBCAGCAGA	ATTTCTGCTCTGACAACCTCCC
PARP9	CTGTCTGCACCGAGGAGAG	GCGCTTCAAAGCATAGACTGT
SLFN5	AGCAAGCCTGTGTGCATTC	ACCACTCTGTCTGAAAATACTGGA
TBP	CCACTCACAGACTCTCACAAC	CCACTCACAGACTCTCACAAC

Target gene	Forward primer	Reverse primer
TGFB1	ACTACTACGCCAAGGAGGTCAC	TGCTTGAACTTGTCATAGATTTCG
TGM2	GGCACCAAGTACCTGCTCA	AGAGGATGCAAAGAGGAACG
TMEM173	ACATTCGCTTCCTGGATAAACT	CTGCTGTCATCTGCAGGTTC
TNFα	TGTAGCCCATGTTGTAGCAAAC	ATGAGGTACAGGCCCTCTGAT
USP18	TCCCGACGTGGAACTCAG	CAGGCACGATGGAATCTCTC
USP22	GAAGATCACCACGTATGTGTCC	CATTCATCCTGCTCTCTTTGC

All primers for qRT-PCR were ordered from Eurofins.

4.1.3.3 Kits and arrays used for gene expression profiling

Table 11: Kits and arrays used for gene expression profiling

Reagent	Company
Clariom™ S array, human	Thermo Fisher Scientific
GeneChip™ WT PLUS Reagent Kit	Thermo Fisher Scientific

4.1.4 Materials used for cytokine analysis

4.1.4.1 Reagents and commercial kits used for cytokine analysis

Table 12: Reagents and commercial kits used for cytokine analysis

Reagent/kit	Company
LEGENDplex™ Human Anti-Virus Response Panel multiplex assay	BioLegend
Quanti-Blue Solution	Invivogen
3,3',5,5'-Tetramethylbenzidine (TMB) substrate	Thermo Fisher Scientific
VeriKine-HS™ Human IFN Beta Serum ELISA Kit	PBL Assay Science

4.1.5 Materials used for protein analysis

4.1.5.1 Reagents and commercial kits used for Western blotting

Table 13: Reagents and commercial kits used for Western blotting

Reagent/kit	Company
Albumin Fraction V (BSA)	Carl Roth
Amersham Hyperfilm™ (High performance chemiluminescence film)	GE Healthcare
AmershamTM Protran 0.2 nitrocellulose Western blotting membrane	GE Healthcare
Ammonium persulfate (APS)	Carl Roth
Bromophenol blue	Amersham
cOmplete™ Protease Inhibitor Cocktail (PIC)	Merck Sigma
Glutathione agarose beads	GE Healthcare
Milk powder	Carl Roth
PageRuler™ Plus Prestained Protein Ladder	Thermo Fisher Scientific
Pierce™ BCA protein assay kit	Thermo Fisher Scientific
Pierce™ ECL Western Blot Substrate	Thermo Fisher Scientific
Pierce™ Universal Nuclease	Thermo Fisher Scientific
Ponceau S	Merck Sigma
ProClin™	Sigma
Rotiphorese® Gel 30, Acrylamide	Carl Roth
Starter for x-ray developer	TETENAL
Superfix MRP x-ray fixing solution	TETENAL
Tetramethyletylenediamine (TEMED)	Carl Roth
Whatman paper	Carl Roth

4.1.5.2 Buffers used for Western blotting

Table 14: Buffers used for Western blotting

Buffer	Composition
RIPA lysis buffer	50 mM Tris hydrochloric acid (HCl) pH, 8.0 1% Nonident-40 (NP-40) 0.5% sodium deoxycholate 150 mM sodium chloride (NaCl) 2 mM $MgCl_2$ 1% Sodium dodecyl sulfate (SDS) Protease Inhibitor Cocktail (PIC) 1 mM sodium orthovanadate 1 mM β-glycerophosphate 5 mM Sodium fluoride 250 U/ml Pierce Universal Nuclease
1% NP-40 lysis buffer for tandem ubiquitin binding entities (TUBE)	50 mM NaCl 20 mM Tris pH 7.5 1% NP-40 5 mM EDTA 10% Glycerol 1 mM sodium orthovanadate 1 mM sodium fluoride 0.5 mM phenylmethylsulfonyl fluoride PIC Pierce Universal Nuclease
Loading buffer (6x)	350 mM Tris Base, pH 6.8 3.8% Glycerol 10% SDS 0.12 mg/ml bromophenol blue
SDS-PAGE running buffer (5x)	15.1 g/l Tris Base 94 g/l glycine 0.5% SDS
Blotting buffer	5.8 g/l Tris Base 2.9 g/l Glycine 0.04% SDS 20% Methanol
Blocking buffer	5% milk powder in PBS-Tween (0.1% Tween)
Phosphate-buffered saline (PBS, 10x, pH 7.4)	80 g/l NaCl 2 g/l KCl 2 g/l Potassium dihydrogen phosphate (KH_2PO_4) 14.4 g/l Disodium hydrogen phosphate (Na_2HPO_4)
PBS-0.1% Tween-20 (PBS-T)	0.1% Tween-20 in PBS
5%/10%/12%/13.5% polyacrylamide gel	5%/10%/12%/13.5% polyacrylamide, 125 mM Tris/HCl pH 6.8, 0.1% SDS, 0.1% APS, 0.1% TEMED
BSA dilution buffer for primary antibodies	2% BSA, 0.1% ProClin™ in PBS

4.1.5.3 Primary antibodies used for Western blotting

Table 15: Primary antibodies used for Western blotting

Target protein	Dilution	Species	Company	Antibody identifier
GAPDH	1:5000	mouse	Hytest	Cat# 5G4cc-6C5cc, RRID:AB_2858176
Histone H2B	1:500	rabbit	Merck Millipore	Cat# 07-371, RRID:AB_310561
IFNGR1	1:100	mouse	Santa Cruz Biotechnology	Cat# sc-12755, AB_673493
IRF1	2:200	Mouse	Santa Cruz Biotechnology	Cat# sc-130761, AB_2126721
IRF-3	1:300	mouse	Santa Cruz Biotechnology	Cat# sc-33641, RRID:AB_627826
IRF-9	1:1000	rabbit	Cell Signaling	Cat# 76684, RRID:AB_2799885
ISG20	1:500	rabbit	Thermo Fisher Scientific	Cat# PA5-30073, RRID:AB_2547547
ISG56	1:5000	mouse	Thermo Fisher Scientific	Cat# PA3-848, RRID:AB_1958733
MDA5	1:1000	rabbit	Cell Signaling	Cat# 5321, RRID:AB_10694490
MLKL	1:1000	rabbit	Cell Signaling	Cat# 14993, RRID:AB 2721822
MX1	1:1000	rabbit	Cell Signaling	Cat# 37849, RRID:AB_2799122
NF-κB p52	1:500	mouse	Merck Millipore	Cat# 05-361, RRID:AB_309692)
NF-κB p65	1:200	rabbit	Santa Cruz Biotechnology	Cat# sc-372, RRID:AB_632037
Phospho-IRF3 (Ser396)	1:1000	rabbit	Cell Signaling	Cat# 4947, RRID:AB_823547
Phospho-MLKL	1:1000	rabbit	Cell Signaling	Cat# 91689 RRID:AB 2732034
Phospho-NF-κB p65 (Ser536)	1:1000	rabbit	Cell Signaling	Cat# 3033, RRID:AB_331284
Phospho-RIPK1	1:1000	rabbit	Cell Signaling	Cat# 65746, RRID:AB 2799693
Phospho-STAT1 (Tyr701)	1:1000	rabbit	Cell Signaling	Cat# 9167, RRID:AB_561284
Phospho-STAT2 (Tyr689)	1:500	rabbit	Merck Millipore	Cat# 07-224, AB_2198439
Phospho-STAT3 (Tyr705)	1:2000	rabbit	Cell Signaling	Cat# 9145, AB_2491009
Phospho-TBK1 (S172)	1:1000	rabbit	Abcam	Cat# ab109272, RRID:AB_10862438
Phospho-TYK2 (Tyr1054/1055)	1:1000	rabbit	Cell Signaling	Cat# 9321, AB_2303972

Target protein	Dilution	Species	Company	Antibody identifier
Phospho-γH2AX (Ser139)	1:1000	rabbit	Novus	Cat# NB 100-384, RRID:AB_350295
RIG-I	1:1000	rabbit	Cell Signaling	Cat# 3743, RRID:AB_2269233
RIPK1	1:1000	Mouse	BD Bioscience	Cat# 610458, RRID:AB_397831
RIPK3	1:1000	Rabbit	Cell Signaling	Cat# 13526, RRID:AB_2687467
STAT1	1:1000	mouse	Cell Signaling	Cat# 9176, RRID:AB_2240087
STING	1:1000	rabbit	Cell Signaling	Cat# 13647, RRID:AB_2732796
TBK1	1:1000	rabbit	Abcam	Cat# ab40676, RRID:AB_776632
TLR3	1:1000	rabbit	Cell Signaling	Cat# 6961, RRID:AB_10829166
TYK2	1:1000	rabbit	Cell Signaling	Cat# 9312, AB_2256719
Ubiquityl-Histone H2B, clone 56	1:500	mouse	Merck Millipore	Cat# 05-1312, RRID:AB_1587119
USP22	1:2000	rabbit	Abcam	Cat# ab195289, RRID:AB_2801585
Vinculin	1:5000	mouse	Sigma	Cat# V9131, RRID:AB_477629

All primary antibodies were diluted in BSA dilution buffer.

4.1.5.4 Secondary antibodies used for Western blotting

Table 16: Secondary antibodies used for Western blotting

Target protein	Dilution	Company	Antibody identifier
Goat Anti-Mouse IgG, HRP Conjugated	1:10000	Abcam	Cat# ab6789, RRID:AB_955439
Goat Anti-Rabbit IgG, HRP Conjugated	1:30000	Abcam	Cat# ab6721, RRID:AB_955447

All secondary antibodies were diluted in 5% milk powder in PBS-T.

4.1.6 Materials used for SARS-CoV-2-related assays

All SARS-CoV-2-related assays were performed by Megan Stanifer at the facilities of the DKFZ in Heidelberg.

4.1.6.1 Cells used for SARS-CoV-2 propagation

Table 17: Cells used for SARS-CoV-2 propagation

Cell line	Origin	Source
Vero E6	African green monkey kidney cells	ATCC

4.1.6.2 SARS-CoV-2 strains

Table 18: SARS-CoV-2 strains

SARS-CoV-2 strain	Source
BavPat1/2020	European Virology Archive

4.1.6.3 Reagents and kits used for analysis of SARS-CoV-2 infections

Table 19: Reagents and kits used for analysis of SARS-CoV-2 infections

Reagent/kit	Company
iSCRIPT reverse transcriptase	BioRad
iTaq SYBR green	BioRad
LI-COR blocking buffer	Li-COR
Paraformaldehyde (PFA)	Sigma
Qiagen RNAeasy Plus Extraction Kit	Qiagen
Triton-X-100	Carl Roth

4.1.6.4 Antibodies and fluorescent dyes used for analysis of SARS-CoV-2-infected cells

Table 20: Antibodies and fluorescent dyes used for analysis of SARS-CoV-2-infected cells

Antibody/fluorescent dye	Company
Alexa Fluor 568	Thermo Fisher Scientific
anti-dsRNA clone J2	Nordic MUbio
anti-mouse CW800	Abcam
anti-SARS-CoV nucleoprotein (NP)	Sino biologicals MM05

Antibody/fluorescent dye	Company
DAPI	Thermo Fisher Scientific
DRAQ5™	Abcam

4.1.6.5 qRT-PCR oligonucleotides used for analysis of SARS-CoV-2-infected cells

Table 21: qRT-PCR oligonucleotides used for analysis of SARS-CoV-2-infected cells

Target protein	Forward primer	Reverse primer
COV1	GCCTCTTCTGTTCCTCATCAC	AGACAGCATCACCGCCATTG
TBP	CCACTCACAGACTCTCACAAC	CCACTCACAGACTCTCACAAC

4.1.7 Chemicals

Table 22: List of chemicals

Chemical	Company
2-propanol	Carl Roth
Adenosine triphosphate (ATP)	Sigma
Digitonin	Sigma
Na_2HPO_4	Merck
DTT	Millipore
Ethanol	Carl Roth
EDTA	Carl Roth
Glycerol	Merck
Glycine	Carl Roth
HEPES	Carl Roth
$MgCl_2$	Merck
Methanol	Carl Roth
NP-40	Carl Roth
Phenylmethylsulfonyl fluoride (PMSF)	Carl Roth
KCl	Carl Roth
KH_2PO_4	Carl Roth
NaCl	Carl Roth
Sodium deoxycholate	Merck

Chemical	Company
SDS	Carl Roth
Sodium fluoride	Carl Roth
Sodium orthovanadate	Sigma
Sucrose	Carl Roth
Tris Base	Carl Roth
Tris HCl	Carl Roth
Tween-20	Carl Roth
β-glycerophosphate	Sigma

4.1.8 Plastic ware and consumables

Table 23: List of plastic ware and consumables

Plastic ware/consumable	Company
8-well Glass Bottom slide	ibidi
Cell culture dishes 100 mm	Greiner Bio-One
Cell culture dishes 150 mm	Greiner Bio-One
Cell culture dishes 60 mm	Greiner Bio-One
Cell scraper	BD Biosciences
CELLSTAR® 12-well tissue culture plates	Greiner Bio-One
CELLSTAR® 24-well tissue culture plates	Greiner Bio-One
CELLSTAR® 6-well tissue culture plates	Greiner Bio-One
CELLSTAR® 96-well tissue culture plates	Greiner Bio-One
CELLSTAR® cell culture flasks T25, T75, T175	Greiner Bio-One
Combitips advanced (0.5 ml, 1 ml, 2.5 ml, 5 ml, 10 ml)	Eppendorf
Conical tubes, polypropylene, 15 ml and 50 ml	Greiner Bio-One
Cryogenic vials (1.8 ml)	Starlab
MicroAmp™ Optical 384-Well Reaction Plate	Thermo Fisher Scientific
MicroAmp™ Optical 96-Well Reaction Plate	Thermo Fisher Scientific
Microcentrifuge tubes (0.5 ml, 1.5 ml, 2 ml)	Starlab
Millex-HA Filter, 0.45 µm	Merck
Nitrile gloves, sterile, powder-free	Kimberly-Clark
PCR tubes	Starlab

Plastic ware/consumable	Company
Sterile pipettes (2 ml, 5 ml, 10 ml, 25 ml, 50 ml)	Greiner Bio-One
Syringes (5 mL)	Braun
TipOne Graduated Tip (10 µl, 200 µl, 1000 µl)	Starlab

4.1.9 Equipment and instruments

Table 24: List of equipment and instruments

Equipment/instrument	Company
Affymetrix GeneChip® Scanner 3000	Thermo Fisher Scientific
ARE heating magnetic stirrer	VELP Scientifica
BD FACSVerse™ flow cytometer	BD Biosciences
BioRAD Mini Protean® Tetra Cell	BioRAD Laboratories
BioRAD Power-Pac HC	BioRAD Laboratories
BioRAD Trans-Blot SD Semi-Dry Transfer Cell	BioRAD Laboratories
CASY® cell counter	OMNI Life Science
Centrifuge MIKRO 200 R	Hettich
Centrifuge ROTANTA 460 R	Hettich
Centrifuge ROTIXA 50 RS	Hettich
Easypet 3	Eppendorf
Freezer (-20°C)	EWALD Innovationstechnik
Freezer (-80°C)	Sanyo Electric Co. Ltd.
Fridge (4°C)	EWALD Innovationstechnik
HERAsafe class II biological safety cabinet	Kendro
ImageXpress Micro XLS Imaging System	Molecular Devices
inCUsafe CO2 incubator model: MCO-20AIC	Sanyo Electric Co. Ltd.
Infinite M200 microplate reader	Tecan
MM-Separator M12+12, MD90001	MagnaMedics
Multipette® M4	Eppendorf
NanoDrop 1000	PeqLab
Nikon Eclipse Ti-S	Nikon
Odyssey® Imaging System	LI-COR Biosciences
Olympus CKX41 Microscope	Olympus

Equipment/instrument	Company
Peqlab PerfectBlue™ Vertical Double Gel System	VWR Life Science
Pipettes Research Plus (2.5 µl, 10 µl, 20 µl, 100 µl, 200 µl, 1000 µl)	Eppendorf
QuantStudio™ 7 Flex Real-Time PCR System	Applied Biosystems
Rocking shaker	MS-L GmbH
Roller mixer	Ratek
Rotator	MS-L GmbH
Steam pressure autoclave Systec VX-150	Systec GmbH
ThermoMixer® comfort	Eppendorf
Vapo.Protect Mastercycler® Pro	Eppendorf
Vortex (ZX classic, wizard X)	VELP Scientifica
Water bath SWB20	Medingen

4.1.10 Software and analysis tools

Table 25: List of software and analysis tools

Software	Company/source
Endnote™ 20	Clarivate
FACSDiva™ (6.1.3)	BD Bioscience, Heidelberg, Germany
FlowJo (10.6.2.)	BD Bioscience, Heidelberg, Germany
Gage R package	Luo et al. 2009 [264]
GraphPad Prism 9	GraphPad
i-control Version 1.10	Tecan Life Sciences
LEGENDplex v.8 software	BioLegend
Linear model-based approach limma R package	Ritchie et al. 2015 [265]
Magellan™ Data Analysis Software Version 7.2	Tecan Life Sciences
MetaXpress® 6.7.2	Molecular Devices
Molecular Signatures Database (MSigDB)	https://www.gsea-msigdb.org
MS Office 2019	Microsoft
oligo R package	Carvalho and Irizarry 2010 [266]
Paint.net 4.3	dotPDN LLC
R	https://www.R-project.org/

4.2 Methods

4.2.1 Cell culture techniques

4.2.1.1 Culturing of cell lines

All cell lines were cultured in recommended medium in humidified incubators at 37 °C and 5% carbon dioxide (CO_2). HT-29 cells were cultivated in McCoy's 5A Medium GlutaMAX™-I, supplemented with 10% fetal calf serum (FCS) and 1% penicillin/streptomycin (P/S). HEK293T, HeLa and Vero E6 cells were cultivated in DMEM GlutaMAX™-I medium, supplemented with 10% FCS and 1% P/S. HEK-Blue IFN reporter cells were cultivated in DMEM GlutaMAX™-I medium, supplemented with 10% FCS, 1% P/S and 100 µg/ml Normocin. Caco-2 cells were maintained in MEM medium, supplemented with 10% FCS, 1% P/S and 2% L-glutamine. HCoEpiC cells were cultivated in EpiCM medium, supplemented with 2% FCS, 1% P/S and 1% Epithelial Cell Growth Supplement.

For general cell culture, cell lines were cultivated in cell culture flasks and passaged 2-3 times per week at 90% confluency. For passaging, adherent cells were washed with pre-warmed PBS to remove remaining culture medium, then incubated with trypsin/EDTA solution at 37 °C, 5% CO_2 for 5-10 minutes until cells were detached. Cells were then resuspended in fresh culture medium and appropriate amounts of cell suspension were transferred to a new cell culture flask for further cultivation. Splitting ratios varied between 1:2 (Caco-2, HCoEpiC) and 1:8 or 1:16 (HT-29, HeLa). After 30 passages, cell culture was terminated, and cell culture continued with freshly thawed cells.

4.2.1.2 Thawing and freezing of cell lines

Cells were initially thawed at early passages by shortly incubating cryogenic tubes in a water bath at 37 °C, followed by dilution in pre-warmed cell culture medium and centrifugation for 5 minutes at 1800 rpm. After removal of residual DMSO, cells were resuspended in appropriate growth medium and transferred to a cell culture flask. For long term-storage, cells were detached and resuspended in freezing medium containing 90% FCS and 10% DMSO, transferred to cryogenic tubes and frozen in freezing containers to -80 °C. After 24 hours, cryogenic vials were stored in liquid nitrogen at -196 °C.

4.2.1.3 Counting, seeding and treatment of cell lines

To ensure equal conditions for every experiment, cells were seeded at pre-defined densities that avoid unfavourable conditions like overgrowth or lack of cell-cell contact. Seeding densities were adapted to reach 90% confluency at the end of the experiment.

For seeding, cells were washed with pre-warmed PBS, then incubated with trypsin/EDTA for 5 minutes at 37 °C until detached. Cells were resuspended in growth medium supplemented

with 10% FCS to block trypsin activity and counted using the Casy Cell Counter. Seeding cell suspension was prepared using the following formula:

$$ml\ cells\ for\ seeding = \frac{confluency\ [\frac{cells}{cm^2}] * well\ area\ [cm^2] * \frac{1}{well\ volume\ [ml]} * total\ seeding\ volume\ [ml]}{cells/10^5}$$

After seeding, cells were cultivated at 37 °C and 5% CO_2 for 24 hours before treatment was performed, or for 48 hours for basal evaluation of cells.

4.2.1.4 Generation of genetically modified cell lines using CRISPR/Cas9

Clustered regularly interspaced short palindromic repeats (CRISPR)/Cas9-mediated knockout (KO) of USP22, MDA5, RIG-I, TLR3 and STING was performed using the pLentiCRISPRv2 system.

CRISPR small guide RNAs (sgRNAs) (Table 8) were designed by Sjoerd J.L. van Wijk and introduced into the pLentiCRISPRv2 vector by Sonja Smith, using standard restriction enzyme cloning methods. Cloned constructs were amplified in bacteria and correct generation verified using DNA sequencing.

For generation of CRISPR virus, two (IFIH1) or three sgRNAs for each target were combined and co-transfected with pMD2.G and psPAX2 into HEK293T cells using FuGENE HD Transfection Reagent in a FuGENE/DNA ratio of 3:1 according to the manufacturer's instructions. After 48 and 72 hours, supernatants containing virus were collected, pooled, sterile filtered (45 µm) and either directly used for target cell transduction or frozen in liquid nitrogen and stored at -80 °C until further use.

For transduction of cell lines with CRISPR virus, cells in early passages were seeded in 6-well plates at a density of 20%. The next day, 8 µg/ml polybrene was added to the cells to enhance the efficiency of lentiviral transfection and incubated with 500 µl virus supernatant for 72 hours. After removal of cell supernatant and remaining virus, cells were incubated with fresh growth medium containing 12.5 µg/ml puromycin for selection. KO was confirmed using Western blot analysis. Where necessary, single-cell dilution was performed after selection to obtain single-cell derived KO cultures. To this end, polyclonal KO culture was diluted in growth medium to contain 0.5 cells/well and seeded into 96-well plates. Cells were regularly checked to ensure growth as single cell colony, expanded for 14 days and knockout efficiency was tested by Western blot analysis.

To obtain USP22 double KO (dKO) cell lines, USP22 KO cells were generated first, then transduced with gRNA-containing viral particles against the secondary target. Puromycin selection was performed with increased concentrations up to 100 µg/ml.

4.2.1.5 Transfection of cells

4.2.1.5.1 Gene silencing using RNAiMAX and the Neon Transfection system

Transient gene silencing was performed using Silencer® and Silencer® select siRNAs in the concentrations indicated in the respective figures. For each experiment, non-silencing siRNA constructs were used as a control.

For reverse transfection using the Lipofectamine RNAiMAX reagent, cells were detached and counted as described above. In the meantime, siRNA in the indicated concentrations and RNAiMAX reagent were pre-mixed separately with OptiMEM according to the manufacturer's protocol, then mixed at a ratio of 1:1 and incubated for 15 min at RT. Transfection mix was then added to the plate surface, and the counted cells were seeded in P/S-free medium on top of the transfection mix and incubated at 37°C, 5% CO_2. Six hours after seeding, medium was replaced with fresh P/S-free medium to reduce toxicity of the transfection mix and further incubated for indicated times until lysis. SiRNA constructs are listed in Table 7.

Gene silencing of USP22 in HCoEpiC cells was performed using the NeonTM Transfection System. Cells were collected and counted as described above, 0.5 x 10^6 cells per condition were centrifuged at 1200 x g and medium removed. Cells were resuspended in resuspension buffer R, mixed with Silencer® select siRNA in a final concentration of 125 nM for each condition. Cells were electroporated using 1 pulse, 1400 V, 30 ms to deliver siRNA and seeded in plates containing P/S-free cell culture medium. After 72 h of incubation, cells were harvested and processed for Western blot analysis.

4.2.1.5.2 Stimulation of PRRs with poly(I:C) and ISD

For stimulation with poly(I:C), HT-29 cells were seeded for treatment the next day. For each 6-well, two µg of ISD were pre-mixed with OptiMEM. In parallel, Lipofectamine2000 was pre-mixed in OptiMEM at a µl Lipofectamine-µg DNA ratio of 3:1, according to the manufacturer's instructions. After 5 minutes, both dilutions were mixed and further incubated at RT for 15 minutes. Transfection mix was then added to cells in P/S free medium. Cell lysis with RIPA or RNA lysis buffer was performed after 24 h.

For stimulation with poly(I:C), cells were seeded as described above. Per well, 2 µg of poly(I:C) was mixed with 20 µl LyoVec and incubated for 15 minutes at RT to allow the formation of lipid-RNA complexes. Transfection mix was then added to cells in P/S free medium at a 1:20 volume ratio. After 24 h of incubation, cells were processed for Western blot or RNA isolation.

4.2.1.6 Stimulation of STING with 2'3'-cGAMP

For the treatment of cells with the STING agonist 2'3'-cGAMP, a protocol using digitonin permeabilization was used. Cells were seeded and cultivated for 24 hours in P/S-free culture medium, then medium was removed and cells were rinsed 1x with PBS. Digitonin permeabilization buffer containing 10 µg/ml 2'3'-cGAMP was added slowly to each well, and cells were incubated at 37 °C, 5% CO_2 to allow delivery of 2'3'-cGAMP into the cell. After 10 minutes, permeabilization buffer was aspirated and replaced with fresh, P/S-free medium and further incubated at 37 °C, 5% CO_2 for the indicated times until lysis.

4.2.2 RNA analysis by quantitative real-time PCR (qRT-PCR)

4.2.2.1 RNA isolation

For RNA isolation using the peqGOLD total RNA isolation kit, cells were seeded 48 hours prior to cell lysis for basal conditions, or 24 hours before indicated treatment, in 6-well plates. At the time point of lysis, medium was discarded and cells were lysed using 350 µl of RNA lysis buffer and the lysate transferred to a peqGOLD RNA homogenizer column. After centrifugation for two minutes at 12000 x g to remove cell debris, column was discarded, flow-through thoroughly mixed with 350 µl of 70% EtOH and loaded on a peqGOLD RNA Mini column. Column was centrifuged for one minute at 10000 x g and flow-through was discarded. The RNA containing columns were washed two times by addition of 500 µl RNA wash buffer I and centrifugation for 30 seconds at 10000 x g, followed by three additional washing steps using 500 µl 80% EtOH. The columns were dried by additional centrifugation for two minutes at 12000 x g and 40-70 µl pre-warmed ddH_2O was added for 4 minutes for RNA elution, depending on sample size. After centrifugation for two minutes at 12000 x g, eluted RNA was stored on ice or at 80 °C for further processing.

For gene expression profiling using the Affymetrix Clariom™ S array, an additional step for DNase digest was performed after the first washing step with RNA wash buffer I. Per sample, 75 µl DNase I mix was prepared by mixing 73.5 µl DNase I Digestion Buffer and 1.5 µl RNase free DNase I per sample and added to the column membrane. After a 15 minutes incubation step at room temperature, the reaction was stopped by addition of 250 µl RNA wash buffer I for two minutes and centrifugation for one minute at 10000 x g to remove remaining DNase and buffer. The RNA isolation protocol was resumed by washing with 80% EtOH and elution with ddH_2O, as described above.

4.2.2.2 cDNA synthesis

Complementary (c) DNA synthesis was performed using the RevertAid H Minus First Strand Kit, using 1 µg of RNA and random hexamer primers, according to the manufacturer's instructions.

4.2.2.3 Analysis of mRNA using qRT-PCR

For the determination of relative mRNA expression levels, qRT-PCR using QuantStudio 7 Flex Real-Time PCR System was performed. 1 µl of transcribed cDNA was mixed with 10 µl of pre-mixed detection-mix containing ddH2O, SYBR-Green PCR Master Mix and 10 pmol/µl forward and reverse primers of the gene of interest (listed in Table 10) in a 384-well MicroAMP™ optical reaction plate. As a negative control, 1 µl ddH2O was mixed with 10 µl of detection mix of the respective gene. Melting curves were analyzed to ensure target specificity of primers. 28S served as housekeeping gene reference in all experiments, and Ct values were analyzed using the $\Delta\Delta C_t$ method.

4.2.3 Gene expression profiling

4.2.3.1 Sample preparation

Gene expression profiling was performed at the DKFZ Genomics and Proteomics Core Facility (Heidelberg, Germany) by Dr. Melanie Bewerunge-Hudler and her team. Cells were seeded at equal densities in 6-well plates to reach 80% confluency at the time of sample collection. After 48 hours, cells were placed on ice, medium removed and RNA isolated using the peqGOLD total RNA isolation kit, as described in 4.2.2.1.

4.2.3.2 Sample processing

RNA was stored at -80 °C and processed using the Affymetrix human Clariom™ S array. The Applied Biosystems™ WT PLUS Reagent Kit was used to generate labelled single strand-cDNA from input amounts of 100 ng total RNA. 5.5 µg of fragmented and labelled ss-cDNA were hybridized for 17 h at 45°C on Applied Biosystems™ human Clariom™ S Array, according to the Affymetrix WT PLUS Reagent Kit user manual. Gene Expression Microarrays were scanned using the Affymetrix GeneChip® Scanner 3000 according to GeneChip® Expression Wash, Stain and Scan Manual for Cartridge Arrays.

4.2.3.3 Data analysis

Data analysis was performed by Geoffroy Andrieux at the Institute of Medical Bioinformatics and Systems Medicine at the University of Freiburg and is described in [267]. Raw.CEL files were analysed using the oligo R package, and the log2 transformed robust multichip average (RMA) method was used to normalize probe intensities. Differential expression between NHT control and USP22 KO cells was identified with the linear model-based approach limma R package [265], and a cut-off was set at the adjusted P-value of <0.05. Gene-set enrichment analysis was performed with gage R package, using the Molecular Signatures Database (MSigDB) [268] as gene set repository.

4.2.4 Cytokine analysis

4.2.4.1 Multiplex quantification of cytokine secretion

Cytokines in cell supernatant were quantified using the LEGENDplex™ Human Anti-Virus Response Panel multiplex assay following the manufacturer's protocol. To this end, cells were seeded in 2 ml cell culture medium in 6-well plates to reach 90% confluency at the time of sample collection. After 48 hours, supernatant was either collected, replaced with fresh or treatment medium, or left further on the cells until collection at indicated time points. Supernatant was collected, centrifuged at 300 x g at 4 °C for 5 minutes, then frozen in liquid nitrogen until analysis. Analysis was performed using the BD FACSVerse™ flow cytometer, where a minimum of 300 events per analyte were acquired, and data was analysed with the LEGENDplex v.8 software.

4.2.4.2 IFNβ ELISA

Cells were seeded in 6-well plates to reach 90% confluency at the time of sample collection. The next day, medium was replaced with 1.5 ml fresh growth medium and further incubated for 24 hours. Supernatant was collected, centrifuged at 300 x g, 4 °C for 5 minutes and frozen in liquid nitrogen until use. IFNβ was quantified using the VeriKine-HS™ Human IFN Beta Serum ELISA Kit according to the manufacturer's protocol. Shortly, 50 µl sample buffer, 50 µl diluted antibody and 50 µl sample or human IFNβ standard were added to the pre-coated microplate and incubated for 2 hours by shaking at 450 rpm. After 3 washing steps with 300 µl wash solution, 100 µl diluted horseradish peroxidase (HRP) solution was added and incubated for 30 minutes by shaking at 450 rpm, followed by 4 washing steps. 100 µl TMB substrate was added to the setup and incubated in the dark without shaking. After 60 minutes, 100 µl stop solution was added to each well and absorbance was immediately measured at 450 nm. As recommended, IFNβ concentrations were calculated by plotting the optical densities using a 4-parameter fit for the standard curve.

4.2.4.3 Detection of type I and type III IFN production

Biologically active type I and type III IFN was detected using HEK-Blue IFNα/β or HEK-Blue IFNλ reporter cells that induce secreted embryonic alkaline phosphatase (SEAP) production when stimulated with IFNα/β or IFNλ, respectively. Per well, 50000 HEK IFN reporter cells were seeded in 180 µl medium and 20 µl cell supernatant added that was collected as described in 4.2.4.2. The next day, 20 µl of HEK-Blue IFN reporter cell supernatant was mixed with 180 µl Quanti-Blue Solution, incubated for 5 minutes at 37 °C, and absorbance at 620 nm was measured for assessment of SEAP expression levels.

4.2.5 Determination of mitochondrial membrane potential

Changes in mitochondrial membrane potential were determined using TMRM, a dye that accumulates in intact mitochondria. Cells were seeded in 24-well plates to reach confluency of 80% for further processing. After 48 hours, cells were incubated with 50 nM TMRM dye for 20 minutes at 37 °C, then cells were detached using trypsin/EDTA, washed two times with PBS and resuspended in PBS for analysis. As a positive control, some samples were additionally exposed to the mitochondrial oxidative phosphorylation uncoupler FCCP (100 µM) 20 minutes before analysis. TMRM fluorescence intensity of living cells was measured using the PE channel and percentual loss of membrane potential calculated using Microsoft Excel.

4.2.6 Protein analysis

4.2.6.1 Harvest and lysis of cells

Depending on the experiment and the amount of protein needed for analysis, cells were seeded in appropriate densities and treatment performed as indicated. For cell lysis, cell supernatant was removed and washed once with ice-cold PBS. All further steps were carried out on ice to decelerate protein degradation processes. Cells were lysed using appropriate amounts of RIPA lysis buffer, if not indicated otherwise, and collected in reagent tubes using a cell scraper. After 30 minutes, cell debris was removed by centrifugation for 25 minutes at 14000 rpm and 4 °C, and supernatants collected. Protein concentration was determined using the Pierce™ BCA protein assay kit, following the manufacturer's instructions. Samples for separation by SDS-PAGE were prepared by mixing a pre-defined amount of protein (25-40 µg) with ddH_2O and 6 x loading buffer to get equally concentrated samples, then denatured at 96 °C for 6 minutes.

4.2.6.2 SDS-polyacrylamide gel electrophoresis (SDS-PAGE) and Western blotting

For the analysis of samples, proteins were first separated by molecular weight using sodium dodecyl sulfate polyacrylamide gel electrophoresis (SDS-PAGE), then transferred to a nitrocellulose membrane using a semi-dry blotting system. For protein separation, previously prepared samples were loaded on self-cast polyacrylamide gels that consisted of a 10-13.5% acrylamide separating gel, depending on the proteins of interest, and a 5% acrylamide stacking gel. In addition to the samples, a dyed protein ladder was run to correlate protein sizes. Gels were run in 1 x running buffer at 60 V until samples reached the separating gel, then at 140 V to get the desired separation. For protein transfer, gels were shortly washed with ddH_2O and equilibrated together with Whatman paper and nitrocellulose membranes for 10 minutes in 1 x blotting buffer. Two Whatman papers were placed on the anode of the transfer system, followed by one nitrocellulose membrane, the gel containing separated samples, and two additional Whatman papers. During the process, excess buffer and air bubbles were removed

to establish complete contact between all components. Protein transfer was carried out at 1 mA/cm^2 of membrane for 90-105 minutes, depending on the molecular weight of the proteins of interest. After transfer, membranes were incubated at room temperature for one hour in 5% milk powder in PBS-0.1% Tween-20 (PBS-T) to block unspecific binding of antibodies, then washed three times for 5 minutes with PBS-T to remove milk.

4.2.6.3 Protein detection

All antibodies used for protein detection were diluted in PBS-T containing 2% BSA and 0.1% ProClin™ as listed in Table 15. Membranes were incubated with primary antibodies overnight at 4 °C, then washed three times with PBS-T. Secondary antibodies conjugated to HRP were diluted in PBS-T containing 5% milk powder as listed in Table 16 and incubated with membranes at room temperature for one hour. After three washing steps, membranes were prepared for enhanced chemiluminescence (ECL) detection using Pierce™ ECL Western Blot Substrate according to the manufacturer's instructions. Where necessary for sequential detection of proteins, membranes were either stripped by incubation with 0.4 M NaOH for 10 minutes, or HRP signal was quenched by incubation with H_2O_2 for 10 minutes, followed by an additional blocking step for 1 hour before the next primary antibody was incubated. If not otherwise indicated, two biologically independent experiments were analyzed with Western blotting, and one representative experiment is presented in this thesis. Proteins within one experiment that were detected on different membranes are shown above their respective loading controls. For improved clarity, Western blots presented in part II of this thesis only display one representative loading control.

4.2.6.4 Immunoprecipitation of ubiquitylated proteins using tandem ubiquitin binding entities

GST-tagged tandem ubiquitin binding entities (TUBEs) were expressed in E. coli as described by Hjerpe et al. [269], purified and immobilized on glutathione agarose beads. For the detection of ubiquitylated proteins, cells were cultivated as described above for 48 hours before treatment with 2'3'-cGAMP or cell lysis. After incubation, medium was first removed and cells were rinsed with ice cold 1x PBS to remove medium, then cells were harvested on ice for 30 minutes in 1% NP-40 lysis buffer supplemented with 25 mM of the deubiquitylase inhibitor NEM to prevent ubiquitin chain degradation as described above. During incubation, cell suspension was thoroughly mixed through resuspension every 5-10 minutes to ensure proper lysis. Protein concentration was determined as described above, and 3 mg of protein lysate was incubated with pre-washed GST-tagged TUBE beads overnight at 4 °C under constant rotation. In the meantime, 20-30 µg lysate was set aside and prepared as input sample for SDS-PAGE as described above (4.2.6.1). On the next day, GST-TUBE beads were separated from the lysate through a magnetic separator, washed four times with ice-cold NP-40 buffer, and bead-bound ubiquitylated proteins were eluted by boiling in 2x loading buffer at 96 °C for

6 minutes. Ubiquitylated proteins were analyzed together with input samples using Western blot analysis. Equal loading of GST-tagged TUBE beads was monitored through staining of membranes with Ponceau S solution for 1 hour.

4.2.7 SARS-CoV-2-related assays

All experiments involving infection of cells with SARS-CoV-2 and analysis of SARS-CoV-2-infected cells were planned in collaboration with Steeve Boulant and Megan Stanifer and performed by Megan Stanifer at the DKFZ facilities in Heidelberg.

4.2.7.1 Infection of cells with SARS-CoV-2

The SARS-CoV-2 strain BavPat1/2020 was obtained from the European Virology Archive, amplified in Vero E6 cells and used at passage 3. For infections, Caco-2 cells were seeded prior to infection, and cells were infected with a MOI of 1 virus particle per cell. After 1 hour of incubation at 37 °C, viral supernatants were removed, and cell culture medium was added after one washing step using PBS. 24 hours post-infection, cells were monitored for virus infection.

4.2.7.2 Indirect immunofluorescence assay

For assessment of virus infection using indirect immunofluorescence, cells were seeded on iBIDI glass bottom 8-well chamber slides and infected as described above. 24 hours post-infection, cells were fixed in 4% PFA for 20 minutes, then washed and incubated with 0.5% Triton-X-100 for 15 minutes for permeabilization. For nucleocapsid staining, primary antibody against SARS-CoV NP was diluted in PBS and incubated with fixed and permeabilized cells for 1 hour. After three washing steps with PBS, cells were incubated with the secondary antibody Alexa Fluor 568 and DAPI for 45 minutes. After three washing steps using PBS, stained cells were maintained in PBS and imaged by epifluorescence on a Nikon Eclipse Ti-S. All incubation steps after cell culture termination were performed at RT.

4.2.7.3 qRT-PCR detection of SARS-CoV-2 genome

Quantification of viral RNA in SARS-CoV-2-infected cells was performed using qRT-PCR. To this end, RNA was extracted from infected or mock-treated Caco-2 cells 24 hours post-infection using the Qiagen RNAeasy Plus Extraction Kit. cDNA was generated using 250 ng of RNA with the BioRad iSCRIPT reverse transcriptase according to the manufacturer's protocol. qRT-PCR was performed according to the manufacturer's instructions using BioRad iTaq SYBR green and normalized on TBP.

4.2.7.4 TCID50 virus titration

The infectious viral titer of supernatants of SARS-CoV-2 infected cells was determined by $TCID_{50}$ endpoint dilution assay. Therefore, 20000 Vero E6 cells per well were seeded in 96-well plates and cultivated for 24 hours. Then, viral supernatant of the indicated SARS-CoV-2-

infected Caco-2 cells was collected and 100 µl added to the first well of the previously seeded Vero E6 cells. Seven dilutions of a 1:10 ratio were made and incubated on the following wells. All infections were performed in triplicate and terminated after 24 hours by fixation in 2% PFA at RT. After 20 minutes, PFA was removed, cells were washed two times in PBS and permeabilized with 0.5% Triton-X-100 diluted in PBS for 10 minutes at RT. After a blocking step in 1:2 diluted LI-COR blocking buffer for 30 minutes at RT, infected cells were stained with anti-dsRNA (J2) at a 1:1000 dilution for 1 hour at RT, followed by three washing steps with 0.1% PBS-T. Secondary antibody anti-mouse CW800 and DNA dye Draq5 was added in a 1:10000 dilution in blocking buffer and incubated for 1 hour at RT. After three washing steps with 0.1% PBS-T, cells were imaged in PBS on a LI-COR imager.

4.2.8 Determination of cell death

Microscopic live/death staining was performed to determine the cytotoxic effect of potential cell death inducing agents. Cells were seeded one day prior to treatment in 96-well to reach 90% confluency at the point of cell death assessment. Percentage of cell death was assessed by double staining with Hoechst 33342 and propidium iodide (PI), followed by fluorescence-based microscopic quantification of PI-positive dead cells and Hoechst-positive total cells. Both imaging and analysis were performed using the ImageXpress Micro XLS Widefield High-Content Analysis System and MetaXpress Software.

4.2.9 Statistical analysis

Data is represented as mean + standard deviation (SD) of at least three independent experiments performed in triplicate, or as stated in the figure legend. Significance was calculated using 2-way ANOVA followed by Tukey’s multiple comparison test using the GraphPad Prism 9 Software. P-values were marked as indicated: * $P < 0.05$, ** $P < 0.01$, *** $P < 0.001$, n.s.: not significant.

4.2.10 Data availability

Microarray data are available on Gene Expression Omnibus under the accession number GSE190036.

5 Results

The main part of the results presented in Chapter 5.1 was published in the international peer-reviewed journal *Cell Death and Disease* in 2022 with the title “USP22 controls type III interferon signaling and SARS-CoV-2 infection through activation of STING” [267].

5.1 Part I: USP22 controls interferon signaling and SARS-CoV-2 infection through activation of STING

USP22 is a deubiquitylase with multiple functions and is implicated in the post-translational modification of a variety of proteins with roles in cell cycle regulation [61-63, 65], proliferation [270], cancer immunoresistance [47, 71, 73] and programmed cell death [68, 69, 72]. In addition, USP22 is integrated into the SAGA complex through which it regulates gene expression by removing ubiquitin from K119 of H2A and K120 of H2B [51-53] and possibly also at promoter distal sites in a SAGA independent manner [271]. To identify the full spectrum of USP22-controlled genes, we profiled USP22-dependent changes in gene expression in the hIEC line HT-29.

5.1.1 Screening of USP22-mediated changes in gene expression in HT-29 cells

In order to investigate USP22-mediated changes in gene expression, two HT-29 USP22 knockout (KO) single clones (#16 and #62), recently generated using CRISPR/Cas9 [72], were used in the following experiments. Complete KO of USP22 was confirmed by probing for USP22 protein expression in HT-29 WT, CRISPR/Cas9 control (NHT, non-human target) and the two USP22 KO single clones #16 and #62 (Figure 6A). As a first step in understanding USP22-mediated changes in gene expression in HT-29 cells, basal gene expression of HT-29 control and USP22 KO cells was assessed by microarray analysis, revealing prominent alterations in gene expression upon loss of USP22, with 182 downregulated and 401 upregulated genes compared to control HT-29 cells (Figure 6B and C).

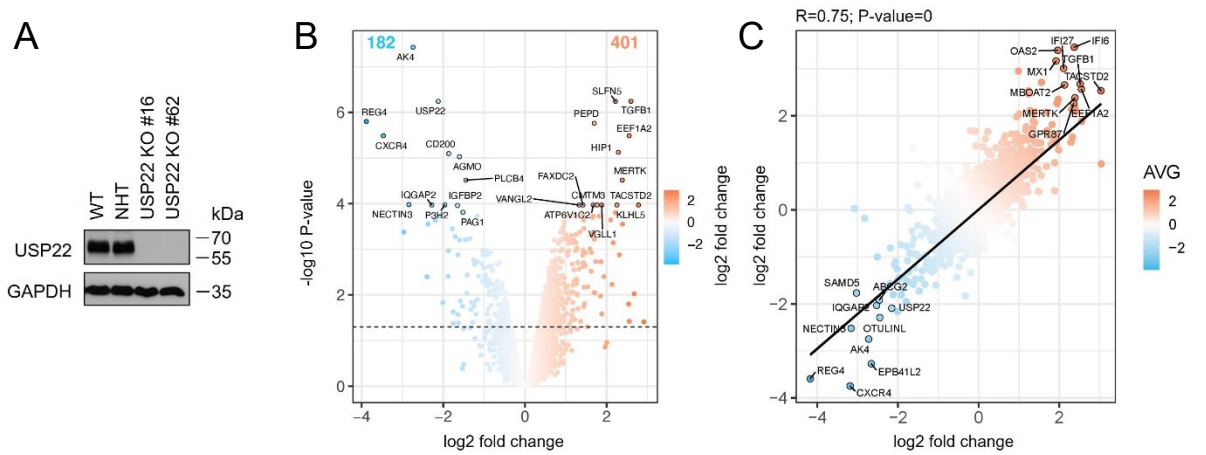

Figure 6: Profiling of USP22-mediated gene expression in HT-29 cells. A. Expression levels of USP22 in HT-29 WT, CRISPR/Cas9 control (NHT) and two independent single-cell HT-29 USP22 CRISPR/Cas9 KO clones (#16 and #62) were investigated using Western blotting. GAPDH served as a loading control. B, C. Differential gene expression of two independent single-cell HT-29 USP22 CRISPR/Cas9 KO clones (#16 and #62) compared to CRISPR/Cas9 control (NHT) HT-29 cells is visualized in a volcano (B) and scatter (C) plot. Color code represents the average log2 fold change compared to NHT. Volcano and scatter plot were generated by Geoffroy Andrieux.

A more detailed look at the top-50 differentially regulated genes revealed 30 genes that were upregulated in both USP22 KO single clones compared to NHT, including genes involved in growth and differentiation (such as tumor-associated calcium signal transducer 2 (TACSTD2), TGFB1 and tyrosine-protein kinase Mer (MERTK)), phospholipid remodeling (membrane bound O-acyltransferase domain containing 2 (MBOAT2)), protein biosynthesis (eukaryotic translation elongation factor 1 alpha 2 (EEF1A2)), and cytosolic RNA- and DNA sensor DDX60 (Figure 7A). Downregulated genes included regenerating family member 4 (REG4), a marker of deep crypt secretory cells in the colon [272], C-X-C motif chemokine receptor (CXCR) 4, which is also a functional receptor for extracellular ubiquitin [273], the mitochondria-localized adenylate kinase 4 (AK4), which protects against oxidative stress by controlling cellular ATP levels [274, 275], the ATP-binding cassette subfamily G member 2 (ABCG2), and USP22. Interestingly, several of the downregulated genes, such as sterile alpha motif domain containing 5 (SAMD5), nectin cell adhesion molecule 3 (NECTIN3) and Prolyl 3-hydroxylase 2 (P3H2), are involved in retinal development and disease (Figure 7A).

To validate the gene expression data, individual genes were selected from the top-50 up- and downregulated genes and their expression levels were assessed by qRT-PCR in biologically independent samples. Indeed, increased mRNA expression of TGFB1, schlafen 5 (SLFN5), transglutaminase 2 (TGM2) and DDX60 and decreased expression of USP22, AK4 and CXCR4 were confirmed (Figure 7B), supporting the findings and confirming the quality of the gene expression analysis.

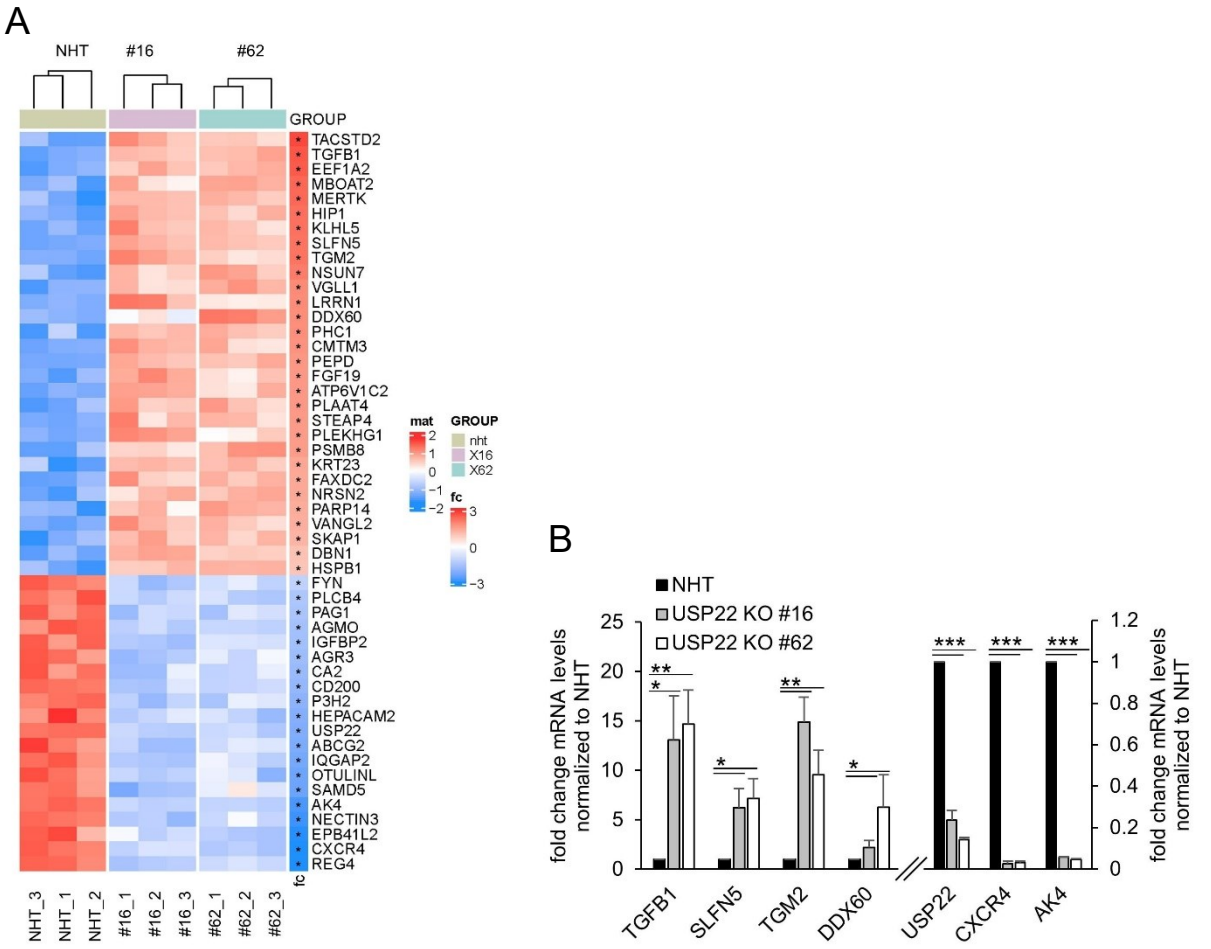

Figure 7: USP22 modulates gene expression in HT-29 cells. A. Heatmap depicting the top 50 differentially regulated genes between HT-29 USP22 KO single clones #16 and #62 and NHT control; and confirmation using qRT-PCR. Color coding represents the row-wise scaled (Z-score) RNA intensities. Genes are sorted according to their log2 fold change, compared to NHT. An adjusted p-value of < 0.05 was used. Heatmap was generated by Geoffroy Andrieux. B. Basal mRNA expression of randomly selected genes was assessed in USP22 KO clones #16 and #62 and NHT HT-29 cells using qRT-PCR. Graph shows fold change mRNA levels compared to NHT. Mean and SD of three independent experiments in triplicate are shown. *P < 0.05; **P < 0.01, ***P < 0.001.

As part of the SAGA complex, USP22 regulates gene expression through mono-ubiquitylation of H2A and H2B. Indeed, USP22 KO in HT-29 increased mono-ubiquitylation of H2B, as described before, but not of H2A (Figure 8A and B).

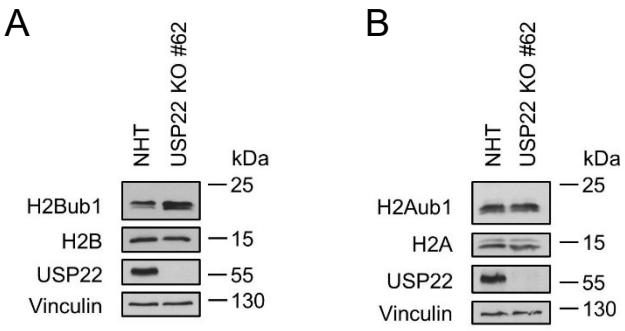

Figure 8: USP22 increases mono-ubiquitylation of H2B. A, B. Basal levels of total and mono-ubiquitylated (ub1) histone 2B (H2B) (A) and histone 2A (H2A) (B) protein as well as levels of USP22 of control and USP22 KO HT-29 cells (USP22 KO #62) were assessed using Western blotting, and Vinculin served as loading control.

Due to the broad spectrum of regulated genes, we performed gene-set enrichment analysis to evaluate whether specific gene ontology (GO) terms were regulated by USP22. To exclude any single clone effects, the differential regulation values of single clones #16 and #62 were combined and used for further analysis of enriched up- and downregulated GO terms. Several GO terms enriched in upregulated genes are associated with type I and type II IFN signaling and regulation of viral processes, including the GO terms “response to IFNγ”, “IFNγ-mediated signaling pathway”, “response to type I IFN”, “regulation of viral genome replication”, and “regulation of viral life cycle” (Figure 9A). Downregulated genes were enriched in ribosome and ribonucleoprotein complex biogenesis, mitochondrial gene expression, and translation and processing of non-coding (nc) RNA, ribosomal (r) RNA, and transfer (t) RNA (Figure 9B).

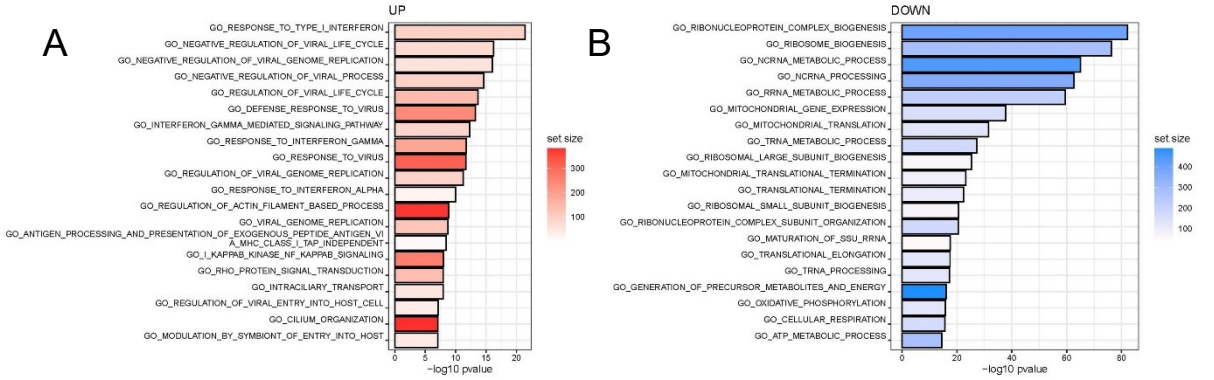

Figure 9: Gene-set enrichment analysis of USP22-regulated genes. A, B. Top-20 GO terms enriched in upregulated (A) and downregulated (B) genes of HT-29 USP22 KO single clones #16 and #62 compared to control HT-29 cells are presented in a bar plot. Color code represents the number of annotated genes within each gene set. Bar plots were generated by Geoffroy Andrieux.

Interestingly, USP22 has previously been reported to regulate IFN signaling, but with controversial effects on the cell types studied [59, 219, 222, 223]. Therefore, we further investigated USP22-mediated effects on genes involved in type I and type II IFN signaling in detail. Several ISGs known for their role in viral defense were upregulated upon loss of USP22,

such as 2'-5'-oligoadenylate synthetase (OAS) 1, -2 and -3, IFN-induced transmembrane protein (IFITM) 1, -2 and -3, MX dynamin like GTPase 1 (MX1), bone marrow stromal cell antigen 2 (BST2) and IFI27 (Figure 10), suggesting an important role of USP22 in the regulation of viral responses. Other upregulated genes included the type I IFN-induced transcription factor IRF9 and the genes encoding ISG15 and USP18, which are core components of the ISGylation machinery (Figure 10).

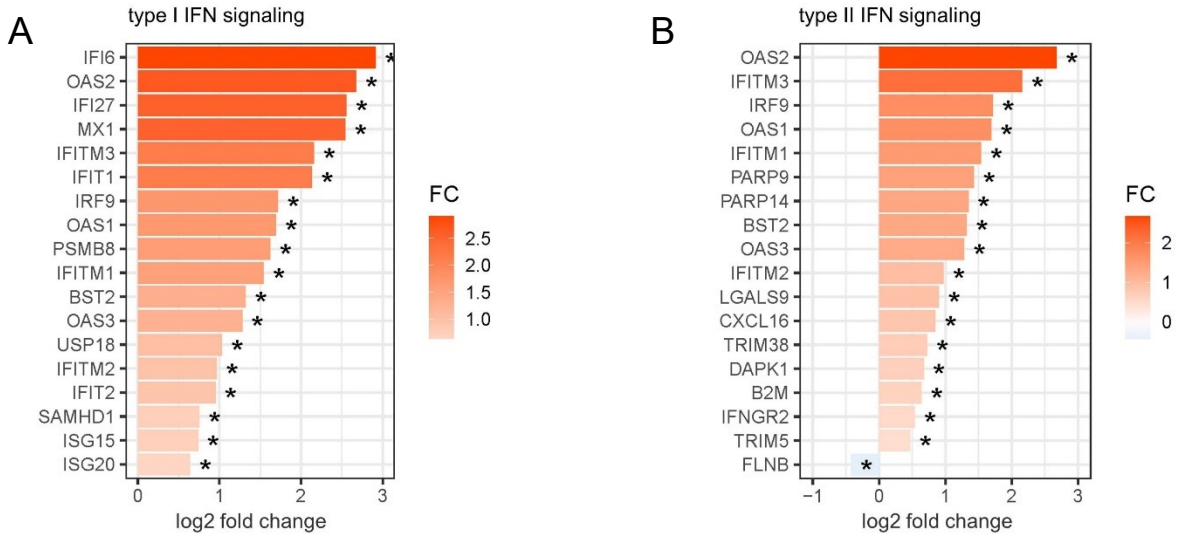

Figure 10: Loss of USP22 leads to differential expression of type I- and type II IFN-associated genes. A, B. Differentially expressed genes contributing to GO terms response to type I (A) and response to type II (B) IFN signaling are presented in a heatmap. Color code represents the log2 fold change of USP22 KO single clones #16 and #62 compared to NHT. Heatmaps were generated by Geoffroy Andrieux.

The increased upregulation of type I and type II IFN-annotated genes regulated by USP22 was again validated by qRT-PCR analysis for selected genes. In both HT-29 USP22 KO single clones, increased mRNA expression of BST2, poly(ADP-Ribose) polymerase family member 9 (PARP9), USP18, OAS3, IFIT1, IRF9, ISG15, OAS2, IFI27 and IFI6 was confirmed (Figure 11A). Although all tested genes except for IFI6 were significantly regulated in both single clones, the strongest regulation of gene expression was detected in single clone #62, which was used for analysis in all further experiments. To further substantiate our findings of USP22-induced regulation of antiviral genes, Western blotting was used to investigate protein expression levels of selected ISGs. Indeed, strongly increased protein expression levels of the ISGs MX1, IRF9, ISG56 and ISG20 were detected upon loss of USP22 (Figure 11B).

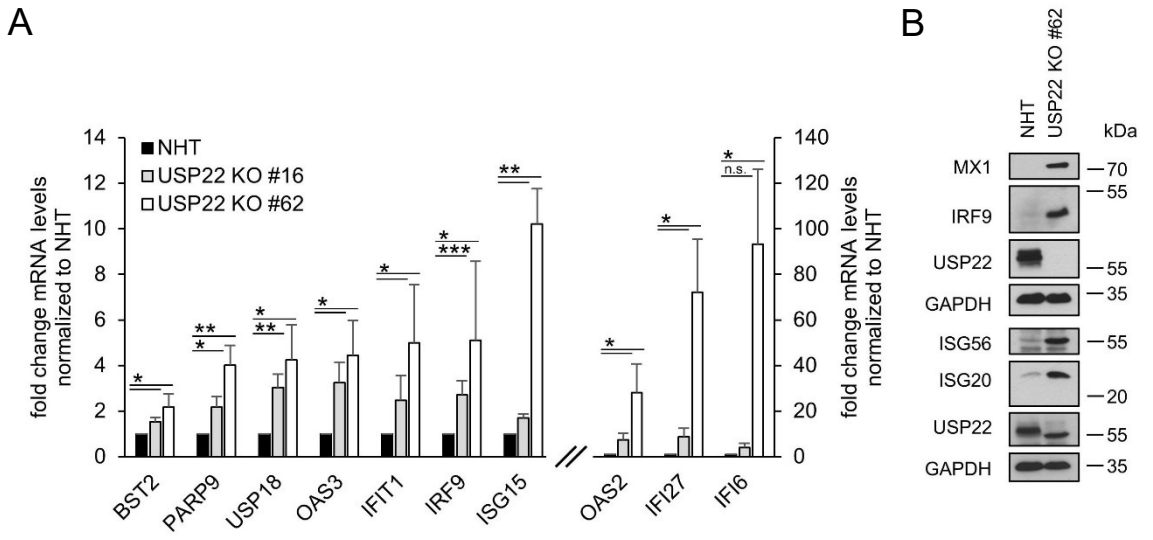

Figure 11: Validation of USP22-mediated regulation of genes annotated to type I- and type II IFN signaling. A. Basal mRNA expression levels of USP22-regulated genes annotated to IFN signaling were assessed in HT-29 NHT and USP22 KO single clones #16 and #62 using qRT-PCR. Data is presented as x-fold mRNA expression compared to NHT and mean and SD of three independent experiments in triplicate are shown. *P < 0.05; **P < 0.01, ***P < 0.001, n.s. not significant. B. Basal protein levels of MX1, IRF9, ISG56 and ISG20, as well as USP22, were assessed in HT-29 NHT and USP22 KO single clone #62 using Western blotting. GAPDH was used as loading control.

5.1.2 Loss of USP22 increases STAT1 signaling and regulates expression and secretion of IFNs and inflammatory cytokines

High expression of ISGs such as BST2, OAS2 and OAS3, IFIT1 and IFI27 usually occurs after induction of IFNs upon detection of self-DNA or pathogen invasion. In the absence of exogenous stimuli, changes in the constitutive expression of IFNs, which normally ensures the basal expression of critical proteins of the immune response, could account for the increase in ISGs observed in Figure 11. Indeed, basal mRNA expression of the type I IFNs IFNα and IFNβ was increased in USP22 KO compared to NHT HT-29 cells (Figure 12A), which was accompanied by increased STAT1 phosphorylation as well as STAT1 expression, an ISG itself (Figure 12B). A detailed analysis of secreted IFNs and related cytokines in the supernatant of HT-29 NHT and USP22 KO clone #62 showed relatively low levels of IFNα2 with minor changes compared to control cells, and no detectable levels of IFNβ (Figure 12C). Surprisingly, USP22 KO in HT-29 cells strongly increased the secretion of the type III IFN IFNL1 as well as the pro-inflammatory cytokines CXCL-10 and IL-8 (Figure 12C). Like IFNα2, granulocyte-macrophage colony-stimulating factor (GM-CSF) expression was only detected at low levels with minor changes upon USP22 KO (Figure 12C).

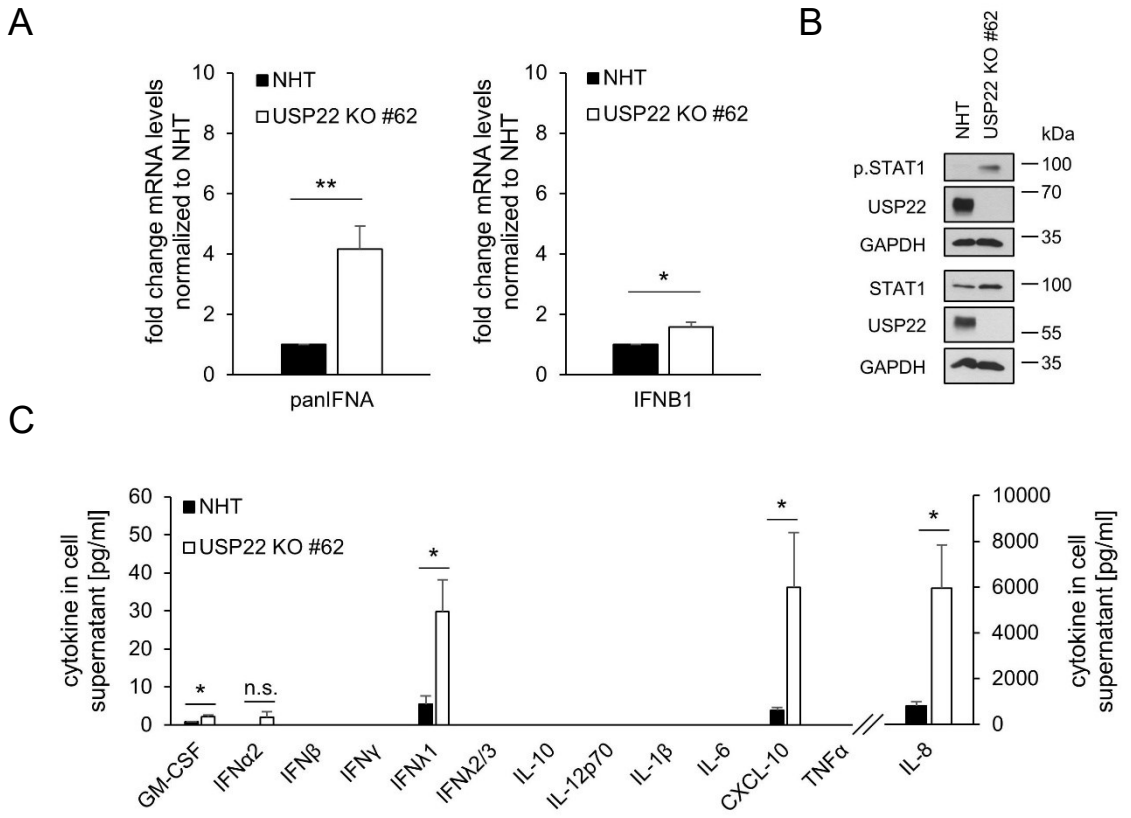

Figure 12: Loss of USP22 leads to increased STAT1 signaling and IFN expression. A. Basal mRNA expression levels of total IFNA and IFNB1 were analyzed in HT-29 control and USP22 KO cells using qRT-PCR. mRNA levels are presented as x-fold change normalized to NHT. Mean and SD of three independent experiments in triplicate are shown. *P < 0.05; **P < 0.01. B. Basal levels of total and phosphorylated STAT1 as well as USP22 were analyzed in HT-29 control and USP22 KO cells. GAPDH was used as loading control. C. Cytokine secretion patterns of the viral defense cytokine panel were analyzed in cell supernatants of NHT and USP22 KO HT-29 cells in a FACS based assay. Data are presented as absolute levels of cytokines (in pg/ml). Samples below the lower detection limit were set to zero, values above upper detection limit were set to the value of the detection limit. Mean and SD of three independent experiments in triplicate are shown. *P < 0.05; n.s. not significant. FACS-based analysis was performed in collaboration with Ralf Schubert.

5.1.3 Type I IFNs are only marginally expressed in HT-29 cells

Although USP22-mediated regulation of IFNα and IFNβ was observed in HT-29 cells based on analysis of mRNA expression, analysis of the absolute levels of secreted IFNs suggested only a minor role for type I and II IFNs in the observed ISG signature (Figure 12). Using isoform-specific primers, IFNA1 and IFNA8 were identified as isoforms highly regulated by USP22 (Figure 13A). Additional analysis of basal and STING agonist 2’3’-cGAMP-induced IFNα and IFNβ in the supernatants of NHT and USP22 KO HT-29 cells revealed very low levels of both type I IFNs (Figure 13B and C), suggesting that type I IFNs contribute only slightly to the increased IFN signaling and ISG expression in USP22 KO HT-29 cells. Notably, mRNA levels of the type II IFN IFNγ could not be detected by qRT-PCR, nor in cell supernatants, suggesting that basal type II IFN expression does not contribute to the ISG signature observed in USP22 KO cells.

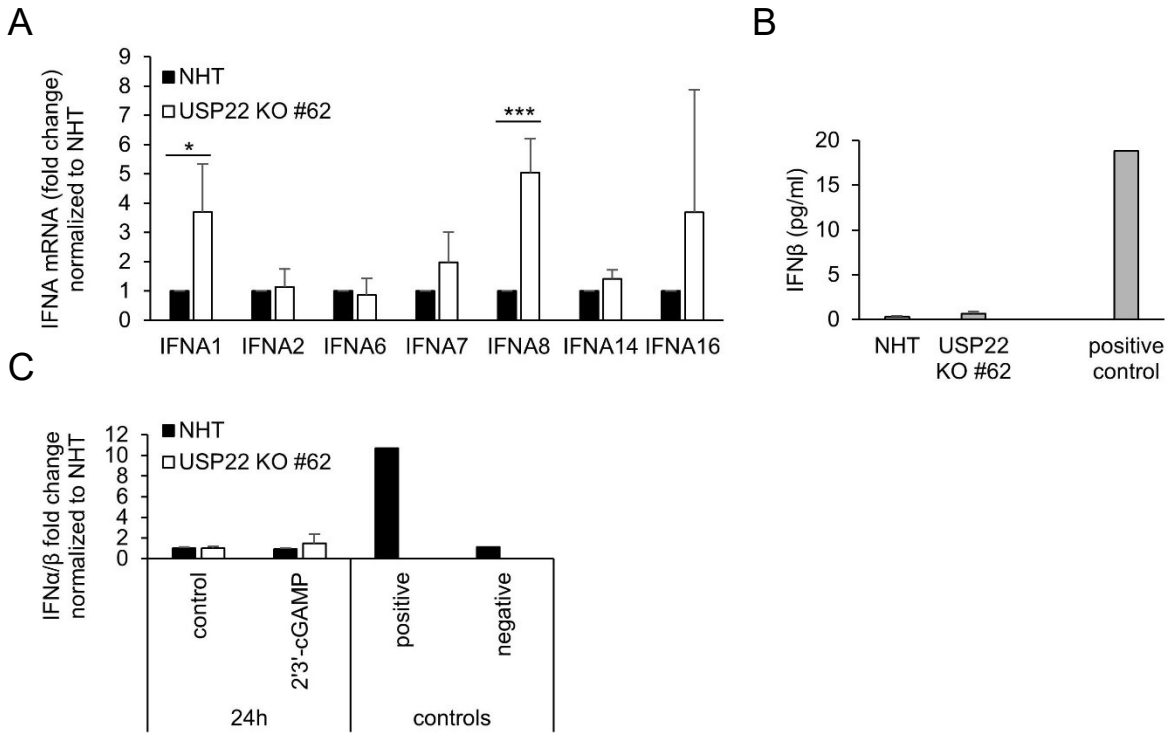

Figure 13: In-depth analysis of type I IFN expression. A. mRNA levels of IFNα isoforms were assessed using qRT-PCR in HT-29 NHT and USP22 KO cells and presented as x-fold mRNA expression compared to NHT. Mean and SD of four independent experiments in triplicate are shown. *P < 0.05, ***P < 0.001. B. Basal levels of IFNβ in the supernatants of HT-29 NHT and USP22 KO cells were measured with ELISA, as well as supernatants of HT-29 USP22 KO cells that were incubated for 24 hours with 10 µg/ml 2'3'-cGAMP as a positive control for IFN expression. Mean and SD of three independent experiments measured in duplicate are shown. C. IFNα/β levels in the supernatant of unstimulated or 2'3'-cGAMP-treated (10 µg/ml for 24 hours) HT-29 NHT and USP22 KO cells were measured by luciferase assay and normalized to unstimulated levels in control cells. Mean and SD of three independent experiments are shown. Luciferase assay was performed in collaboration with Denisa Bojkova.

5.1.4 IFNL1 is the main regulated IFN contributing to the ISG signature observed in USP22 KO HT-29 cells

Based on the strong regulation of IFNL1 mediated by USP22 that was observed in HT-29 cells in the FACS-based cytokine screen, we further analyzed USP22-dependent changes in the expression and secretion of type III IFNs (Figure 14). Increased basal and 2'3'-cGAMP-induced levels of IFNλ were detected in the supernatants of HT-29 USP22 KO cells compared to the control (Figure 14A). In addition, loss of USP22 increased IFNL1 mRNA expression (Figure 14B). Furthermore, inhibition of the type I IFN receptor IFNAR2 did not affect USP22-induced STAT1 phosphorylation (Figure 14C), suggesting that IFNλs are the main IFNs that contribute to the induction of ISG expression and STAT1 activation observed in HT-29 USP22 KO cells. Interestingly, when comparing the response of USP22 KO and control cells to treatment with type I, II or III IFNs, the strongest difference in induction of the ISGs OAS3 and IRF9 between NHT and USP22 KO cells was observed after treatment with IFNλ (Figure 14D and E), highlighting the important role of USP22 in the regulation of IFNλ signaling.

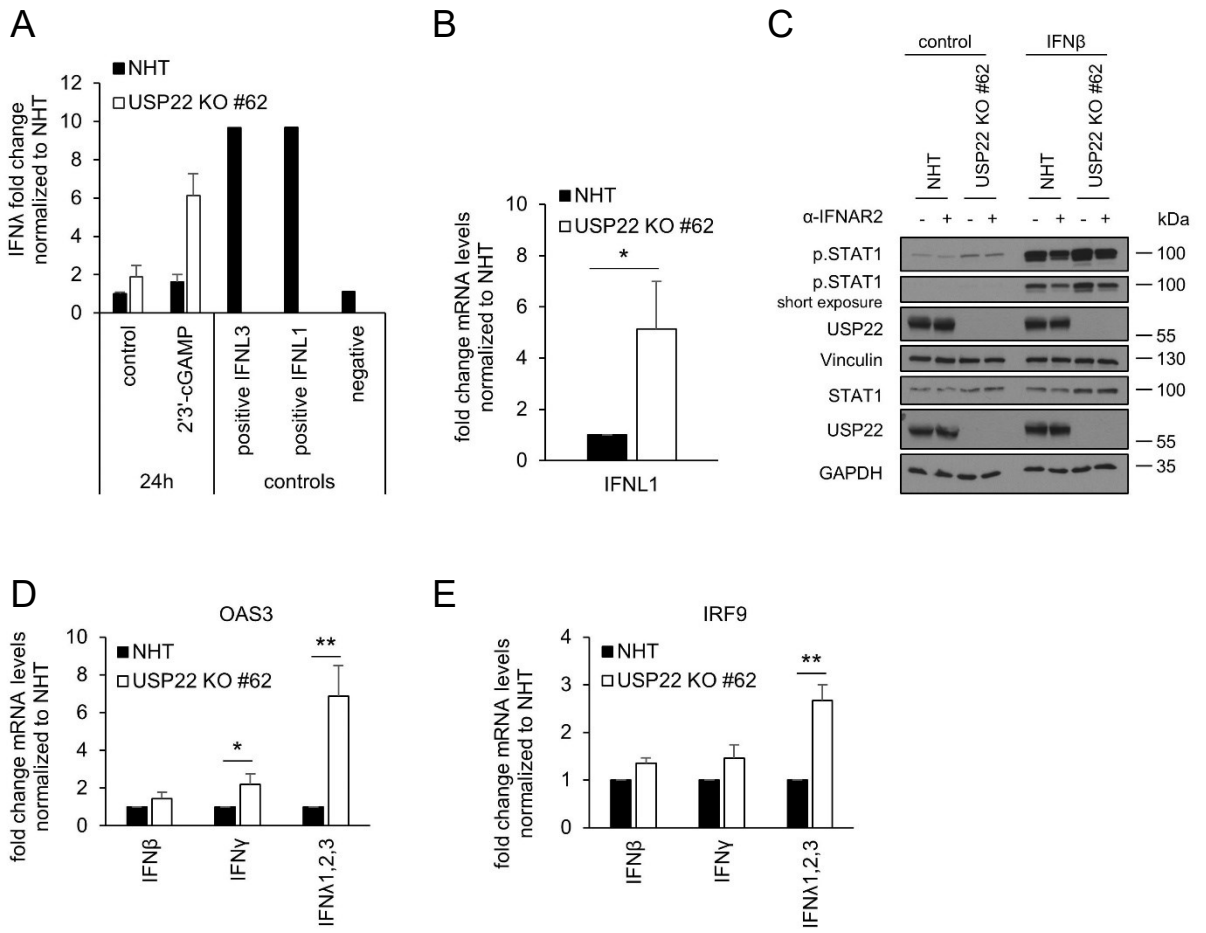

Figure 14: IFNλ is the main regulated IFN contributing to the ISG signature of USP22 KO HT-29 cells. A. IFNλ levels in supernatants of NHT and USP22 KO HT-29 cells were assessed using luciferase assays at basal levels and 24 hours after stimulation with 10 µg/ml 2'3'-cGAMP. IFN levels were normalized to unstimulated control cells and mean and SD of three independent experiments are shown. Luciferase assay was performed in collaboration with Denisa Bojkova. B. Basal mRNA expression levels of IFNL1 were assessed using qRT-PCR in control and USP22 KO HT-29 cells and presented as x-fold mRNA expression compared to NHT. Mean and SD of three independent experiments in triplicate are shown. *P < 0.05. C. Phosphorylated and total levels of STAT1 were analyzed in HT-29 NHT and USP22 KO cells using Western blotting after 24 hours of incubation with 1 µg/ml IFNAR2 blocking antibody. As positive control for STAT1 activation, cells were treated for 1 hour with IFNAR2 blocking antibody before incubation with 0.05 ng/ml IFNβ for 1 hour. Vinculin and GAPDH were used as a loading control. D. E. HT-29 NHT and USP22 KO cells were incubated with 10 ng/ml IFNβ, 10 ng/ml IFNγ or 300 ng/ml IFNλ1/2/3. Changes in OAS3 (D) and IRF9 (E) mRNA expression after 12 hours of treatment with IFNβ, IFNγ and IFNλ were assessed with qRT-PCR. The mRNA expression levels are presented as x-fold change and normalized to expression levels of IFNβ-, IFNγ- or IFNλ-stimulated NHT cells, respectively. Mean and SD of three independent experiments in triplicate are shown. *P < 0.05; **P < 0.01.

5.1.5 Knockout of PRRs does not restore USP22-mediated changes in STAT1 signaling

We have shown that depletion of USP22 in HT-29 cells is accompanied by the specific upregulation of genes involved in IFN and immune signaling pathways. As first-in-line immune signaling molecules, the pattern-recognition receptors RIG-I, MDA5 and TLR3 specifically detect pathogenic threats, such as viral dsRNA and dsDNA, in the cytosol and endosomal compartments and activate IFN signaling and strong antiviral responses. RIG-I, MDA5 and

TLR3 protein levels were increased in HT-29 USP22 KO cells compared to control cells (Figure 15).

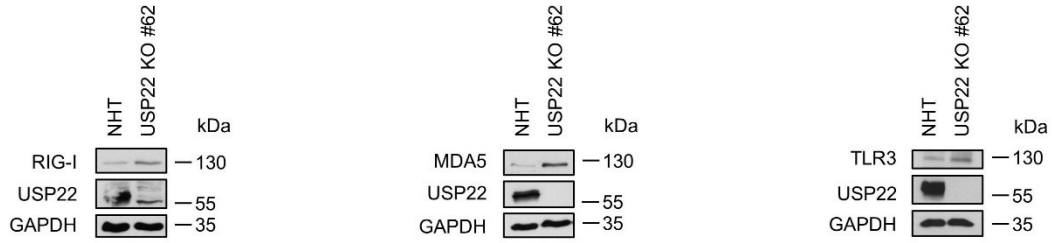

Figure 15: Expression of PRRs upon USP22 KO. Basal protein levels of RIG-I, MDA5, TLR3, and USP22 were analyzed in HT-29 NHT and USP22 KO cells using Western blotting, GAPDH served as loading control.

Using CRISPR/Cas9 technology, expression of RIG-I (DDX58), MDA5 (IFIH1) or TLR3 was ablated in NHT control cells and USP22 KO clone #62 to investigate their contribution to the USP22-mediated IFN signature. Although KO of the respective PRRs was successful, as confirmed by Western blot analysis, neither the observed elevated levels of STAT1 phosphorylation nor ISG56 expression in HT-29 USP22 KO cells could be reduced upon additional knockout of RIG-I, MDA5 or TLR3 (Figure 16A, B and C). Interestingly, in TLR3-USP22 dKO cells, STAT1 phosphorylation and ISG56 expression were even increased, suggesting a further regulatory role of USP22 on TLR3-mediated signaling (Figure 16C).

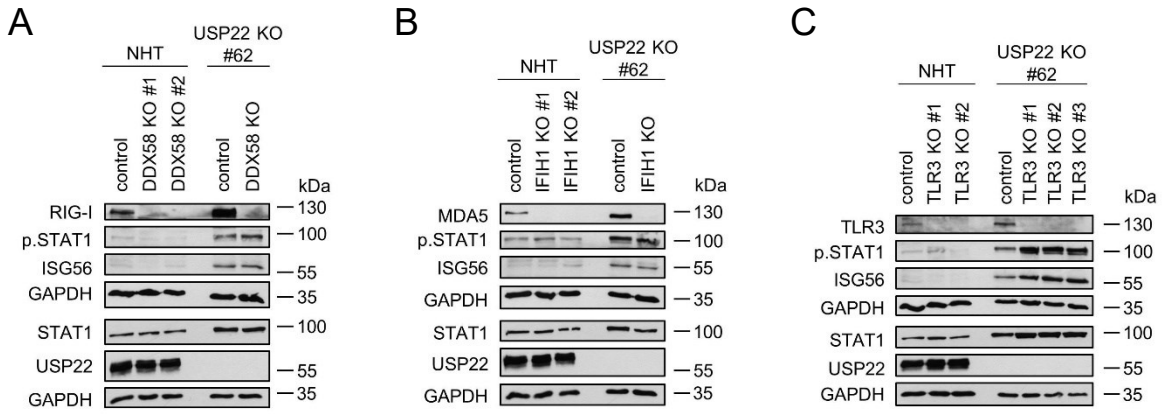

Figure 16: Assessment of IFN signaling in CRISPR/Cas9-mediated KO of PRRs in HT-29 USP22 KO cells. A. Protein expression of basal RIG-I, phosphorylated and total STAT1, ISG56 and USP22 levels in control, USP22 KO HT-29 cells (USP22 KO #62) as well as two NHT-control and one USP22-DDX58 dKO HT-29 single clones was assessed using Western blotting. GAPDH served as loading control. B: idem as A, analysis of MDA5 expression in two NHT control-IFIH1 KO HT-29 single clone and polyclonal USP22-IFIH1 dKO cells. C: idem as A, analysis of TLR3 expression in two NHT-TLR3 KO single clone and three USP22-TLR3 dKO single clone HT-29 cells.

Although CRISPR/Cas9-mediated depletion of the PRRs RIG-I, MDA5 or TLR3 failed to reduce STAT1 phosphorylation and ISG expression, it cannot be excluded that these PRRs act redundantly, or that additional PRRs are regulated by USP22 and contribute to the ISG

signature of USP22 KO HT-29 cells. To address this issue, HT-29 NHT and USP22 KO cells were stimulated with polyinosinic:polycytidylic acid (poly(I:C)), a synthetic dsRNA analog that activates TLR3, RIG-I, and MDA5, or with interferon-stimulatory DNA (ISD), a *Listeria monocytogenes* 45-bp non-CpG oligomer, a ligand for STING-TBK1-IRF3 activation [154, 276] (Figure 17A-C). Interestingly, whereas poly(I:C) treatment induced a strong increase in total and phosphorylated levels of STAT1 in both NHT and USP22 KO cells, treatment with the STING activator ISD specifically increased STAT1 expression and phosphorylation in USP22 KO cells, but not in NHT cells (Figure 17A). In all cases, STAT1 phosphorylation was accompanied by an upregulation of the ISGs STAT1 and RIG-I, whereas treatment with ISD specifically led to the activation of STING (Figure 17A), suggesting USP22 as a specific regulator of STING signaling. ISD-mediated mRNA upregulation of the representative ISGs OAS3 and IRF9 in HT-29 USP22 KO cells, but not in NHT cells (Figure 17B), underlines the importance of USP22 in the mediation of STING signaling. Interestingly, both mRNA levels and protein expression of STING were increased in HT-29 USP22 KO cells, compared to NHT cells (Figure 17A and C). Basal STING protein levels were also increased in HCoEpiC primary human colon epithelial cells upon RNAi-mediated transient depletion of USP22 (Figure 17D) and CRISPR/Cas9-mediated USP22 KO (Figure 17E).

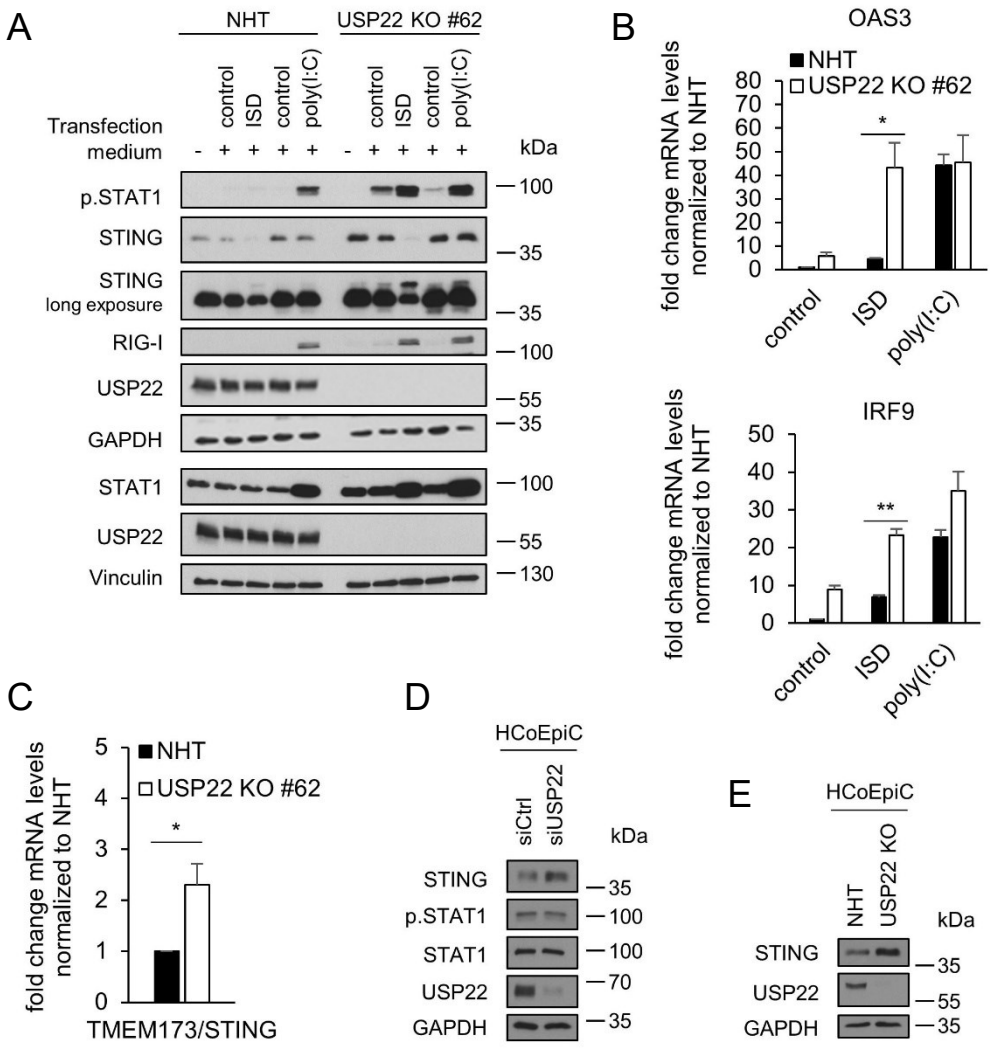

Figure 17: Loss of USP22 positively regulates STING signaling and expression in hIECs. A. Levels of phosphorylated and total STAT1, STING, RIG-I and USP22 were assessed with Western blotting in HT-29 NHT and USP22 KO cells after transfection with transfection reagent alone (control) or with 2 µg/well ISD or poly(I:C) for 24 hours. GAPDH and Vinculin were used as loading controls. B. Treated as described for A, OAS3 and IRF9 mRNA expression levels were measured after 24 hours in HT-29 NHT and USP22 KO cells. Fold change mRNA levels were normalized to mRNA expression of NHT cells treated with transfection reagent. Mean and SD of three independent experiments in triplicate are shown. *P < 0.05; **P < 0.01. C. Basal mRNA expression levels of TMEM173/STING in HT-29 NHT and USP22 KO cells were assessed with qRT-PCR and are presented as x-fold change normalized to NHT. Mean and SD of three independent experiments in triplicate are shown. *P < 0.05. D. Phosphorylated and total levels of STAT1, STING and USP22 expression in HCoEpiC cells were assessed with Western blotting upon RNAi-mediated silencing of USP22 and a non-silencing control (siCtrl) for 96 hours (final siRNA concentration of 125 nM for each condition). GAPDH was used as a loading control. E. Basal expression of STING and USP22 was analyzed with Western blotting in CRISPR/Cas9-generated control and USP22 KO HCoEpiC cells. GAPDH was used as a loading control.

5.1.6 Investigation of self-DNA as activator of IFN signaling in USP22-deficient cells

In addition to activation upon pathogenic threats, IFNs can be expressed upon recognition of self-DNA by PRRs, including cGAS-STING. Self-DNA, which can result from DNA damage, double-strand breaks or leakage of mitochondrial DNA into the cytosol, leads to the induction of IFNα and IFNλ through NF-κB signaling [277], and may explain the elevated levels of STING

in USP22 KO cells. Interestingly, USP22 has also been described to regulate the DNA damage response by regulating classical non-homologous end joining and V(D)J recombination [278] and by promoting γH2AX formation after irradiation [279]. However, no increases in γH2AX levels could be observed in USP22 KO cells compared to NHT (Figure 18A), despite increased activation of both canonical and non-canonical NF-κB signaling (Figure 18B). Interestingly, the mitochondrial membrane potential, an indicator of mitochondrial homeostasis, was decreased in USP22 KO HT-29 cells compared to control cells (Figure 18C), possibly facilitating leakage of mitochondrial DNA into the cytosol, activation of PRRs and the induction of IFN expression. However, siRNA-mediated knockdown of the mitochondrial (mt) DNA-binding protein mitochondrial transcription factor A (TFAM) that induces aberrant mtDNA packaging, leakage of mtDNA into the cytosol and induction of ISG expression, as described in other studies [280], does not induce increases in STAT1 phosphorylation (Figure 18D). At present, the potential contribution of mitochondrial DNA to the elevated ISG and IFN expression in USP22 KO HT-29 cells remain subject of further research.

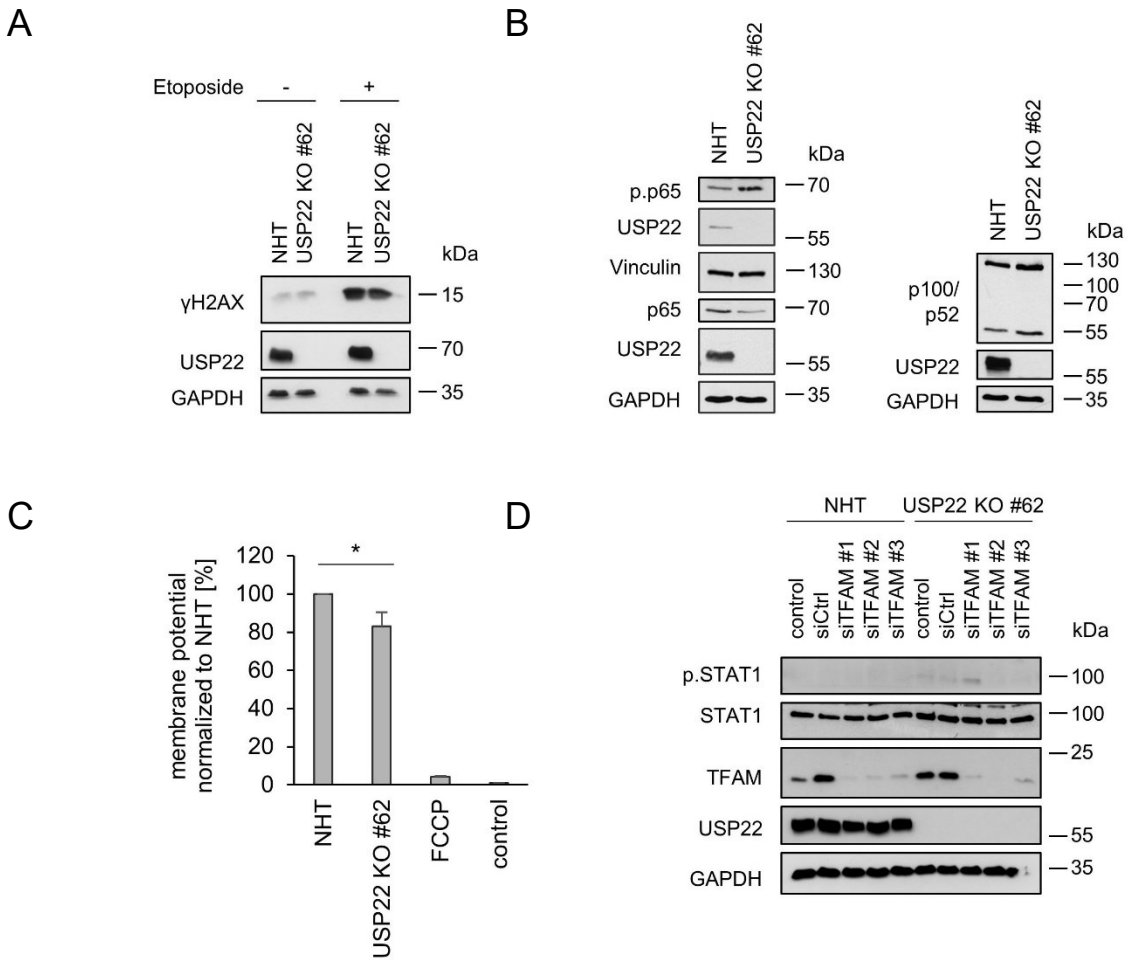

Figure 18: The role of alternative IFN-inducing intracellular processes. A. Basal expression levels of γH2AX and USP22 were analyzed with Western blotting in HT-29 NHT and USP22 KO cells. As a positive control, cells were additionally treated with 100 µM etoposide for 2 hours to induce DNA damage and H2AX phosphorylation. GAPDH was used as a loading control. B. Basal phosphorylated and total

levels of the NF-κB signaling proteins p65 and of p100/p52, as well as USP22, were analyzed with Western blotting in HT-29 NHT and USP22 KO cells. Vinculin and GAPDH served as loading controls. C. Mitochondrial membrane potential of HT-29 NHT and USP22 KO cells was measured with TMRM staining. As a positive control, cells were treated with 100 µM FCCP 20 minutes before analysis. TMRM-negative cells were used as a negative control. Mitochondrial membrane potential is shown as percentage of signal measured in NHT cells as mean and SD of three independent experiments. *P < 0.05. D. HT-29 NHT and USP22 KO cells were subjected to RNAi-mediated silencing of TFAM using three TFAM-specific siRNA constructs (#1-3, 20 nM each), as well as a siRNA control (siCtrl) for 48 hours. Protein levels of phosphorylated and total STAT1, TFAM and USP22 were analyzed with Western blotting, and GAPDH was used as a loading control.

5.1.7 USP22 regulates type III IFN signaling via STING

In the absence of DNA damage or cytosolic leakage of mitochondrial DNA that could potentially explain the observed IFN signature of USP22 KO cells, we further focused on the role of STING in USP22-induced type III IFN signaling. To this end, we used CRISPR/Cas9 to generate HT-29 NHT-STING KO and USP22-STING dKO cells. USP22-STING dKO in HT-29 cells reduced STAT1 phosphorylation and total STAT1 levels to levels comparable to NHT cells (Figure 19A). Furthermore, USP22-mediated upregulation of the ISGs USP18, OAS3, IRF9, BST2 and IFIT1 was reversed upon additional STING KO in HT-29 cells (Figure 19B). USP22-STING dKO also reduced the USP22-mediated increase in IFNL1 mRNA expression, while IFNA and IFNB mRNA expression levels remained largely unchanged (Figure 19C). These results support the important regulatory role of USP22 in STING-mediated ISG induction and type III IFN signaling in HT-29 cells.

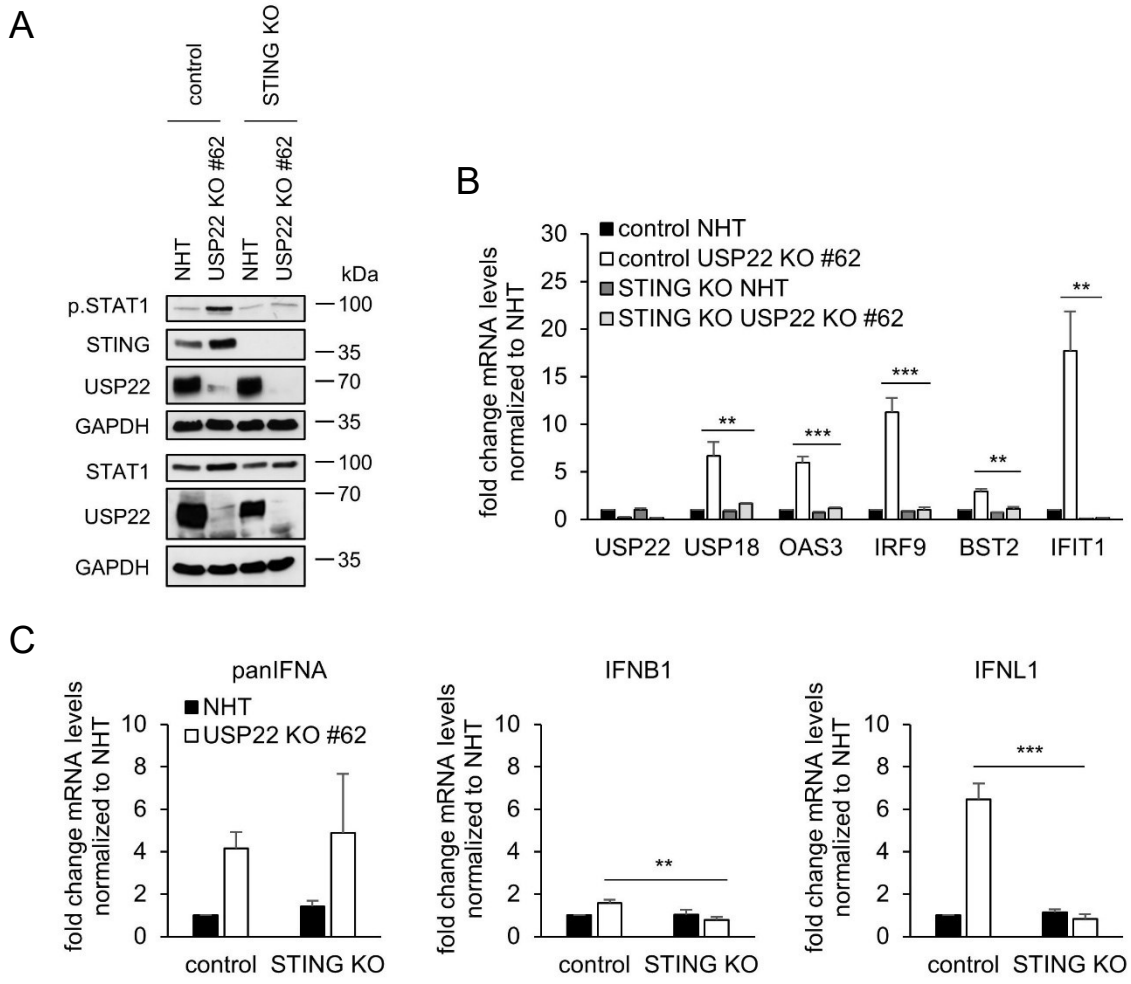

Figure 19: STING is essential for USP22-dependent type III IFN signatures. A. HT-29 NHT and USP22 KO cells were subjected to CRISPR/Cas9-mediated depletion of USP22 and analyzed for expression of STING, USP22, and total and phosphorylated levels of STAT1. GAPDH was used as a loading control. B. Basal mRNA levels of USP22, USP18, OAS3, IRF9, BST2 and IFIT1 in HT-29 NHT and USP22 KO as well as NHT-STING KO and USP22-STING dKO cells were assessed with qRT-PCR and presented as x-fold change normalized to NHT. Mean and SD of three independent experiments in triplicate are shown. **P < 0.01; ***P < 0.001. C. Basal panIFNA, IFNB1 and IFNL1 mRNA expression levels of HT-29 NHT, USP22 KO, NHT-STING KO and USP22-STING dKO cells were assessed with qRT-PCR and presented as x-fold change normalized to NHT. Mean and SD of three independent experiments in triplicate are shown. **P < 0.01; ***P < 0.001.

5.1.8 USP22 is a negative regulator of STING activation and ubiquitylation

The selective induction of ISG expression and STAT1 activation in USP22 KO cells upon stimulation with ISD, as well as the reversal of IFNL1 expression in USP22-STING dKO HT-29 cells, suggests an important role for USP22 in the negative regulation of STING signaling and IFNλ induction. However, it is unclear how USP22 regulates STING function. To investigate the impact of USP22 loss on STING-mediated signaling, HT-29 NHT and USP22 KO cells were treated with the STING agonist 2'3'-cGAMP. STING agonism resulted in faster, stronger and more prolonged activation and phosphorylation of STING, TBK1 and IRF3 in USP22 KO cells compared to NHT cells (Figure 20A). To test the generality of USP22-mediated regulation of STING, HeLa NHT and USP22 KO cells were subjected to treatment

with 2’3’-cGAMP or diABZI, a diamidobenzimidazole STING agonist, both of which induced a stronger and more prolonged STAT1 response and activation of STING in USP22 KO cells compared to control cells (Figure 20B,C). In addition, while STING agonism increased the expression of IFNA, IFNB and IFNL1 in both HT-29 NHT and USP22 KO cells, we detected the strongest increase in IFNL1 mRNA expression in USP22 KO cells (Figure 20D), contributing to the observation that USP22 specifically regulates IFNL1 expression via STING.

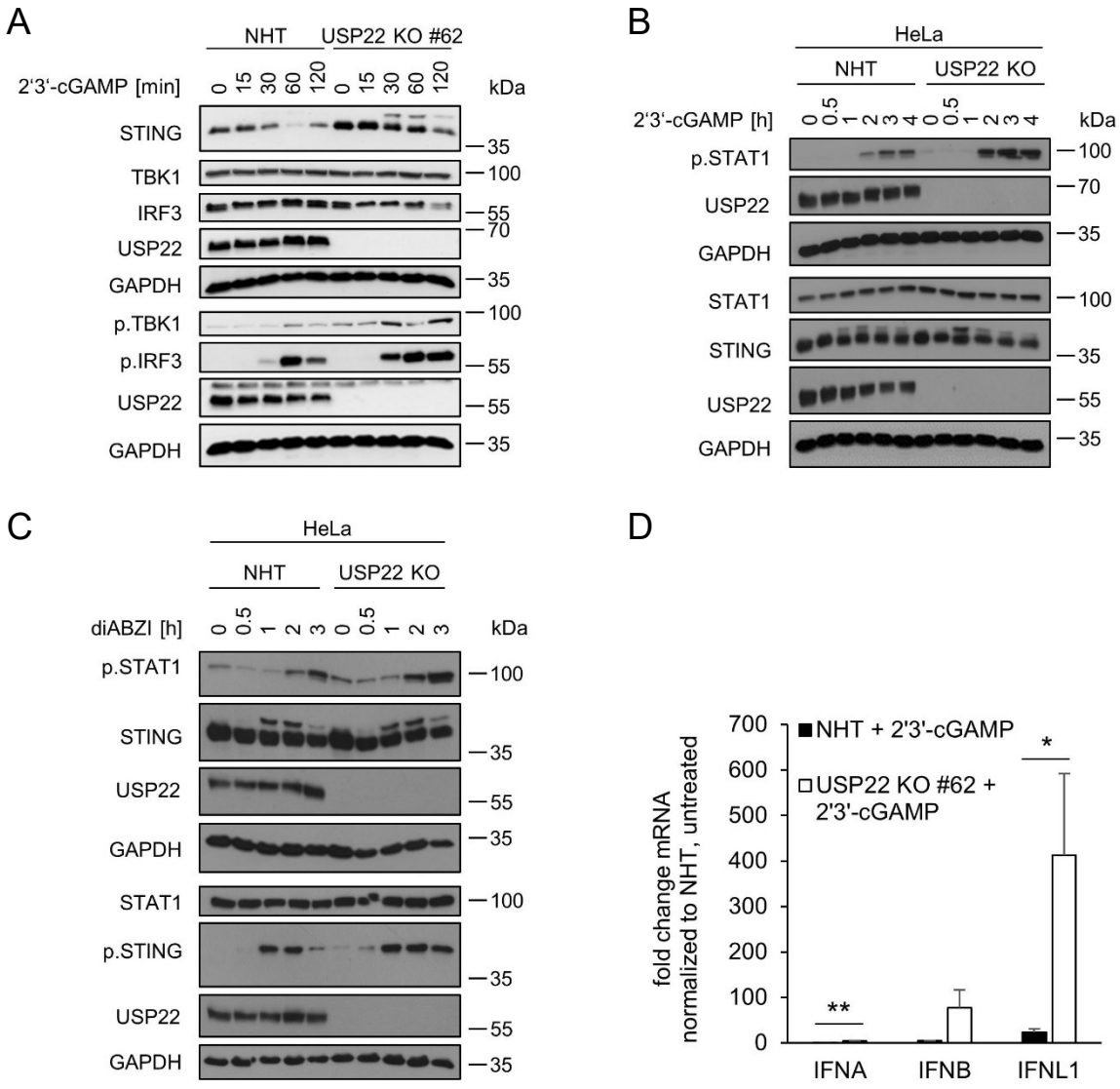

Figure 20: STING signaling and IFNL1 induction are increased upon USP22 KO in HT-29 and HeLa cells. A. HT-29 NHT and USP22 KO cells were analyzed for expression levels of STING, total and phosphorylated TBK1, total and phosphorylated IRF3, and USP22 with Western blotting upon treatment with 10 µg/ml 2’3’-cGAMP for the indicated time points. GAPDH was used as a loading control. B. HeLa NHT and USP22 KO cells were analyzed for expression levels of phosphorylated and total STAT1, STING and USP22 after treatment with 10 µg/ml 2’3’-cGAMP for the indicated time points. GAPDH was used as loading control C. HeLa NHT and USP22 KO cells were treated with 1 µM diABZI for indicated time points and analyzed for expression levels of total and phosphorylated STAT1, total and phosphorylated levels of STING and USP22 with Western blotting. GAPDH was used as a loading control. D. IFNA, IFNB, and IFNL1 mRNA expression levels of HT-29 NHT and USP22 KO cells were analyzed with qRT-PCR after treatment with 10 µg/ml 2’3’-cGAMP for 3 hours. Gene expression is

presented as x-fold mRNA expression compared to unstimulated NHT. Mean and SD of three independent experiments in triplicate are shown. *P < 0.05; **P < 0.01.

In addition, HT-29 and HeLa USP22 KO cells showed an increased response to different concentrations of 2'3'-cGAMP compared to NHT cells, supporting previous results (Figure 21A and B).

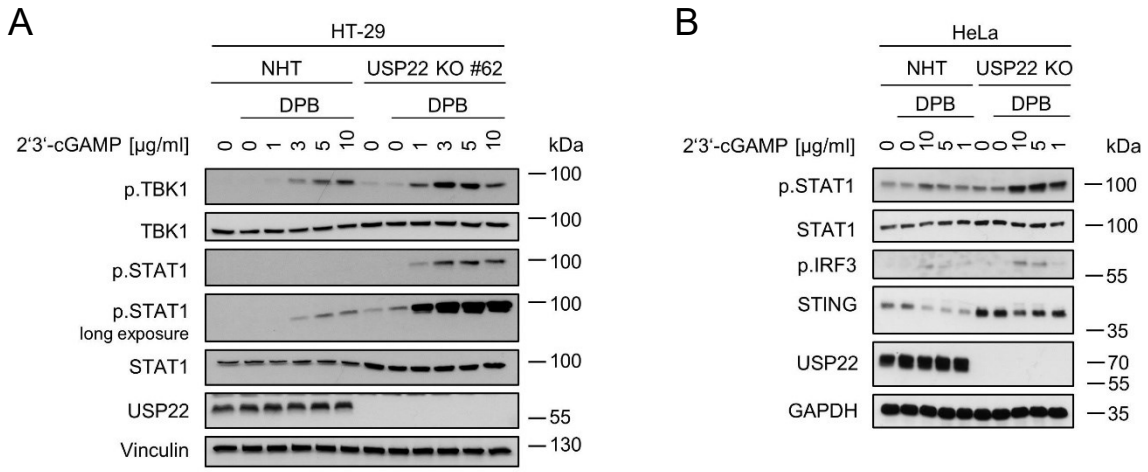

Figure 21: Preliminary assessment of concentration-dependent activation of STING in HT-29 and HeLa cells. HT-29 (A) and HeLa (B) NHT and USP22 KO cells were subjected to treatment with digitonin permeabilization buffer (DPB) in combination with increasing concentrations of 2'3'-cGAMP for 2 hours. A. Expression levels of total and phosphorylated TBK1 and STAT1 as well as USP22 were analyzed with Western blotting, and Vinculin was used as a loading control. Experiment was performed once. Only one representative blot of USP22 and Vinculin is shown, although proteins were detected on separate membranes. B. Expression levels of total and phosphorylated STAT1, phosphorylated IRF3, STING and USP22 were analyzed with Western blotting. GAPDH was used as a loading control, and only one representative blot of USP22 and GAPDH are shown, whereas other proteins were detected on separate membranes. Experiment was performed once.

Since STING itself is an ISG, there is a possibility that the increased expression of STING in USP22 KO cells is caused by a positive feedback loop through constitutive IFN signaling and the subsequent increase in ISG expression. To test the possibility of auto- and paracrine upregulation of STING by IFNs, HT-29 NHT and USP22 KO cells were treated with the JAK/STAT inhibitor ruxolitinib. While the decrease in phosphorylated STAT1 demonstrated the functionality of JAK/STAT1 inhibition, both STING protein and mRNA levels were actually increased after ruxolitinib treatment compared to controls (Figure 22A and B), making any form of IFN-dependent activation of STING expression upon USP22 KO unlikely. Interestingly, elevated mRNA expression of STAT1 in USP22 KO cells could be reversed by JAK/STAT inhibition (Figure 22C), whereas elevated mRNA levels of OAS3 and ISG56 in USP22 KO cells remained largely unchanged (Figure 22D and E).

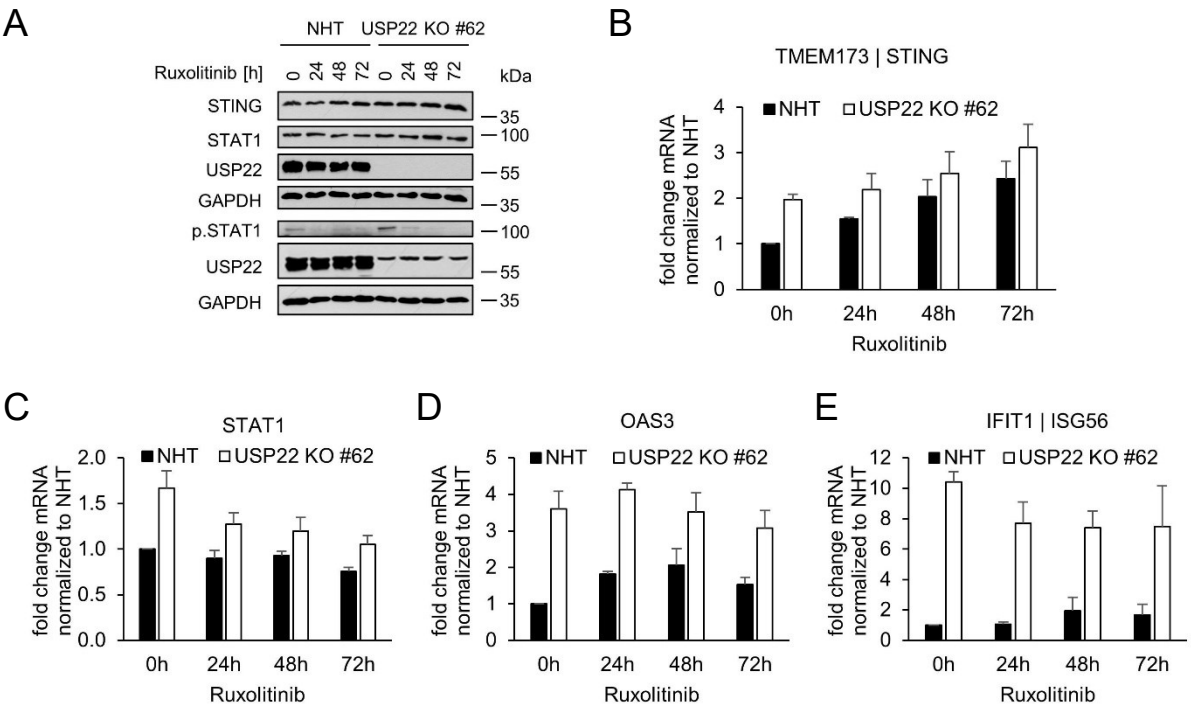

Figure 22: Inhibition of JAK/STAT signaling does not reverse USP22-induced STING expression. A. HT-29 NHT and USP22 cells were subjected to treatment with 5 µM JAK/STAT inhibitor ruxolitinib for 24, 48 or 72 hours. Expression of STING, total and phosphorylated STAT1, and USP22 was analyzed with Western blotting. GAPDH served as a loading control. B-E. Ruxolitinib-treated (5 µM) HT-29 NHT and USP22 KO cells were analyzed for expression of TMEM173/STING (B), STAT1 (C), OAS3 (D) and IFIT1/ISG56 (E) mRNA after 24, 48 and 72 hours. Gene expression is presented as x-fold mRNA expression compared to NHT. Mean and SD of three independent experiments in triplicate are shown.

Surprisingly, while RIG-I mRNA expression in USP22 KO cells remained largely unchanged upon JAK/STAT inhibition (Figure 23A), RIG-I protein levels still increased (Figure 23B). In NHT cells, RIG-I mRNA and protein levels increased continuously over time (Figure 23A and B). Interestingly, USP22-STING dKO could reverse RIG-I mRNA expression to the level of NHT cells (Figure 23C), suggesting another USP22-mediated regulatory mechanism on RIG-I expression and stability.

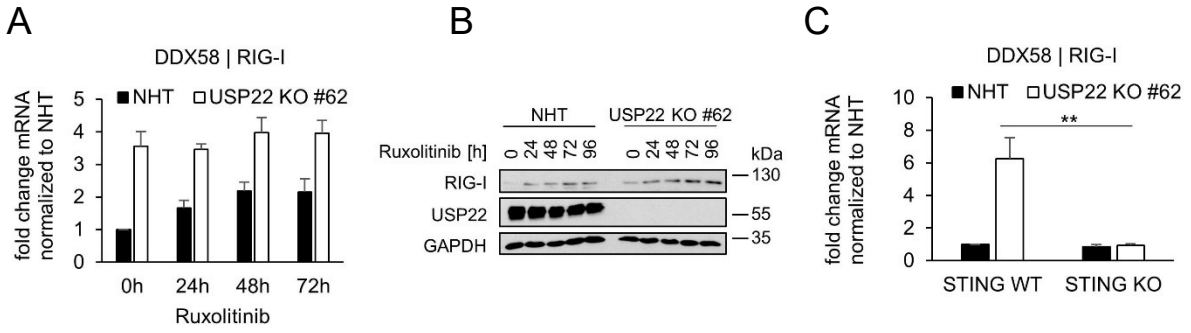

Figure 23: RIG-I expression is differentially regulated by JAK/STAT inhibition and is dependent on STING. A. Ruxolitinib-treated (5 µM) HT-29 NHT and USP22 KO cells were analyzed for expression of RIG-I (DDX58) mRNA after 24, 48 and 72 hours. Gene expression is presented as x-fold mRNA expression compared to NHT. Mean and SD of three independent experiments in triplicate are shown.

B. HT-29 NHT and USP22 KO cells were analyzed for RIG-I and USP22 protein expression with Western blotting 24, 48, 72 and 96 hours after treatment with 5 µM of JAK/STAT inhibitor ruxolitinib. GAPDH was used as a loading control. C. Basal RIG-I mRNA expression was assessed in HT-29 NHT, USP22 KO, NHT-STING KO and USP22-STING dKO cells. Gene expression is presented as x-fold mRNA expression compared to NHT. Mean and SD of three independent experiments in triplicate are shown. **P < 0.01.

The activation and stability of STING depends on the precise execution of post-translational modifications, mediated by several kinases and (de)ubiquitylases, as is reviewed in detail in Chapter 2.5. Indeed, treatment with the translational inhibitor cycloheximide (CHX) resulted in slightly more stabilized STING protein levels in USP22 KO cells compared to NHT control cells (Figure 24).

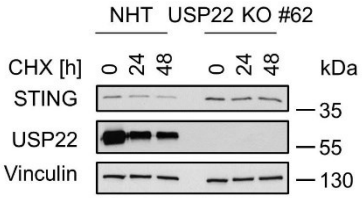

Figure 24: Analysis of STING stability. HT-29 NHT and USP22 KO cells were incubated with the translational inhibitor cycloheximide (CHX; 100 µg/ml) for 24 and 48 hours, and protein levels of STING and USP22 were analyzed with Western blotting. Vinculin served as a loading control.

Interestingly, the E3 ubiquitin ligase TRIM29 appeared among the genes regulated by USP22 KO in the RNA-sequencing analysis. TRIM29 targets STING for K48-linked ubiquitylation and degradation [206, 281]. TRIM29 protein levels were indeed decreased in HT-29 USP22 KO cells compared to NHT cells (Figure 25A), which could explain the increased STING stability observed in Figure 24. However, despite a marked reduction of TRIM29, no further increase in STING protein levels was observed in either NHT or USP22 KO cells (Figure 25B), making it unlikely that TRIM29 is involved in the USP22-mediated regulation of STING stability. Notably, total and phosphorylated levels of STAT1 were strongly increased after TRIM29 knockdown (Figure 25B).

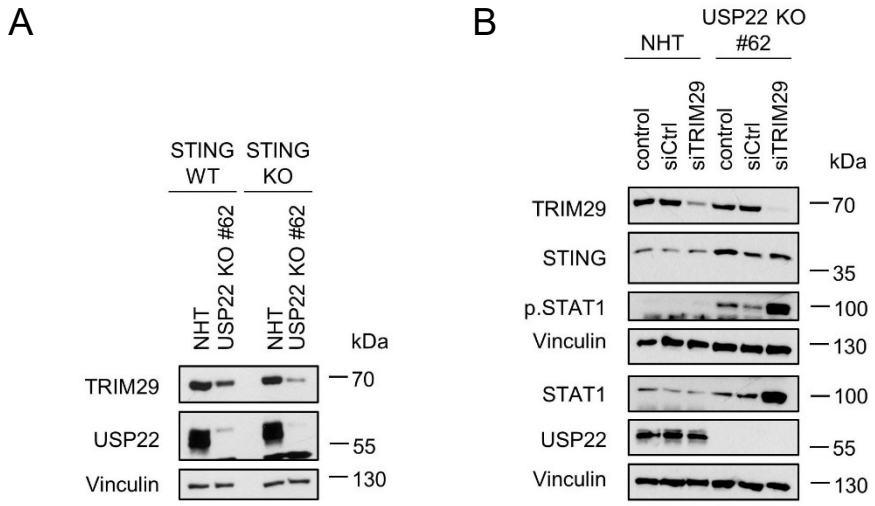

Figure 25: TRIM29 is positively regulated by USP22. A. Basal TRIM29 and USP22 protein expression levels were analyzed with Western blotting in HT-29 NHT and USP22 KO cells, as well as NHT-STING KO and USP22-STING dKO cells. Vinculin served as a loading control. B. Protein expression levels of TRIM29, STING, USP22 and total and phosphorylated STAT1 were analyzed with Western blotting after RNAi mediated silencing of TRIM29 or transfection with siRNA control (siCtrl) for 48 hours in HT-29 NHT and USP22 KO cells. Three constructs of TRIM29 siRNA were pooled to a total concentration of 40 nM. Vinculin was used as a loading control.

To further characterize USP22-mediated regulation on STING, tandem ubiquitin binding entity (TUBE) enrichments were performed in control and 2'3'-cGAMP treated HT-29 NHT and USP22 KO cells. Indeed, ubiquitylated STING was detected in all conditions, but enriched in unstimulated HT-29 USP22 KO cells compared to NHT cells (Figure 26). Treatment with 2'3'-cGAMP further increased the enrichment of ubiquitylated STING in both NHT and USP22 KO cells, with a stronger increase observed in USP22 KO cells (Figure 26). Taken together, these data suggest that USP22-mediated expression of type III IFN and several other ISGs may be predominantly regulated by an increase in activating and stabilizing STING ubiquitylation and only to a lesser extent by auto- or paracrine IFN priming.

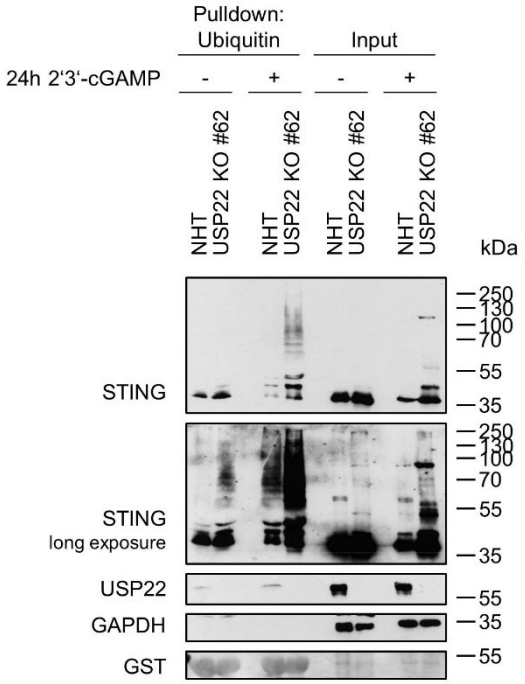

Figure 26: Loss of USP22 increases STING ubiquitylation. Ubiquitylated STING was enriched in control and 2'3'-cGAMP treated HT-29 NHT and USP22 KO cells (10 µg/ml, 24 h) using tandem ubiquitin binding entities (TUBE), followed by immunoprecipitation and analyzed with Western blotting. GAPDH served as loading control, and Ponceau S staining confirmed equal loading of GST-tagged TUBE beads.

5.1.9 USP22 KO in Caco-2 cells mediates IFN upregulation and SARS-CoV-2 resistance in a STING-dependent manner

STING is a known regulator of IFN signaling and is critical in mediating antiviral resistance. Moreover, both STING and type III IFNs have been described to control SARS-CoV-2 infection, but with effects ranging from poorer outcomes to antiviral failure [193, 282-284]. Most interestingly, USP22 has previously been described to confer resistance to viral infection but has also been implicated in the positive control of viral signaling [219, 223]. We therefore aimed to investigate the significance of USP22 and the resulting STING-mediated changes in type III and ISG expression for viral defense in hIECs in the context of SARS-CoV-2 infection. In line with previous observations, HT-29 cells could not be infected with SARS-CoV-2 [285] (data not shown). Therefore, we used CRISPR/Cas9 in the SARS-CoV-2-susceptible colon carcinoma cell line Caco-2 to generate USP22 KO and NHT control cells. Single USP22 KO clones were obtained by serial dilution, and clones #1 and #6 were selected for further experiments based on USP22 expression levels (Figure 27A).

USP22 depletion in Caco-2 cells was accompanied by increased STAT1 phosphorylation and STING expression (Figure 27A). In addition, mRNA expression of the representative antiviral ISGs IRF9 and OAS3 was upregulated in USP22 KO clones compared to both WT and NHT control cells (Figure 27B). Of the IFNs tested, only IFNL1 expression was increased upon

USP22 KO (Figure 27C), highlighting the important role of USP22 in regulating type III IFN signaling. USP22 KO also sensitized to diABZI-induced STING agonism, marked by increased activation of STAT1 signaling, as well as activation and degradation of STING, in USP22 KO Caco-2 cells compared to control cells (Figure 27D).

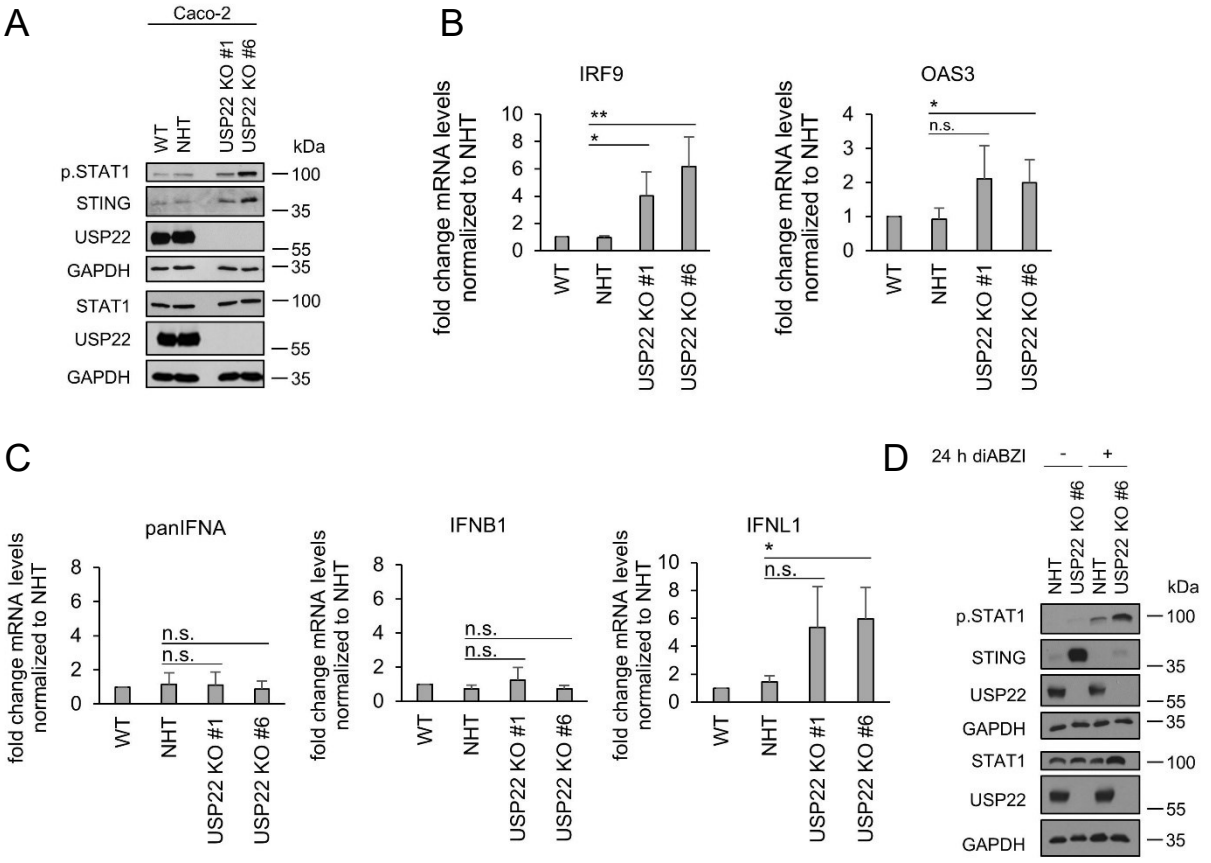

Figure 27: Loss of USP22 in Caco-2 cells increases ISG and IFNL1 expression and amplifies STING signaling. A. WT, CRISPR/Cas9-generated NHT control and CRISPR/Cas9-generated USP22 KO Caco-2 single clones (USP22 KO #1 and #6) were analyzed for expression levels of total and phosphorylated STAT1, STING, and USP22 with Western blotting. GAPDH was used as a loading control. B. WT, CRISPR/Cas9-generated NHT control and CRISPR/Cas9-generated USP22 KO Caco-2 single clones (USP22 KO #1 and #6) were analyzed for mRNA expression of IRF9 and OAS3 with qRT-PCR. Gene expression is presented as x-fold mRNA expression compared to NHT. Mean and SD of three independent experiments in triplicate are shown. *P < 0.05; **P < 0.01, n.s. not significant. C. Basal mRNA expression of panIFNA, IFNB1 and IFNL1 were analyzed in Caco-2 WT, NHT and USP22 KO clones #1 and #6 with qRT-PCR. Expression levels are presented as x-fold change compared to NHT. Mean and SD of four (IFNA, IFNB) or three (INFL1) independent experiments in triplicate are shown. *P < 0.05, n.s. not significant. D. Caco-2 NHT and USP22 clone #6 were subjected to treatment with STING agonist diABZI (1 µM) for 24 hours, followed by analysis of expression levels of total and phosphorylated STAT1, STING and USP22 with Western blotting. GAPDH was used as loading control.

The functional relevance of USP22-mediated changes in antiviral signaling was assessed by infection of Caco-2 NHT and USP22 KO cells with SARS-CoV-2 particles. Infected cells were fixed 24 hours after infection, and SARS-CoV-2 replication was quantified by immunofluorescence-staining of the SARS nucleocapsid protein. Indeed, the number of SARS-CoV-2-infected Caco-2 cells at 24 hours was greatly reduced upon loss of USP22 compared

to WT and NHT control cells (Figure 28A), accompanied by reduced SARS-CoV-2 genome copy number (Figure 28B) and reduced *de novo* infectious SARS-CoV-2 particles in the supernatant of Caco-2 USP22 KO cells at 6 and 24 hours after infection (Figure 28C).

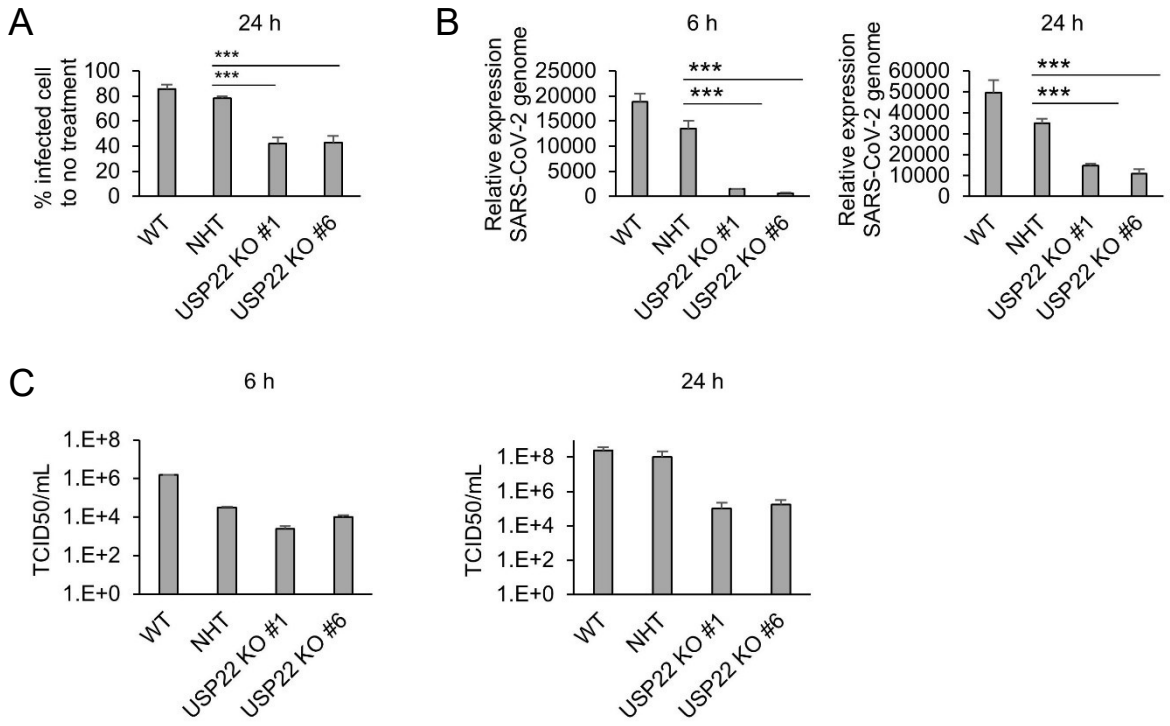

Figure 28: Loss of USP22 protects against SARS-CoV-2 infection in Caco-2 cells. A. Caco-2 WT, NHT and USP22 KO clones #1 and #6 were infected with SARS-CoV-2, stained for SARS-CoV-2 nucleocapsid protein at 24 hours post-infection (hpi) and number of infected cells was normalized against non-infected cells. Mean and SD of three independent experiments in triplicate are shown. ***P < 0.001. B. Relative SARS-CoV-2 genome expression of SARS-CoV-2-infected WT, control and USP22 KO Caco-2 cells (USP22 KO #1 and #6) at 6 hpi (left) and 24 hpi (right) was quantified with qRT-PCR, normalized against non-infected cells. Mean and SD of three independent experiments in triplicate are shown. ***P < 0.001. C. TCID50/ml of Caco-2 WT, NHT and USP22 KO cells was determined via titration on Vero cells 6 and 24 hours after infection with SARS-CoV-2. Mean and SD of three independent experiments in triplicate are shown. SARS-CoV-2 infections and related assays were performed by Megan Stanifer.

As demonstrated above, additional loss of STING restored USP22-mediated changes in antiviral signaling in HT-29 cells. To test whether this was also the case in Caco-2 cells, we generated NHT-STING KO and USP22-STING dKO Caco-2 cells. Intriguingly, additional loss of STING resulted in increased expression of the SARS-CoV-2 genome and increased release of infectious particles into the supernatant compared to USP22 KO Caco-2 cells (Figure 29A and B), confirming the importance of STING in the USP22-mediated regulation of antiviral signaling. In line with previous findings in HT-29, USP22-mediated upregulation of STAT1 phosphorylation was reduced by additional STING KO in Caco-2 cells (Figure 29C).

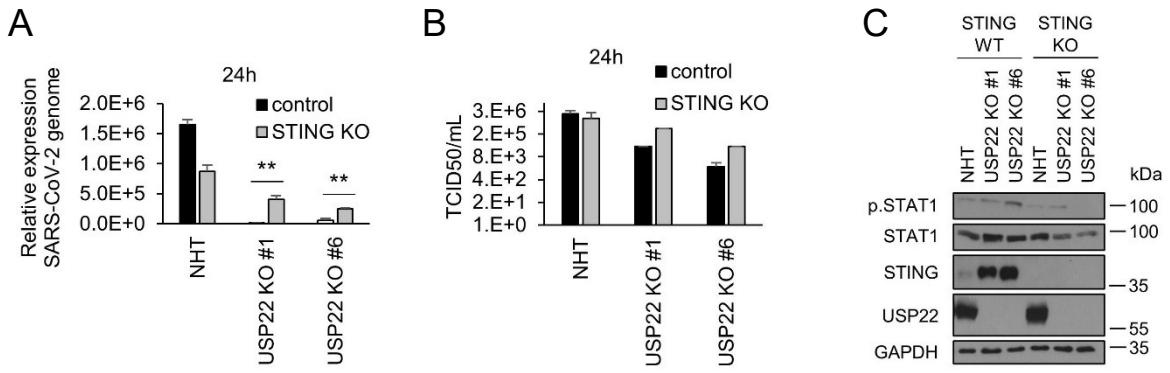

Figure 29: SARS-CoV-2 infection in Caco-2 USP22 KO cells is increased after additional KO of STING. Caco-2 NHT and USP22 KO clones #1 and #6 were subjected to CRISPR/Cas9-mediated depletion of STING. A. Caco-2 NHT, USP22 KO clones #1 and #6 as well as their respective STING dKOs were infected with SARS-CoV-2 and relative expression of SARS-CoV-2 genome was determined with qRT-PCR 24 hpi. Mean and SD of three independent experiments in triplicate are shown. **P < 0.005. B. Supernatant of SARS-CoV-2-infected Caco-2 NHT, USP22 KO clones #1 and #6 as well as their respective STING dKOs were titrated on Vero cells 24 hpi, and TCID50/ml was determined. Mean and SD of three independent experiments in triplicate are shown. C. Basal protein expression levels of total and phosphorylated STAT1, STING and USP22 were analyzed in Caco-2 NHT cells, USP22 KO clones #1 and #6 as well as their respective STING dKOs with Western blotting. GAPDH was used as a loading control. SARS-CoV-2 infections and related assays were performed by Megan Stanifer.

In accordance with reduced STAT1 phosphorylation, USP22-mediated upregulation of IFNL1 mRNA was restored in Caco-2 USP22-STING dKO cells compared to Caco-2 USP22 KO cells, whereas STING KO did not affect IFNB1 or IFNA mRNA expression (Figure 30). In line, IRF9 and OAS3 mRNA expression was restored after USP22-STING dKO in Caco-2 cells (Figure 30). Taken together, these results suggest USP22 as a critical regulator of SARS-CoV-2 infection, replication and *de novo* production of viral particles, an effect that could be partially attributed to USP22-mediated regulation of STING signaling.

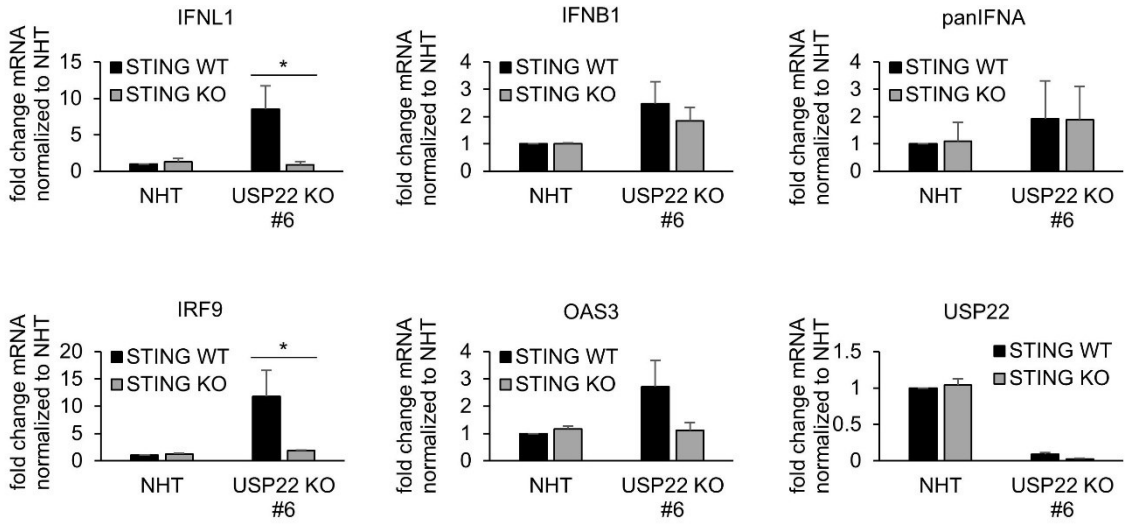

Figure 30: Additional KO of STING in Caco-2 USP22 KO cells reverses IFNL1 and ISG expression previously elevated by USP22 KO. Basal mRNA expression of the IFNs IFNL1, IFNB1 and total IFNA, the ISGs IRF9 and OAS3, and USP22 in Caco-2 NHT and USP22 KO (#6) cells was assessed with qRT-PCR. Expression levels are displayed as x-fold change mRNA normalized to Caco-2 NHT cells. Mean and SD of three independent experiments in triplicate are shown. *P < 0.05.

5.2 Part II: USP22 regulates IFN-induced necroptotic cell death

Induction of necroptosis in cancer cells has become a valuable tool to overcome primary or acquired treatment resistance. Since colon cancer is the second most fatal type of cancer with high relapse numbers despite initial remission, it is indispensable to find alternate treatments [286, 287]. Induction of necroptosis with TNFα, Smac mimetics and the pan-caspase inhibitor zVAD.fmk is a well-studied approach, however, treatment alternatives to TNFα such as administration of IFNs or activation of STING are promising emerging concepts to overcome treatment resistance and to additionally stimulate the tumor microenvironment for enhanced tumor clearance. The successful induction of apoptotic or necroptotic cell death using IFNs in combination with Smac mimetics was previously published in various cancer cell lines, including HT-29 [260, 288-291].

Findings presented in the first part of this thesis identified USP22 as an important regulator of IFN and STING signaling. Additionally, USP22 is described as part of an 11 gene signature that is associated with critical tumor progression and patient outcome and could therefore be vital to explore as an approach for cancer treatment [42]. Therefore, the aim of this part of the thesis is to understand the role of USP22 in IFN- and STING-mediated necroptosis.

5.2.1 USP22 deficiency promotes interferon-induced necroptotic cell death

IFNs have been previously used to induce necroptotic cell death [256, 288, 289, 291]. In light of the findings that loss of USP22 confers a state of elevated IFN signaling in hIECs, and previous studies described that priming with IFN sensitizes cells to necroptosis [292], we aimed to evaluate the ability of IFNs to stimulate cell death in HT-29 cells and to investigate effects of loss of USP22 during the process. To this end, HT-29 control and USP22 KO cells were incubated for 24 hours with IFNγ in the presence of the Smac mimetic BV6 (B) and zVAD.fmk (Z). Cell death was assessed by quantifying the uptake of propidium iodide (PI) by dying cells as a marker for membrane permeabilization and cell death, compared to the number of total cells stained by Hoechst 33342. To exclude any CRISPR/Cas9-mediated off-target effects on cell death, HT-29 wildtype (WT) cells were also included, as well as a USP22 KO single clone with approximately half the USP22 expression of WT cells (#8) and two full KO single clones (#16 and #62).

Indeed, when assessing the levels of cell death after 24 hours of IBZ treatment, all tested clones demonstrated a robust increase in PI-positive cells, with slightly increased cell death levels in USP22 KO cells compared to controls (Figure 31). Cell death could be prevented using inhibitors of the necroptotic proteins RIPK1 (Nec-1s) and RIPK3 (GSK’872), confirming necroptosis as mode of cell death (Figure 31).

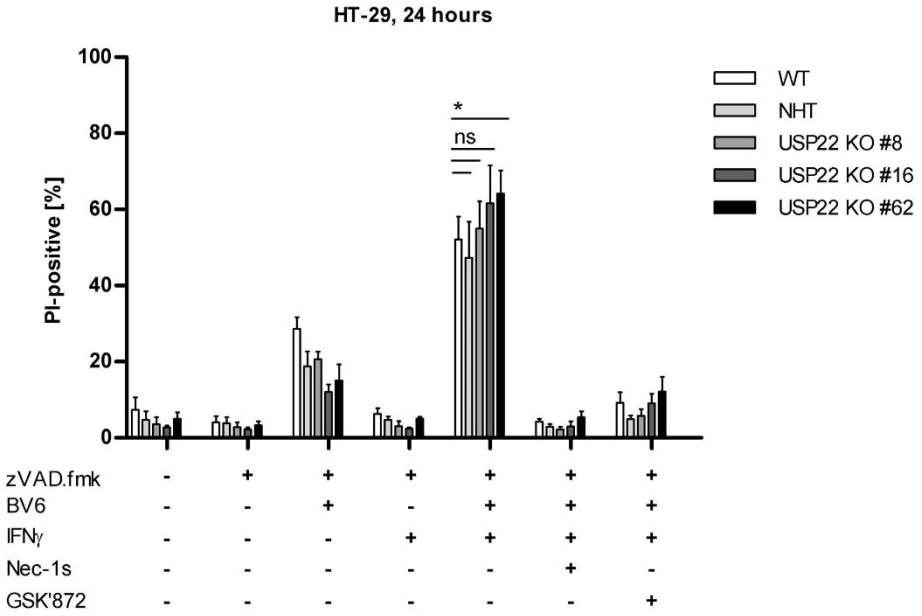

Figure 31: Treatment with IFNγ, BV6 and zVAD.fmk induces necroptosis in HT-29 cells. HT-29 control (WT, NHT) and USP22 KO single clone cells (#8: intermediate expression levels of USP22, #16, #62: full USP22 KO) were subjected to treatment with 1 ng/ml IFNγ, 0.5 µM BV6, 20 µM zVAD.fmk, 30 µM Nec-1s and 20 µM GSK'872 as indicated and amount of cell death was measured using fluorescence-based PI/Hoechst staining. Data is represented as mean and SD of three independent experiments performed in triplicates. *P < 0.05, ns: not significant.

To evaluate if the observed differences between control and USP22 KO cells were caused by USP22-dependent regulation of the kinetics of necroptotic cell death, we tested shorter incubation periods. Indeed, PI-positive USP22 KO cells were already detected between 6 and 12 hours after treatment, while control cells displayed a much slower increase in PI-positive cells, starting around 15 hours (Figure 32). Of note, USP22 KO clone #8, which comprises reduced USP22 expression levels, displayed cell death kinetics that lie between HT-29 WT and complete USP22 KO, revealing a gradual sensitivity towards IFN-induced necroptosis that is dependent on USP22 expression levels (Figure 32).

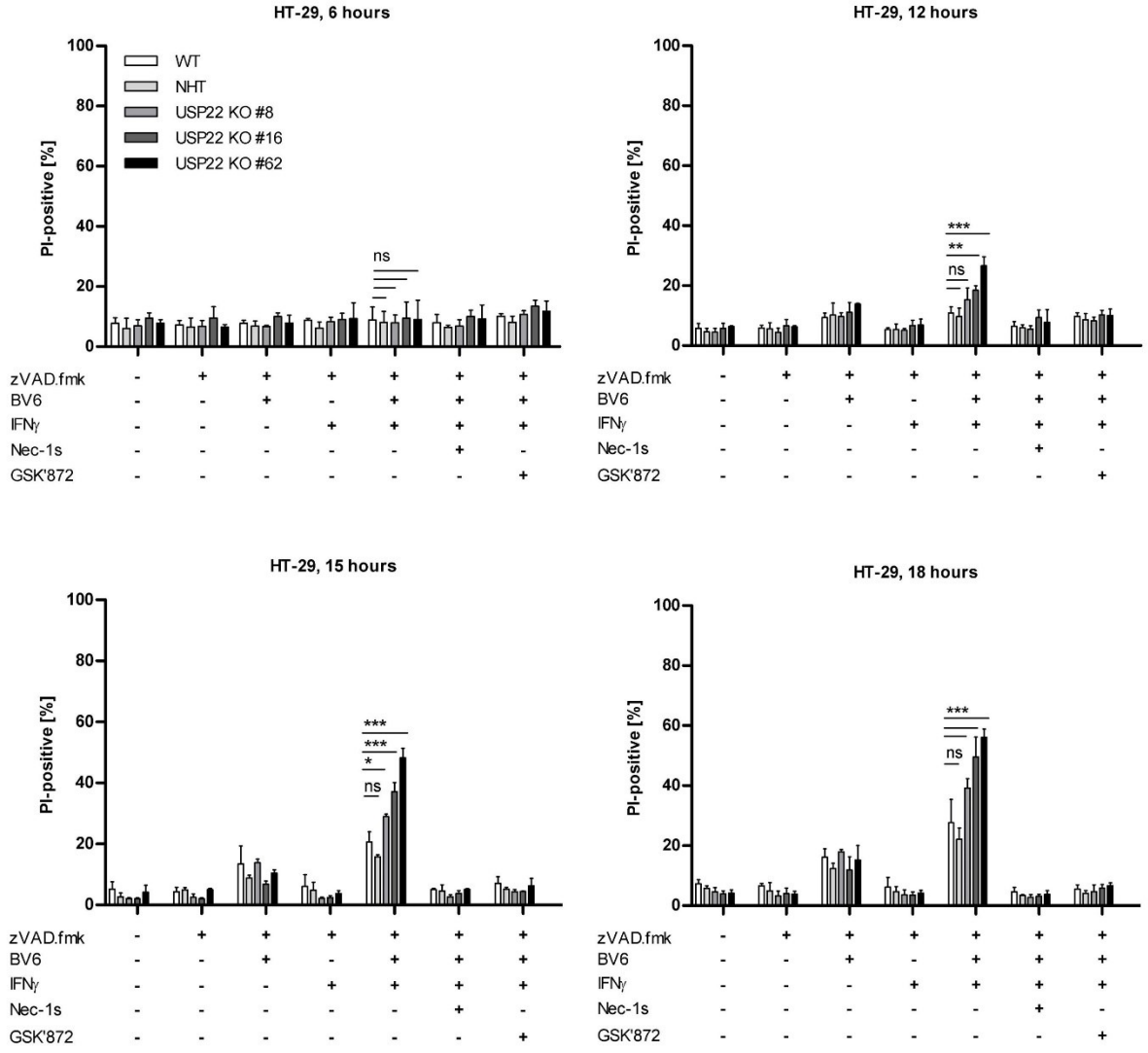

Figure 32: USP22-dependent kinetics of IFNγ-BV6-zVAD.fmk-induced necroptosis. Treatment with IFNγ, BV6 and zVAD.fmk induces necroptosis in HT-29 cells. HT-29 control (WT, NHT) and USP22 KO single clone cells (#8: intermediate expression levels of USP22, #16, #62: full USP22 KO) were subjected to treatment with 1 ng/ml IFNγ, 0.5 µM BV6, 20 µM zVAD.fmk, 30 µM Nec-1s and 20 µM GSK'872 as indicated and amount of cell death was measured using fluorescence-based PI/Hoechst staining after 6, 12, 15 or 18 hours. Data is represented as mean and SD of three independent experiments performed in triplicates. *P < 0.05, **P < 0.01, ***P < 0.001, ns: not significant.

5.2.2 Both type I and II IFNs induce USP22-regulated necroptosis

GO term analysis performed after RNA sequencing in NHT and USP22 KO HT-29 cells had revealed an enrichment of genes of the GO terms "response to type I IFN", "IFNγ mediated signaling pathway", "response to IFNγ" and "response to IFNα", among others (Chapter 5.1). Therefore, we investigated the ability of USP22 to regulate necroptosis induced by type I or II IFNs in combination with BZ (Figure 33). To this end, HT-29 control and USP22 KO cells were subjected to IFNα, IFNβ or IFNγ treatment combined with BV6 and zVAD.fmk. Analysis was focused on 18 hours of IBZ induced cell death, where the differences between control and USP22 KO clones were most pronounced. Interestingly, USP22-dependent regulation of

necroptosis was not restricted to IFNγ-, but also present in type I IFN-treated HT-29 cells. Whereas with IFNβ-BZ treatment cell death levels were comparable to those induced with IFNγ-BZ treatment, IFNα had less cytotoxic effects on both control and USP22 KO cells (Figure 33A). Using Western blot analysis, we detected the phosphorylation of RIPK1 and MLKL as well as phosphorylated (p.) RIPK3, indicated by its upward shift, after treatment with IFNα-BZ, IFNβ-BZ or IFNγ-BZ (Figure 33B). Interestingly, while phosphorylation was stronger in IFNβ- and IFNγ-treated NHT cells, USP22 KO cells did not reflect the cell death pattern of type I and II IFNs observed in PI/Hoechst experiments. Since USP22 KO cells already reach a high percentage of cell death, which is in general accompanied by swelling and the release of proteins into the cell culture medium or degradation of necroptosis-associated proteins [229-231], this could account for lesser amounts of detectable protein of RIPK3, RIPK1 and MLKL and their respective phosphorylated forms in USP22 KO cells (Figure 33B). Also, other factors may account for this observation, such as a transfer of the respective proteins to insoluble phases or IFN-specific differences in signaling kinetics, which should be addressed in future experiments.

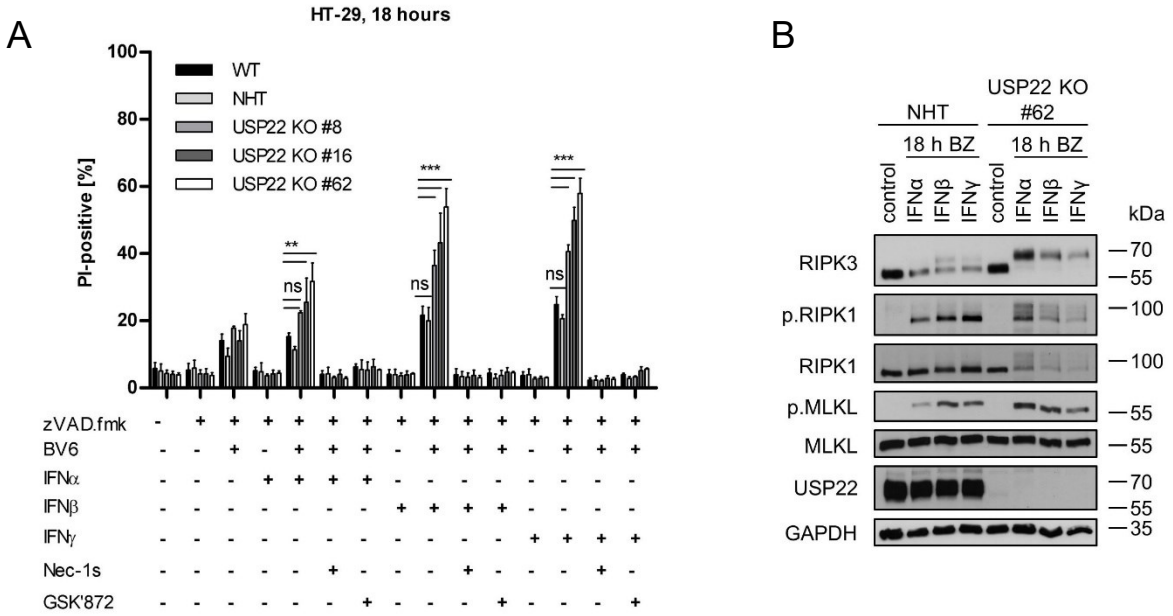

Figure 33: Type I and type II IFN-BZ induced necroptotic cell death is regulated by USP22 KO. HT-29 control and USP22 KO single clone cells were subjected to treatment with 1 ng/ml IFNα, IFNβ or IFNγ, 0.5 μM BV6, 20 μM zVAD.fmk, 30 μM Nec-1s and 20 μM GSK'872 as indicated for 18 hours. A. Amount of cell death was measured using fluorescence-based PI/Hoechst staining. Data is represented as mean and SD of three independent experiments performed in triplicates. **P < 0.01, ***P < 0.001, ns: not significant. B. Protein levels of basal or phosphorylated forms of RIPK3, RIPK1 and MLKL were assessed using Western blot. Levels of USP22 were detected as control of USP22 KO, GAPDH served as loading control. Blot is representative of two independent experiments.

In addition to the proteins of the necroptotic signaling pathway, we investigated components of the IFN signaling pathway in early phases of treatment with BZ and IFNα, IFNβ or IFNγ after 0.5 hours (Figure 34A), and later signaling after 18 hours (Figure 34B). Although type I and II

IFNs share similar features, they signal through different receptors complexes and could therefore be regulated differently by USP22. Binding of IFNα or IFNβ to the heterodimeric IFNα receptor activates the receptor-associated tyrosine kinases JAK1 and TYK2, while IFNγ is recognized by the IFNγ receptor that is associated with JAK1 and JAK2. This leads to kinase cross-phosphorylation, phosphorylation of the respective receptors and recruitment of STAT proteins [293]. Both treatment with IFNα- and IFNβ-BZ led to early STAT1 and STAT2 phosphorylation, while IFNγ-BZ treatment induced STAT1 phosphorylation (Figure 34A). STAT3 was only activated after treatment with IFNβ-BZ and IFNγ-BZ. Interestingly, only IFNγ-BZ treatment activated TYK2, which is surprising because TYK2 is not associated with the IFNγ receptor, but with IFNAR and IFNLR. However, no striking differences between NHT and USP22 KO cells were detected in IFNα, IFNβ or IFNγ treated HT-29 cells 30 minutes after treatment (Figure 34A).

IFN signaling starts immediately at the point of treatment, however, prolonged IFN signaling can occur due to feedback loops activated when cells are dying. After 18 hours, we detected increased STAT1 as well as p.STAT1 levels in all IFN-treated conditions that could not explain the differences in cell death between NHT and USP22 KO cells (Figure 34B). The only difference between NHT and USP22 KO cells was observed in p.STAT1 and IFNGR1 levels. Although consistently upregulated after IFN treatment, IFNGR1 levels were lower in USP22 KO cells compared to NHT cells in untreated, IFNβ- and IFNγ-treated cells (Figure 34B).

All in all, we did not find strong indications for USP22-dependent regulation of JAK/STAT signaling after IBZ treatment, or for differences in necroptosis signaling between type I and II IFNs, except for the differences in IFNGR1 abundance. Since we observed the highest amount of cell death and increase in JAK/STAT1 signaling upon IFNγ-BZ treatment, we focused our further research on IFNγ-BZ-induced cell death.

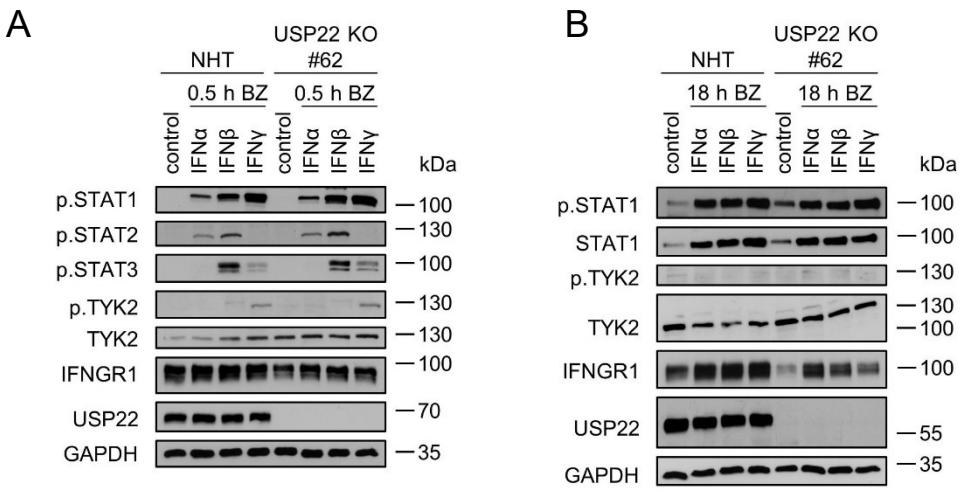

Figure 34: Western blot assessment of proteins of the IFN signaling pathway after activation of necroptosis using IFNα, IFNβ or IFNγ in combination with BZ. HT-29 NHT and USP22 KO cells were treated with 1 ng/ml IFNα, IFNβ or IFNγ in combination with 0.5 µM BV6 and 20 µM zVAD.fmk for 0.5 (A) or 18 (B) hours. Indicated protein levels of the IFN-STAT signaling pathway were detected using Western blot. Levels of USP22 were detected as control of USP22 KO, GAPDH served as loading control. Blots are representative of two independent experiments.

5.2.3 USP22-mediated necroptotic cell death does not require STING expression

As a sensor of cytosolic DNA, STING is an indispensable part of the innate immune system through its role as a mediator of IFN signaling [294]. In addition, studies emphasize that priming with IFN sensitizes cells to necroptosis [292]. STING is a negative regulator of basal IFN expression upon loss of USP22 which could be responsible for priming cells towards necroptosis. To investigate the role of STING and STING-mediated IFN priming upon USP22 loss in IBZ-mediated necroptosis, STING KO cells were generated using CRISPR/Cas9 in NHT and USP22 KO HT-29 cells and subjected to IBZ-induced cell death. Of note, as demonstrated in part I of this thesis, additional USP22 STING dKO reduced the increased IFNL1 levels and basal STAT1 phosphorylation levels observed upon loss of USP22. Surprisingly, despite complete loss of both STING and USP22 expression, loss of STING could not reduce the levels of cell death in USP22 KO cells, nor did it change the amount of cell death induced in NHT cells (Figure 35). This suggests that USP22-mediated necroptosis occurs independent from STING expression or posttranslational modification deposited on STING. Of note, TNFα-BZ induced necroptosis, that was previously described to be negatively

regulated upon loss of USP22 through USP22-mediated changes in RIPK3 ubiquitylation [72], was also not affected by additional STING KO (Figure 35).

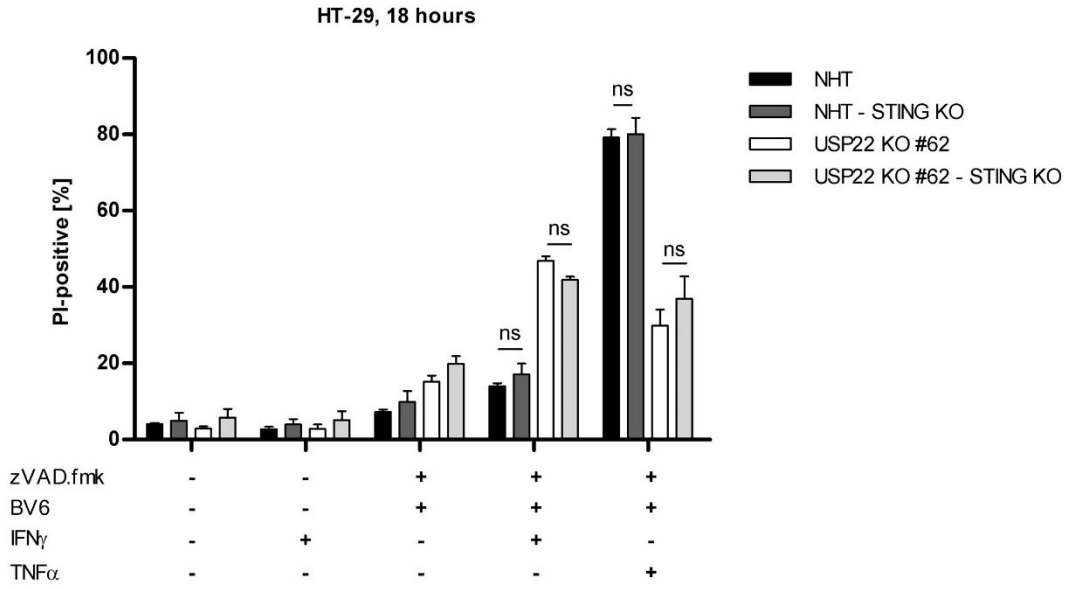

Figure 35: Loss of STING does not affect IBZ-induced necroptosis sensitivity in USP22 KO HT-29 cells. HT-29 NHT, NHT-STING KO, USP22 KO and USP22-STING dKO cells were treated with 1 ng/ml IFNγ, 1 ng/ml TNFα, 0.5 µM BV6 and 20 µM zVAD.fmk as indicated for 18 h. Percentages of PI positive cells were assessed by fluorescence-based PI/Hoechst staining and represented as mean and SD of three independent experiments performed in triplicates. ns: not significant.

5.2.4 IBZ-induced necroptosis is dependent on IRF1

IRF1 is among the genes upregulated upon IFN treatment [295, 296] and has previously been suggested as a mediator of IFNγ-induced cell death [288]. We therefore aimed to investigate the relevance of IRF1 for USP22-dependent IBZ-induced necroptosis.

Using an siRNA-mediated approach, IRF1 expression was silenced in HT-29 NHT and USP22 KO cells and knockdown efficiency was confirmed using Western blot analysis. Since IRF1 expression is not detectable in unstimulated cells, transfection control and siIRF1 HT-29 cells were additionally treated with IFNγ one hour prior to lysis to induce IRF1 expression for confirmation of successful knockdown (Figure 36A). While treatment of HT-29 NHT and USP22 KO cells with non-silencing constructs resulted in slightly less cell death than in control cells after 18 hours of IBZ treatment, the increased cell death of USP22 KO cells was still observed. Interestingly, silencing of IRF1 reduced necroptotic cell death in USP22 KO cells while only slightly reducing NHT cell death levels (Figure 36B). This strongly suggests an important role of IRF1 in USP22-mediated IBZ-induced necroptotic cell death.

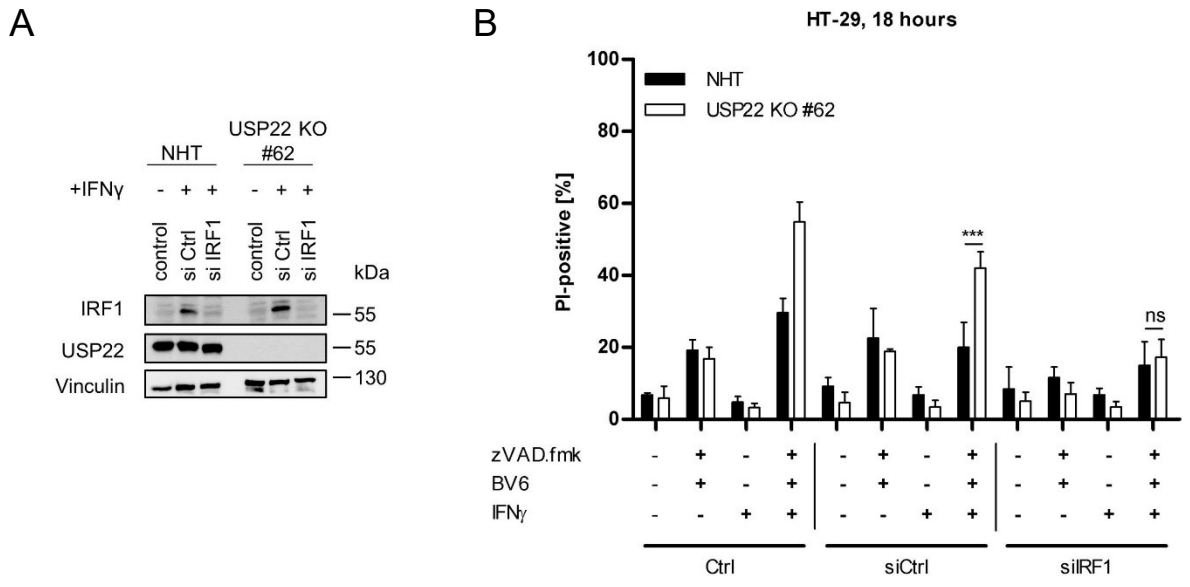

Figure 36: IBZ-induced necroptosis in HT-29 USP22 KO cells is partially dependent on IRF1. Expression of IRF1 was reduced with an siRNA mediated approach using three pooled siRNA constructs of a total concentration of 40 nM for 48 hours, and non-silencing siRNA constructs (siCtrl) were used as transfection control. A. Reduction of protein expression of IRF1 was assessed using Western blot analysis. For confirmation of successful IRF1 silencing, cells were stimulated with 1 ng/ml IFNγ one hour before harvesting to induce IRF1 expression. Probing for USP22 served as an additional control of USP22 KO, Vinculin served as loading control. Western blot experiments were performed at least two times. B. 48 hours after silencing, HT-29 NHT, USP22 KO and respective silenced cells were stimulated with 1 ng/ml IFNγ, 0.5 µM BV6, 20 µM zVAD.fmk and 30 µM Nec-1s for 18 hours as indicated. Percentages of PI positive cells were assessed by fluorescence-based PI/Hoechst staining and represented as mean and SD of three independent experiments performed in triplicates. ***P < 0.001, ns: not significant.

5.2.5 Loss of USP22 regulates the expression of signaling molecules during IFN- and TNFα-induced necroptosis

Treatment with IFNs induces the expression of several ISGs, including inflammatory cytokines or type I, II or III IFNs themselves, enhancing IFN signaling in a positive feedback-loop [297]. In addition, necroptotic cell death is accompanied by the release of DAMPs that can activate PRRs, leading to a second wave of IFN expression, e.g. through activation of MDA5, TLRs or cGAS/STING [298, 299]. Interestingly, also RIPK3 or MLKL activation can result in increased expression and secretion of cytokines [299-303]. To address the role of signaling molecules during necroptosis, IBZ- and TBZ-induced cyto- and chemokine expression was quantified using a FACS-based approach (Figure 37). To temporally resolve a first and second wave of cytokine expression, cytokines were measured in cell supernatants six and 18 hours after treatment.

Treatment with IBZ induced early secretion of IFN-gamma induced protein 10 kDa (IP-10), detectable six hours post treatment in the supernatant of both NHT and USP22 KO cells (Figure 37A). At a later time point of 18 hours post treatment, IP-10 expression was even more elevated compared to levels detected after six hours. In addition, IFNβ, IFNλ1, -2 and -3, TNFα,

IL-6, IL-8 and GM-CSF levels were increased compared to unstimulated HT-29 cells (Figure 37B). USP22-dependent regulation was observed in most cytokine profiles, with USP22 KO HT-29 cells displaying increased cytokine levels compared to NHT cells. This was most pronounced for levels of IP-10 six hours after IBZ treatment, and after 18 hours for IFNλ and GM-CSF, a factor that is involved in macrophage stimulation and has also been reported to induce necroptosis in human neutrophils [304]. Interestingly, after 18 hours, IP-10 levels of NHT and USP22 KO HT-29 cells were again at comparable levels.

Contrasting to the IBZ-induced cytokine expression pattern, treatment with TBZ led to an early increase in IL-8 expression, observable six hours post treatment, and later increase of IFNλ1, IL-6 and GM-CSF (Figure 37C and D). Again, USP22 KO cells displayed an overall increased cytokine expression pattern compared to NHT cells, most pronounced for IFNλ1, IL-8 and GM-CSF, indicating a USP22-dependent regulation of these cytokines during necroptosis.

Of note, basal expression levels were generally increased 18 hours after treatment compared to six hours, which may be attributed to longer incubation times during which cytokines could accumulate in cell supernatants. In addition, the levels of IFNγ measured during IBZ treatment and TNFα measured after TBZ treatment are therefore difficult to interpret since the treatment itself increases the respective cytokine levels in the cell supernatants, and would need to be investigated in a separate assay (Figure 37A-D).

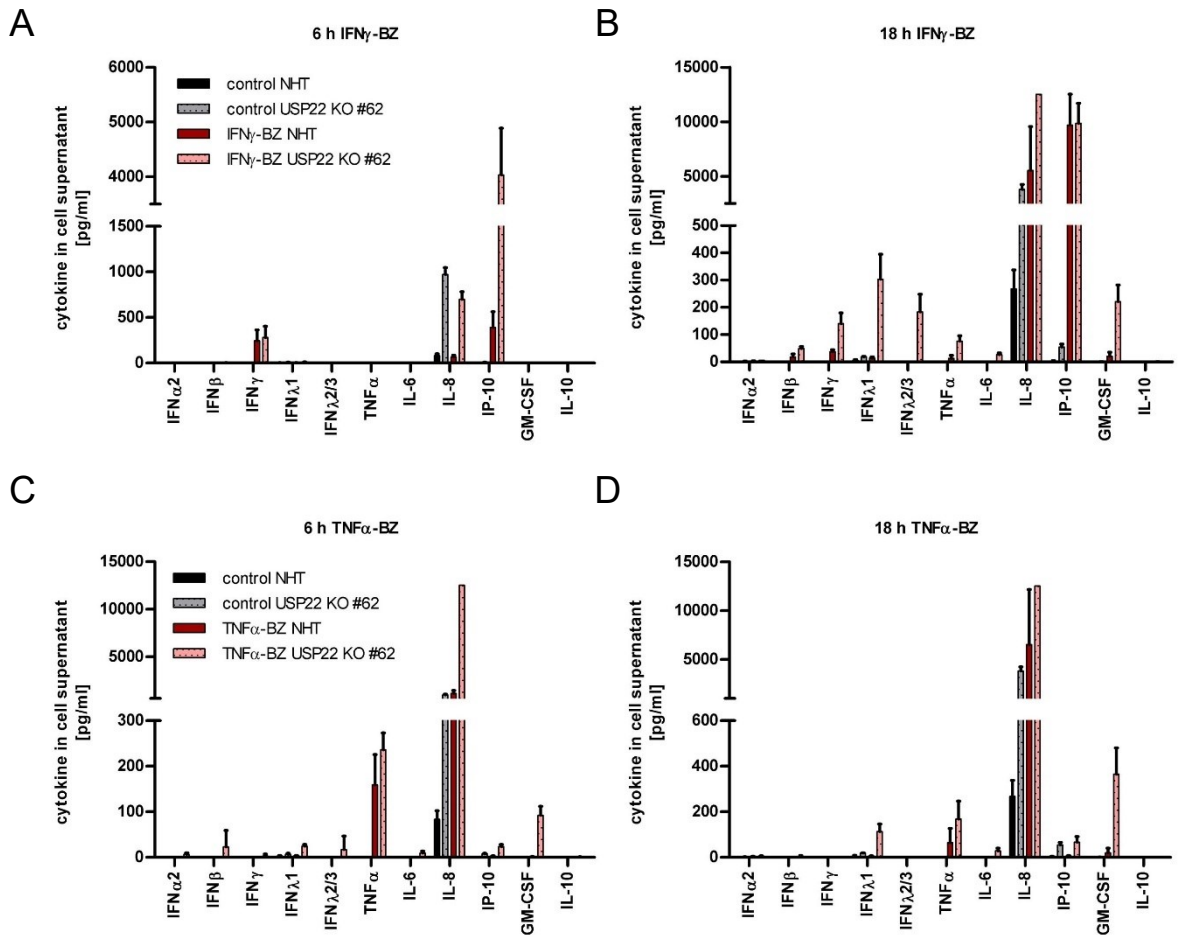

Figure 37: FACS-based analysis of secreted cytokines during IBZ- (A, B) and TBZ- (C, D) induced necroptosis in HT-29. Cytokine secretion of HT-29 NHT and USP22 KO cells was assessed 6 and 18 hours after treatment with 1 ng/ml TNFα or 1 ng/ml IFNγ in combination with 0.5 µM BV6 and 20 µM zVAD.fmk using a FACS-based multiplex assay. Data is represented as mean and SD of three independent samples.

5.2.6 IBZ-induced necroptosis is partially dependent on TNFα expression

Several of the induced cytokines upon IBZ treatment are ISGs, and are naturally upregulated upon IFN stimulation, like IFNs themselves or IP-10. However, IP-10 is not only induced in response to IFNs, but is also described as both a downstream target of TNFα signaling and an upstream inducer of TNFα production through the JNK-c-Jun signaling pathway [305]. In addition, IL-8, a major mediator of the inflammatory response, is increased during early timepoints upon TBZ treatment, but only after 18 hours upon IBZ treatment, proposing the possibility of TNFα-dependent necroptotic signaling and cytokine expression during later stages of necroptosis progression. Therefore, we aimed to investigate the dependence of IBZ-induced necroptotic cell death on TNFα expression.

Indeed, by scavenging secreted TNFα during IBZ-induced necroptosis, cell death could be partially blocked in both NHT and USP22 KO HT-29 cells, while Enbrel completely abrogated TBZ-induced necroptosis (Figure 38A). In addition, USP22-dependent differences in the

induction of TNFα mRNA levels could be detected at early stages of IBZ-induced necroptosis (Figure 38B). Taken together, these experiments reveal the dependency on TNFα for IFN-induced necroptosis and suggest an additional role for USP22 in the regulation of IBZ-induced necroptosis.

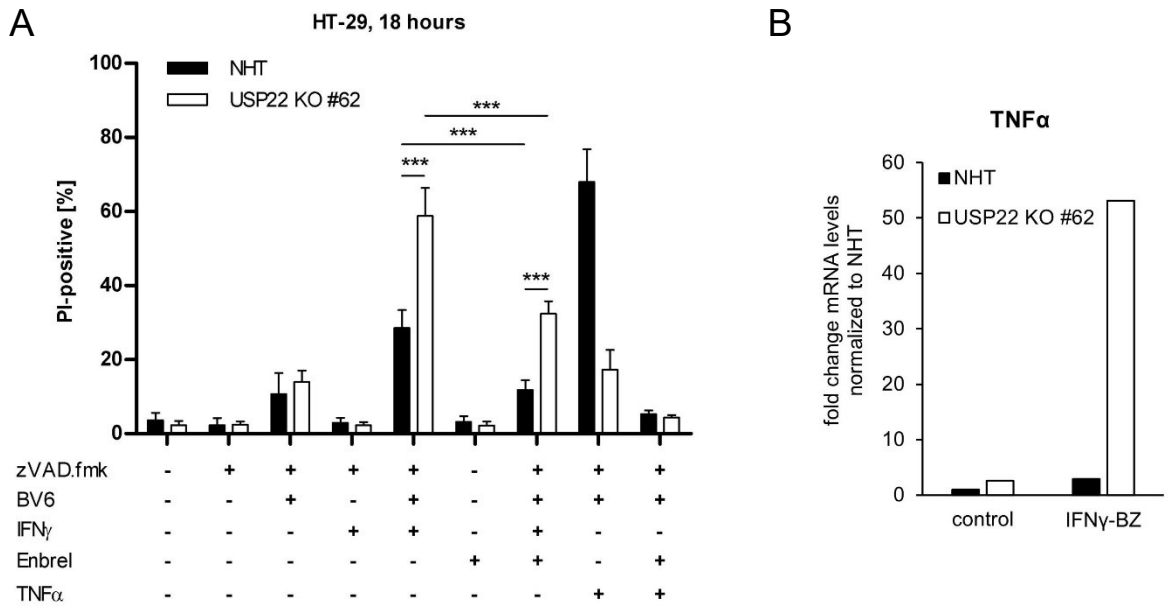

Figure 38: TNFα contributes to IBZ-induced necroptotic cell death. A. HT-29 NHT and USP22 KO cells were treated with 1 ng/ml IFNγ or 1 ng/ml TNFα in combination with 0.5 µM BV6 and 20 µM zVAD.fmk as indicated for 18 hours. TNFα was scavenged using 50 µg/ml Enbrel in combination with TBZ or IBZ. Data is represented as mean and SD of three independent experiments performed in triplicates. ***P < 0.001. B. Expression of TNFα mRNA was assessed using qRT-PCR 4.5 hours after IBZ treatment. Data is represented as mean of two independent experiments performed in triplicates.

5.2.7 Loss of USP22 promotes 2'3'-cGAMP-induced necroptotic cell death

Our investigations revealed that IBZ-induced necroptosis is at least partially mediated through IRF1 and TNFα signaling. Given that our previous research in PC cells demonstrated that also STING agonism using 2'3'-cGAMP in combination with BV6 and zVAD.fmk induced necroptotic cell death through a mechanism that depends on IRF1 and partially on TNFα signaling [291], we aimed to explore the ability of 2'3'-cGAMP to induce necroptotic cell death in HT-29 cells. Indeed, while treatment with 2'3'-cGAMP alone caused only negligible amounts of PI-positive cells, combined treatment with BZ for 24 hours led to the induction of cell death, with significantly increased levels of cell death in HT-29 USP22 KO cells that could be rescued by inhibition of RIPK1 with Nec-1s, again confirming necroptosis as mode of cell death (Figure 39A).

To further characterize 2'3'-cGAMP-induced cell death and differences in regulation through USP22, key players of STING signaling and necroptosis were analyzed during cell death progression by Western blotting (Figure 39B). In line with the finding that loss of USP22

sensitized cells to STING activation, treatment with 2’3’-cGAMP-BZ induced prolonged and stronger TBK1 phosphorylation three to 24 hours after treatment, and distinctly stronger IRF3 phosphorylation after three hours in USP22 KO HT-29 cells. In addition, STING activation was more persisting in USP22 KO HT-29 cells, marked by an upward shift of STING protein which represents phosphorylated STING (this was confirmed using an anti-p.STING antibody in previous experiments that are not shown in this study), and more quickly degraded in NHT HT-29 cells. Western blot analysis of the necroptotic key players RIPK1, RIPK3 and MLKL confirmed necroptosis as mode of cell death (Figure 39B). While MLKL was phosphorylated to a similar extent in NHT and USP22 KO cells after 24 hours, RIPK3 phosphorylation was increased in USP22 KO cells, indicating higher levels of cell death. Phosphorylated RIPK1 was already detectable six hours after treatment in USP22 KO cells, but not in control cells, matching the increased cell death. Interestingly, while levels of RIPK1 phosphorylation were similar in NHT and USP22 KO cells after 24 hours, RIPK1 was not detectable in USP22 KO cells. Several possibilities may explain the depletion of RIPK1 in Western blot lysates, including advanced progression of necroptosis and accompanied protein degradation, or RIPK1 becoming insoluble during necroptosis progression, as demonstrated by Jens Rödig for RIPK3 [72]. Further research is necessary to elucidate USP22-dependent regulation of RIPK1 and necroptosis progression upon 2’3’-cGAMP-BZ treatment. Taken together, these findings confirm that 2’3’-cGAMP induces necroptotic cell death and strengthen the role of USP22 as a regulator of necroptosis.

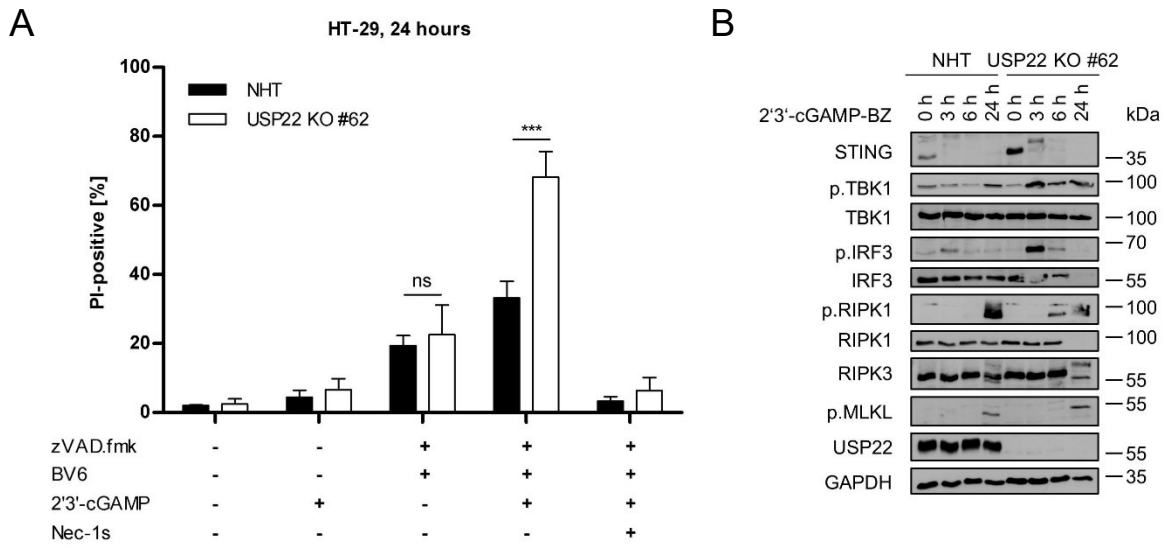

Figure 39: Combined treatment with STING agonist 2'3'-cGAMP, BV6 and zVAD.fmk induces necroptotic cell death in HT-29 control and USP22 KO cells. A. HT-29 NHT and USP22 KO cells were stimulated with 10 ng/ml 2’3’-cGAMP, 0.5 µM BV6, 20 µM zVAD.fmk and 30 µM Nec-1s for 24 hours as indicated. Percentages of PI positive cells were assessed by fluorescence-based PI/Hoechst staining and represented as mean and SD of three independent experiments performed in triplicates. ***P < 0.001, ns: not significant. B. HT-29 NHT and USP22 KO cells were stimulated with 10 ng/ml 2’3’-cGAMP, 0.5 µM BV6 (B) and 20 µM zVAD.fmk (Z) for the indicated time points. Indicated proteins of the

STING and necroptosis signaling pathway were analyzed using Western blot, GAPDH served as loading control.

6 Discussion

6.1 Part I: USP22 controls interferon signaling and SARS-CoV-2 infection through activation of STING

Regulation of IFN signaling and maintaining a baseline IFN expression is critical for the alertness and preparedness of organisms to be armed for pathogen invasion. With this study, we are the first to extensively investigate the effects of USP22 on constitutive IFN expression, STAT signaling and baseline ISG expression in hIECs. We identify USP22 as a negative regulator of type III IFN and ISG expression in unstimulated conditions and in the absence of IFNs or virus infection. We reveal that loss of USP22 increases both basal and 2'3'-cGAMP-induced activation and ubiquitylation of STING, which we identify as major mediator of IFNλ1 expression and basal upregulation of ISGs in a USP22 dependent manner. Finally, we test the functional relevance of USP22-regulated basal IFN signaling and ISG expression in antiviral defense and identify USP22 as critical regulator of SARS-CoV-2 infection, replication, and formation of infectious viral particles in a STING-dependent manner.

6.1.1 USP22 selectively regulates gene expression

Using a genome-wide screening, we identified a broad spectrum of USP22-regulated genes in the colon carcinoma cell line HT-29. Although not readily apparent within the top 50 regulated genes, GO analysis prominently highlighted type I and II signaling and regulation of viral processes such as genome replication and life cycle as key pathways modulated by USP22. In addition, the expression of several IFN-unrelated genes is changed upon loss of USP22, including the majority of downregulated genes.

Very few studies have performed screens to explore alterations in global gene expression dependent on USP22, leaving the basis for the selectivity of USP22 in the regulation of gene expression unsolved. In line with our findings, Gong et al. revealed selective regulation of gene expression in HeLa cells, however, the regulation of antiviral or IFN signaling did not emerge as major pathways influenced by USP22 [271]. Instead, the study revealed additional regulated pathways, such as focal adhesion, ubiquitin mediated proteolysis and phosphatidylinositol signaling [271]. However, in accordance with our findings, a screen by Dietlein et al. observed a significant increase in the expression of ISGs in cells of the hematopoietic system of USP22-deficient mice in the absence of IFNs, that could be traced back to increased H2B ubiquitylation at ISG loci [222]. It is well established that USP22, as part of the SAGA complex, modulates H2A and H2B ubiquitylation [51-53], which typically correlates with transcriptionally active chromatin [306-308]. Indeed, in line with previous observations [52, 309], our findings suggest increased H2B ubiquitylation in HT-29 cells, which may account for the abundance of ISGs regulated by loss of USP22. However, the expression of several ISGs and IFNL1 is dependent

on STING, suggesting that USP22 could directly regulate gene transcription via deubiquitylation of H2B and indirectly via modifications on STING. This opens the additional possibility that USP22-dependent modifications on STING and subsequent upregulation of IFNs increase H2B ubiquitylation at specific ISG loci. This would be in line with the observation that during adenovirus infection, type I IFN expression increases H2Bub1 levels via the hBre1/RNF20 complex [310]. Indeed, USP22-dependent regulation of type I and III IFN expression was observed in this study and could account for an increase in total H2Bub1 levels. Of note, type III IFNs have not been studied regarding H2Bub1 status and ISG induction, however it is likely that USP22-mediated IFNλ1 expression promotes H2Bub1 and drives ISG expression in our model since type I and III IFNs generally share features regarding viral defense and ISG induction [311]. Interestingly, the work by Dietlein et al. did not extend their investigation of IFN secretion on type III IFNs, although stating that they did not observe an increased systemic secretion of IFNs in USP22 KO mice [222]. Therefore, USP22-mediated changes on STING could indeed also be responsible for the increased levels of H2Bub1 in their model.

It is to consider that apart from regulation via H2B ubiquitylation, USP22 may also control transcription through deubiquitylation of additional non-histone targets besides STING to cause the diversity of regulation as seen in the top regulated genes of the microarray. Possible candidates are SIRT1 that was already demonstrated to regulate expression of several genes, including genes of the mitochondrial metabolism [312] and transcription of antioxidant genes [313], or telomeric repeat factor 1 (TRF1) and Cyclin B that control cell cycle progression and telomere elongation [314].

6.1.2 Type III IFN selectivity of USP22-mediated regulation in hIECs

Our investigation revealed that the loss of USP22 results in selective upregulation of IFNλ1 expression, with only minor effects on type I IFN expression. While type I and II IFN-regulated genes were strongly represented in the GO analysis despite their minimal expression and secretion in HT-29 cells, the highly expressed type III IFNs were not reflected in the GO terms regulated by KO of USP22. This discrepancy is likely due to the limited representation of type III IFNs in the current GO databases and the overlapping gene expression patterns induced by type I and III IFNs [311].

During our investigations, we observed both a strong basal upregulation of type III IFNs upon USP22 KO in the epithelial cell lines HT-29 and Caco-2, as well as an increased response to IFNλ treatment, rather than to type I or II IFN treatment. This selectivity of signaling towards type III IFNs agrees with several other studies. Type III IFN signaling is dependent on the IFNLR1, whose expression is primarily restricted to epithelial cells of various tissues and cell types, such as the intestine, lung, vaginal tissue, and hepatocytes [315, 316]. Accordingly, in

a study conducted in mice, tissues with a high proportion of epithelial cells and elevated IFNLR1 expression, including the stomach, intestine, skin, and lung, exhibited the strongest response to IFNλ treatment and subsequent induction of ISGs dependent on IFNλ signaling [317]. In line, Stanifer et al. reported a bias towards IFNλ rather than type I IFN expression in mouse IECs during viral infection [315]. These findings may explain the weak response to type I and II IFNs observed in HT-29 cells, as well as the low expression of IFNα, β, and γ, with important implications for the role of USP22 in the pathogen defense in hIECs of the gastrointestinal tract.

In all tested cell lines, loss of USP22 was accompanied by elevated expression of STING. Notably, STING is a key mediator of IFNλ expression, e.g. in response to gamma-radiation in HT-29 cells [318] and in response to sensing of DNA by the cytosolic DNA sensor Ku70 in primary human macrophages [319]. Accordingly, we demonstrated that elevated IFNλ1 expression in HT-29 and Caco-2 cells was dependent on STING expression. Since STING was demonstrated to normally also stimulate the expression of type I IFNs [320, 321], it is unclear how loss of USP22 and subsequent changes in STING signaling positively regulates type III, but not type I IFN expression. Sui et al. propose a mechanism by which STING-dependent IRF3 activation induces the expression of IRF1 and IRF7, which were both necessary in the induction of IFNλ1 upon activation of Ku70 [319], however, IRF1 and IRF7-independent activation of IFNλ1 upon activation of STING through IFI16 was also described [322]. Given these findings, it would be interesting to further investigate whether USP22-mediated deubiquitylation of STING directly affects the selectivity of STING towards IFNλ1 production, or if USP22 regulates expression or ubiquitylation of additional proteins that affect IFN expression.

Despite originating from different sources, all cell lines tested, HT-29, Caco-2, HeLa and HCoEpiC, are of epithelial origin. Interestingly, STING expression is notably pronounced in endo- and epithelial cells of the respiratory tract, the fallopian tube, and cells of the hematopoietic system, such as T cells, macrophages, and dendritic cells [154, 323]. This heightened STING expression in respiratory epithelial cells, together with the importance of IFNλ signaling in epithelial cells, may render them particularly sensitive to regulation via USP22. It would be intriguing to investigate whether our findings extend to epithelial cells of the respiratory tract, particularly considering our observation that USP22 also controls SARS-CoV-2 infection.

Despite the strong bias towards IFNλ1 production in HT-29 and Caco-2 USP22 KO cells, we also observed a USP22-dependent regulation of IFNα and IFNβ transcription that did not rely on USP22-mediated changes on STING. As discussed above, USP22-mediated changes in H2Bub1 levels could be responsible for selective regulation of IFNα and IFNβ [308]. Since type

I IFN expression also underlies regulation via IRFs and NF-κB [83, 324], it is also possible that the increased NF-κB signaling observed in USP22 KO HT-29 cells promotes type I IFN expression, given that NF-κB signaling is not strictly dependent on STING expression.

6.1.3 USP22 regulates ubiquitylation of STING and STING-associated proteins

As a major signaling hub protein, STING is known for its important role in the response to viral infections. However, modulation of tonic STING signaling in the absence of external stimuli is an emerging area of investigation [152], e.g. for its role in several diseases such as SAVI or COPA syndrome, that are governed by aberrant regulation and activation of STING signaling [325-327]. Previous studies have investigated the posttranslational regulation of STING and identified a variety of proteins, including E3 ligases and deubiquitylases, as described in Chapter 2.5.

With this study, we are the first to identify USP22 as a central host factor regulating basal STING signaling, ubiquitylation and transcriptional expression in USP22-deficient hIECs without the addition of external stimuli. We observe a marked increase in STING ubiquitylation in HT-29 cells upon loss of USP22. Moreover, activation of STING using 2'3'-cGAMP also led to an increase in STING ubiquitylation which was even stronger in USP22 KO cells. In line with our findings, USP13 was previously identified as a STING-specific DUB that cooperates with USP22 to remove overexpressed K27-linked ubiquitin from overexpressed STING upon HSV-1 infection in HEK293T cells [219]. Interestingly, Liu et al. revealed that instead of directly deubiquitylating STING, USP22 serves as a scaffold to enable USP13-mediated STING-deubiquitylation, with the interaction between USP22 and USP13 being augmented by viral stimuli [219]. It could be that also in our model, USP22 might act as scaffold for USP13-mediated removal of K27-linked ubiquitin chains on STING, even under basal, untreated conditions. The hypothesis that also in our model USP22 mediates removal of K27-linked ubiquitin chains of STING aligns with the previously described functions of K27-linked ubiquitylation of STING. For instance, The E3 ligases AMFR and TRIM10 both mediate K27-linked ubiquitylation of STING, promoting TBK1 recruitment and positively regulating STING trafficking to the Golgi, respectively [203, 328], with positive implications for type I IFN and response to HSV-1 infection. Correspondingly, we observe that increased STING ubiquitylation upon USP22 KO correlates with an increase in both basal activation of STING signaling, and activation upon STING agonism, resulting in increased transcription of IFNL1, antiviral ISGs, and a heightened response to SARS-CoV-2 infection. In line, Liu et al. also reported increased antiviral properties of USP22 KO or USP13 KO HEK293T cells, while Sun et al. described USP13-mediated removal of K27- and K33-linked ubiquitin chains from STING with implications for TBK1 recruitment and HSV-1 replication [211, 219].

It is noteworthy that previous investigations of USP22 in IFN and antiviral signaling exclusively used overexpression models that often artificially amplify IFN signaling pathways, making it challenging to assess the basal effects resulting from either the lack of USP22 expression or basal STING signaling. By examining the impact of USP22 KO on STING ubiquitylation and STING signaling under endogenous conditions we go beyond the limitations of overexpression models and demonstrate for the first time that USP22 regulates tonic IFN signaling by modulating STING under basal conditions and in the absence of viral infection or exogenous IFN. Future investigations should extend the exploration of the interplay between USP22, USP13, and STING under endogenous, unstimulated conditions, and elucidate whether USP22 DUB activity is necessary for USP22-mediated changes in STING ubiquitylation.

Besides USP22-USP13-mediated deubiquitylation of STING, USP22 may modulate the addition of K48-linked ubiquitin to STING by regulating TRIM29 transcription. TRIM29 is an E3 ligase that mediates the addition of degradative K48-linked ubiquitin chains to STING [281] that was downregulated upon USP22 KO in HT-29 cells. Future studies will shed light on the regulatory mechanism that USP22 exerts over TRIM29 expression and whether TRIM29-dependent modifications on STING would account for the increased STING stability observed upon USP22 KO. Indeed, the loss of USP22 might indirectly impact tonic STING signaling by modulating additional effectors involved in STING stability and degradation, such as TRIM29, or regulate expression or activity of upstream PRRs. It was long thought that STING is only activated upon cell-intrinsic or -extrinsic stimuli, e.g. by cyclic di-nucleotides through cGAS, or mtDNA [142, 154]. However, recent studies have demonstrated that STING is also active at homeostasis, and that signaling strength and the extent of the resulting tonic IFN signaling can be modulated by several cofactors that regulate either STING trafficking from Golgi to lysosomal compartments, or by factors that otherwise regulate STING degradation [150]. Interestingly, the USP22 target STAT3 has been shown to regulate the RAB GTPase RAB14 in colorectal cancer [329], an oncogene that is also involved in the regulation of STING post-Golgi trafficking, thereby affecting Golgi dwell-time of STING and tonic IFN signaling [150]. In addition, direct posttranslational modification of STING signaling effectors mediated by USP22 are thinkable, such as demonstrated for the DUB USP8 that stabilizes ESCRT proteins [330, 331], which have been described to mediate termination of STING signaling by facilitating degradation of ubiquitylated STING in murine macrophages [332].

It cannot be excluded that STING may act as a physical scaffold for USP22-mediated ubiquitin modifications on other proteins, as observed with USP7 and USP9X, which employ OTUD4 as a scaffold for the DNA demethylases alkylation B (AlkB) homolog (ALKBH) 2 and ALKBH3 [333]. One potential target for STING-scaffolded regulation is IRF3, which is recruited to STING only in the presence of TBK1 and may be negatively regulated by USP22 to prevent excessive

IFN signaling. Consistent with this proposal, Liu et al. observed interactions of USP22 with IRF3, supported by the observation that FLAG-tagged USP22 interacts with green fluorescent protein (GFP)-tagged IRF3 in HEK293T cells [219, 223]. The possibility that USP22 may act as a scaffold for USP13 to mediate deubiquitylation, or that USP22 may use STING as a scaffold for further ubiquitin modifications, may be owed to the lack of the USP22 ZnF domain to bind ubiquitin [46]. Therefore, USP22 may rely on protein substrate specificity or recruitment through adaptor proteins, rather than ubiquitin specificity, to be directed to its substrates and exert deubiquitylating action, analogous to its role within the SAGA complex.

6.1.4 The role of STING and IFNλ1 in SARS-CoV-2 infection

In the last part of this part of the study, we demonstrate that loss of USP22 in the hIEC cell line Caco-2 protects from SARS-CoV-2 infection. Moreover, we can show that the protective role that loss of USP22 exerts on Caco-2 cells is, at least partially, mediated by USP22-dependent changes on STING, and most likely is mediated by the high expression of IFNλ1 and upregulation of antiviral ISGs.

Interestingly, profiling studies conducted on COVID-19 patients have revealed compromised induction of both type I and III IFNs, impaired type I IFN responses, and elevated viral load in the bloodstream [334, 335]. Furthermore, a comparative analysis of human lung tissue infected with SARS-CoV-2 and SARS-CoV has demonstrated significantly reduced expression of IFNs and proinflammatory cytokines and chemokines upon SARS-CoV-2 infection. The ability of SARS-CoV-2 to suppress or evade an adequate IFN response emphasizes the crucial preventive role played by type I and III IFNs in the regulation of viral infections and supports our hypothesis that USP22 mediates antiviral properties through STING-mediated upregulation of the type III IFN IFNλ1 and subsequent induction of antiviral ISGs. Indeed, type I and type III IFNs are known to elicit a robust antiviral response [79, 336], and prophylactic treatment with type I or III IFNs has shown promise against several respiratory viruses. For instance, administration of pegylated IFNα has exhibited a protective effect against SARS-CoV infection in cynomolgus macaques [337], and both type I and III IFNs have impeded the replication of a novel human coronavirus, HCoV-EMC, in primary human airway epithelial cells [338]. Additionally, IFNλ4 has demonstrated antiviral effects on MERS-CoV infection [339]. Consequently, exogenous administration of IFNs to induce antiviral immunity has been proposed as a potential treatment for more severe cases of COVID-19 [340, 341]. Consistent with the preventive role of type III IFNs in viral infections highlighted by these studies, we propose USP22 as a central host factor regulating the cell-intrinsic antiviral state by modulating IFNλ1 expression via regulation of STING. Accordingly, we observe a reduced number of SARS-CoV-2-infected cells, decreased SARS-CoV-2 copy numbers, and a decline in the

production of *de novo* infectious viral particles in the supernatants of Caco-2 cells lacking USP22.

In our study, elevated IFNλ and ISG expression in USP22 KO cells, as well as decreased replication and de novo virus formation, were mediated by USP22-dependent changes on STING. Interestingly, STING signaling itself is regulated heavily by SARS-CoV-2 proteins, often with redundant mechanisms. Certain viral proteins directly interact with STING to inhibit signaling. For example, ORF3a binds to STING and hampers NF-κB signaling by impeding nuclear accumulation of NF-κB [342]. The protease 3C-like protease (3CLpro) interferes with the assembly of STING complexes by inhibiting K63-linked ubiquitylation of STING [342]. Furthermore, ORF10 attenuates ER-to-Golgi trafficking by anchoring STING in the ER, thereby impairing STING-TBK1 interaction, oligomerization, and STING-mediated autophagy [343]. Additionally, both 3CLpro and PLpro directly cleave IRF3, which disrupts downstream signaling [344], and Nsp1 interferes with the translation of IFNλ1, IFNβ and IL-8 [345, 346].

It remains elusive why loss of USP22, and subsequent regulation of STING, provides such a pronounced effect on SARS-CoV-2 replication and *de novo* virus particle formation. Given the potent ability of SARS-CoV-2 to modulate the cGAS-STING pathway and IFN signaling at various stages, further studies will be necessary to explore the long-term implications of USP22 KO and STING signaling during SARS-CoV-2 infection. It is important to consider whether the protective state induced by the loss of USP22 in hIECs endures during later stages of SARS-CoV-2 infection. Alternatively, it is conceivable that the loss of USP22 merely prophylactically impedes SARS-CoV-2 infection by enhancing the antiviral state through upregulation of IFNs and ISGs, such as RNA-sensing PRRs like RIG-I and MDA5 [187], OAS1, -2, -3 or IFITM1, -2, -3 [347]. During later stages of COVID-19, the counteractive mechanisms employed by SARS-CoV-2 against STING and IFN signaling may potentially silence the effects mediated by USP22 and facilitate progression of the viral life cycle.

6.1.5 Limitations and outlook

6.1.5.1 USP22 may modulate STING signaling beyond its role in STING ubiquitylation

Despite our identification of USP22 as a mediator of STING ubiquitylation, it is still unclear which USP22-mediated modifications on STING lead to the observed phenotype of increased IFN and ISG expression and increased resistance to SARS-CoV-2 infection. In addition to modulating K27-linked activating ubiquitylation of STING, loss of USP22 might indirectly impact tonic STING signaling by modulating additional effectors involved in STING stability and degradation or regulate expression or activity of upstream PRRs.

Although we demonstrate that the observed increased expression of three PRRs important for viral signaling, namely RIG-I, MDA5 and TLR3, is not involved in STING-mediated elevated

IFN signatures observed in HT-29 USP22 KO cells, we cannot exclude the possibility that USP22 regulates the expression or activation of upstream sensors of STING. Intriguingly, various PRR signaling pathways converge at STING [168], and emerging studies unravel the existence of previously unknown PRRs that activate STING signaling, some of which specifically affect IFNλ1 expression through STING, such as IFI16 and Ku70 [319, 322, 348, 349]. A more comprehensive investigation that includes exploring the interaction of USP22 with STING-inducing PRRs under basal conditions could unveil additional target proteins of USP22.

Although we could not find evidence of DNA damage or leakage of mtDNA into the cytosol, it is still possible that minimal amounts of DNA leaking from the nucleus or mitochondria into the cytosol trigger a constant basal activation of STING, as observed in certain tumor cells [350, 351]. Furthermore, it would be intriguing to further examine the effect of USP22 KO on mitochondrial metabolism and translation, as our study observed both a decline in mitochondrial membrane potential and a strong representation of genes related to mitochondrial processes. Indeed, a study by De Luca et al. suggests a role of USP22 in the survival of tumor cells under hypoxic conditions [352]. Consistent with our GO analysis results, a previous study by Chipumuro et al. reported that USP22 contributes to 3'-end processing of JAK-STAT-inducible genes through the regulation of H2B ubiquitylation, recruitment of polyadenylation factors, and phosphorylation of serine 2 at the RNA polymerase II C-terminal domain [353, 354]. Further investigations will elucidate whether USP22-mediated changes in mitochondrial processes contribute to the increase in basal STING activity.

It is to note that we did not extend our research on the observed increase in NF-κB signaling upon USP22 KO. Since STING does affect both IRF3 and NF-κB signaling [355], it would be worthwhile to investigate the role of USP22 in the regulation of STING-mediated NF-κB signaling. However, it should be acknowledged that STING is frequently dysregulated in colon carcinoma, including HT-29 cells, as demonstrated in a comprehensive study by Xia et al. [356]. In HT-29 cells, only a moderate response to dsDNA transfection was observed, characterized by robust IRF3 translocation but impeded STING trafficking and p65 activation [356]. Therefore, it would be more suitable to continue further investigations in cells of other origins, such as non-malignant cells or lung cells, where STING is highly expressed [323, 357].

Lastly, USP22 might regulate STING transcription independently of its influence on IFN expression, potentially as a direct target of SAGA-mediated H2B ubiquitylation and subsequent increase in transcription at STING gene loci. This hypothesis aligns with our observation of increased basal STING mRNA expression, even in the presence of JAK/STAT inhibition, in HT-29 cells lacking USP22. Consequently, it is plausible that the loss of USP22 also affects

STING signaling by directly regulating STING transcription itself, but further investigations are required to establish this relationship.

6.1.5.2 USP22 extends its antiviral properties beyond STING and IFNλ1 signaling in the regulation of SARS-CoV-2 infection

Although we provide strong evidence of the inhibitory effect of loss of USP22 on SARS-CoV-2 infection, we were not able to elucidate the precise mechanism underlying this regulatory process. Considering the substantial body of literature supporting the protective role of type III IFNs, it is reasonable to propose that the upregulation of IFNλ1 mediated by the USP22-STING axis, and subsequent induction of ISGs even prior to infection, plays a significant role in the antiviral effects observed in USP22-deficient hIECs. However, more detailed experiments, including IFN silencing, knockout or inhibition are required to elucidate the contribution of STING-mediated IFN regulation to the response against SARS-CoV-2 infection.

While our findings demonstrate that the protective effect of USP22 KO during SARS-CoV-2 infection is dependent on STING, most likely due to STING-mediated upregulation of IFNL1 and ISG expression, it should be noted that additional KO of STING only partially rescues the effects observed in the absence of USP22. Little is known regarding the role of USP22 in the regulation of antiviral signaling pathways that extends beyond its regulation of STING signaling. The screening of DUBs for antiviral properties performed by Liu et al. additionally revealed that USP22 interacts with IRF3 downstream of STING [219], which may be worth investigating also in hIECs, particularly considering the antiviral properties of USP22 KO despite additional STING deficiency in our study. Interestingly, USP22 has also been shown to positively control antiviral signaling by deubiquitylating the importin protein KPNA2 to promote IRF3 translocation during SeV infection [223], contrasting with our observations and the findings of Liu et al., which suggest a negative regulatory role of USP22 in antiviral signaling [219].

Furthermore, the regulatory influence of USP22 on immune signaling may extend beyond the 2D model utilized in our study to a more physiological context. For instance, loss of USP22 in PC has been shown to promote T cell and NK cell infiltration, thereby enhancing the response to immunotherapy [358]. Similarly, loss of USP22 in liver cancer leads to increased lymphocyte infiltration and improved efficacy of immunotherapy through programmed death-ligand 1 (PD-L1) deubiquitylation [359], highlighting the significance of USP22 in the modulation of immune cell recruitment. Thus, further investigations are warranted to elucidate the broader implications of USP22 in immune modulation in the context of antiviral responses.

6.1.5.3 Importance of activation of STING signaling during SARS-CoV-2 infection

It is interesting to ponder why several other RNA viruses, including the coronaviruses SARS-CoV and HCoV, have emerged with mechanisms interfering with the cGAS-STING pathway and modulate STING oligomerization and ubiquitylation [39, 360, 361], especially since the major hosts for coronaviruses, bats, express defective STING variants and comprise impaired type I IFN responses [362]. The success of SARS-CoV-2 and other coronaviruses may be attributed to their capacity to modulate the cGAS-STING response, which surprisingly becomes activated during coronavirus infections. Intriguingly, the cGAS-STING pathway is not directly triggered by coronavirus infection since cGAS is not activated by RNA. Instead, the spike protein of SARS-CoV-2 induces the fusion of infected cells with neighboring cells, resulting in the formation of multinucleated syncytial cells [363]. The generation of micronuclei within these syncytial cells instigates an increased DNA damage response and activation of the cGAS-STING pathway [364-366]. Interestingly, IFITM proteins, which were also highly expressed in our study upon USP22 KO, dependent on STING expression, were able to block S-mediated fusion [363]. This underscores the expanded antiviral function of STING in the recognition and prevention of SARS-CoV-2 infection.

6.1.5.4 Adverse effects of STING activation in SARS-CoV-2 infection

When contemplating the therapeutic implications of STING activation and the prophylactic administration of type III IFNs in the context of SARS-CoV-2 infection, it is crucial to acknowledge the adverse role that STING and IFNs have been shown to play in the progression of COVID-19. Investigations utilizing lung samples from COVID-19 patients and lung-on-chip models infected with SARS-CoV-2 have demonstrated that cGAS-STING signaling drives type I IFN responses, culminating in tissue destruction and cell death [367]. Remarkably, pharmacological inhibition of STING has improved disease outcomes and reduced the extent of lung inflammation [367].

In accordance, a study conducted in hACE2 transgenic mice has provided evidence that type I IFNs strongly contribute to a pathological response rather than effectively controlling SARS-CoV-2 infection [368]. Intriguingly, Neufeldt et al. discovered that SARS-CoV-2 redirects the cGAS-STING-mediated signaling from IRF3-mediated IFN induction towards NF-κB-mediated pro-inflammatory signaling in infected human epithelial cells [169]. This shift from IFN expression to pro-inflammatory NF-κB signaling may also explain the observations made in severe COVID-19 cases, where diminished IFN expression coincides with increased levels of proinflammatory cytokines [335, 369, 370] and the manifestation of extensive lung inflammation [371].

Accordingly, the potential significance of USP22-controlled signaling during SARS-CoV-2 infection may lie in the activation of the STING-IRF3-type III IFN axis, instead of NF-κB signaling or the induction of type I IFNs, which have been associated with unfavorable outcomes for patients [368].

6.2 Part II: USP22 regulates IFN-induced necroptotic cell death

Despite increasing progress in the development of cancer therapies, tumors rapidly acquire resistance mechanisms or are initially unresponsive to treatment. Recently, the use of IFNs or STING agonism to induce necroptotic cell death has emerged as a promising treatment strategy in apoptosis-resistant settings, potentially combining activation of the innate cell death program with activation of the tumor microenvironment. In addition, the identification of host factors that regulate cell fate, particularly programmed cell death, has become critical in the fight against cancer. Recently, the deubiquitylase USP22 has been reported to positively regulate necroptosis by affecting RIPK3 ubiquitylation upon TBZ treatment [72]. Here, we describe a novel role for USP22 in the negative regulation of necroptosis induced by the synergistic action of BV6 together with IFNs when caspases are blocked. We show that although USP22-mediated changes on STING increase basal IFN signaling in HT-29 cells, which may sensitize to IFN-induced necroptosis, USP22-dependent regulation of IBZ-induced necroptosis signaling is not dependent on STING but relies on a yet unknown mechanism. Finally, we shed light on how IBZ-induced necroptosis is regulated in HT-29 cells by identifying TNFα and IRF1 as mediators of necroptosis signaling and demonstrate the potential of STING agonism in the induction of necroptosis, especially when combined with USP22 inhibition.

6.2.1 IFN-induced necroptosis is dependent on IRF1 and partially on TNFα signaling

Several studies before have proposed type I or type II IFN administration in combination with BV6 as a treatment strategy to successfully activate apoptosis in various cell types [289, 290, 372]. With a better understanding of other regulated cell death pathways, it has become clear that the combination of IFN administration with other stimuli also enables the activation of the necroptotic pathway, as demonstrated by Thapa et al. in mice and HeLa cells [234]. However, while TNFα-induced cell death is well understood, the mechanisms and factors regulating IFN- and STING-mediated necroptosis remain unclear.

In this study, we identify IRF1 as a critical mediator of IFN-induced necroptotic cell death in HT-29 cells, consistent with previous findings from our group in HT-29 cells [255, 288] and a panel of PC cells [291]. Our data aligns with several other studies, which have reported the importance of IRF1 during IFN-induced necroptosis, inflammasome activation, and PANoptosis [373-376]. Interestingly, IRF1 is also among the basally upregulated ISGs following USP22 KO in the acute myeloid leukemia (AML) cell line NB4, as demonstrated by my colleague Lisa Kowald (Manuscript submitted). It is possible that also in HT-29 cells, IRF1 is one of the ISGs transcriptionally regulated upon USP22 KO, which positively affects necroptosis outcomes. Future investigations should explore the regulation of IRF1 by USP22 in HT-29 cells, given that both NHT and USP22 KO cells rely on IRF1 during IBZ-induced necroptosis. Interestingly, both TBZ- and IFNγ-induced cell death in the present study are

accompanied by IP-10 secretion. This is consistent with previous studies reporting MLKL-dependent upregulation of inflammatory cytokines, including the IP-10 gene CXCL10 and CXCL1, during necroptosis [302, 303]. Since IP-10 has been reported to be transcriptionally regulated by concomitant binding of IRF1 to ISRE sequences and IKKβ-dependent p65 translocation and binding to kB sites of the CXCL10 promoter [377, 378], this may imply the involvement of NF-κB signaling during IBZ-induced necroptosis, as previously observed in PC cells following STING agonism [291].

In this study, we demonstrate that 2'3'-cGAMP, a STING agonist, efficiently induces necroptotic cell death, accompanied by activation of the STING-TBK1-IRF3 axis and phosphorylation of the necroptotic signaling components RIPK1, RIPK3 and MLKL. While we focused our mechanistic studies on IFN- and not on 2'3'-cGAMP-induced necroptosis, previous studies in PC have suggested the relevance of both IRF1 and p65 in the progression of STING-mediated necroptotic cell death [291]. Given that STING agonism induces expression of IFNs via the STING-TBK1-IRF3 axis, as demonstrated in the first part of this thesis, it is reasonable to assume that once IFNs are induced, 2'3'-cGAMP-BZ employs the signaling pathway of IFN-induced necroptosis to execute cell death. However, the involvement of additional mechanisms is conceivable given that STING can activate not only IRF3 but also NF-κB signaling, or autophagy [146, 355], e.g. through expression of genes that rely both on IRF and NF-κB transcription factors [377, 378], as discussed above. Indeed, a study by Brault et al. emphasizes the need for synergistic expression of type I IFNs and TNFα to induce necroptosis upon STING agonism in bone marrow-derived macrophages [257]. Interestingly, TNFα-IFNγ-synergy was also reported to induce the inflammatory cell death PANoptosis during SARS-CoV-2 infection in several cell types and in mice through the JAK-STAT1-IRF1-axis [379]. Indeed, IFNγ-dependent TNFα-expression was also reported in the murine macrophage cell line RAW 264.7 where IFNγ-treated macrophages responded with expression of TNFα, dependent on the combined binding of IRF1 and IRF8 to the TNFα promoter [380].

While the need for IFN-TNFα-synergism for the induction of necroptosis upon IFN-treatment was confirmed in the present study for HT-29 cells, as well as in a previous study of our group in a subset of PC cells using the TNFα scavenger Enbrel [291], surprisingly, neither knockdown of TNFR1 nor TNFα scavenging was reported to affect IBZ-induced necroptosis in a previous study in HT-29 cells under similar conditions [288]. It is possible that during earlier time points of necroptosis, like investigated in the present study, the observed IFN-induced expression of TNFα is involved in the progression of cell death through an auto-/paracrine loop, but that loss of TNFα signaling does not prevent from IFN-induced effects at later time points, as Cekay et al. investigated later time points of 48 hours. These findings suggest that while TNFα may drive the initial stages of necroptosis progression, IBZ treatment ultimately leads to necroptotic cell

death without the necessity of TNFα signaling. This possibility may explain the residual cell death observed despite the blocking of TNFα in USP22-KO HT-29 cells in the present study, implying the involvement of different signaling pathways besides TNFα in the execution of IBZ-induced cell death. Additionally, it is plausible that TNFα and IFNγ initially synergistically drive IBZ-induced necroptosis, especially under USP22-deficient conditions, as implicated by an increased transcriptional upregulation of TNFα in USP22 KO cells upon IBZ treatment.

In conclusion, the study identifies IRF1 as a critical mediator of IFN-induced necroptotic cell death in HT-29 cells, aligning with previous studies. Furthermore, the study shows that the STING agonist 2'3'-cGAMP efficiently induces necroptotic cell death, accompanied by activation of the STING-TBK1-IRF3 axis and phosphorylation of the necroptotic signaling components RIPK1, RIPK3, and MLKL. The involvement of additional mechanisms, including TNFα, NF-κB signaling or autophagy, is also conceivable, emphasizing the need for further investigation.

6.2.2 IFN specific effects during IBZ-induced necroptosis

Although the type I IFNs IFNα and IFNβ both bind to the same receptor and downstream signaling components, IFNβ was more potent in activating necroptosis, as evidenced by the greater percentage of PI-positive cells after IFNβ-BZ treatment. Different biological outcome despite binding to the same receptor may be explained by IFN-specific receptor affinities, as investigated for IFNα subtypes and IFNβ [103, 104] and may be the reason for differentially regulated downstream signaling [105, 108]. In addition, the amount of receptor expression could potentially compensate for weaker binding affinities and modulate the strength and mode of downstream signaling, at least as observed for IFNα subtypes [106].

Apart from differences in the downstream execution of necroptosis between the type I IFNs IFNα and IFNβ, we observed differences in the strength of STAT1, -2, and -3 activation, mostly during early time points after stimulation with BZ in combination with type I or II IFNs. As discussed above, differences in IFNα- and IFNβ-mediated signaling, despite the fact that both engage the IFNAR1/2-JAK1/TYK2 complex to recruit STAT1 and STAT2, may be explained by different receptor affinities. However, it is surprising that only IFNβ induces a strong activation of STAT3, whereas no STAT3 phosphorylation was detected after IFNα-BZ treatment. The fact that IFNγ-BZ, like IFNβ-BZ treatment, also induces a STAT3 response, although weaker, suggests the possibility of the involvement of non-canonical STAT3 signaling in the progression of necroptosis. In contrast, we observed STAT3 activation especially under conditions that result in high percentage of cell death, and STAT3 is actually described as negative regulator of apoptotic cell death, e.g. upon treatment with TRAIL in cervical cancer [381], in hepatocarcinoma [382] and in human ALL cells [383], and constitutive STAT3 activation was also reported in several cancer types, also suggesting pro-survival functions

[384-386]. Interestingly enough, USP22 reportedly controls STAT3 activation via deubiquitylating and stabilizing its deacetylase SIRT1 [220, 387]. Consequently, loss of USP22 should reduce SIRT1 levels and promote STAT3 acetylation, phosphorylation and subsequent activation. However, since we only monitored STAT3 phosphorylation upon IBZ treatment, and not basal STAT3 protein levels, no statement can be made about USP22-dependent basal regulation of STAT3. It does not seem, however, that USP22 in this setting would strongly modulate STAT3 activation during the first half hour of IBZ treatment.

Although not shown in the present study, preliminary experiments suggest no induction of necroptosis after treatment with IFNλ1, -2 or -3 in combination with BZ up to investigated time points of 24 hours. However, experiments concerning IFNλ-induced cell death were performed only once and would need to be repeated to substantiate any conclusions. Overall, the role of IFNλ in inducing cell death remains controversial, with some studies suggesting that IFNλ signaling has regenerative functions in the mouse colon [388], while others have reported that IFNλ expression promotes apoptosis or necroptosis in severely inflamed regions of Crohn's Disease, depending on the cell type [389]. As IFNλ administration is currently being investigated as a more moderate form of immunotherapy due to its lower but more sustained signaling [79], it is critical to clarify the potential of type III IFNs to induce cell death and avoid the activation of a highly inflammatory state.

6.2.3 USP22 may control necroptosis through regulation of type I IFNs, independent from STING

We initially hypothesized that the USP22-mediated increase in IFN and ISG expression, and STING regulation, were responsible for the increased necroptosis levels of HT-29 USP22 KO cells observed upon treatment with either 2'3'-cGAMP-BZ or IBZ. Several previous reports have highlighted the importance of IFN priming in accelerating necroptosis, specifically mediated by cGAS/STING-dependent DNA sensing that licenses necroptosis in macrophages [292] and by increasing the expression of RIPK3 and MLKL [292, 390]. It comes as a surprise that in this study HT-29 cells lacking STING, especially in combination with USP22 KO, were not impaired in their ability to execute necroptosis. The increase in IFNλ1 and ISG protein levels and basal STAT1 phosphorylation could indeed have been a valid explanation for the difference in necroptosis induction observed between control and USP22 KO cells through initially sensitizing HT-29 USP22 KO cells to necroptosis. Interestingly, there remains the possibility that (lack of) USP22 amplifies IBZ-induced signaling by controlling the expression of type I IFNs, which were regulated independently of STING expression status, either by initial priming mediated by IFNα or IFNβ, or by the increased expression of type I IFNs and IFN-regulated ISGs during necroptosis.

Previously, Dietlein et al. have proposed a model in which loss of USP22 in mouse hematopoietic stem cells results in increased H2B monoubiquitylation at ISG loci, which is consistent with our observations of increased global H2B monoubiquitylation in HT-29 cells [222]. Increased H2Bub1 levels usually correlate with increased transcription of the affected gene regions [308], and although no studies to date have directly observed higher H2Bub1 levels at type I IFN loci, it is possible that USP22 selectively regulates type I IFNs via control of H2B ubiquitylation, thereby promoting necroptosis. However, it is uncertain whether the very low levels of type I IFNs detected by ELISA and luciferase assays would account for the proposed IFN priming and sensitization to necroptosis in this system, especially since no increase in STAT1 phosphorylation was observed in USP22 KO cells upon additional STING KO.

6.2.4 Limitations and outlook

6.2.4.1 Proposing potential IFN- and USP22-regulated players during IBZ-induced necroptosis

In this study, we could demonstrate that IBZ treatment leads to necroptosis in HT-29 cells through activation of IRF1 and partially through TNFα signaling. However, the exact mechanism by which necroptosis is induced and how USP22 regulates the outcome of necroptosis requires further study. Several candidates come to mind when suggesting potential proteins whose regulation by USP22 during IBZ-induced necroptosis, either through type I IFN-mediated priming or (in)direct (de)ubiquitylation, would account for the increased necroptotic outcome observed in this study.

First, both transcription and activation of the serine-threonine kinase PKR are triggered upon IFN stimulation, enabling interaction with RIPK1 to induce necrosome formation [234, 391]. Interestingly, IRF1 controls PKR transcription by binding to its promoter element and correlates with PKR expression in several cell lines [392]. PKR KO in mice also prevented IP-10 expression upon viral infection [393]. Based on these studies, it would be interesting to see if USP22 controls IBZ-induced necroptosis by modulating PKR transcription or activation.

Second, IFN-induced USP22-dependent regulation of RIP homotypic interaction motif (RHIM)-containing proteins could de- or increase interactions with RIPK1 or RIPK3 and modulate the formation of RIPK3 amyloid oligomers, MLKL recruitment and subsequent cell membrane permeabilization and cell death [394]. Both TRIF and ZBP1 share the highly conserved RHIM domain with RIPK1 and RIPK3 [394]. Like PKR, ZBP1 is transcriptionally regulated by IRF1 and has been suggested in various studies to promote apoptosis and inflammatory cell death [373, 376, 395]. It is known that both TLR3 and TLR4 induce necroptosis via TRIF without the use of the TNF system [232, 396]. The prospect of TLR3 participation in the activation or

amplification of necroptotic signaling in USP22 KO is particularly interesting because TLR3 levels were consistently elevated in USP22 KO cells, and overexpression of TLR3 may indeed lead to acceleration of cell death through increased activation of TRIF and subsequent increased oligomerization with RIPK3. Testing the level of TRIF dimerization or interaction with RIPK3 would shed light on the question of USP22-mediated necroptosis regulation, provided that TLR3 is not one of the ISGs regulated by USP22-dependent STING regulation. In addition, defects in autophagy can also sensitize to necroptosis through accumulation of the RHIM domain proteins TRIF, RIPK1 and RIPK3 [397], which is especially interesting due to the implication of USP22 in the regulation of autophagy [398-400].

Interestingly, given the role of USP22 in viral defense, many viruses have evolved to contain RHIM domain proteins that can counteract either PRR-dependent signaling and/or necroptosis to promote infection, such as the murine cytomegalovirus (MCMV), which can bind to RIPK1, RIPK3 and ZBP1 through its RHIM-containing M45 protein, preventing cell death [401], or the cowpoxvirus protein viral inducer of RIPK3 degradation (vIRD), an orthopoxvirus protein that binds RIPK3 RHIM and promotes RIPK3 degradative ubiquitylation [402]. Also, the SARS-CoV-2 protein Nsp13 contains a RHIM and inhibits the binding of ZBP1 to RIPK1 and RIPK3 [403]. Nevertheless, a recent study observed activation of the ZBP1-RIPK3 axis during SARS-CoV-2 infection, leading to RIPK3-MLKL-mediated necroptosis signaling and subsequent inflammatory signaling [404]. Given that we did not observe remarkable levels of cell death during SARS-CoV-2 infections presented in the first part of the thesis, it is rather unlikely that loss of USP22 affected SARS-CoV-2 replication through increasing ZBP1-mediated necroptosis in infected cells. This also matches the findings of the previously mentioned study that showed that ZBP1 did not affect SARS-CoV-2 replication, but promoted inflammatory signaling through increased infiltration of leukocytes, macrophages, neutrophils and T cells [404].

Lastly, even MLKL expression is known to be transcriptionally upregulated upon IFN treatment [255], and could induce necrotic cell death through STAT1 signaling in human autoimmune hepatitis, independently from RIPK3 activation [405]. Here, more in-depth analysis of the kinetics of IBZ-induced cell death regarding MLKL expression, phosphorylation and membrane translocation would be necessary to dissect USP22-dependent regulations on necroptosis.

6.2.4.2 Contrast to TNFα-induced necroptosis

In the study previously published in *EMBO reports*, my former colleague Jens Rödig identified three possible ubiquitylation sites on RIPK3 that are affected by USP22 during TBZ-induced necroptosis and proposes that USP22 (in)directly affects RIPK3 ubiquitylation and phosphorylation, thereby controlling necrosome formation and necroptosis progression [72]. Surprisingly, loss of USP22 and consequently increased phosphorylation and ubiquitylation of

RIPK3 resulted in decelerated cell death upon TBZ treatment, whereas loss of USP22 leads to increased necroptotic cell death upon IBZ treatment, as demonstrated in this study. This now presents both positive and negative roles of USP22 in the regulation of necroptotic cell death and emphasizes the need for further investigations of how USP22 controls necroptosis signaling.

It would be interesting to further investigate if RIPK3 ubiquitylation is indeed decreased upon IBZ-induced necroptosis in USP22 deficient cells, opposite to observations in TBZ-induced necroptosis. Since we could (partially) block IBZ-induced necroptosis by scavenging TNFα, cell death can be at least partially accounted to TBZ-induced necroptosis, most likely as a result of IFN-induced TNFα upregulation and auto-/paracrine signaling via TNFR1 and would encounter the same block in necroptosis progression observed under TBZ conditions.

Although Roedig et al. were able to demonstrate the importance of RIPK3 ubiquitylation sites in the progression of necroptosis [72], it is possible that these are only required for the classical induction of necroptosis during TNFα-RIPK1-RIPK3 (or Fas/TRAIL-RIPK1-RIPK3) signaling and are bypassed by engaging an alternative necroptosis signaling pathway, e.g. by directly inducing RIPK3 oligomerization through the RHIM-containing proteins ZBP1 or TRIF, as discussed above. However, the described studies differ in the necessity of RIPK1 in RIPK3 activation [233], and even if those pathways were RIPK1-independent, we observe RIPK1 phosphorylation, which again would pose the question of USP22-dependent regulation of RIPK3 ubiquitylation sites.

There is the possibility that USP22 regulates IBZ-induced cell death through modulation of signaling downstream of MLKL activation, like proposed in detail by Jens Rödig for TBZ-induced necroptosis [72]. However, preliminary data in IBZ-treated HT-29 cells showed that MLKL phosphorylation levels correlated with the levels of cell death observed through fluorescence imaging, making it more plausible that USP22 regulates necroptosis signaling upstream of MLKL.

6.2.4.3 Clinical relevance of USP22-regulated IBZ- and TBZ-induced necroptosis

Colorectal cancer remains one of the most prevalent cancers worldwide and is difficult to target with immunotherapy due to its immunosuppressive properties [406, 407]. Necroptotic cells have been successfully employed as a vaccine to prime $CD8^+$ T cells in various cancer entities [408, 409]. In addition, type I IFNs have been widely used for cancer immunotherapy, with recombinant IFNα2 being the first human immunotherapeutic approved by the Food and Drug Administration (FDA) for cancer in 1986 [410]. Both monotherapy or combination with other treatments resulted in disease regression in myeloma, lymphomas, melanoma and Kaposi's sarcoma, to only name few [411], and IFN priming facilitated Fas-mediated apoptosis and cell

death through chemotherapeutics, also in colorectal carcinoma [412]. However, several adverse effects like fever, chills and later onset fatigue and depression have been observed upon IFN treatment, which most likely can be attributed to over-activation of immune effector cells [413]. Moreover, STING agonists, which play a crucial role in antigen-presenting cells during the antitumor response, are currently being evaluated in clinical trials, with STING recognizing DNA derived from phagocytosed dying tumor cells, leading to IFN production and tumor antigen presentation, as well as stimulation of $CD8^+$ T cells and tumor clearance [414-416].

Here, we demonstrate that both IFN treatment and STING agonism in combination with BV6 and zVAD.fmk in a USP22-deficient setting enhances the necroptotic response in HT-29 cells. Since IFN administration, or STING-mediated IFN expression, was shown to have severe adverse effects during cancer immunotherapy [413], it would be interesting to explore the potential of USP22 inhibition to sensitize cells to IFN- or STING-induced necroptotic cell death and recruit the tumor microenvironment, while reducing the amount of administered IFNs or STING agonists. This combination is particularly promising since STING expression is frequently epigenetically silenced at promoter regions in colorectal cancer [414], which may enable immune escape. Therefore, USP22 inhibition to enhance STING-mediated immune responses and necroptosis could be a valuable tool to improve the efficacy of immunotherapy in colorectal cancer. However, this approach has some limitations. STING activity in some cancer types can also enable tumor growth by inducing indoleamine-2,3-dioxygenase activity, thereby even increasing tumor growth [417]. Therefore, it is essential to investigate the effects of STING activation under USP22-deficient conditions in co-cultivation spheroid models and mouse models. It is also important to evaluate how USP22 loss affects T cell response and cell death. Additionally, necroptosis itself has been associated with not only tumor reduction but also the promotion of metastasis through death receptor 6 signaling [418] or the release of E-cadherin [419]. Lastly, TBZ treatment in USP22-deficient cells decreased necroptotic cell death, which is in contrast to our observations of IBZ- or 2’3’-cGAMP-BZ-induced necroptosis [72]. Since both TNFα and IFNs are secreted during either form of necroptosis, it is not yet foreseeable how USP22 will affect necroptosis and the tumor microenvironment in 3D-tumor models or patients.

In conclusion, we demonstrate that either STING agonism or IFN treatment, combined with the Smac mimetic BV6, can activate necroptosis in HT-29 cells under caspase-deficient conditions, depending on IRF1 and TNFα. Although not depending on IFN priming through STING, both STING agonism and IFN treatment in combination with BZ led to increased necroptosis in USP22-deficient cells, which can be leveraged for developing novel treatment strategies for colorectal cancer to increase necroptosis and recruit the tumor

microenvironment. However, the implications of USP22 loss or overexpression need to be explored in future studies in advanced tumor models, given the contrasting results upon TBZ-treatment in USP22-deficient cells. It is crucial to ensure that the combined treatment of USP22 inhibitors and STING activators does not dampen the necroptotic response and tumor decline, but instead, aids in curing the patient.

7 Deutsche Zusammenfassung

Lebende Organismen stehen ständig der Bedrohung durch innere und äußere Faktoren gegenüber, die das Gleichgewicht wichtiger Prozesse zu stören drohen, was letzten Endes zum Tod führen kann. Mehr denn je stehen wir vor der Herausforderung, zelluläre Faktoren zu identifizieren, die in der Abwehr gegen Infektionen, wie zuletzt mit dem Coronavirus SARS-CoV-2, einen entscheidenden Vorteil bieten können. Darüber hinaus wird es auch im Kampf gegen Krebs immer wichtiger, Marker zu identifizieren, die für eine gezielte Therapie eingesetzt werden können, um zelluläre Prozesse und damit das Überleben fehlregulierter Zellen zu beeinflussen.

Die Ubiquitin-spezifische Peptidase 22 (USP22) gehört zur Superfamilie der Ubiquitin-Peptidasen. Ubiquitin ist ein 76 Aminosäuren großes Protein, das durch den Vorgang der Ubiquitinierung in einem mehrstufigen Prozess, vermittelt durch eine Reihe von Ubiquitin-aktivierenden (E1), -konjugierenden (E2) und -ligierenden (E3) Enzymen, unter Verbrauch von Adenosintriphosphat (ATP) kovalent an Substratproteine gebunden wird. Dabei ist die Verknüpfung einzelner Ubiquitin-Moleküle an Zielproteine möglich (Mono-Ubiquitinierung) sowie die Verknüpfung mehrerer Ubiquitin-Moleküle (Poly-Ubiquitinierung) durch ihr N-terminales Amin (M1) oder durch eines ihrer sieben Lysin-Reste (K6, K11, K27, K29, K33, K48, K63). Die vielfältige Signalwirkung ubiquitinierter Proteine lässt sich auf die Variabilität der Ubiquitin-Verknüpfungen zurückführen, die durch die Unterschiede ihrer dreidimensionalen Topologien die präzise Erkennung durch Proteine mit Ubiquitin-bindender Domäne (UBD) ermöglichen. Die Art der Verknüpfung und die Rekrutierung Ubiquitin-bindender Proteine spezifiziert den Output der Ubiquitinierung und kann unter anderem zum Abbau oder Aktivierung des ubiquitinierten Proteins führen oder als Gerüst für die Rekrutierung weiterer Signalkomponenten dienen.

Der Ubiquitinierung wird durch die Superfamilie der deubiquitinierenden Enzyme (oder Deubiquitylasen, DUBs) entgegengewirkt. Bis heute wurden etwa 100 DUBs identifiziert, von denen die meisten, wie auch USP22, der Gruppe der Cystein-Proteasen angehören, die Ubiquitin durch die katalytische Triade bestehend aus einem Cystein, Histidin und einem azidischen Rest von ihrem Zielprotein spalten. Die Balance zwischen Ubiquitinierung und Deubiquitinierung ist ein wesentlicher Bestandteil der Feinabstimmung und Regulation vieler zellulärer Prozesse. So lassen sich viele Krankheiten, darunter auch Krebs, auf eine Fehlfunktion des Ubiquitinsystems zurückführen, wie z.B. CYLD-assoziierte Hauttumore und mehrere autosomal-dominante juvenile autoinflammatorische Störungen. Darüber hinaus enthalten zahlreiche Viren die genetische Information für virale DUBs, die dem fortgeschrittenen Ubiquitin-System der angeborenen Immunantwort entgegenwirken, um eine Neutralisierung durch die Immunantwort des Wirts zu verhindern.

USP22 wurde zunächst als Teil einer 11-Gen-Signatur beschrieben, die mit schlechtem Ausgang bei Patienten mit einer Krebserkrankung korreliert, wie zum Beispiel einem kurzen Intervall bis zum Wiederauftreten der Krankheit, Metastasierung und Tod. In diesem Kontext spielt USP22 eine wichtige Rolle, indem es K63-gebundenes Ubiquitin von FBP1 entfernt und dadurch die Stabilität des Zellzyklusregulators p21 beeinflusst und die Zellzyklusprogression vorantreibt. Weiter vermittelt USP22 durch die Deubiquitinierung von SIRT1 und die daraus resultierende Regulation der Transkriptionsfaktoren c-Myc und p53 Resistenz gegen die Induktion von Zelltod, ein weiteres wichtiges Merkmal von Krebs. Zusätzlich wurde USP22 kürzlich als positiver Regulator der TNFα-induzierten Nekroptose identifiziert. Als Nekroptose wird eine Form des programmierten Zelltods bezeichnet, die sich durch einen inflammatorischen Phänotyp auszeichnet und durch die Aktivierung der Proteine RIPK1, RIPK3 und MLKL ausgeführt wird, deren Oligomerisierung zur Porenbildung in der Zellmembran und so zum Zelltod führt.

Der Einfluss von USP22 auf zelluläre Signalwege ist auch durch seine Einbindung in den Spt-Ada-Gcn5-Acetyltransferase (SAGA)-Transkriptionskomplex gegeben, der in fünf Module mit funktionell unterschiedlichen Aufgaben unterteilt ist. USP22 als Teil des DUB-Moduls vermittelt hier die Deubiquitinierung der Histone H2B und H2A an K120 bzw. K119, was maßgeblich zur Regulation der Genexpression beiträgt. Während die Regulierung der H2A-Mono-Ubiquitinierung durch USP22 die Transkription einer Reihe von Polycomb-Genen unterdrückt, führt eine erhöhte Ubiquitinierung von H2B zu einer verstärkten Transkription, indem sie die enge Packung von Histonen hemmt und so die Rekrutierung von Histon-modifizierenden und -umbauenden Proteinen ermöglicht. Zusätzlich beschreiben neuere Studien USP22 auch als Regulator von Signalwegen, die zur Detektion zellinterner Schäden und zur Abwehr von Pathogenen beitragen.

Eine wichtige Komponente des angeborenen Immunsystems ist die Expression von sogenannten *Pattern Recognition Receptors* (PRRs, „Mustererkennungsrezeptoren“) in einer Vielzahl von Zelltypen, einschließlich Epithelzellen. PRRs sind in der Lage, spezifische Sequenzen bakterieller oder viraler Komponenten sowie schädigungsassoziierte molekulare Muster zu erkennen, z. B. abnorme Desoxyribonukleinsäure (DNA). Letztendlich führt die Erkennung dieser Muster zur Expression von Interferonen und zur Induktion von Prozessen zur Bekämpfung der Infektion oder Schädigung. Ein Schlüsselfaktor in der intrinsischen Signaltransduktion des angeborenen Immunsystems ist das dimere, in der Membran des endoplasmatischen Retikulums (ER) lokalisierte Protein STING. STING wird durch den Botenstoff zyklisches GMP-AMP (2'3'-cGAMP) aktiviert, der durch den DNA-Sensor cGAS synthetisiert wird. Die Bindung von 2‘3‘-cGAMP in der Liganden-Bindungsdomäne von STING führt zu einer Konformationsänderung, die die Bildung von STING-Oligomeren höherer

Ordnung erlaubt. Dadurch wird die Aktivierung der Serin/Threonin-Proteinkinase TBK1 sowie des Transkriptionsfaktors IRF3 ermöglicht, der dann die Transkription nachgeschalteter Gene, zum Beispiel Interferone, induziert.

Interferone spielen eine wichtige Rolle bei der antiviralen und antiproliferativen Signalübertragung sowie bei der Immunmodulation als Reaktion auf die Erkennung von Pathogenen oder geschädigten Zellen. In humanen Zellen werden abhängig von Zelltyp und Stimulus drei Klassen von Interferonen exprimiert, sogenannte Typ I-, Typ II- und Typ III-Interferone. Die Bindung der Interferone an die spezifischen Rezeptoren führt zur Aktivierung von Mitgliedern der Januskinase-Familie, die wiederum die Transkriptionsfaktoren der STAT-Proteine rekrutieren und durch Phosphorylierung aktivieren. Dies führt zur Bildung von STAT-Homo- oder Heterodimeren, die in den Zellkern translozieren und als Transkriptionsfaktoren für die Expression einer bestimmten Untergruppe von Zielgenen, den sogenannten Interferon-stimulierten Genen (ISGs), sorgen. Primär werden Interferone in Reaktion auf die Erkennung abnormaler zytosolischer DNA, bakterieller Komponenten oder viraler Infektionen exprimiert. Zusätzlich werden in vielen Zelltypen, einschließlich Epithelzellen, konstitutiv in geringen Mengen exprimiert und spielen dadurch eine entscheidende Rolle in der Vermittlung der zelleigenen Abwehr, indem sie die basale Expression wichtiger Signalkomponenten wie IRF- und STAT-Proteine sicherstellen. Darüber hinaus ist es möglich, durch die präventive Verabreichung von Interferonen das Immunsystem zusätzlich zu sensitivieren. Dies wurde auch für eine Infektion mit dem Coronavirus SARS-CoV-2 gezeigt, bei der die präventive Verabreichung von Typ I- und Typ III-Interferonen vor einer Infektion zu einer erhöhten Transkription antiviraler Gene und maßgeblichen Inhibierung der viralen Replikation führte.

Wir beobachteten in früheren Studien, dass USP22 selektiv die Genexpression reguliert, während die Transkription anderer Gene durch ein Fehlen von USP22 unverändert bleibt. Darauf basierend führten wir zunächst ein genomweites Screening in der menschlichen Kolonkarzinom-Zelllinie HT-29 und einer durch die CRISPR/Cas9-Methode modifizierten HT-29 USP22-Knockout (KO) Zelllinie durch, um Signalwege zu identifizieren, die spezifisch von USP22 beeinflusst werden. Wir identifizierten ein breites Spektrum an USP22-regulierten Genen, deren weitere Analyse zeigte, dass USP22 spezifisch an der Regulierung der Signaltransduktion von Typ I- und Typ II-Interferonen sowie der Regulation viraler Prozesse beteiligt ist. Angesichts des wachsenden Wissens über die Bedeutung der Ubiquitinierung bei Virusinfektionen und die komplexen Strategien von Viren wie SARS-CoV-2, Ubiquitinierungsprozesse zu beeinflussen, fokussierten wir unsere weiteren Untersuchungen auf die Rolle, die USP22 in der Regulierung der Interferon-Signalwege spielt.

Durch erste RNA-, Western Blot- und FACS-basierte Analysen konnten wir zeigen, dass der Verlust von USP22 zu einer erhöhten Expression sowie Sekretion des Typ-III-Interferons IFNλ und einer verstärkten Aktivierung von STAT1 führt. Auf der Suche nach der Grundlage der USP22-vermittelten Regulierung der Interferonexpression transfizierten wir Kontroll- und USP22-KO-Zellen mit PRR-aktivierenden Substanzen und beobachteten eine verstärkte Antwort des STAT-Signalwegs in USP22-defizienten Zellen nach Behandlung mit der STING-aktivierenden Substanz ISD. Dies legte nahe, dass USP22 Komponenten des STING-Signalwegs reguliert. Durch weiterführende Experimente an verschiedenen Zelllinien epithelialen Ursprungs konnten wir zeigen, dass der Verlust von USP22 mit einer erhöhten Proteinexpression von STING einhergeht. Zusätzlich beobachteten wir einen signifikanten Anstieg der STING-Ubiquitinierung in HT-29 Zellen nach Verlust von USP22. Darüber hinaus führte die Aktivierung von STING durch 2'3'-cGAMP ebenfalls zu einer erhöhten Aktivierung des STING-Signalwegs und einem Anstieg der STING-Ubiquitinierung in USP22-defizienten Zellen.

In den folgenden Experimenten konnten wir mit Hilfe von HT-29 USP22-STING Doppel-KO Zellen zeigen, dass die erhöhte Expression von IFNλ sowie repräsentativer ISGs in USP22-KO Zellen auf eine USP22-vermittelte Regulierung von STING zurückzuführen ist. STING ist ein wichtiges Signalprotein, das für seine Rolle in der Abwehr von Virusinfektionen bekannt ist. Folglich fokussierten wir im letzten Teil der Studie die Bedeutung von USP22 und der daraus resultierenden Veränderungen der Typ III- und ISG-Expression für die Virusabwehr in humanen Darmepithelzellen. Hierfür generierten wir ein USP22-KO Modell der Darmkrebsepithel-Zelllinie Caco-2, die sich, im Kontrast zu den zuvor verwendeten HT-29 Zellen, mit SARS-CoV-2 infizieren lässt. Tatsächlich konnten wir zeigen, dass der Verlust von USP22 in Caco-2 Zellen die Replikation von SARS-CoV-2, die Produktion neuer infektiöser Viruspartikel und die Zahl der infizierten Zellen maßgeblich reduziert. Darüber hinaus konnten wir zeigen, dass der Verlust von USP22 und die dadurch verbundenen protektiven Eigenschaften gegenüber Virusinfektionen zumindest teilweise auf USP22-abhängige Veränderungen an STING zurückzuführen sind und sehr wahrscheinlich durch die erhöhte Expression von IFNλ1 und antiviralen ISGs vermittelt werden.

Mit diesen Ergebnissen zeigen wir zum ersten Mal die wichtige Rolle auf, die USP22 in der Regulierung der basalen, konstitutiven Interferon-Expression und -Signalweiterleitung innehat, indem USP22 Veränderungen an STING vermittelt. Darüber hinaus identifizieren wir USP22 als einen kritischen Wirtsfaktor in der Regulierung der antiviralen Antwort auf eine Infektion mit SARS-CoV-2.

Im zweiten Teil der Studie knüpften wir an die Erkenntnisse des ersten Teils an und untersuchten den Einfluss von USP22 auf den Signalweg der Interferon-induzierten

Nekroptose. Die Induktion von Nekroptose in Krebszellen hat sich als wertvolles Werkzeug zur Überwindung von Therapieresistenz erwiesen. Besonders bei Darmkrebs, der häufig hohe Rückfallraten aufweist, ist die Erforschung alternativer Behandlungen dringend notwendig. Die etablierte Methode der Nekroptoseinduktion durch Verabreichung von TNFα, Smac-Mimetika und zVAD.fmk wird durch neuere Konzepte wie Interferone oder STING-Aktivierung ergänzt, um Resistenzen zu überwinden und die Tumorumgebung für verbesserte Abwehrreaktionen zu stimulieren. Die erfolgreiche Induktion von apoptotischem und nekroptotischem Zelltod durch Interferone und Smac-Mimetika wurde bereits in verschiedenen Krebszelllinien, darunter HT-29, gezeigt. Die Mechanismen, durch die Interferone den nekroptotischen Zelltod auslösen, bedürfen jedoch weiterer Aufklärung. Ausgehend von früheren Erkenntnissen unserer Forschungsgruppe, dass USP22 die nekroptotische Signaltransduktion durch eine Modulierung der RIPK3-Ubiquitinierung reguliert, war das Ziel dieser Studie, den Signalweg der Interferon- und STING-induzierten Nekroptose näher zu untersuchen sowie zu verstehen, wie USP22 diese beeinflusst.

Zu diesem Zweck inkubierten wir HT-29 Kontroll- und USP22-KO Zellen in Gegenwart des Smac-Mimetikums BV6 und des Caspase-Inhibitors zVAD.fmk mit IFNγ. Durch die Analyse der Nekroptoseproteine RIPK1, RIP3 und MLKL mittels Western Blot Analyse und durch Inhibierung nekroptotischer Proteine konnten wir die Nekroptose als Form des programmierten Zelltods bestätigen. Weitere Analysen mittels Propidiumiodid-Färbung zeigten jedoch, dass USP22 die Interferon-induzierte Nekroptose, im Gegensatz zur TNF-induzierten Nekroptose, negativ reguliert und das Fehlen von USP22 in HT-29 Zellen zu beschleunigtem Zelltod führt. Die USP22-abhängige Regulierung von Zelltod konnte zusätzlich auch für die Induktion von Nekroptose durch die Behandlung mit Typ I Interferonen übertragen werden.

Im weiteren Verlauf wollten wir untersuchen, welchen Einfluss die USP22-vermittelte Regulierung von Interferon-assoziierten Signalwegen auf die Induktion von Nekroptose hat. Beispielsweise könnte eine erhöhte USP22-vermittelte Expression von Interferonen, wie sie im ersten Teil gezeigt wurde, Zellen für Nekroptose sensitivieren. Überraschenderweise war die von USP22 vermittelte Verstärkung des nekroptotischen Zelltods jedoch unabhängig von der STING-Expression und basiert auf einem noch unbekannten Mechanismus. In weiteren Experimenten konnten wir zeigen, dass Interferon-BV6-zVAD.fmk-induzierte Nekroptose in HT-29 Zellen durch TNFα und IRF1 vermittelt wird. Abschließend zeigten wir auf, dass auch eine Behandlung mit dem STING-Agonisten 2’3’-cGAMP nekroptotischen Zelltod induziert, der ebenfalls von USP22 negativ reguliert wird, was nochmals die wichtige Rolle von USP22 als Regulator der Nekroptose bestätigt und seine vielseitige Funktion in der Regulation von zellulären Prozessen aufzeigt.

8 References

1. Popovic, D., D. Vucic, and I. Dikic, *Ubiquitination in disease pathogenesis and treatment.* Nature Medicine, 2014. **20**(11): p. 1242-1253.
2. Komander, D. and M. Rape, *The ubiquitin code.* Annu Rev Biochem, 2012. **81**: p. 203-29.
3. Kerscher, O., R. Felberbaum, and M. Hochstrasser, *Modification of proteins by ubiquitin and ubiquitin-like proteins.* Annu Rev Cell Dev Biol, 2006. **22**: p. 159-80.
4. Clague, M.J., S. Urbé, and D. Komander, *Breaking the chains: deubiquitylating enzyme specificity begets function.* Nature Reviews Molecular Cell Biology, 2019. **20**(6): p. 338-352.
5. Zhang, W. and S.S. Sidhu, *Development of inhibitors in the ubiquitination cascade.* FEBS Lett, 2014. **588**(2): p. 356-67.
6. Hershko, A., et al., *Components of ubiquitin-protein ligase system. Resolution, affinity purification, and role in protein breakdown.* J Biol Chem, 1983. **258**(13): p. 8206-14.
7. Pickart, C.M. and M.J. Eddins, *Ubiquitin: structures, functions, mechanisms.* Biochimica et Biophysica Acta (BBA) - Molecular Cell Research, 2004. **1695**(1): p. 55-72.
8. Dittmar, G. and K.F. Winklhofer, *Linear Ubiquitin Chains: Cellular Functions and Strategies for Detection and Quantification.* Frontiers in Chemistry, 2020. **7**.
9. Metzger, M.B., et al., *RING-type E3 ligases: master manipulators of E2 ubiquitin-conjugating enzymes and ubiquitination.* Biochim Biophys Acta, 2014. **1843**(1): p. 47-60.
10. Weber, J., S. Polo, and E. Maspero, *HECT E3 Ligases: A Tale With Multiple Facets.* Frontiers in Physiology, 2019. **10**.
11. Qian, H., et al., *Structure and Function of HECT E3 Ubiquitin Ligases and their Role in Oxidative Stress.* J Transl Int Med, 2020. **8**(2): p. 71-79.
12. Dove, K.K. and R.E. Klevit, *RING-Between-RING E3 Ligases: Emerging Themes amid the Variations.* J Mol Biol, 2017. **429**(22): p. 3363-3375.
13. Wang, X.S., et al., *The unifying catalytic mechanism of the RING-between-RING E3 ubiquitin ligase family.* Nature Communications, 2023. **14**(1): p. 168.
14. Geis-Asteggiante, L., A.E. Lee, and C. Fenselau, *Analysis of the topology of ubiquitin chains.* Methods Enzymol, 2019. **626**: p. 323-346.
15. Akutsu, M., I. Dikic, and A. Bremm, *Ubiquitin chain diversity at a glance.* J Cell Sci, 2016. **129**(5): p. 875-80.
16. Kliza, K. and K. Husnjak, *Resolving the Complexity of Ubiquitin Networks.* Frontiers in Molecular Biosciences, 2020. **7**.
17. Guzzo, C.M., et al., *RNF4-dependent hybrid SUMO-ubiquitin chains are signals for RAP80 and thereby mediate the recruitment of BRCA1 to sites of DNA damage.* Sci Signal, 2012. **5**(253): p. ra88.
18. Dikic, I. and B.A. Schulman, *An expanded lexicon for the ubiquitin code.* Nature Reviews Molecular Cell Biology, 2022.
19. van Wijk, S.J., et al., *Visualizing ubiquitination in mammalian cells.* EMBO Rep, 2019. **20**(2).
20. Swatek, K.N. and D. Komander, *Ubiquitin modifications.* Cell Research, 2016. **26**(4): p. 399-422.
21. Kwasna, D., et al., *Discovery and Characterization of ZUFSP/ZUP1, a Distinct Deubiquitinase Class Important for Genome Stability.* Mol Cell, 2018. **70**(1): p. 150-164.e6.
22. Abdul Rehman, S.A., et al., *MINDY-1 Is a Member of an Evolutionarily Conserved and Structurally Distinct New Family of Deubiquitinating Enzymes.* Mol Cell, 2016. **63**(1): p. 146-55.
23. Zeng, C., et al., *Machado-Joseph Deubiquitinases: From Cellular Functions to Potential Therapy Targets.* Front Pharmacol, 2020. **11**: p. 1311.
24. Komander, D., M.J. Clague, and S. Urbé, *Breaking the chains: structure and function of the deubiquitinases.* Nature Reviews Molecular Cell Biology, 2009. **10**(8): p. 550-563.
25. Mevissen, T.E.T. and D. Komander, *Mechanisms of Deubiquitinase Specificity and Regulation.* Annu Rev Biochem, 2017. **86**: p. 159-192.
26. Basters, A., et al., *Structural basis of the specificity of USP18 toward ISG15.* Nat Struct Mol Biol, 2017. **24**(3): p. 270-278.
27. An, T., et al., *Insights Into the Properties, Biological Functions, and Regulation of USP21.* Frontiers in Pharmacology, 2022. **13**.
28. Basters, A., K.-P. Knobeloch, and G. Fritz, *How USP18 deals with ISG15-modified proteins: structural basis for the specificity of the protease.* The FEBS Journal, 2018. **285**(6): p. 1024-1029.
29. Zhu, X., R. Ménard, and T. Sulea, *High incidence of ubiquitin-like domains in human ubiquitin-specific proteases.* Proteins, 2007. **69**(1): p. 1-7.

30. Ronau, J.A., J.F. Beckmann, and M. Hochstrasser, *Substrate specificity of the ubiquitin and Ubl proteases.* Cell Research, 2016. **26**(4): p. 441-456.
31. Sloper-Mould, K.E., et al., *Distinct functional surface regions on ubiquitin.* J Biol Chem, 2001. **276**(32): p. 30483-9.
32. Liu, X., et al., *Colon cancer bears overexpression of OTUB1.* Pathol Res Pract, 2014. **210**(11): p. 770-3.
33. Saldana, M., et al., *Otubain 1: a non-canonical deubiquitinase with an emerging role in cancer.* Endocr Relat Cancer, 2019. **26**(1): p. R1-r14.
34. Greenwood, E., *Cylindromatosis: cause and treatment.* Nature Reviews Cancer, 2003. **3**(10): p. 716-717.
35. Sokolova, O. and M. Naumann, *Manifold role of ubiquitin in Helicobacter pylori infection and gastric cancer.* Cell Mol Life Sci, 2021. **78**(10): p. 4765-4783.
36. Sato, S., et al., *Juvenile onset autoinflammatory disease due to a novel mutation in TNFAIP3 (A20).* Arthritis Research & Therapy, 2018. **20**(1): p. 274.
37. Isaacson, M.K. and H.L. Ploegh, *Ubiquitination, ubiquitin-like modifiers, and deubiquitination in viral infection.* Cell Host Microbe, 2009. **5**(6): p. 559-70.
38. Bailey-Elkin, B.A., et al., *Structure and Function of Viral Deubiquitinating Enzymes.* J Mol Biol, 2017. **429**(22): p. 3441-3470.
39. Chen, X., et al., *SARS coronavirus papain-like protease inhibits the type I interferon signaling pathway through interaction with the STING-TRAF3-TBK1 complex.* Protein Cell, 2014. **5**(5): p. 369-81.
40. Shin, D., et al., *Papain-like protease regulates SARS-CoV-2 viral spread and innate immunity.* Nature, 2020. **587**(7835): p. 657-662.
41. Nomaguchi, M., M. Fujita, and A. Adachi, *Role of HIV-1 Vpu protein for virus spread and pathogenesis.* Microbes and Infection, 2008. **10**(9): p. 960-967.
42. Glinsky, G.V., O. Berezovska, and A.B. Glinskii, *Microarray analysis identifies a death-from-cancer signature predicting therapy failure in patients with multiple types of cancer.* J Clin Invest, 2005. **115**(6): p. 1503-21.
43. Glinsky, G.V., *Genomic Models of Metastatic Cancer: Functional Analysis of Death-from-Cancer Signature Genes Reveals Aneuploid, Anoikis-Resistant, Metastasis-Enabling Phenotype with Altered Cell Cycle Control and Activated PcG Protein Chromatin Silencing Pathway.* Cell Cycle, 2006. **5**(11): p. 1208-1216.
44. Gavin, A.C., et al., *Functional organization of the yeast proteome by systematic analysis of protein complexes.* Nature, 2002. **415**(6868): p. 141-7.
45. Ho, Y., et al., *Systematic identification of protein complexes in Saccharomyces cerevisiae by mass spectrometry.* Nature, 2002. **415**(6868): p. 180-3.
46. Bonnet, J., et al., *Zinc-finger UBPs: regulators of deubiquitylation.* Trends in Biochemical Sciences, 2008. **33**(8): p. 369-375.
47. Jeusset, L.M.P. and K.J. McManus *Ubiquitin Specific Peptidase 22 Regulates Histone H2B Mono-Ubiquitination and Exhibits Both Oncogenic and Tumor Suppressor Roles in Cancer*. Cancers, 2017. **9**, DOI: 10.3390/cancers9120167.
48. Soffers, J.H.M. and J.L. Workman, *The SAGA chromatin-modifying complex: the sum of its parts is greater than the whole.* Genes Dev, 2020. **34**(19-20): p. 1287-1303.
49. Herbst, D.A., et al., *Structure of the human SAGA coactivator complex.* Nature Structural & Molecular Biology, 2021. **28**(12): p. 989-996.
50. Cheon, Y., et al., *Dynamic modules of the coactivator SAGA in eukaryotic transcription.* Experimental & Molecular Medicine, 2020. **52**(7): p. 991-1003.
51. Zhang, X.Y., et al., *The putative cancer stem cell marker USP22 is a subunit of the human SAGA complex required for activated transcription and cell-cycle progression.* Mol Cell, 2008. **29**(1): p. 102-11.
52. Zhao, Y., et al., *A TFTC/STAGA module mediates histone H2A and H2B deubiquitination, coactivates nuclear receptors, and counteracts heterochromatin silencing.* Mol Cell, 2008. **29**(1): p. 92-101.
53. Zhang, X.Y., et al., *USP22, an hSAGA subunit and potential cancer stem cell marker, reverses the polycomb-catalyzed ubiquitylation of histone H2A.* Cell Cycle, 2008. **7**(11): p. 1522-4.
54. Liu, S., et al., *H2A ubiquitination is essential for Polycomb Repressive Complex 1-mediated gene regulation in Marchantia polymorpha.* Genome Biology, 2021. **22**(1): p. 253.
55. Wang, H., et al., *Role of histone H2A ubiquitination in Polycomb silencing.* Nature, 2004. **431**(7010): p. 873-878.

56. Shema-Yaacoby, E., et al., *Systematic identification of proteins binding to chromatin-embedded ubiquitylated H2B reveals recruitment of SWI/SNF to regulate transcription.* Cell Rep, 2013. **4**(3): p. 601-8.
57. Fierz, B., et al., *Histone H2B ubiquitylation disrupts local and higher-order chromatin compaction.* Nat Chem Biol, 2011. **7**(2): p. 113-9.
58. Pavri, R., et al., *Histone H2B Monoubiquitination Functions Cooperatively with FACT to Regulate Elongation by RNA Polymerase II.* Cell, 2006. **125**(4): p. 703-717.
59. Hong, A., J.E. Lee, and K.C. Chung, *Ubiquitin-specific protease 22 (USP22) positively regulates RCAN1 protein levels through RCAN1 de-ubiquitination.* J Cell Physiol, 2015. **230**(7): p. 1651-60.
60. Wyce, A., et al., *H2B ubiquitylation acts as a barrier to Ctk1 nucleosomal recruitment prior to removal by Ubp8 within a SAGA-related complex.* Mol Cell, 2007. **27**(2): p. 275-288.
61. Atanassov, B.S. and S.Y. Dent, *USP22 regulates cell proliferation by deubiquitinating the transcriptional regulator FBP1.* EMBO Rep, 2011. **12**(9): p. 924-30.
62. Abbas, T. and A. Dutta, *p21 in cancer: intricate networks and multiple activities.* Nat Rev Cancer, 2009. **9**(6): p. 400-14.
63. Ning, Z., et al., *USP22 promotes the G1/S phase transition by upregulating FoxM1 expression via β-catenin nuclear localization and is associated with poor prognosis in stage II pancreatic ductal adenocarcinoma.* Int J Oncol, 2014. **45**(4): p. 1594-608.
64. Li, Z.H., et al., *RNA interference-mediated USP22 gene silencing promotes human brain glioma apoptosis and induces cell cycle arrest.* Oncol Lett, 2013. **5**(4): p. 1290-1294.
65. Lin, Z., et al., *Ubiquitin-specific protease 22 is a deubiquitinase of CCNB1.* Cell Discov, 2015. **1**: p. 15028-.
66. Hanahan, D. and R.A. Weinberg, *Hallmarks of cancer: the next generation.* Cell, 2011. **144**(5): p. 646-74.
67. Schrecengost, R.S., et al., *USP22 regulates oncogenic signaling pathways to drive lethal cancer progression.* Cancer Res, 2014. **74**(1): p. 272-86.
68. Lin, Z., et al., *USP22 antagonizes p53 transcriptional activation by deubiquitinating Sirt1 to suppress cell apoptosis and is required for mouse embryonic development.* Mol Cell, 2012. **46**(4): p. 484-94.
69. Li, L., et al., *SIRT1 activation by a c-MYC oncogenic network promotes the maintenance and drug resistance of human FLT3-ITD acute myeloid leukemia stem cells.* Cell Stem Cell, 2014. **15**(4): p. 431-446.
70. Prokakis, E., et al., *USP22 promotes HER2-driven mammary carcinoma aggressiveness by suppressing the unfolded protein response.* Oncogene, 2021. **40**(23): p. 4004-4018.
71. Jiang, S., et al., *Ubiquitin-Specific Peptidase 22 Contributes to Colorectal Cancer Stemness and Chemoresistance via Wnt/β-Catenin Pathway.* Cellular Physiology and Biochemistry, 2018. **46**(4): p. 1412-1422.
72. Roedig, J., et al., *USP22 controls necroptosis by regulating receptor-interacting protein kinase 3 ubiquitination.* EMBO Rep, 2021. **22**(2): p. e50163.
73. Levine, B. and G. Kroemer, *Autophagy in the pathogenesis of disease.* Cell, 2008. **132**(1): p. 27-42.
74. Isaacs, A. and J. Lindenmann, *Virus interference. I. The interferon.* Proc R Soc Lond B Biol Sci, 1957. **147**(927): p. 258-67.
75. Platanias, L.C., *Mechanisms of type-I- and type-II-interferon-mediated signalling.* Nature Reviews Immunology, 2005. **5**(5): p. 375-386.
76. Pestka, S., et al., *The interferon gamma (IFN-γ) receptor: a paradigm for the multichain cytokine receptor.* Cytokine & Growth Factor Reviews, 1997. **8**(3): p. 189-206.
77. Kotenko, S.V., et al., *IFN-lambdas mediate antiviral protection through a distinct class II cytokine receptor complex.* Nat Immunol, 2003. **4**(1): p. 69-77.
78. Prokunina-Olsson, L., et al., *A variant upstream of IFNL3 (IL28B) creating a new interferon gene IFNL4 is associated with impaired clearance of hepatitis C virus.* Nat Genet, 2013. **45**(2): p. 164-71.
79. Lazear, H.M., J.W. Schoggins, and M.S. Diamond, *Shared and Distinct Functions of Type I and Type III Interferons.* Immunity, 2019. **50**(4): p. 907-923.
80. Kagan, J.C., et al., *TRAM couples endocytosis of Toll-like receptor 4 to the induction of interferon-beta.* Nat Immunol, 2008. **9**(4): p. 361-8.
81. Odendall, C., A.A. Voak, and J.C. Kagan, *Type III IFNs Are Commonly Induced by Bacteria-Sensing TLRs and Reinforce Epithelial Barriers during Infection.* J Immunol, 2017. **199**(9): p. 3270-3279.

82. Honda, K., et al., *IRF-7 is the master regulator of type-I interferon-dependent immune responses.* Nature, 2005. **434**(7034): p. 772-777.
83. Honda, K., A. Takaoka, and T. Taniguchi, *Type I Inteferon Gene Induction by the Interferon Regulatory Factor Family of Transcription Factors.* Immunity, 2006. **25**(3): p. 349-360.
84. Lazear, H.M., et al., *IRF-3, IRF-5, and IRF-7 Coordinately Regulate the Type I IFN Response in Myeloid Dendritic Cells Downstream of MAVS Signaling.* PLOS Pathogens, 2013. **9**(1): p. e1003118.
85. Odendall, C., et al., *Diverse intracellular pathogens activate type III interferon expression from peroxisomes.* Nature Immunology, 2014. **15**(8): p. 717-726.
86. Osterlund, P.I., et al., *IFN regulatory factor family members differentially regulate the expression of type III IFN (IFN-lambda) genes.* J Immunol, 2007. **179**(6): p. 3434-42.
87. Kasahara, T., et al., *Interleukin 2-mediated immune interferon (IFN-gamma) production by human T cells and T cell subsets.* J Immunol, 1983. **130**(4): p. 1784-9.
88. Matsushita, H., et al., *Cytotoxic T lymphocytes block tumor growth both by lytic activity and IFNγ-dependent cell-cycle arrest.* Cancer Immunol Res, 2015. **3**(1): p. 26-36.
89. Yu, J., et al., *Pro- and antiinflammatory cytokine signaling: reciprocal antagonism regulates interferon-gamma production by human natural killer cells.* Immunity, 2006. **24**(5): p. 575-90.
90. Sercan, O.z., et al., *Cutting Edge: Innate Immune Cells Contribute to the IFN-γ-Dependent Regulation of Antigen-Specific CD8+ T Cell Homeostasis1.* The Journal of Immunology, 2006. **176**(2): p. 735-739.
91. Mesev, E.V., R.A. LeDesma, and A. Ploss, *Decoding type I and III interferon signalling during viral infection.* Nature Microbiology, 2019. **4**(6): p. 914-924.
92. Kotenko, S.V., et al., *Type III IFNs: Beyond antiviral protection.* Semin Immunol, 2019. **43**: p. 101303.
93. Ye, L., D. Schnepf, and P. Staeheli, *Interferon-λ orchestrates innate and adaptive mucosal immune responses.* Nat Rev Immunol, 2019. **19**(10): p. 614-625.
94. Zanin, N., et al., *Interferon Receptor Trafficking and Signaling: Journey to the Cross Roads.* Frontiers in Immunology, 2021. **11**.
95. Egli, A., et al., *The impact of the interferon-lambda family on the innate and adaptive immune response to viral infections.* Emerg Microbes Infect, 2014. **3**(7): p. e51.
96. Kumar, K.G., et al., *SCF(HOS) ubiquitin ligase mediates the ligand-induced down-regulation of the interferon-alpha receptor.* Embo j, 2003. **22**(20): p. 5480-90.
97. Kumar, K.G., J.J. Krolewski, and S.Y. Fuchs, *Phosphorylation and specific ubiquitin acceptor sites are required for ubiquitination and degradation of the IFNAR1 subunit of type I interferon receptor.* J Biol Chem, 2004. **279**(45): p. 46614-20.
98. Kumar, K.G., et al., *Site-specific ubiquitination exposes a linear motif to promote interferon-alpha receptor endocytosis.* J Cell Biol, 2007. **179**(5): p. 935-50.
99. Marchetti, M., et al., *Stat-mediated signaling induced by type I and type II interferons (IFNs) is differentially controlled through lipid microdomain association and clathrin-dependent endocytosis of IFN receptors.* Mol Biol Cell, 2006. **17**(7): p. 2896-909.
100. Blouin, C.M., et al., *Glycosylation-Dependent IFN-γR Partitioning in Lipid and Actin Nanodomains Is Critical for JAK Activation.* Cell, 2016. **166**(4): p. 920-934.
101. Darnell, J.E., Jr., I.M. Kerr, and G.R. Stark, *Jak-STAT pathways and transcriptional activation in response to IFNs and other extracellular signaling proteins.* Science, 1994. **264**(5164): p. 1415-21.
102. Boehm, U., et al., *Cellular responses to interferon-gamma.* Annu Rev Immunol, 1997. **15**: p. 749-95.
103. Jaks, E., et al., *Differential receptor subunit affinities of type I interferons govern differential signal activation.* J Mol Biol, 2007. **366**(2): p. 525-39.
104. Lavoie, T.B., et al., *Binding and activity of all human alpha interferon subtypes.* Cytokine, 2011. **56**(2): p. 282-9.
105. Cull, V.S., et al., *Type I interferon differential therapy for erythroleukemia: specificity of STAT activation.* Blood, 2003. **101**(7): p. 2727-35.
106. Moraga, I., et al., *Receptor density is key to the alpha2/beta interferon differential activities.* Mol Cell Biol, 2009. **29**(17): p. 4778-87.
107. Maher, S.G., et al., *IFNalpha and IFNlambda differ in their antiproliferative effects and duration of JAK/STAT signaling activity.* Cancer Biol Ther, 2008. **7**(7): p. 1109-15.
108. Gibbert, K., et al., *IFN-α subtypes: distinct biological activities in anti-viral therapy.* Br J Pharmacol, 2013. **168**(5): p. 1048-58.
109. Gough, D.J., et al., *Constitutive type I interferon modulates homeostatic balance through tonic signaling.* Immunity, 2012. **36**(2): p. 166-174.

110. Hsu, A.C.Y., et al., *Critical Role of Constitutive Type I Interferon Response in Bronchial Epithelial Cell to Influenza Infection.* PLOS ONE, 2012. **7**(3): p. e32947.
111. Tsugawa, Y., et al., *Critical Role of Interferon-α Constitutively Produced in Human Hepatocytes in Response to RNA Virus Infection.* PLOS ONE, 2014. **9**(2): p. e89869.
112. Silginer, M., et al., *Autocrine activation of the IFN signaling pathway may promote immune escape in glioblastoma.* Neuro-oncology, 2017. **19**(10): p. 1338-1349.
113. Kurokawa, C., et al., *Constitutive Interferon Pathway Activation in Tumors as an Efficacy Determinant Following Oncolytic Virotherapy.* JNCI: Journal of the National Cancer Institute, 2018. **110**(10): p. 1123-1132.
114. Akamatsu, M.A., et al., *Off balance: Interferons in COVID-19 lung infections.* eBioMedicine, 2021. **73**.
115. Dempsey, P.W., S.A. Vaidya, and G. Cheng, *The art of war: Innate and adaptive immune responses.* Cell Mol Life Sci, 2003. **60**(12): p. 2604-21.
116. Chaplin, D.D., *Overview of the immune response.* J Allergy Clin Immunol, 2010. **125**(2 Suppl 2): p. S3-23.
117. Amarante-Mendes, G.P., et al., *Pattern Recognition Receptors and the Host Cell Death Molecular Machinery.* Frontiers in Immunology, 2018. **9**.
118. Rai, V., G. Mathews, and D.K. Agrawal, *Translational and Clinical Significance of DAMPs, PAMPs, and PRRs in Trauma-induced Inflammation.* Arch Clin Biomed Res, 2022. **6**(5): p. 673-685.
119. Li, D. and M. Wu, *Pattern recognition receptors in health and diseases.* Signal Transduction and Targeted Therapy, 2021. **6**(1): p. 291.
120. Bell, J.K., et al., *Leucine-rich repeats and pathogen recognition in Toll-like receptors.* Trends Immunol, 2003. **24**(10): p. 528-33.
121. Liu, L., et al., *Structural basis of toll-like receptor 3 signaling with double-stranded RNA.* Science (New York, N.Y.), 2008. **320**(5874): p. 379-381.
122. Chuenchor, W., et al., *Structures of pattern recognition receptors reveal molecular mechanisms of autoinhibition, ligand recognition and oligomerization.* Curr Opin Immunol, 2014. **26**: p. 14-20.
123. Kawai, T. and S. Akira, *The role of pattern-recognition receptors in innate immunity: update on Toll-like receptors.* Nature Immunology, 2010. **11**(5): p. 373-384.
124. Kawasaki, T. and T. Kawai, *Toll-like receptor signaling pathways.* Front Immunol, 2014. **5**: p. 461.
125. Li, W.W., et al., *Ubiquitination of TLR3 by TRIM3 signals its ESCRT-mediated trafficking to the endolysosomes for innate antiviral response.* Proc Natl Acad Sci U S A, 2020. **117**(38): p. 23707-23716.
126. Matsumoto, M., H. Oshiumi, and T. Seya, *Antiviral responses induced by the TLR3 pathway.* Rev Med Virol, 2011. **21**(2): p. 67-77.
127. Kato, H., et al., *Length-dependent recognition of double-stranded ribonucleic acids by retinoic acid-inducible gene-I and melanoma differentiation-associated gene 5.* J Exp Med, 2008. **205**(7): p. 1601-10.
128. Rehwinkel, J. and M.U. Gack, *RIG-I-like receptors: their regulation and roles in RNA sensing.* Nature Reviews Immunology, 2020. **20**(9): p. 537-551.
129. Jakobsen, M.R., et al., *IFI16 senses DNA forms of the lentiviral replication cycle and controls HIV-1 replication.* Proc Natl Acad Sci U S A, 2013. **110**(48): p. E4571-80.
130. Takaoka, A., et al., *DAI (DLM-1/ZBP1) is a cytosolic DNA sensor and an activator of innate immune response.* Nature, 2007. **448**(7152): p. 501-5.
131. Bürckstümmer, T., et al., *An orthogonal proteomic-genomic screen identifies AIM2 as a cytoplasmic DNA sensor for the inflammasome.* Nat Immunol, 2009. **10**(3): p. 266-72.
132. Chiu, Y.H., J.B. Macmillan, and Z.J. Chen, *RNA polymerase III detects cytosolic DNA and induces type I interferons through the RIG-I pathway.* Cell, 2009. **138**(3): p. 576-91.
133. Sun, L., et al., *Cyclic GMP-AMP synthase is a cytosolic DNA sensor that activates the type I interferon pathway.* Science, 2013. **339**(6121): p. 786-91.
134. Zhang, X., et al., *Cyclic GMP-AMP containing mixed phosphodiester linkages is an endogenous high-affinity ligand for STING.* Mol Cell, 2013. **51**(2): p. 226-35.
135. Ablasser, A., et al., *cGAS produces a 2'-5'-linked cyclic dinucleotide second messenger that activates STING.* Nature, 2013. **498**(7454): p. 380-4.
136. Gao, P., et al., *Cyclic [G(2',5')pA(3',5')p] is the metazoan second messenger produced by DNA-activated cyclic GMP-AMP synthase.* Cell, 2013. **153**(5): p. 1094-107.
137. Diner, E.J., et al., *The innate immune DNA sensor cGAS produces a noncanonical cyclic dinucleotide that activates human STING.* Cell Rep, 2013. **3**(5): p. 1355-61.

138. Shang, G., et al., *Cryo-EM structures of STING reveal its mechanism of activation by cyclic GMP-AMP.* Nature, 2019. **567**(7748): p. 389-393.
139. Liu, S., et al., *Phosphorylation of innate immune adaptor proteins MAVS, STING, and TRIF induces IRF3 activation.* Science, 2015. **347**(6227): p. aaa2630.
140. Decout, A., et al., *The cGAS–STING pathway as a therapeutic target in inflammatory diseases.* Nature Reviews Immunology, 2021. **21**(9): p. 548-569.
141. Shang, M., et al., *2',3'-Cyclic GMP-AMP Dinucleotides for STING-Mediated Immune Modulation: Principles, Immunotherapeutic Potential, and Synthesis.* ChemMedChem, 2022. **17**(2): p. e202100671.
142. Ishikawa, H. and G.N. Barber, *STING is an endoplasmic reticulum adaptor that facilitates innate immune signalling.* Nature, 2008. **455**(7213): p. 674-678.
143. Saitoh, T., et al., *Atg9a controls dsDNA-driven dynamic translocation of STING and the innate immune response.* Proc Natl Acad Sci U S A, 2009. **106**(49): p. 20842-6.
144. Dobbs, N., et al., *STING Activation by Translocation from the ER Is Associated with Infection and Autoinflammatory Disease.* Cell Host Microbe, 2015. **18**(2): p. 157-68.
145. Srikanth, S., et al., *The Ca(2+) sensor STIM1 regulates the type I interferon response by retaining the signaling adaptor STING at the endoplasmic reticulum.* Nat Immunol, 2019. **20**(2): p. 152-162.
146. Gui, X., et al., *Autophagy induction via STING trafficking is a primordial function of the cGAS pathway.* Nature, 2019. **567**(7747): p. 262-266.
147. Zhang, B.C., et al., *STEEP mediates STING ER exit and activation of signaling.* Nat Immunol, 2020. **21**(8): p. 868-879.
148. Zhang, C., et al., *Structural basis of STING binding with and phosphorylation by TBK1.* Nature, 2019. **567**(7748): p. 394-398.
149. Ogawa, E., et al., *The binding of TBK1 to STING requires exocytic membrane traffic from the ER.* Biochem Biophys Res Commun, 2018. **503**(1): p. 138-145.
150. Tu, X., et al., *Interruption of post-Golgi STING trafficking activates tonic interferon signaling.* Nature Communications, 2022. **13**(1): p. 6977.
151. Prabakaran, T., et al., *Attenuation of cGAS-STING signaling is mediated by a p62/SQSTM1-dependent autophagy pathway activated by TBK1.* Embo j, 2018. **37**(8).
152. Mukai, K., et al., *Homeostatic regulation of STING by retrograde membrane traffic to the ER.* Nature Communications, 2021. **12**(1): p. 61.
153. Liu, D., et al., *STING directly activates autophagy to tune the innate immune response.* Cell Death Differ, 2019. **26**(9): p. 1735-1749.
154. Ishikawa, H., Z. Ma, and G.N. Barber, *STING regulates intracellular DNA-mediated, type I interferon-dependent innate immunity.* Nature, 2009. **461**(7265): p. 788-792.
155. Oeckinghaus, A. and S. Ghosh, *The NF-kappaB family of transcription factors and its regulation.* Cold Spring Harb Perspect Biol, 2009. **1**(4): p. a000034.
156. Sun, S.C., J.H. Chang, and J. Jin, *Regulation of nuclear factor-κB in autoimmunity.* Trends Immunol, 2013. **34**(6): p. 282-9.
157. Sun, S.C. and S.C. Ley, *New insights into NF-kappaB regulation and function.* Trends Immunol, 2008. **29**(10): p. 469-78.
158. Karin, M. and M. Delhase, *The I kappa B kinase (IKK) and NF-kappa B: key elements of proinflammatory signalling.* Semin Immunol, 2000. **12**(1): p. 85-98.
159. Sun, S.C., *The noncanonical NF-κB pathway.* Immunol Rev, 2012. **246**(1): p. 125-40.
160. Balka, K.R., et al., *TBK1 and IKKε Act Redundantly to Mediate STING-Induced NF-κB Responses in Myeloid Cells.* Cell Reports, 2020. **31**(1).
161. Abe, T. and G.N. Barber, *Cytosolic-DNA-Mediated, STING-Dependent Proinflammatory Gene Induction Necessitates Canonical NF-κB Activation through TBK1.* Journal of Virology, 2014. **88**(10): p. 5328-5341.
162. Bakhoum, S.F., et al., *Chromosomal instability drives metastasis through a cytosolic DNA response.* Nature, 2018. **553**(7689): p. 467-472.
163. Hopfner, K.-P. and V. Hornung, *Molecular mechanisms and cellular functions of cGAS–STING signalling.* Nature Reviews Molecular Cell Biology, 2020. **21**(9): p. 501-521.
164. Zhang, Z., et al., *Multifaceted functions of STING in human health and disease: from molecular mechanism to targeted strategy.* Signal Transduction and Targeted Therapy, 2022. **7**(1): p. 394.
165. Unterholzner, L., et al., *IFI16 is an innate immune sensor for intracellular DNA.* Nat Immunol, 2010. **11**(11): p. 997-1004.
166. Zhang, Z., et al., *The helicase DDX41 senses intracellular DNA mediated by the adaptor STING in dendritic cells.* Nat Immunol, 2011. **12**(10): p. 959-65.

167. Ferguson, B.J., et al., *DNA-PK is a DNA sensor for IRF-3-dependent innate immunity.* Elife, 2012. **1**: p. e00047.
168. Zevini, A., D. Olagnier, and J. Hiscott, *Crosstalk between Cytoplasmic RIG-I and STING Sensing Pathways.* Trends in immunology, 2017. **38**(3): p. 194-205.
169. Neufeldt, C.J., et al., *SARS-CoV-2 infection induces a pro-inflammatory cytokine response through cGAS-STING and NF-κB.* bioRxiv, 2020: p. 2020.07.21.212639.
170. Chan, J.F., et al., *Genomic characterization of the 2019 novel human-pathogenic coronavirus isolated from a patient with atypical pneumonia after visiting Wuhan.* Emerg Microbes Infect, 2020. **9**(1): p. 221-236.
171. Kim, D., et al., *The Architecture of SARS-CoV-2 Transcriptome.* Cell, 2020. **181**(4): p. 914-921.e10.
172. Hoffmann, M., et al., *SARS-CoV-2 Cell Entry Depends on ACE2 and TMPRSS2 and Is Blocked by a Clinically Proven Protease Inhibitor.* Cell, 2020. **181**(2): p. 271-280.e8.
173. Shang, J., et al., *Structural basis of receptor recognition by SARS-CoV-2.* Nature, 2020. **581**(7807): p. 221-224.
174. Walls, A.C., et al., *Structure, Function, and Antigenicity of the SARS-CoV-2 Spike Glycoprotein.* Cell, 2020. **181**(2): p. 281-292.e6.
175. Klein, S., et al., *SARS-CoV-2 structure and replication characterized by in situ cryo-electron tomography.* Nat Commun, 2020. **11**(1): p. 5885.
176. Brant, A.C., et al., *SARS-CoV-2: from its discovery to genome structure, transcription, and replication.* Cell Biosci, 2021. **11**(1): p. 136.
177. Hartenian, E., et al., *The molecular virology of coronaviruses.* J Biol Chem, 2020. **295**(37): p. 12910-12934.
178. Lu, Q., et al., *SARS-CoV-2 exacerbates proinflammatory responses in myeloid cells through C-type lectin receptors and Tweety family member 2.* Immunity, 2021. **54**(6): p. 1304-1319.e9.
179. Thépaut, M., et al., *DC/L-SIGN recognition of spike glycoprotein promotes SARS-CoV-2 trans-infection and can be inhibited by a glycomimetic antagonist.* PLOS Pathogens, 2021. **17**(5): p. e1009576.
180. Amraei, R., et al., *CD209L/L-SIGN and CD209/DC-SIGN Act as Receptors for SARS-CoV-2.* ACS Central Science, 2021. **7**(7): p. 1156-1165.
181. Zheng, M., et al., *TLR2 senses the SARS-CoV-2 envelope protein to produce inflammatory cytokines.* Nature Immunology, 2021. **22**(7): p. 829-838.
182. Proud, P.C., et al., *Prophylactic intranasal administration of a TLR2/6 agonist reduces upper respiratory tract viral shedding in a SARS-CoV-2 challenge ferret model.* EBioMedicine, 2021. **63**: p. 103153.
183. Sohn, K.M., et al., *COVID-19 Patients Upregulate Toll-like Receptor 4-mediated Inflammatory Signaling That Mimics Bacterial Sepsis.* J Korean Med Sci, 2020. **35**(38): p. e343.
184. Choudhury, A. and S. Mukherjee, *In silico studies on the comparative characterization of the interactions of SARS-CoV-2 spike glycoprotein with ACE-2 receptor homologs and human TLRs.* Journal of Medical Virology, 2020. **92**(10): p. 2105-2113.
185. Zhang, Q., et al., *Inborn errors of type I IFN immunity in patients with life-threatening COVID-19.* Science, 2020. **370**(6515).
186. Kouwaki, T., et al., *RIG-I-Like Receptor-Mediated Recognition of Viral Genomic RNA of Severe Acute Respiratory Syndrome Coronavirus-2 and Viral Escape From the Host Innate Immune Responses.* Front Immunol, 2021. **12**: p. 700926.
187. Thorne, L.G., et al., *SARS-CoV-2 sensing by RIG-I and MDA5 links epithelial infection to macrophage inflammation.* Embo j, 2021. **40**(15): p. e107826.
188. Wu, J., et al., *SARS-CoV-2 ORF9b inhibits RIG-I-MAVS antiviral signaling by interrupting K63-linked ubiquitination of NEMO.* Cell Rep, 2021. **34**(7): p. 108761.
189. Felgenhauer, U., et al., *Inhibition of SARS-CoV-2 by type I and type III interferons.* J Biol Chem, 2020. **295**(41): p. 13958-13964.
190. Kuri, T., et al., *Interferon priming enables cells to partially overturn the SARS coronavirus-induced block in innate immune activation.* The Journal of general virology, 2009. **90**(Pt 11): p. 2686-2694.
191. Vanderheiden, A., et al., *Type I and Type III Interferons Restrict SARS-CoV-2 Infection of Human Airway Epithelial Cultures.* J Virol, 2020. **94**(19).
192. Busnadiego, I., et al., *Antiviral Activity of Type I, II, and III Interferons Counterbalances ACE2 Inducibility and Restricts SARS-CoV-2.* mBio, 2020. **11**(5).
193. Li, M., et al., *Pharmacological activation of STING blocks SARS-CoV-2 infection.* Science Immunology, 2021. **6**(59): p. eabi9007.

194. Liu, W., et al., *Activation of STING Signaling Pathway Effectively Blocks Human Coronavirus Infection.* J Virol, 2021. **95**(12).
195. Song, P., et al., *Cytokine storm induced by SARS-CoV-2.* Clin Chim Acta, 2020. **509**: p. 280-287.
196. Guan, W.J., et al., *Clinical Characteristics of Coronavirus Disease 2019 in China.* N Engl J Med, 2020. **382**(18): p. 1708-1720.
197. Chen, G., et al., *Clinical and immunological features of severe and moderate coronavirus disease 2019.* J Clin Invest, 2020. **130**(5): p. 2620-2629.
198. Jiang, S., C. Hillyer, and L. Du, *Neutralizing Antibodies against SARS-CoV-2 and Other Human Coronaviruses.* Trends in Immunology, 2020. **41**(5): p. 355-359.
199. Tsuchida, T., et al., *The ubiquitin ligase TRIM56 regulates innate immune responses to intracellular double-stranded DNA.* Immunity, 2010. **33**(5): p. 765-76.
200. Zhang, J., et al., *TRIM32 protein modulates type I interferon induction and cellular antiviral response by targeting MITA/STING protein for K63-linked ubiquitination.* J Biol Chem, 2012. **287**(34): p. 28646-55.
201. Ni, G., H. Konno, and G.N. Barber, *Ubiquitination of STING at lysine 224 controls IRF3 activation.* Sci Immunol, 2017. **2**(11).
202. Zhang, Z.D., et al., *RNF115 plays dual roles in innate antiviral responses by catalyzing distinct ubiquitination of MAVS and MITA.* Nat Commun, 2020. **11**(1): p. 5536.
203. Wang, Q., et al., *The E3 ubiquitin ligase AMFR and INSIG1 bridge the activation of TBK1 kinase by modifying the adaptor STING.* Immunity, 2014. **41**(6): p. 919-33.
204. Zhong, B., et al., *The ubiquitin ligase RNF5 regulates antiviral responses by mediating degradation of the adaptor protein MITA.* Immunity, 2009. **30**(3): p. 397-407.
205. Wang, Y., et al., *TRIM30α Is a Negative-Feedback Regulator of the Intracellular DNA and DNA Virus-Triggered Response by Targeting STING.* PLoS Pathog, 2015. **11**(6): p. e1005012.
206. Xing, J., et al., *TRIM29 promotes DNA virus infections by inhibiting innate immune response.* Nature Communications, 2017. **8**(1): p. 945.
207. Li, X., et al., *The transmembrane endoplasmic reticulum-associated E3 ubiquitin ligase TRIM13 restrains the pathogenic-DNA-triggered inflammatory response.* Sci Adv, 2022. **8**(4): p. eabh0496.
208. Fenech, E.J., et al., *Interaction mapping of endoplasmic reticulum ubiquitin ligases identifies modulators of innate immune signalling.* Elife, 2020. **9**.
209. Qin, Y., et al., *RNF26 Temporally Regulates Virus-Triggered Type I Interferon Induction by Two Distinct Mechanisms.* PLOS Pathogens, 2014. **10**(9): p. e1004358.
210. Luo, W.-W., et al., *iRhom2 is essential for innate immunity to DNA viruses by mediating trafficking and stability of the adaptor STING.* Nature Immunology, 2016. **17**(9): p. 1057-1066.
211. Sun, H., et al., *USP13 negatively regulates antiviral responses by deubiquitinating STING.* Nature Communications, 2017. **8**(1): p. 15534.
212. Zhang, J., et al., *Deubiquitinase USP35 restrains STING-mediated interferon signaling in ovarian cancer.* Cell Death & Differentiation, 2021. **28**(1): p. 139-155.
213. Zhang, L., et al., *The deubiquitinase CYLD is a specific checkpoint of the STING antiviral signaling pathway.* PLOS Pathogens, 2018. **14**(11): p. e1007435.
214. Chen, Y., et al., *p38 inhibition provides anti-DNA virus immunity by regulation of USP21 phosphorylation and STING activation.* J Exp Med, 2017. **214**(4): p. 991-1010.
215. Tian, M., et al., *MYSM1 Represses Innate Immunity and Autoimmunity through Suppressing the cGAS-STING Pathway.* Cell Rep, 2020. **33**(3): p. 108297.
216. Zhang, M., et al., *USP18 recruits USP20 to promote innate antiviral response through deubiquitinating STING/MITA.* Cell Res, 2016. **26**(12): p. 1302-1319.
217. Zhang, M.X., et al., *USP20 Promotes Cellular Antiviral Responses via Deconjugating K48-Linked Ubiquitination of MITA.* J Immunol, 2019. **202**(8): p. 2397-2406.
218. Guo, Y., et al., *OTUD5 promotes innate antiviral and antitumor immunity through deubiquitinating and stabilizing STING.* Cell Mol Immunol, 2021. **18**(8): p. 1945-1955.
219. Liu, Q., et al., *Broad and diverse mechanisms used by deubiquitinase family members in regulating the type I interferon signaling pathway during antiviral responses.* Sci Adv, 2018. **4**(5): p. eaar2824.
220. Ao, N., et al., *Ubiquitin-specific peptidase USP22 negatively regulates the STAT signaling pathway by deubiquitinating SIRT1.* Cell Physiol Biochem, 2014. **33**(6): p. 1863-75.
221. Wang, R., P. Cherukuri, and J. Luo, *Activation of Stat3 sequence-specific DNA binding and transcription by p300/CREB-binding protein-mediated acetylation.* J Biol Chem, 2005. **280**(12): p. 11528-34.

222. Dietlein, N., et al., *Usp22 is an intracellular regulator of systemic emergency hematopoiesis.* Sci Immunol, 2022. **7**(78): p. eabq2061.
223. Cai, Z., et al., *USP22 promotes IRF3 nuclear translocation and antiviral responses by deubiquitinating the importin protein KPNA2.* J Exp Med, 2020. **217**(5).
224. Li, M., et al., *USP22 deficiency in melanoma mediates resistance to T cells through IFNγ-JAK1-STAT1 signal axis.* Mol Ther, 2021. **29**(6): p. 2108-2120.
225. Nagata, S. and M. Tanaka, *Programmed cell death and the immune system.* Nature Reviews Immunology, 2017. **17**(5): p. 333-340.
226. Lockshin, R.A. and C.M. Williams, *PROGRAMMED CELL DEATH--I. CYTOLOGY OF DEGENERATION IN THE INTERSEGMENTAL MUSCLES OF THE PERNYI SILKMOTH.* J Insect Physiol, 1965. **11**: p. 123-33.
227. Galluzzi, L., et al., *Molecular mechanisms of cell death: recommendations of the Nomenclature Committee on Cell Death 2018.* Cell Death & Differentiation, 2018. **25**(3): p. 486-541.
228. Bedoui, S., M.J. Herold, and A. Strasser, *Emerging connectivity of programmed cell death pathways and its physiological implications.* Nature Reviews Molecular Cell Biology, 2020. **21**(11): p. 678-695.
229. Degterev, A., et al., *Chemical inhibitor of nonapoptotic cell death with therapeutic potential for ischemic brain injury.* Nat Chem Biol, 2005. **1**(2): p. 112-9.
230. Newton, K. and G. Manning, *Necroptosis and Inflammation.* Annual Review of Biochemistry, 2016. **85**(1): p. 743-763.
231. Dhuriya, Y.K. and D. Sharma, *Necroptosis: a regulated inflammatory mode of cell death.* Journal of Neuroinflammation, 2018. **15**(1): p. 199.
232. He, S., et al., *Toll-like receptors activate programmed necrosis in macrophages through a receptor-interacting kinase-3-mediated pathway.* Proc Natl Acad Sci U S A, 2011. **108**(50): p. 20054-9.
233. Kaiser, W.J., et al., *Toll-like receptor 3-mediated necrosis via TRIF, RIP3, and MLKL.* J Biol Chem, 2013. **288**(43): p. 31268-79.
234. Thapa, R.J., et al., *Interferon-induced RIP1/RIP3-mediated necrosis requires PKR and is licensed by FADD and caspases.* Proceedings of the National Academy of Sciences, 2013. **110**(33): p. E3109-E3118.
235. Rajput, A., et al., *RIG-I RNA helicase activation of IRF3 transcription factor is negatively regulated by caspase-8-mediated cleavage of the RIP1 protein.* Immunity, 2011. **34**(3): p. 340-51.
236. McComb, S., et al., *Type-I interferon signaling through ISGF3 complex is required for sustained Rip3 activation and necroptosis in macrophages.* Proc Natl Acad Sci U S A, 2014. **111**(31): p. E3206-13.
237. Upton, J.W., W.J. Kaiser, and E.S. Mocarski, *Virus inhibition of RIP3-dependent necrosis.* Cell Host Microbe, 2010. **7**(4): p. 302-313.
238. Balkwill, F., *Tumour necrosis factor and cancer.* Nature Reviews Cancer, 2009. **9**(5): p. 361-371.
239. Annibaldi, A. and P. Meier, *Checkpoints in TNF-Induced Cell Death: Implications in Inflammation and Cancer.* Trends Mol Med, 2018. **24**(1): p. 49-65.
240. Bertrand, M.J.M., et al., *cIAP1 and cIAP2 Facilitate Cancer Cell Survival by Functioning as E3 Ligases that Promote RIP1 Ubiquitination.* Molecular Cell, 2008. **30**(6): p. 689-700.
241. Park, S.M., J.B. Yoon, and T.H. Lee, *Receptor interacting protein is ubiquitinated by cellular inhibitor of apoptosis proteins (c-IAP1 and c-IAP2) in vitro.* FEBS Lett, 2004. **566**(1-3): p. 151-6.
242. Dumétier, B., A. Zadoroznyj, and L. Dubrez *IAP-Mediated Protein Ubiquitination in Regulating Cell Signaling*. Cells, 2020. **9**, DOI: 10.3390/cells9051118.
243. Kovalenko, A., et al., *The tumour suppressor CYLD negatively regulates NF-κB signalling by deubiquitination.* Nature, 2003. **424**(6950): p. 801-805.
244. Trompouki, E., et al., *CYLD is a deubiquitinating enzyme that negatively regulates NF-κB activation by TNFR family members.* Nature, 2003. **424**(6950): p. 793-796.
245. Cho, Y.S., et al., *Phosphorylation-driven assembly of the RIP1-RIP3 complex regulates programmed necrosis and virus-induced inflammation.* Cell, 2009. **137**(6): p. 1112-23.
246. Zhang, D.W., et al., *RIP3, an energy metabolism regulator that switches TNF-induced cell death from apoptosis to necrosis.* Science, 2009. **325**(5938): p. 332-6.
247. He, S., et al., *Receptor interacting protein kinase-3 determines cellular necrotic response to TNF-alpha.* Cell, 2009. **137**(6): p. 1100-11.
248. Mompeán, M., et al., *The Structure of the Necrosome RIPK1-RIPK3 Core, a Human Hetero-Amyloid Signaling Complex.* Cell, 2018. **173**(5): p. 1244-1253.e10.

249. Wang, H., et al., *Mixed lineage kinase domain-like protein MLKL causes necrotic membrane disruption upon phosphorylation by RIP3.* Mol Cell, 2014. **54**(1): p. 133-146.
250. Dondi, E., et al., *A dual role of IFN-alpha in the balance between proliferation and death of human CD4+ T lymphocytes during primary response.* J Immunol, 2004. **173**(6): p. 3740-7.
251. Sekiya, M., et al., *IFN-gamma upregulates anti-apoptotic gene expression and inhibits apoptosis in IL-3-dependent hematopoietic cells.* Biochem Biophys Res Commun, 1997. **239**(2): p. 401-6.
252. Hao, Q., et al., *Interferon-γ Preferentially Promotes Necroptosis of Lung Epithelial Cells by Upregulating MLKL.* Cells, 2022. **11**(3).
253. Yang, D., et al., *ZBP1 mediates interferon-induced necroptosis.* Cellular & Molecular Immunology, 2020. **17**(4): p. 356-368.
254. Frank, T., et al., *Cell cycle arrest in mitosis promotes interferon-induced necroptosis.* Cell Death Differ, 2019. **26**(10): p. 2046-2060.
255. Knuth, A.-K., et al., *Interferons Transcriptionally Up-Regulate MLKL Expression in Cancer Cells.* Neoplasia, 2019. **21**(1): p. 74-81.
256. Thapa, R.J., et al., *NF-κB Protects Cells from Gamma Interferon-Induced RIP1-Dependent Necroptosis.* Molecular and Cellular Biology, 2011. **31**(14): p. 2934-2946.
257. Brault, M., et al., *Intracellular Nucleic Acid Sensing Triggers Necroptosis through Synergistic Type I IFN and TNF Signaling.* J Immunol, 2018. **200**(8): p. 2748-2756.
258. Zhang, X., et al., *mtDNA-STING pathway promotes necroptosis-dependent enterocyte injury in intestinal ischemia reperfusion.* Cell Death & Disease, 2020. **11**(12): p. 1050.
259. Yang, Y., et al., *ZBP1-MLKL necroptotic signaling potentiates radiation-induced antitumor immunity via intratumoral STING pathway activation.* Science Advances, 2021. **7**(41): p. eabf6290.
260. Hao, Q. and H. Tang, *Interferon-γ and Smac mimetics synergize to induce apoptosis of lung cancer cells in a TNFα-independent manner.* Cancer Cell Int, 2018. **18**: p. 84.
261. Kotredes, K.P. and A.M. Gamero, *Interferons as inducers of apoptosis in malignant cells.* J Interferon Cytokine Res, 2013. **33**(4): p. 162-70.
262. Tekautz, T.M., et al., *Evaluation of IFN-γ effects on apoptosis and gene expression in neuroblastoma—Preclinical studies.* Biochimica et Biophysica Acta (BBA) - Molecular Cell Research, 2006. **1763**(10): p. 1000-1010.
263. Sanjana, N.E., O. Shalem, and F. Zhang, *Improved vectors and genome-wide libraries for CRISPR screening.* Nat Methods, 2014. **11**(8): p. 783-784.
264. Luo, W., et al., *GAGE: generally applicable gene set enrichment for pathway analysis.* BMC Bioinformatics, 2009. **10**(1): p. 161.
265. Ritchie, M.E., et al., *limma powers differential expression analyses for RNA-sequencing and microarray studies.* Nucleic Acids Res, 2015. **43**(7): p. e47.
266. Carvalho, B.S. and R.A. Irizarry, *A framework for oligonucleotide microarray preprocessing.* Bioinformatics, 2010. **26**(19): p. 2363-7.
267. Karlowitz, R., et al., *USP22 controls type III interferon signaling and SARS-CoV-2 infection through activation of STING.* Cell Death Dis, 2022. **13**(8): p. 684.
268. Subramanian, A., et al., *Gene set enrichment analysis: A knowledge-based approach for interpreting genome-wide expression profiles.* Proceedings of the National Academy of Sciences, 2005. **102**(43): p. 15545-15550.
269. Hjerpe, R., et al., *Efficient protection and isolation of ubiquitylated proteins using tandem ubiquitin-binding entities.* EMBO Rep, 2009. **10**(11): p. 1250-8.
270. Xiao, H., et al., *USP22 acts as an oncogene by regulating the stability of cyclooxygenase-2 in non-small cell lung cancer.* Biochem Biophys Res Commun, 2015. **460**(3): p. 703-8.
271. Gong, Z., et al., *Identification of potential target genes of USP22 via ChIP-seq and RNA-seq analysis in HeLa cells.* Genet Mol Biol, 2018. **41**(2): p. 488-495.
272. Sasaki, N., et al., *Reg4+ deep crypt secretory cells function as epithelial niche for Lgr5+ stem cells in colon.* Proc Natl Acad Sci U S A, 2016. **113**(37): p. E5399-407.
273. Saini, V., A. Marchese, and M. Majetschak, *CXC chemokine receptor 4 is a cell surface receptor for extracellular ubiquitin.* J Biol Chem, 2010. **285**(20): p. 15566-15576.
274. Fujisawa, K., et al., *Modulation of anti-cancer drug sensitivity through the regulation of mitochondrial activity by adenylate kinase 4.* J Exp Clin Cancer Res, 2016. **35**: p. 48.
275. Lanning, N.J., et al., *A mitochondrial RNAi screen defines cellular bioenergetic determinants and identifies an adenylate kinase as a key regulator of ATP levels.* Cell Rep, 2014. **7**(3): p. 907-17.
276. Stetson, D.B. and R. Medzhitov, *Recognition of cytosolic DNA activates an IRF3-dependent innate immune response.* Immunity, 2006. **24**(1): p. 93-103.

277. Brzostek-Racine, S., et al., *The DNA damage response induces IFN.* J Immunol, 2011. **187**(10): p. 5336-45.
278. Li, C., et al., *The H2B deubiquitinase Usp22 promotes antibody class switch recombination by facilitating non-homologous end joining.* Nature Communications, 2018. **9**(1): p. 1006.
279. Ramachandran, S., et al., *The SAGA Deubiquitination Module Promotes DNA Repair and Class Switch Recombination through ATM and DNAPK-Mediated γH2AX Formation.* Cell Rep, 2016. **15**(7): p. 1554-1565.
280. West, A.P., et al., *Mitochondrial DNA stress primes the antiviral innate immune response.* Nature, 2015. **520**(7548): p. 553-557.
281. Li, Q., et al., *TRIM29 negatively controls antiviral immune response through targeting STING for degradation.* Cell Discovery, 2018. **4**(1): p. 13.
282. Stanifer, M.L., et al., *Critical Role of Type III Interferon in Controlling SARS-CoV-2 Infection in Human Intestinal Epithelial Cells.* Cell Rep, 2020. **32**(1): p. 107863.
283. Zhu, Q., et al., *Inhibition of coronavirus infection by a synthetic STING agonist in primary human airway system.* Antiviral Research, 2021. **187**: p. 105015.
284. Humphries, F., et al., *A diamidobenzimidazole STING agonist protects against SARS-CoV-2 infection.* Science Immunology, 2021. **6**(59): p. eabi9002.
285. Wurtz, N., et al., *Culture of SARS-CoV-2 in a panel of laboratory cell lines, permissivity, and differences in growth profile.* Eur J Clin Microbiol Infect Dis, 2021. **40**(3): p. 477-484.
286. Hossain, M.S., et al., *Colorectal Cancer: A Review of Carcinogenesis, Global Epidemiology, Current Challenges, Risk Factors, Preventive and Treatment Strategies.* Cancers (Basel), 2022. **14**(7).
287. Gupta, R., et al., *Colon cancer stem cells: Potential target for the treatment of colorectal cancer.* Cancer Biol Ther, 2019. **20**(8): p. 1068-1082.
288. Cekay, M.J., et al., *Smac mimetics and type II interferon synergistically induce necroptosis in various cancer cell lines.* Cancer Lett, 2017. **410**: p. 228-237.
289. Roesler, S., et al., *Cooperative TRAIL production mediates IFNα/Smac mimetic-induced cell death in TNFα-resistant solid cancer cells.* Oncotarget, 2016. **7**(4): p. 3709-25.
290. Reiter, M., et al., *Smac mimetic sensitizes renal cell carcinoma cells to interferon-α-induced apoptosis.* Cancer Lett, 2016. **375**(1): p. 1-8.
291. Hannes, S., R. Karlowitz, and S.J.L. van Wijk, *The Smac mimetic BV6 cooperates with STING to induce necroptosis in apoptosis-resistant pancreatic carcinoma cells.* Cell Death & Disease, 2021. **12**(9): p. 816.
292. Sarhan, J., et al., *Constitutive interferon signaling maintains critical threshold of MLKL expression to license necroptosis.* Cell Death Differ, 2019. **26**(2): p. 332-347.
293. Hu, X., et al., *The JAK/STAT signaling pathway: from bench to clinic.* Signal Transduction and Targeted Therapy, 2021. **6**(1): p. 402.
294. Zhu, Y., et al., *STING: a master regulator in the cancer-immunity cycle.* Molecular Cancer, 2019. **18**(1): p. 152.
295. Schoggins, J.W., et al., *A diverse range of gene products are effectors of the type I interferon antiviral response.* Nature, 2011. **472**(7344): p. 481-5.
296. Forero, A., et al., *Differential Activation of the Transcription Factor IRF1 Underlies the Distinct Immune Responses Elicited by Type I and Type III Interferons.* Immunity, 2019. **51**(3): p. 451-464.e6.
297. Ma, F., et al., *Positive feedback regulation of type I interferon by the interferon-stimulated gene STING.* EMBO Rep, 2015. **16**(2): p. 202-12.
298. Lee, A.J. and A.A. Ashkar, *The Dual Nature of Type I and Type II Interferons.* Frontiers in Immunology, 2018. **9**.
299. Zhu, K., et al., *Necroptosis promotes cell-autonomous activation of proinflammatory cytokine gene expression.* Cell Death & Disease, 2018. **9**(5): p. 500.
300. Morgan, M.J. and Y.-S. Kim, *Roles of RIPK3 in necroptosis, cell signaling, and disease.* Experimental & Molecular Medicine, 2022. **54**(10): p. 1695-1704.
301. Orozco, S.L., et al., *RIPK3 Activation Leads to Cytokine Synthesis that Continues after Loss of Cell Membrane Integrity.* Cell Rep, 2019. **28**(9): p. 2275-2287.e5.
302. Gong, Y.N., et al., *ESCRT-III Acts Downstream of MLKL to Regulate Necroptotic Cell Death and Its Consequences.* Cell, 2017. **169**(2): p. 286-300.e16.
303. Weinelt, N., et al., *Species-specific LUBAC-mediated M1 ubiquitination regulates necroptosis by segregating the cellular distribution and fate of activated MLKL.* bioRxiv, 2022: p. 2022.12.08.519265.
304. Wang, X., et al., *Neutrophil Necroptosis Is Triggered by Ligation of Adhesion Molecules following GM-CSF Priming.* J Immunol, 2016. **197**(10): p. 4090-4100.

305. Wang, K., et al., *IP-10 Promotes Blood–Brain Barrier Damage by Inducing Tumor Necrosis Factor Alpha Production in Japanese Encephalitis.* Frontiers in Immunology, 2018. **9**.
306. Lee, J.S., et al., *Histone crosstalk between H2B monoubiquitination and H3 methylation mediated by COMPASS.* Cell, 2007. **131**(6): p. 1084-96.
307. Xiao, T., et al., *Histone H2B ubiquitylation is associated with elongating RNA polymerase II.* Mol Cell Biol, 2005. **25**(2): p. 637-51.
308. Minsky, N., et al., *Monoubiquitinated H2B is associated with the transcribed region of highly expressed genes in human cells.* Nat Cell Biol, 2008. **10**(4): p. 483-8.
309. Wang, Z., et al., *Decreased H2B monoubiquitination and overexpression of ubiquitin-specific protease enzyme 22 in malignant colon carcinoma.* Hum Pathol, 2015. **46**(7): p. 1006-14.
310. Fonseca, G.J., et al., *Adenovirus evasion of interferon-mediated innate immunity by direct antagonism of a cellular histone posttranslational modification.* Cell Host Microbe, 2012. **11**(6): p. 597-606.
311. Stanifer, M.L., K. Pervolaraki, and S. Boulant, *Differential Regulation of Type I and Type III Interferon Signaling.* Int J Mol Sci, 2019. **20**(6).
312. Wan, X. and N.J. Garg, *Sirtuin Control of Mitochondrial Dysfunction, Oxidative Stress, and Inflammation in Chagas Disease Models.* Front Cell Infect Microbiol, 2021. **11**: p. 693051.
313. Olmos, Y., et al., *SirT1 regulation of antioxidant genes is dependent on the formation of a FoxO3a/PGC-1α complex.* Antioxid Redox Signal, 2013. **19**(13): p. 1507-21.
314. Atanassov, B.S., et al., *Gcn5 and SAGA regulate shelterin protein turnover and telomere maintenance.* Mol Cell, 2009. **35**(3): p. 352-64.
315. Stanifer, M.L., et al., *Importance of Type I and III Interferons at Respiratory and Intestinal Barrier Surfaces.* Front Immunol, 2020. **11**: p. 608645.
316. Mordstein, M., et al., *Lambda interferon renders epithelial cells of the respiratory and gastrointestinal tracts resistant to viral infections.* J Virol, 2010. **84**(11): p. 5670-7.
317. Sommereyns, C., et al., *IFN-Lambda (IFN-λ) Is Expressed in a Tissue-Dependent Fashion and Primarily Acts on Epithelial Cells In Vivo.* PLOS Pathogens, 2008. **4**(3): p. e1000017.
318. Chen, J., et al., *STING-Dependent Interferon-λ1 Induction in HT29 Cells, a Human Colorectal Cancer Cell Line, After Gamma-Radiation.* Int J Radiat Oncol Biol Phys, 2018. **101**(1): p. 97-106.
319. Sui, H., et al., *STING is an essential mediator of the Ku70-mediated production of IFN-λ1 in response to exogenous DNA.* Sci Signal, 2017. **10**(488).
320. Barber, G.N., *Cytoplasmic DNA innate immune pathways.* Immunol Rev, 2011. **243**(1): p. 99-108.
321. Sharma, S. and K.A. Fitzgerald, *Innate immune sensing of DNA.* PLoS Pathog, 2011. **7**(4): p. e1001310.
322. Sui, H., et al., *siRNA enhances DNA-mediated interferon lambda-1 response through crosstalk between RIG-I and IFI16 signalling pathway.* Nucleic Acids Res, 2014. **42**(1): p. 583-98.
323. Digre, A. and C. Lindskog, *The Human Protein Atlas-Spatial localization of the human proteome in health and disease.* Protein Sci, 2021. **30**(1): p. 218-233.
324. Jefferies, C.A., *Regulating IRFs in IFN Driven Disease.* Frontiers in Immunology, 2019. **10**.
325. Frémond, M.L. and Y.J. Crow, *STING-Mediated Lung Inflammation and Beyond.* J Clin Immunol, 2021. **41**(3): p. 501-514.
326. David, C. and M.L. Frémond, *Lung Inflammation in STING-Associated Vasculopathy with Onset in Infancy (SAVI).* Cells, 2022. **11**(3).
327. Lepelley, A., et al., *Mutations in COPA lead to abnormal trafficking of STING to the Golgi and interferon signaling.* J Exp Med, 2020. **217**(11).
328. Kong, L., et al., *The ubiquitin E3 ligase TRIM10 promotes STING aggregation and activation in the Golgi apparatus.* Cell Rep, 2023. **42**(4): p. 112306.
329. Du, C., et al., *STAT3-induced upregulation of lncRNA DUXAP8 functions as ceRNA for miR-577 to promote the migration and invasion in colorectal cancer through the regulation of RAB14.* Eur Rev Med Pharmacol Sci, 2019. **23**(14): p. 6105-6118.
330. Doherty, L.M., et al., *Integrating multi-omics data reveals function and therapeutic potential of deubiquitinating enzymes.* eLife, 2022. **11**: p. e72879.
331. Reyes-Turcu, F.E., K.H. Ventii, and K.D. Wilkinson, *Regulation and cellular roles of ubiquitin-specific deubiquitinating enzymes.* Annu Rev Biochem, 2009. **78**: p. 363-97.
332. Balka, K.R., et al., *Termination of STING responses is mediated via ESCRT-dependent degradation.* Embo j, 2023: p. e112712.
333. Zhao, Y., et al., *Noncanonical regulation of alkylation damage resistance by the OTUD4 deubiquitinase.* Embo j, 2015. **34**(12): p. 1687-703.

334. Blanco-Melo, D., et al., *Imbalanced Host Response to SARS-CoV-2 Drives Development of COVID-19.* Cell, 2020. **181**(5): p. 1036-1045.e9.
335. Hadjadj, J., et al., *Impaired type I interferon activity and inflammatory responses in severe COVID-19 patients.* Science, 2020. **369**(6504): p. 718-724.
336. Park, A. and A. Iwasaki, *Type I and Type III Interferons - Induction, Signaling, Evasion, and Application to Combat COVID-19.* Cell Host Microbe, 2020. **27**(6): p. 870-878.
337. Haagmans, B.L., et al., *Pegylated interferon-alpha protects type 1 pneumocytes against SARS coronavirus infection in macaques.* Nat Med, 2004. **10**(3): p. 290-3.
338. Kindler, E., et al., *Efficient replication of the novel human betacoronavirus EMC on primary human epithelium highlights its zoonotic potential.* mBio, 2013. **4**(1): p. e00611-12.
339. Hamming, O.J., et al., *Interferon lambda 4 signals via the IFNλ receptor to regulate antiviral activity against HCV and coronaviruses.* Embo j, 2013. **32**(23): p. 3055-65.
340. O'Brien, T.R., et al., *Weak Induction of Interferon Expression by Severe Acute Respiratory Syndrome Coronavirus 2 Supports Clinical Trials of Interferon-λ to Treat Early Coronavirus Disease 2019.* Clin Infect Dis, 2020. **71**(6): p. 1410-1412.
341. Pan, H., et al., *Repurposed Antiviral Drugs for Covid-19 - Interim WHO Solidarity Trial Results.* N Engl J Med, 2021. **384**(6): p. 497-511.
342. Rui, Y., et al., *Unique and complementary suppression of cGAS-STING and RNA sensing-triggered innate immune responses by SARS-CoV-2 proteins.* Signal Transduct Target Ther, 2021. **6**(1): p. 123.
343. Han, L., et al., *SARS-CoV-2 ORF10 antagonizes STING-dependent interferon activation and autophagy.* J Med Virol, 2022.
344. Moustaqil, M., et al., *SARS-CoV-2 proteases PLpro and 3CLpro cleave IRF3 and critical modulators of inflammatory pathways (NLRP12 and TAB1): implications for disease presentation across species.* Emerg Microbes Infect, 2021. **10**(1): p. 178-195.
345. Thoms, M., et al., *Structural basis for translational shutdown and immune evasion by the Nsp1 protein of SARS-CoV-2.* Science, 2020. **369**(6508): p. 1249-1255.
346. Lei, X., et al., *Activation and evasion of type I interferon responses by SARS-CoV-2.* Nat Commun, 2020. **11**(1): p. 3810.
347. Jouvenet, N., C. Goujon, and A. Banerjee, *Clash of the titans: interferons and SARS-CoV-2.* Trends Immunol, 2021. **42**(12): p. 1069-1072.
348. Ong, L.T., et al., *IFI16-dependent STING signaling is a crucial regulator of anti-HER2 immune response in HER2+ breast cancer.* Proc Natl Acad Sci U S A, 2022. **119**(31): p. e2201376119.
349. Almine, J.F., et al., *IFI16 and cGAS cooperate in the activation of STING during DNA sensing in human keratinocytes.* Nature Communications, 2017. **8**(1): p. 14392.
350. Shen, Yu J., et al., *Genome-Derived Cytosolic DNA Mediates Type I Interferon-Dependent Rejection of B Cell Lymphoma Cells.* Cell Reports, 2015. **11**(3): p. 460-473.
351. Li, T. and Z.J. Chen, *The cGAS-cGAMP-STING pathway connects DNA damage to inflammation, senescence, and cancer.* J Exp Med, 2018. **215**(5): p. 1287-1299.
352. De Luca, V., et al., *Role of yUbp8 in Mitochondria and Hypoxia Entangles the Finding of Human Ortholog Usp22 in the Glioblastoma Pseudo-Palisade Microlayer.* Cells, 2022. **11**(10).
353. Davidson, L., L. Muniz, and S. West, *3' end formation of pre-mRNA and phosphorylation of Ser2 on the RNA polymerase II CTD are reciprocally coupled in human cells.* Genes Dev, 2014. **28**(4): p. 342-56.
354. Chipumuro, E. and M.A. Henriksen, *The ubiquitin hydrolase USP22 contributes to 3'-end processing of JAK-STAT-inducible genes.* Faseb j, 2012. **26**(2): p. 842-54.
355. Yum, S., et al., *TBK1 recruitment to STING activates both IRF3 and NF-κB that mediate immune defense against tumors and viral infections.* Proc Natl Acad Sci U S A, 2021. **118**(14).
356. Xia, T., et al., *Deregulation of STING Signaling in Colorectal Carcinoma Constrains DNA Damage Responses and Correlates With Tumorigenesis.* Cell Reports, 2016. **14**(2): p. 282-297.
357. Gao, K.M., et al., *Radioresistant cells initiate lymphocyte-dependent lung inflammation and IFNγ-dependent mortality in STING gain-of-function mice.* Proc Natl Acad Sci U S A, 2022. **119**(25): p. e2202327119.
358. Li, J., et al., *Tumor Cell–Intrinsic USP22 Suppresses Antitumor Immunity in Pancreatic Cancer.* Cancer Immunology Research, 2020. **8**(3): p. 282-291.
359. Huang, X., et al., *USP22 Deubiquitinates CD274 to Suppress Anticancer Immunity.* Cancer Immunology Research, 2019. **7**(10): p. 1580-1590.
360. Ma, Z. and B. Damania, *The cGAS-STING Defense Pathway and Its Counteraction by Viruses.* Cell Host Microbe, 2016. **19**(2): p. 150-8.
361. Sun, L., et al., *Coronavirus papain-like proteases negatively regulate antiviral innate immune response through disruption of STING-mediated signaling.* PLoS One, 2012. **7**(2): p. e30802.

362. Xie, J., et al., *Dampened STING-Dependent Interferon Activation in Bats.* Cell Host Microbe, 2018. **23**(3): p. 297-301.e4.
363. Buchrieser, J., et al., *Syncytia formation by SARS-CoV-2-infected cells.* Embo j, 2020. **39**(23): p. e106267.
364. Ren, H., et al., *Micronucleus production, activation of DNA damage response and cGAS-STING signaling in syncytia induced by SARS-CoV-2 infection.* Biol Direct, 2021. **16**(1): p. 20.
365. Liu, X., et al., *SARS-CoV-2 spike protein-induced cell fusion activates the cGAS-STING pathway and the interferon response.* Science Signaling, 2022. **15**(729): p. eabg8744.
366. Zhou, Z., et al., *Sensing of cytoplasmic chromatin by cGAS activates innate immune response in SARS-CoV-2 infection.* Signal Transduct Target Ther, 2021. **6**(1): p. 382.
367. Domizio, J.D., et al., *The cGAS–STING pathway drives type I IFN immunopathology in COVID-19.* Nature, 2022. **603**(7899): p. 145-151.
368. Israelow, B., et al., *Mouse model of SARS-CoV-2 reveals inflammatory role of type I interferon signaling.* J Exp Med, 2020. **217**(12).
369. Chua, R.L., et al., *COVID-19 severity correlates with airway epithelium-immune cell interactions identified by single-cell analysis.* Nat Biotechnol, 2020. **38**(8): p. 970-979.
370. Mehta, P., et al., *COVID-19: consider cytokine storm syndromes and immunosuppression.* Lancet, 2020. **395**(10229): p. 1033-1034.
371. Wang, L.L., J.W. Yang, and J.F. Xu, *Severe acute respiratory syndrome coronavirus 2 causes lung inflammation and injury.* Clin Microbiol Infect, 2022. **28**(4): p. 513-520.
372. Bake, V., et al., *Synergistic interaction of Smac mimetic and IFNα to trigger apoptosis in acute myeloid leukemia cells.* Cancer Lett, 2014. **355**(2): p. 224-31.
373. Kuriakose, T., et al., *IRF1 Is a Transcriptional Regulator of ZBP1 Promoting NLRP3 Inflammasome Activation and Cell Death during Influenza Virus Infection.* J Immunol, 2018. **200**(4): p. 1489-1495.
374. Man, S.M., et al., *The transcription factor IRF1 and guanylate-binding proteins target activation of the AIM2 inflammasome by Francisella infection.* Nat Immunol, 2015. **16**(5): p. 467-75.
375. Benaoudia, S., et al., *A genome-wide screen identifies IRF2 as a key regulator of caspase-4 in human cells.* EMBO Rep, 2019. **20**(9): p. e48235.
376. Karki, R., et al., *Interferon regulatory factor 1 regulates PANoptosis to prevent colorectal cancer.* JCI Insight, 2020. **5**(12).
377. Shultz, D.B., et al., *Roles of IKK-beta, IRF1, and p65 in the activation of chemokine genes by interferon-gamma.* J Interferon Cytokine Res, 2009. **29**(12): p. 817-24.
378. Shultz, D.B., et al., *Activation of a subset of genes by IFN-gamma requires IKKbeta but not interferon-dependent activation of NF-kappaB.* J Interferon Cytokine Res, 2007. **27**(10): p. 875-84.
379. Karki, R., et al., *Synergism of TNF-α and IFN-γ Triggers Inflammatory Cell Death, Tissue Damage, and Mortality in SARS-CoV-2 Infection and Cytokine Shock Syndromes.* Cell, 2021. **184**(1): p. 149-168.e17.
380. Vila-del Sol, V., C. Punzón, and M. Fresno, *IFN-γ-Induced TNF-α Expression Is Regulated by Interferon Regulatory Factors 1 and 8 in Mouse Macrophages1.* The Journal of Immunology, 2008. **181**(7): p. 4461-4470.
381. Nakamura, H., et al., *STAT3 activity regulates sensitivity to tumor necrosis factor-related apoptosis-inducing ligand-induced apoptosis in cervical cancer cells.* Int J Oncol, 2016. **49**(5): p. 2155-2162.
382. Kusaba, M., et al., *Abrogation of constitutive STAT3 activity sensitizes human hepatoma cells to TRAIL-mediated apoptosis.* J Hepatol, 2007. **47**(4): p. 546-55.
383. Lanuti, P., et al., *Enhancement of TRAIL cytotoxicity by AG-490 in human ALL cells is characterized by downregulation of cIAP-1 and cIAP-2 through inhibition of Jak2/Stat3.* Cell Res, 2009. **19**(9): p. 1079-89.
384. Schoppmann, S.F., et al., *Phosphorylation of signal transducer and activator of transcription 3 (STAT3) correlates with Her-2 status, carbonic anhydrase 9 expression and prognosis in esophageal cancer.* Clin Exp Metastasis, 2012. **29**(6): p. 615-24.
385. Takemoto, S., et al., *Expression of activated signal transducer and activator of transcription-3 predicts poor prognosis in cervical squamous-cell carcinoma.* Br J Cancer, 2009. **101**(6): p. 967-72.
386. Benekli, M., et al., *Constitutive activity of signal transducer and activator of transcription 3 protein in acute myeloid leukemia blasts is associated with short disease-free survival.* Blood, 2002. **99**(1): p. 252-7.

387. Sestito, R., et al., *STAT3-dependent effects of IL-22 in human keratinocytes are counterregulated by sirtuin 1 through a direct inhibition of STAT3 acetylation.* Faseb j, 2011. **25**(3): p. 916-27.
388. Chiriac, M.T., et al., *Activation of Epithelial Signal Transducer and Activator of Transcription 1 by Interleukin 28 Controls Mucosal Healing in Mice With Colitis and Is Increased in Mucosa of Patients With Inflammatory Bowel Disease.* Gastroenterology, 2017. **153**(1): p. 123-138.e8.
389. Günther, C., et al., *Interferon Lambda Promotes Paneth Cell Death Via STAT1 Signaling in Mice and Is Increased in Inflamed Ileal Tissues of Patients With Crohn’s Disease.* Gastroenterology, 2019. **157**(5): p. 1310-1322.e13.
390. Chen, D., et al., *PUMA amplifies necroptosis signaling by activating cytosolic DNA sensors.* Proc Natl Acad Sci U S A, 2018. **115**(15): p. 3930-3935.
391. Barber, G.N., et al., *Translational regulation by the interferon-induced double-stranded-RNA-activated 68-kDa protein kinase.* Proc Natl Acad Sci U S A, 1993. **90**(10): p. 4621-5.
392. Beretta, L., et al., *Expression of the protein kinase PKR in modulated by IRF-1 and is reduced in 5q- associated leukemias.* Oncogene, 1996. **12**(7): p. 1593-6.
393. Kapil, P., et al., *PKR mediated regulation of inflammation and IL-10 during viral encephalomyelitis.* Journal of Neuroimmunology, 2014. **270**(1): p. 1-12.
394. Riebeling, T., U. Kunzendorf, and S. Krautwald, *The role of RHIM in necroptosis.* Biochem Soc Trans, 2022. **50**(4): p. 1197-1205.
395. Karki, R., et al., *ADAR1 restricts ZBP1-mediated immune response and PANoptosis to promote tumorigenesis.* Cell Rep, 2021. **37**(3): p. 109858.
396. Kaiser, W.J. and M.K. Offermann, *Apoptosis induced by the toll-like receptor adaptor TRIF is dependent on its receptor interacting protein homotypic interaction motif.* J Immunol, 2005. **174**(8): p. 4942-52.
397. Lim, J., et al., *Autophagy regulates inflammatory programmed cell death via turnover of RHIM-domain proteins.* Elife, 2019. **8**.
398. Liang, J.X., et al., *Ubiquitin-specific protease 22-induced autophagy is correlated with poor prognosis of pancreatic cancer.* Oncol Rep, 2014. **32**(6): p. 2726-34.
399. Di, Q., et al., *USP22 suppresses the NLRP3 inflammasome by degrading NLRP3 via ATG5-dependent autophagy.* Autophagy, 2023. **19**(3): p. 873-885.
400. Guo, J., et al., *Immune Evasion and Drug Resistance Mediated by USP22 in Cancer: Novel Targets and Mechanisms.* Frontiers in Immunology, 2022. **13**.
401. Upton, J.W., W.J. Kaiser, and E.S. Mocarski, *Cytomegalovirus M45 cell death suppression requires receptor-interacting protein (RIP) homotypic interaction motif (RHIM)-dependent interaction with RIP1.* J Biol Chem, 2008. **283**(25): p. 16966-70.
402. Liu, Z., et al., *A class of viral inducer of degradation of the necroptosis adaptor RIPK3 regulates virus-induced inflammation.* Immunity, 2021. **54**(2): p. 247-258.e7.
403. Herbert, A. and M. Poptsova, *Z-RNA and the Flipside of the SARS Nsp13 Helicase: Is There a Role for Flipons in Coronavirus-Induced Pathology?* Front Immunol, 2022. **13**: p. 912717.
404. Li, S., et al., *SARS-CoV-2 Z-RNA activates the ZBP1-RIPK3 pathway to promote virus-induced inflammatory responses.* Cell Research, 2023. **33**(3): p. 201-214.
405. Günther, C., et al., *The pseudokinase MLKL mediates programmed hepatocellular necrosis independently of RIPK3 during hepatitis.* J Clin Invest, 2016. **126**(11): p. 4346-4360.
406. Evans, C., A.G. Dalgleish, and D. Kumar, *Review article: immune suppression and colorectal cancer.* Aliment Pharmacol Ther, 2006. **24**(8): p. 1163-77.
407. Zhang, Y., et al., *Mechanisms of Immunosuppression in Colorectal Cancer.* Cancers (Basel), 2020. **12**(12).
408. Snyder, A.G., et al., *Intratumoral activation of the necroptotic pathway components RIPK1 and RIPK3 potentiates antitumor immunity.* Sci Immunol, 2019. **4**(36).
409. Aaes, T.L., et al., *Vaccination with Necroptotic Cancer Cells Induces Efficient Anti-tumor Immunity.* Cell Rep, 2016. **15**(2): p. 274-87.
410. Borden, E.C., *Interferons α and β in cancer: therapeutic opportunities from new insights.* Nature Reviews Drug Discovery, 2019. **18**(3): p. 219-234.
411. Borden, E.C., et al., *Interferons at age 50: past, current and future impact on biomedicine.* Nature Reviews Drug Discovery, 2007. **6**(12): p. 975-990.
412. Schwartzberg, L.S., et al., *Modulation of the Fas signaling pathway by IFN-gamma in therapy of colon cancer: phase I trial and correlative studies of IFN-gamma, 5-fluorouracil, and leucovorin.* Clin Cancer Res, 2002. **8**(8): p. 2488-98.
413. Borden, E.C. and D. Parkinson, *A perspective on the clinical effectiveness and tolerance of interferon-alpha.* Semin Oncol, 1998. **25**(1 Suppl 1): p. 3-8.

414. Konno, H., et al., *Suppression of STING signaling through epigenetic silencing and missense mutation impedes DNA damage mediated cytokine production.* Oncogene, 2018. **37**(15): p. 2037-2051.
415. Le, D.T., et al., *Safety and survival with GVAX pancreas prime and Listeria Monocytogenes-expressing mesothelin (CRS-207) boost vaccines for metastatic pancreatic cancer.* J Clin Oncol, 2015. **33**(12): p. 1325-33.
416. Fu, J., et al., *STING agonist formulated cancer vaccines can cure established tumors resistant to PD-1 blockade.* Sci Transl Med, 2015. **7**(283): p. 283ra52.
417. Lemos, H., et al., *STING Promotes the Growth of Tumors Characterized by Low Antigenicity via IDO Activation.* Cancer Res, 2016. **76**(8): p. 2076-81.
418. Strilic, B., et al., *Tumour-cell-induced endothelial cell necroptosis via death receptor 6 promotes metastasis.* Nature, 2016. **536**(7615): p. 215-8.
419. Hu, Q.-P., et al., *Beyond a tumor suppressor: Soluble E-cadherin promotes the progression of cancer.* International Journal of Cancer, 2016. **138**(12): p. 2804-2812.